© 1975

ALAN AUGUST VETTER

ALL RIGHTS RESERVED

KINETICS AND STRUCTURE OF THE CS_2/O_2 FLAME LASER

Thesis by

Alan August Vetter

In Partial Fulfillment of the Requirements

for the Degree of

Doctor of Philosophy

California Institute of Technology

Pasadena, California

1975

(Submitted April 1, 1975)

ACKNOWLEDGMENTS

First, I would like to thank Dr. F. E. C. Culick, my research adviser, who planted the seeds for the majority of the fruitful work which is presented in this thesis. I should also like to thank him for allowing me the freedom to go merrily along paths that I chose.

Designs of many of the pieces of the apparatuses used in the experimental phases of this thesis were significantly improved after discussions with Mr. F. T. Linton. I would also like to thank him, along with M. Ono, J. Shlachter, and M. Rodgers for construction of parts of these apparatuses.

I would like to acknowledge the assistance of E. Sovero, P. Moynihan, M. Ono, J. Shlachter, and M. Rodgers in testing of the apparatuses. I also would like to thank my wife Sylvia for her meticulous laboratory assistance.

I would like to acknowledge the aid of G. Nickerson of Ultrasystems, Inc., who arranged for my use of the GKAP program. I would like to thank D. Atkinson for adapting the modified version of the GKAP program to the Caltech computer, and B. Luke for helping with the utilization of the program. I also want to acknowledge the aid of E. Sovero, who allowed me access to his version of the CEC72 program.

I wish to thank my wife Sylvia for her aid in preparation of the drafts of this thesis, and in particular for her conversion of almost illegible text to a typed version. I also would like to thank the beautiful eurhythmist who typed the final version of this thesis.

Support for my residence at Caltech was provided in part by a

NDEA title IV fellowship. Caltech contributed by supporting me as a Graduate Teaching Assistant and, due to the efforts of Dr. F. S. Buffington, a one-term discretionary tuition scholarship. I was also supported on a Graduate Research Assistantship by AFOSR contract number 74-2674.

Support for equipment and supplies was furnished by the President's Fund and AFOSR contract number 74-2674. The monochrometor and Ge:Au detector were provided by a grant from the Sloan Fund. The lock-in amplifier and chart recorder were obtained, with assistance by L. Strand, from the JPL loan pool.

I wish to acknowledge very important contributions from the three women who provided the motivation for continuation of these studies. Willa Kay Wiener enabled me to survive the toughest times. Susan Lyn McGaha suffered the lean years with me. And finally, Sylvia, who helped me through my thesis preparation.

ABSTRACT

This thesis is a study of the interactions of chemical kinetics, relaxation processes, and low-speed fluid mechanics for the deflagration of gaseous carbon disulfide and oxygen under conditions for which laser action has been demonstrated. A four-reaction branching chain reaction mechanism is deduced from experimental evidence and reaction rates to represent the chemical kinetics of CS_2/O_2 combustion. This chain mechanism is used to explain some explosion phenomena and to obtain the initial conditions and initial chemical kinetics expected for the different types of CS_2/O_2 chemical lasers. The dynamics of chemical population and relaxation, including selective depopulation, of the vibrational levels of CO are discussed.

Three analytical methods are employed to solve the premixed laminar flame problem for the CS_2/O_2 flame. The von Kármán approximations and the thermal theory approximation are two of these methods; the third, which considers diffusion of only the chain carrier, is termed the single-species diffusion approximation. The flame speed, which is the eigenvalue of laminar flame propagation theories, was experimentally determined for the low-pressure CS_2/O_2 flame and compared to the magnitude and dependencies calculated by the analytic methods. Some qualitative measures of flame structure are compared to the calculated structure.

Details are given for a multi-slit injector whose design allows complete control over mixing. Results for this burner and premixed configuration burners are discussed.

CO emission spectra were taken from CS_2/O_2 flames and the relative vibrational populations determined. The rates of population of the upper vibrational levels are calculated from these experimental spectra.

TABLE OF CONTENTS

	Page
Acknowledgments	ii
Abstract	iv
Table of Contents	vi
Nomenclature	ix
INTRODUCTION	1
Summary	3
1. CHEMICAL KINETICS OF CS_2/O_2 COMBUSTION	6
1.1 Macroscopic Behavior	6
1.2 Ancillary Chemistry	8
1.3 Primary Chemistry	11
1.4 Deduction of Chain Mechanism	15
Tables and Figure	20
2. INITIAL CONDITIONS, INITIAL REACTIONS, AND INDUCTION PERIOD	30
2.1 Induction Period	30
2.2 Early Stages of the Induction Period	33
2.3 Induction Time Estimate	34
2.4 Initial Conditions for the Flame Laser	37
2.5 Initial Conditions after Flash Photolysis	38
2.6 Initial Conditions for the Pulse Discharge Laser	38
2.7 Thermal Dissociation Laser	39
2.8 Electric Discharge Laser	40
2.9 Microwave Discharge Laser	42
Table	43
3. HISTORY OF THE CS_2/O_2 CHEMICAL LASER AND CHAIN MECHANISM	44
3.1 Chemical Lasers	44
3.2 Compendium of CO Chemical Lasers	46
3.3 Chain Mechanism	48
Tables	50
4. VIBRATIONAL QUANTA KINETICS OF CO	56
4.1 Energy Levels	56

	Page
4.2 Chemical Excitation	57
4.3 Radiative Decay	59
4.4 Collisional Decay	61
Tables and Figures	65
5. VON KÁRMÁN APPROXIMATION APPLIED TO THE CS_2/O_2 FLAME	73
5.1 Development of the Problem	73
5.2 Zeroth Order Approximation	80
5.3 First Order Approximation	81
5.4 Second Order Approximation	81
5.5 Numerical Results	85
5.6 Sensitivity of Numerical Results	88
Tables and Figures	90
6. THERMAL THEORY APPROXIMATION TO THE CS_2/O_2 FLAME	101
6.1 Thermal Theory Formulation	102
6.2 Numerical Solution	105
6.3 Sensitivity of Numerical Results	108
Tables and Figures	110
7. SINGLE SPECIES DIFFUSION APPROXIMATION	115
7.1 Formulation	116
7.2 First Case, Thermal Conduction Ignored	118
7.3 Second Case, Thermal Conduction Considered	119
7.4 Numerical Solution	121
7.5 Sensitivity of the Numerical Calculation	124
Tables and Figures	125
8. APPARATUS	132
8.1 Gas Supplies	132
8.2 Exhaust, Ignition, and Cooling Water	134
8.3 Chamber	135
8.4 Injector	137
8.5 Optical Subsystem	139
8.6 Observational Notes	142
Tables and Figures	144

	Page
9. FLAME SPEED	155
9.1 Technique	155
9.2 Data Acquisition	157
9.3 Estimate of the Limit of Error	160
9.4 Calculated Flame Speeds	161
Tables and Figures	164
10. EMISSION MEASUREMENTS	172
10.1 Vibrational Populations from Overtone Spectra	172
10.2 Experimental Arrangement	175
10.3 Experimental Data	177
10.4 Rate of Population of CO(v)	178
Tables and Figures	181
11. GENERALIZED KINETICS AND THERMODYNAMICS PROGRAMS	186
11.1 The CEC 72 Program	186
11.2 The GKAP Program	187
Tables and Figures	191
CONCLUDING REMARKS	195
REFERENCES	200
APPENDIX A	214
APPENDIX B	231
APPENDIX C	246

NOMENCLATURE

A_i	pre-exponential coefficient of reaction rate i
A_f	flame area
$A_{v, v'}$	spontaneous emission coefficient for the transition from level v to v'
a_{ji}	coefficients for polynomial fit to enthalpy
B_e	spectroscopic constant
$B_{v, v'}$	stimulated emission coefficient
b	constant for induction time calculation
C_p	specific heat capacity
$\bar{C}_p$	molar heat capacity
C_{pi}	heat capacity of species i
C_1, C_2, C_3, C_4	constants
c	concentration
D, D_{ij}	diffusion coefficient
D_e	spectroscopic constant
E	energy
E_i	activation energy of reaction i
e	electron
f	flow rate
G	function which is independent of the species
H_e	spectroscopic constant
H_i	molar enthalpy of species i
h_i	specific enthalpy of species i
h^o_j	standard heat of formation of species j
h	Planck's constant; flame arc length

I	ionization potential
$I_{v, v-2}$	relative emission intensity
J	rotational level
K	rate of reaction or deactivation
k	Boltzmann's constant
ℓ	length of flame along the optical axis
ℓ_i	heat conduction constant for species i
M	number of reactions
m	mass of molecule; mass flow rate
N	number of species
N_V	relative population of CO(v)
n	particle density
$P_{v, v-1}$	probability of vibrational deactivation from level v
p	pressure
q	parameter
R	ideal gas constant
R_v	relative role of population of CO(v)
r	initial ratio of SO to O
S_{ij}	collision cross section between species i and j
T	absolute temperature
t	time
u	gas speed
V_i	diffusion velocity of species i
v	vibrational level; flame speed
W_i	molecular weight of species i
$\overline{W}$	average molecular weight

w_i	rate of production or destruction of species i
X_i	mole fraction of species i
X_0	initial mole fraction of CS_2
x	correction for mole fraction approximation
$\underline{x}$	vector function for induction time calculation
Y_i	mass fraction for species i
y	non-dimensional function related to mass flux fraction
Z	collision frequency
z	distance
α	coefficient for first VKA ; influence coefficient
α_e	spectroscopic constant
β_e	spectroscopic constant
γ_e	spectroscopic constant
δ	non-dimensional ignition temperature
ϵ	non-dimensional function related to mass flux fraction of CO
ϵ_i	mass flux fraction of species i
ζ	distance related variable
η	non-dimensional temperature
θ	non-dimensional temperature
θ_a	non-dimensional activation energy
Λ	eigenvalue of VKA
λ	coefficient of thermal conduction
$\lambda_\pm$	eigenvalues for induction time calculation
μ_i	stoichiometric coefficients of the overall reaction

ν	frequency
$\nu'_{i,j}, \nu''_{i,j}$	stoichiometric coefficients
ρ	mass density
σ_i	molecular diameter of species i
τ_I	induction time
ω_e	spectroscopic constant
LE	Lewis number
ΔE	energy defect
ΔH^o_{300}	standard molar heat of formation at 300 K
Δp	pressure drop
$\Delta \nu_D$	Doppler linewidth
$\Delta \nu_L$	Lorentz linewidth

INTRODUCTION

This thesis is a study of the interactions of chemical kinetics, relaxation processes, and low-speed fluid mechanics for the deflagration of gaseous carbon disulfide and oxygen under conditions which are similar to those for which laser action has been demonstrated. Some of the macroscopic phenomena associated with CS_2/O_2 combustion are explained from a basis of the underlying microscopic behavior of molecular interactions. The problem of a chemically-reacting gas which is coupled to fluid mechanical constraints is solved by a few different techniques; numerical solutions are presented. Some characteristics of CS_2/O_2 combustion are experimentally explored to provide a link between the real world and the analytical models.

The CS_2/O_2 chemical lasers operate from the fundamental and first overtone vibrational transitions of carbon monoxide. The CO is chemically formed in high vibrational states (maximum population in the 13^{th} vibrational level) and with a large vibrational population inversion. Laser emission from the overtone bands has a wavelength of around 2.7 μm, while laser emission for the fundamental bands is centered at 5.3 μm.

Both carbon disulfide and molecular oxygen are very ordinary chemicals which are stable in the normal environment. The products of combustion of CS_2 in O_2, sulfur dioxide, carbon monoxide, and carbon dioxide, are all normal combustion products of petroleum based fuels and are normally found in the atmosphere of any industrial area. Thus, no special considerations need be taken for handling of the reactants or products of CS_2/O_2 lasers. This is a clear ad-

vantage over other chemical lasers and, in particular, the hydrogen halide chemical lasers.

The CS_2/O_2 flame is a low-speed flame which can be run in a premixed configuration. Analysis of the CS_2/O_2 flame laser is aided by the significant development of the theories for laminar flame propagation for both premixed and diffusion flames. The complexities of supersonic flow are not present for this type of laser, and many approximations for low-speed flow, which are not possible for other chemical lasers, become available. Because of the relatively simple flow field, the CS_2/O_2 flame laser can be subjected to analysis which realistically represents the actual behavior of the deflagration. Hence, it is possible to realistically relate experimental evidence to the fundamental chemical kinetics of combustion.

The CS_2/O_2 flame is a very stable flame. It can be run over a large pressure range including one thousandth of an atmosphere to over one atmosphere. Propagation is possible over an extremely wide range of fuel/oxidizer ratios with an extraordinarily low lower limit. CS_2 and O_2 can be burned with or without diluents. Since the CS_2/O_2 flame can be stabilized over a large range of experimental conditions, it is ideally suited for study, as it is possible to choose the experimental conditions.

The kinetics of CS_2/O_2 combustion are dominated by a branching chain mechanism. The limitations of combustion efficiency which are present in a straight chain mechanism, such as for the hydrogen halide chemical lasers, are not present in CS_2/O_2 chemical lasers. This means that vast amounts of diluents are not required to maintain

the chain reaction. The branching chain mechanism, however, means that the chemical kinetics of CS_2/O_2 chemical lasers cannot be approximated by a simple scheme.

Summary

The experimental evidence pertaining to CS_2/O_2 combustion is reviewed in the first chapter. Experimental reaction rates are presented and inspected. The experimental evidence and reactions rates are used to deduce a mechanism, based on four reactions, to represent the chemical kinetics of CS_2/O_2 combustion.

The branching chain mechanism deduced in the first chapter is used in the second chapter to explain some of the chemical dynamics of particular CS_2/O_2 lasers and of explosion phenomena. The initial conditions and initial chemical kinetics of the different types of CS_2/O_2 lasers are also discussed in Chapter 2.

The history of the CS_2/O_2 chemical lasers is presented in the third chapter. The relation of each type of laser to the chain mechanism is explicitly given. The evolution of the understanding of the chain mechanism is traced in Chapter 3.

The dynamics of chemical population and relaxation of the vibrational levels of carbon monoxide are discussed in the fourth chapter. Selective relaxation of the vibrational levels by reactants and additive gases is also discussed.

The fifth chapter develops the first of three analytical approximations which are applied to the particular case of the CS_2/O_2 flame laser. The von Kármán approximations for laminar flame propagation are applied to a lean CS_2/O_2 flame in this chapter. Rough functional

dependencies are obtained by this method.

The thermal theory approximation is developed in the sixth chapter. This approximation ignores diffusion, but does provide a reasonable model of the flame structure. A reasonable model of the flame structure is also obtained by the single-species diffusion approximation which is developed in the seventh chapter. The single-species diffusion approximation considers diffusion effects in an approximate manner by allowing for back diffusion of the most important chain carrier.

The experimental apparatuses which were developed to study the CS_2/O_2 flame are detailed in the eighth chapter. Of particular note is the development of a multi-slit injector whose design provides for significant flexibility in choice of mixing conditions. The observational characteristics of various injector and flame holder configurations is discussed in Chapter 8.

Experimental behavior of the eigenvalue of the laminar flame problem is presented and correlated with the theoretical results in the ninth chapter. The temperature profile of the flame is qualitatively discussed in this chapter.

Experimental CO emission spectra from the flame are quantitatively discussed in the tenth chapter. The vibrational populations are obtained, and with the aid of a few theoretical assumptions, the rate of population of the upper levels of CO is estimated.

Equilibrium and kinetics computer programs which were developed for general use are applied to CS_2/O_2 chemical laser conditions in the eleventh chapter. The results of these programs are cor-

related with the results obtained in other parts of this thesis.

1. CHEMICAL KINETICS OF CS_2/O_2 COMBUSTION

The combustion of carbon disulfide and oxygen provides a chemiluminescent reaction which produces an inverted vibrational population in carbon monoxide. The chemical kinetics of this combustion determine the characteristics of the chemical lasers, and thus chemical kinetics analyses provide a useful tool to find an understanding of the processes on which these lasers are based. The flame laser provides the most difficult case from a kinetic standpoint, as this case couples the problems of kinetics with the fluid mechanics of steady deflagration. Because only three elements are involved, and the largest reactant is a triatomic, reasonable models of the kinetics can be constructed. The intermediate species and elementary reactions which are essential to the flame laser provide a basic understanding from which models of the other types of CS/O chemical lasers can be built.

1.1 Macroscopic Behavior

The global equilibrium reaction for the burning of carbon disulfide in oxygen is expected[1] to be:

$$CS_2 + 3O_2 \rightarrow 2SO_2 + CO_2 + 1105 \text{ kJ mol}^{-1} \quad . \qquad (1.1)$$

However, for low pressure flames, the stoichiometric ratio of CS_2/O_2 has been experimentally determined to be 1:2.5,[2,3] and at this ratio the products were SO_2 and CO in a ratio of 2 to 1, respectively[3]. This corresponds to a global reaction which has carbon monoxide as one of its products:

$$CS_2 + \frac{5}{2} O_2 \rightarrow 2SO_2 + CO + 821 \text{ kJ mol}^{-1} \quad . \qquad (1.2)$$

Since carbon dioxide formation from carbon monoxide and atomic oxygen is a termolecular reaction at low pressures and predissociation is important[4], the carbon dioxide formation can be expected to be slow. The bimolecular reaction between carbon monoxide and molecular oxygen does not contribute much carbon dioxide due to a large activation energy of 210 kJ mol^{-1}.[5]

The visible and UV emission from the CS_2/O_2 flame is the result of a termolecular reaction between atomic oxygen and sulfur monoxide to form electronically-excited SO_2. Comparison of the CS_2/O_2 flame spectra with the SO_2 afterglow and the spectra of oxidation of other simple molecules which contain sulfur confirm that the emission is attributable to the SO_2 molecule.[6] Since the radiative lifetime for SO_2 fluorescence is 4×10^{-5} s[7], the SO_2 emission can define the reaction zone for low velocity flames. This visible emission could terminate before the overall reaction was complete, as evidenced in the SO_2 afterglow where O atom concentration decays faster than that of SO.[8] Electronically-excited SO_2 is also formed from the bimolecular reaction between sulfur monoxide and ozone,[8] but the low concentration of ozone in the flame minimizes the contribution from this reaction.

The CS_2/O_2 system exhibits first, second, and third ignition limits characteristic of a chain reaction mechanism.[9] It is also characterized by an induction period,[10] which is a characteristic of a branched chain reaction (ref. 11, pp. 619-623). This system was identified as an example of a quadratic branching chain reaction,[12] but with CS and SO_2 identified as the two active centers. Sulfur mon-

oxide has been proposed as the principal carrier of the chain,[13] as has the combination of atomic oxygen and sulfur monoxide.[14] A compilation of the chain mechanisms which have been proposed for CS_2/O_2 combustion is presented in Chapter 3. At the close of this chapter, a chain mechanism, which has atomic oxygen as the principal chain carrier, will be deduced.

1.2 Ancillary Chemistry

There are a few types of chemical reactions which have only a minor influence on the steady flame laser. First, heterogeneous reactions are not important since the kinetics of combustion all occur in the gas phase.

Ion chemistry has been excluded from present considerations due to the very small ion concentrations expected. The equilibrium concentration of ions can be calculated from the Saha equation.[15]

A simplified version for the first ionization stage in flames is given by[11]

$$\log\left\{ \frac{[A^+][e]m^3}{[A]\,\mathrm{mol}} \right\} = -3.15 \times 10^5 \left(\frac{K}{T}\right)\left(\frac{I}{aJ}\right) + \frac{5}{2}\log\left\{\frac{T}{K}\right\} - 24.28 \quad (1.3)$$

where

$[A]$ = concentration of species A ,

I = ionization potential from A to $A^+ + e$,

T = temperature

The first ionization potentials of the gaseous species present in the CS_2/O_2 flame are listed in Table 1-1. Since the lowest ionization potential is greater than 1.5 aJ (900 kJ mol^{-1}), there will be negligible ionization. The nonequilibrium ion concentration may be much larger

than that for equilibrium,[11] but it remains quite small.

Due to the large activation energies, the dissociation reactions should not have much importance in the kinetics of the flame. Estimates for the activation energies of the triatomics SO_2, CO_2, CS_2, and COS are 460, 320 to 460, 330 to 370, and 250 to 280 kJ mol^{-1} respectively,[16] and the diatomic O_2 has an activation energy of 496.8 kJ mol^{-1}.[17] Therefore, temperatures of many thousands of degrees Kelvin are required before thermal dissociation can be an influence on the kinetics; since sufficiently high flame temperatures occur only for near stoichiometric mixture with no diluent and then only towards the end of the reaction zone, thermal dissociation is not too important. The reaction rates for thermal dissociation of some of the species associated with the CS_2/O_2 flame are listed in the first part of Table 1-2, numbers 1 through 7.

Consideration should not be given to carbon atom chemistry because there is a much greater probability that the CS radical will react in a collision that it will break its bond. The CS radical is stable, with a bond dissociation energy of 762 ±21 kJ mol^{-1},[26] but is quite reactive. Heterogeneous reaction of the CS radical, not heterogeneous carbon atom polymerization, is the most probable cause of carbon deposits found in some systems.[24, 27, 28] The wall reaction of the CS radicals produces CS_2 molecules which return to the gas phase leaving a carbon-rich deposit.[29] When carbon atoms exist in the gas phase, they react with molecular oxygen in about five collisions[24] to form carbon monoxide and atomic oxygen; carbon dioxide is not found as a product of carbon atoms and molecular oxygen (see

refs. 23, 24, 30). Carbon formation was searched for but not found in the CS_2/O_2 flame.[31] The reaction rates of three carbon atom reactions which might occur in CS_2/O_2 combustion are listed in Table 1-2, reactions 7, 8, and 9.

Polymerization of sulfur will be significant when there is a discharge in CS_2 and when the reaction occurs in a CS_2-rich mixture (refs. 2, 9, 10, 13, 32, 33). However, when molecular oxygen is present in excess, diatomic sulfur is not detected in CS_2 oxidation.[2, 34-39] The reaction of carbon disulfide with atomic sulfur has a low probability; since sulfur polymerization is more probable[40] the reaction between CS_2 and S can be ignored. Thus, with molecular oxygen present, the only important reaction involving atomic sulfur is with molecular oxygen.

The SOO isomer of sulfur dioxide has been claimed to be the primary reaction product, with later rearrangement to form the common OSO isomer.[13] However, both its existence and absence in the flame have been claimed.[13, 38, 39, 41] The results attributed to the SOO isomer have been explained by consideration of the higher electronic transitions of SO[42] and the presence of vibrationally-excited SO_2.[43] Since the evidence of the existence of the SOO isomer is weak and its influence on the laser kinetics would be small, it will be ignored.

Two SO molecules may be converted to the dimer $(SO)_2$, which was thought to be observed in non-exploding mixtures of CS_2 and O_2 (ref. 13). This dimer is formed by a bimolecular reaction and is the first step in SO decomposition into sulfur suboxide, S_2O, and sulfur

dioxide.[44] Since the absorption and emission characteristics which lead to the identification of this dimer probably are attributable to other sulfur oxides,[43] the kinetics of S_2O_2 shall be ignored.

1.3 Primary Chemistry

Carbon disulfide can react with atomic oxygen in three ways. The primary products are CS and SO for a reaction in which O attacks either end of the CS_2 molecule and retreats having captured a sulfur atom. In this reaction channel the remaining diatomic CS retains some of the reaction energy as vibrational excitation.[45] The second and most exothermic possibility has CO and S_2 as the products, but this reaction has a low probability due to the large energy required to break two bonds. The third reaction channel involves the exchange of the incoming atomic oxygen for one of the sulfur atoms; because of the positional rearrangement, this will be less probable than the first reaction. Rates for these three reactions are listed in Table 1-3, numbers 1, 2, and 3, respectively.

The fast chemiluminescent reaction between carbon monosulfide and atomic oxygen provides vibrationally-inverted CO for the chemical laser. The reaction of CS with molecular oxygen was once considered important to the CS_2/O_2 system,[14, 34, 72, 73] but even with most of the gas being O_2, this reaction has been shown not to contribute much to the decay of CS. This reaction requires the breaking of two strong bonds with rearrangement to form two new bonds, which indicates a high activation energy and small pre-exponential factor. The large difference between the reaction rates of CS with O and O_2 is found from the reaction rates which are listed in Table 1-3, num-

bers 4 and 5. Electronically-excited CS does react with molecular oxygen while the ground state does not.[39]

The atomic sulfur produced in the chemiluminescent reaction will most likely combine with molecular oxygen in the chain branching reaction discussed previously. This reaction is fast, with a relatively low activation energy as shown in the rates given in Table 1-3, number 6. The termolecular chain terminating polymerization reaction between two sulfur atoms is not too important in low pressure CS_2/O_2 flames; the rate of this reaction is given in Table 1-3, number 7.

Sulfur monoxide is a critical link in the chain reaction. It can produce atomic oxygen in a reaction with O_2 and reacts with atomic oxygen in a double chain termination reaction, which can be either bimolecular or termolecular, producing electronically, excited SO_2 whose emission is characteristic of the flame. The rates of these reactions are given in Table 1-3, numbers 8 - 10. The electronic state of SO_2 has not been noted for these reactions, as that level of sophistication is not required here. Sulfur dioxide is also a product of the reaction between two SO molecules. This reaction, whose rate is given in Table 1-3, number 11, also produces an atomic sulfur to continue one of the two chains.

The reaction of carbon monoxide with atomic oxygen to yield carbon dioxide has been studied extensively, but there is still much controversy over the order and activation energy of the reaction (refs. 4, 5, 43, 67-69, 74, 75). A few of the rates attributed to the termolecular reaction are given in Table 1-3, number 12. The discrepancy in the measured reaction rates is possibly due to the tendency for the

electronically-excited CO_2 to predissociate before it is stabilized by emission or non-radiative processes. Carbon monoxide can oxidize to CO_2 in a reaction with molecular oxygen which has an atomic oxygen as a product. The rates of this reaction, which can aid the chain reaction with its production of a bonus active center, and its reverse are given in Table 1-3, numbers 13 and 14.

The chain terminating recombination reaction of O atoms is, fortunately and necessarily, slower than the reactions in the chain. The rate of this termolecular reaction is well known and is given in Table 1-3, number 15. Atomic oxygen can react with molecular oxygen to form ozone; the termolecular reaction rate for this reaction is given in Table 1-3, number 16. There does not seem to be any evidence showing that ozone has any significance in CS_2/O_2 combustion. Atomic oxygen reacts with diatomic sulfur in a chain branching reaction to produce SO and atomic sulfur; the rate of this reaction is given in Table 1-3, number 17.

The reaction between carbonyl sulfide, COS, and atomic oxygen has SO and CO as its predominant products.[64] In a manner similar to its reaction with CS_2, the oxygen atom attacks the COS molecule at the sulfur atom end and retreats as the diatomic SO. The absence of CS among the products[64, 66] indicates that oxygen atom attack on the oxygen end is not very successful, the activation energy for this reaction being higher due to the carbon-oxygen bond at 628 kJ mol^{-1} [26] being much stronger than the carbon-sulfur bond which is 310.5 kJ mol^{-1}.[26] The stronger oxygen-carbon bond also explains the higher activation energy for the COS reaction, which is indicated in

the reaction rates for this reaction, given in Table 1-4, number 1, than the CS_2 reaction with atomic oxygen, given in Table 1-4, number 1. The CO and SO should be formed vibrationally excited from the reaction of COS and atomic oxygen. Since the total energy released in this reaction is about 100 kJ mol^{-1} smaller than that of the CS and atomic oxygen reaction (Table 1-3, number 4) and both diatomics should share the vibrational energy, the CO should be formed in the lower vibrational states. This vibrationally-excited CO would then tend to decrease the populations inversion produced by the O plus CS reaction alone.

Atomic sulfur can react with carbonyl sulfide in a manner analogous to that of atomic oxygen. The predominant products are carbon monosulfide and diatomic sulfur for the same reasons. This reaction, whose rate is given in Table 1-4, number 2, is less exothermic than that with atomic oxygen, and hence any carbon monoxide formed from this reaction should be in even lower vibrational levels.

Carbon disulfide reacts slowly with sulfur monoxide, as expected from the rearrangement that is required to form carbonyl sulfide and diatomic sulfur. The rate of this reaction and the analogous reaction with COS as a reactant and CO_2 as a product are given in Table 1-4, numbers 3 and 4, respectively. Sulfur trioxide is formed in a termolecular reaction between atomic oxygen and sulfur dioxide, and it can revert back to SO_2 in another exothermic chain terminating reaction which has molecular oxygen as its product; the rates for these reactions are given in Table 1-4, numbers 5 and 6.

Because of a high activation energy, ozone cannot be expected

to be generated in a reaction between two O_2 molecules (Table 1-4, number 7) but the chain terminating inverse reaction (Table 1-4, number 8) might occur if ozone is produced by the previously discussed mechanism. Ozone also can react in a chain terminating and highly exothermic reaction with sulfur monoxide (Table 1-4, number 9) but does not react significantly with SO_2 [82] or CS_2 [83].

1.4 Deduction of Chain Mechanism

Typical conditions found in free-burning CS_2/O_2 chemical lasers will be chosen for the deduction of the chain mechanism. The mechanisms important to other types of CS_2/O_2 lasers can be easily obtained as they are subsets of this chain. Non-diluted, oxygen-rich mixtures of CS_2/O_2 are of primary interest in the free-burning laser. In order to explore the kinetics of this system, a homogeneous mixture of reacting gases will be considered; the problems of fluid mechanics, heat transfer, and diffusion shall be ignored.

With only three atomic species there are relatively few simple molecules. Since the reactants of the overall reaction are a diatomic and a triatomic, as are the products, the elementary reaction steps in the homogeneous mixture should involve only the lower order molecules. The previously mentioned reactions contain 17 species which include all three monatomics (C, O, S) and all six diatomics (C_2, CO, CS, O_2, SO, S_2) along with six of the ten triatomics (CO_2, COS, CS_2, O_3, SO_2, S_2O) and two higher molecules (SO_3, S_2O_2). The aforementioned arguments concerning reactions of secondary importance result in small production and importance of eight species (C, C_2, S_2, CO_2, O_3, S_2O, SO_3, and S_2O_2). Thus, there are nine species of pri-

mary interest (O, S, CO, CS, O_2, SO, COS, CS_2, SO_2). Since two species are reactants (O_2, CS_2) and two are products (CO, SO_2), there are five species which can be termed intermediates.

There are 45 possible bimolecular and implied termolecular reactant pairs between these nine species, as illustrated in Table 1-5. These are the only ones to be considered, since unimolecular (implied bimolecular) decompositions have been shown to be unimportant and termolecular and implied tetramolecular reactions do not have a high probability of occurrence. Also, only exchange, spearing, and recombination reactions have been considered. The 45 bimolecular reactant pairs were first screened by the requirement that all of the product species are among the other seven species; this left 23 reactant pairs, each with at least one eligible reaction. Highly endothermic reactions were omitted while noting that their inverses were still candidates. A third screening eliminated those reactions which have a large activation energy and corresponding low reaction rate. The remaining 11 reactant pairs yield the 13 candidate reactions listed in Table 1-6.

The chemiluminescent reaction (Table 1-6, number 3) between CS and O must be the cornerstone of any reaction scheme, and within these reactions it is the only method of CO production. Following back the CS yields the reaction between CS_2 and O (Table 1-6, number 1) as the single source of CS. Thus, the path of the carbon atom from reactant to product is established:

$$CS_2 + O \rightarrow CS + SO \quad \text{followed by} \quad CS + O \rightarrow CO + S \ . \qquad (1.4)$$

This implies that COS is a by-product, being formed in the lower probability channel of the CS_2 and O reaction (Table 1-6, number 2), the chain terminating step between CS and SO_2 (Table 1-5, number 4), and the recombination reaction between CO and S (Table 1-6, number 9).

Those reactions which provide paths which lead to the formation of reactants may slow the rate of combustion but cannot be considered as part of the chain propagation mechanism. The termolecular recombination reaction to CS_2 (Table 1-6, number 8) is such a step backwards.

The atomic oxygen recombination reaction (Table 1-6, number 13), although possibly important for determination of atomic oxygen concentration and thus the rate of the reaction, also cannot help to propagate the chain mechanism as it can ultimately be only a sink of atomic oxygen.

The efficiency of the bimolecular reaction between atomic sulfur and molecular oxygen (Table 1-6, number 6) along with the large concentration of O_2 make this reaction the most probable path for the sulfur atoms as compared to the termolecular reactions given in Table 1-6, numbers 11 and 12. The termolecular double chain terminating reaction between SO and O (Table 1-6, number 10) or its slow bimolecular counterpart (Table 1-3, number 9) are slower than the fast chain kinetics. These reactions cannot dominate since the consequences would be the inability to sustain a chain reaction. The sulfur dioxide which appears as a product of the fast chain mechanism must come from either the reaction between two SO molecules (Table

1-6, number 5) or SO and O_2 (Table 1-5, number 7), or both. These two reactions have the same molecular orbital arrangements and similar activation energies,[26] but the latter should have a higher steric factor. It should be noted that the reaction between two SO molecules followed by the fast reaction between S and O_2 nets the same as the reaction between SO and O_2:

$$\begin{aligned} SO + SO &\rightarrow SO_2 + S \\ S + O_2 &\rightarrow SO + O \\ \text{net:} \quad SO + O_2 &\rightarrow SO_2 + O \end{aligned} \qquad (1.5)$$

The abundance of molecular oxygen as compared to the scarcity of the intermediate SO provides the reason for choice of the chain propagation reaction between SO and O_2 as the more important one.

The result of this process is the construction of a branching chain mechanism which models the kinetics of the flame laser. It is composed of the two elementary reactions which convert CS_2 to CO by removal of the one sulfur atom per reaction, and two reactions which provide the atomic oxygen required in the first two reactions of the chain. This mechanism involves eight species and is given by:

$$\begin{aligned} CS_2 + O &\rightarrow CS + SO \\ CS + O &\rightarrow CO + S \\ S + O_2 &\rightarrow SO + O \\ SO + O_2 &\rightarrow SO_2 + O \end{aligned} \qquad (1.6)$$

The details of this branching chain mechanism are illustrated in Figure 1-1. The principal chain carrier, therefore called the active center, is atomic oxygen with SO as a vital, but less important,

chain carrier. Both of the intermediate species CS and S are chain carriers with single functions. The critical branching reaction, between atomic sulfur and molecular oxygen, produces both an active center and a chain carrier. The reaction between CS_2 and atomic oxygen is also a chain branching reaction. If the last reaction of this scheme occurs twice for once each of the preceding three, then the net reaction yields an extra atomic oxygen (the product of the branching chain) and a stoichiometric ratio of 1:3,

$$CS_2 + 3O_2 \rightarrow 2SO_2 + CO + O \quad . \qquad (1.7)$$

This net reaction can be made to fit exactly the overall reaction for CS_2/O_2 combustion, given in equation (1.2), with the addition of atomic oxygen recombination and/or the double chain termination reaction between SO and atomic oxygen.

TABLE 1-1.

Approximate First Ionization Potentials for Gas Phase Species*

Species	IP/aJ
C	1.81
C_2	2.1
CO	2.24
CO_2	2.21
CS	1.73
CS_2	1.62
O	2.17
O_2	1.94
O_3	2.1
COS	1.79
S	1.67
S_2	1.53
S_2O	1.65
SO	2.60
SO_2	1.99

*data from ref. 16

TABLE 1-2. Rate Constants for Some Reactions of Limited Interest in CS_2/O_2 Combustion

Reaction	$-\Delta H^o_{300}$	K	T	M	Ref.
dissociation reactions					
1. $CS_2+M \rightarrow CS+S+M$	-392.1	$3.6\times10^{9}\exp(-\frac{40400}{T})$	1800-3700		19
2. $SO_2+M \rightarrow SO+O+M$	-553.1	$2.5\times10^{8}\exp(-\frac{55000}{T})$	4500-7500	Ar	17, 20
3. $COS+M \rightarrow CO+S+M$	-307.0	$1.5\times10^{8}\exp(-\frac{30500}{T})$	1600-3100		17
4. $O_2+M \rightarrow O+O+M$	-498.5	$2.77\times10^{13}T^{-1}\exp(-\frac{59900}{T})$	1000-8000		18
5. $O_3+M \rightarrow O_2+O+M$	-106.6	$4.3\times10^{8}\exp(-\frac{11400}{T})$	200-1000		18
6. $SO_3+M \rightarrow SO_2+O+M$	-348.2	8×10^{2}	1740	N_2	21
carbon atom reactions					
7. $CO+M \rightarrow C+O+M$	-1074.7	$8.0\times10^{32}T^{-5.5}\exp\{-\frac{1.29\times10^{5}}{T}\}$	5500-12000	CO, C, O	22
8. $C+O_2 \rightarrow CO+O$	576.5	2.0×10^{7}	300		23
9. $C + C \rightarrow C_2$	592.4	1.3×10^{7}	300		24

ΔH^o_{300} in kJ mol^{-1} (data from ref. 25)

T in K

K in $(m^3\ mol^{-1})^{n-1}\ s^{-1}$, where n is the order of the reaction

TABLE 1-3. Rate Constants for the CS_2/O_2 System

Reaction	$-\Delta H^o_{300}$	K	T	M	Ref.
1. $CS_2+O \rightarrow CS+SO$	129.3	$5\times10^7 \exp(-\frac{960}{T})$	300-920		46
		$2.2\times10^7 \exp(-\frac{750}{T})$	341-415		14
		$1.2\times10^7 \exp(-\frac{530}{T})$	227-538		47
		$6.3\times10^6 \exp(-\frac{300}{T})$	305-410		48-50
		2.1×10^6	300		51
		2.2×10^6	302		52
2. $CS_2+O \rightarrow CO+S_2$	347.8	$< 2\times10^4$	300		35
3. $CS_2+O \rightarrow COS+S$	225.7	$<2\times10^4$	300		35
		$< 10^2$	300		30
		2×10^5	302		52
		$\sim 10^6$	1100		46
4. $CS+O \rightarrow CO+S$	310.9	2.1×10^7	300		51
		8.4×10^6	300		35
		$\sim 10^8$	1100		46
5. $CS+O_2 \rightarrow CO+SO$	333.9	2	300		35
		$2.3\times10^8 \exp(-\frac{24200}{T})$	440-530		34

ΔH^o_{300} in kJ mol^{-1} (data from ref. 25)

T in K

K in $(m^3\ mol^{-1})^{n-1}\ s^{-1}$, where n is the order of the reaction

TABLE 1-3 (continued). Rate Constants for the CS_2/O_2 System

Reaction	$-\Delta H^o_{300}$	K	T	M	Ref.
6. $S+O_2 \rightarrow SO+O$	22.9	$1.3\times10^6 \exp(-\frac{0}{T})$	252-423		53
		$1\times10^7 \exp(-\frac{2800}{T})$	675-1090		46
		$2.35\times10^7 \exp(-\frac{1200}{T})$			54
		1.0×10^6	295		37
		1.7×10^6	298		55
		1.2×10^6	298		1
7. $S+S+M \rightarrow S_2+M$	429.1	1.0×10^{13}	298		48
		7×10^2			56
		10^6			57
		5×10^5			58
8. $SO+O_2 \rightarrow SO_2+O$	54.5	$3.5\times10^5 \exp(-\frac{3300}{T})$	580-1145		46
		$9.7\times10^7 \exp(-\frac{14600}{T})$	1600-2100		34
		$2\times10^7 \exp(-\frac{5000}{T})$	440-530		33
		$5.2\times10^8 \exp(-\frac{9710}{T})$			59
9. $SO+O \rightarrow SO_2$	553.1	3.4×10^3			60
		$<2\times10^2$	298		61
		4×10^2	300		62
10. $SO+O+M \rightarrow SO_2+M$	553.1	3.2×10^5	300	Ar	63
		8.0×10^4			60

TABLE 1-3 (continued). Rate Constants for the CS_2/O_2 System

	Reaction	$-\Delta H^o_{300}$	K	T	M	Ref.
11.	$SO+SO \rightarrow SO_2+S$	31.6	$< 4 \times 10^3$	300		63
			2.6×10^6	300		64
			$<5 \times 10^3$	223-303		65
			$<7 \times 10^4$	300		41
			$<10^4$	300		66
			$<10^4$	500		46
12.	$CO+O+M \rightarrow CO_2+M$	532.3	$6.8\times10^{-1}\exp(+\frac{1500}{T})$	410-500		67
			$4\times10^5\exp(-\frac{1800}{T})$			4
			$2.8\exp(+\frac{12000}{T})$	1500-3000		68
			$2\times10^1 - 1\times10^2$	2800-3600		69
13.	$CO+O_2 \rightarrow CO_2+O$	33.8	$3.5\times10^6\exp(-\frac{26000}{T})$	1500-3000		5
			$2.5\times10^6\exp(-\frac{24000}{T})$			70
14.	$CO_2+O \rightarrow CO+O_2$	-33.8	$1.7\times10^7\exp(-\frac{27000}{T})$			70
15.	$O+O+M \rightarrow O_2+M$	498.5	$1.37\times10^6 T^{-1}\exp(-\frac{171}{T})$	1000-8000		18
			$<2.5 \times 10^2$	350		71
16.	$O+O_2+M \rightarrow O_3+M$	106.6	2×10^2	300	O_2	5
17.	$O+S_2 \rightarrow SO+S$	92.4	4×10^6	1100		46

TABLE 1-4. Rate Constants for Some Other Reactions

Reaction	$-\Delta H^{o}_{300}$	K	T	M	Ref.
1. $COS+O \rightarrow CO+SO$	214.5	$6.5\times10^{7}\exp(-\frac{2800}{T})$	300-1150		46
		$1.9\times10^{7}\exp(-\frac{2280}{T})$	273-808		47
		$9.6\times10^{6}\exp(-\frac{2300}{T})$	300-523		76
		$1.2\times10^{8}\exp(-\frac{2900}{T})$	290-465		66
		5.5×10^{3}	300		64
2. $COS+S \rightarrow CO+S_2$	122.1	2×10^{4}			57
3. $CS_2+SO \rightarrow COS+S_2$	133.3	2×10^{1}	341		14, 46
4. $COS+SO \rightarrow CO_2+S_2$	133.3	10^{5}	300		63
5. $SO_2+O+M \rightarrow SO_3+M$	348.2	3×10^{4}	295	O_2	77, 78
		2.7×10^{3}	299	O_2	79
		3×10^{3}	300	O_2	63
		1.1×10^{3}	300	Ar	80
		2×10^{3}	2150		21
		4.9×10^{3}			81
6. $SO_3+O \rightarrow SO_2+O_2$	150.3	$2.8\times10^{8}\exp(-\frac{6000}{T})$			17

ΔH^{o}_{300} in kJ mol^{-1} (data from ref. 27)

T in K

K in $(m^3\ mol^{-1})^{n-1}\ s^{-1}$, where n is the order of the reaction

TABLE 1-4 (continued). Rate Constants for Some Other Reactions

Reaction	$-\Delta H^{o}_{300}$	K	T	M	Ref.
7. $O_2+O_2 \rightarrow O+O_3$	-392.0	$1.28\times10^{7}\exp(-\frac{50630}{T})$	200-1000		18
8. $O+O_3 \rightarrow O_2+O_2$	+392.0	$1.20\times10^{7}\exp(-\frac{2410}{T})$	200-1000		18
9. $SO+O_3 \rightarrow SO_2+O_2$	446.5	$1.5\times10^{6}\exp(-\frac{1100}{T})$	223-303		8, 65

TABLE 1-5. Elimination of Bimolecular Pairs from Importance in CS_2/O_2 Kinetics

	O	S	CO	CS	O_2	SO	COS	CS_2	SO_2
SO_2	P	E	E	*	P	P	P	P	P
CS_2	*, *	P	E	P	A	P	P	P	
COS	E, A	E, A	P	A	A	E	P		
SO	$*_t$, E	P	E	E	*	*			
O_2	P	*, $*_t$	P	A	P				
CS	*	$*_t$	P	P					
CO	P	$*_t$, E	P						
S	$*_t$	P							
O	$*_t$								

Key:

E: endothermic reaction, inverse is considered

A: large activation energy, reaction doesn't go

P: products necessarily include species which are not considered

*: candidate reaction

subscript t: implied termolecular reaction

TABLE 1-6. Candidate Reactions for the Chain Mechanism

1. $CS_2 + O \rightarrow CS + SO$
2. $CS_2 + O \rightarrow COS + S$
3. $CS + O \rightarrow CO + S$
4. $CS + SO_2 \rightarrow COS + SO$
5. $SO + SO \rightarrow SO_2 + S$
6. $S + O_2 \rightarrow SO + O$
7. $SO + O_2 \rightarrow SO_2 + O$
8. $CS + S + M \rightarrow CS_2 + M$
9. $CO + S + M \rightarrow COS + M$
10. $SO + O + M \rightarrow SO_2 + M$
11. $S + O_2 + M \rightarrow SO_2 + M$
12. $S + O + M \rightarrow SO + M$
13. $O + O + M \rightarrow O_2 + M$

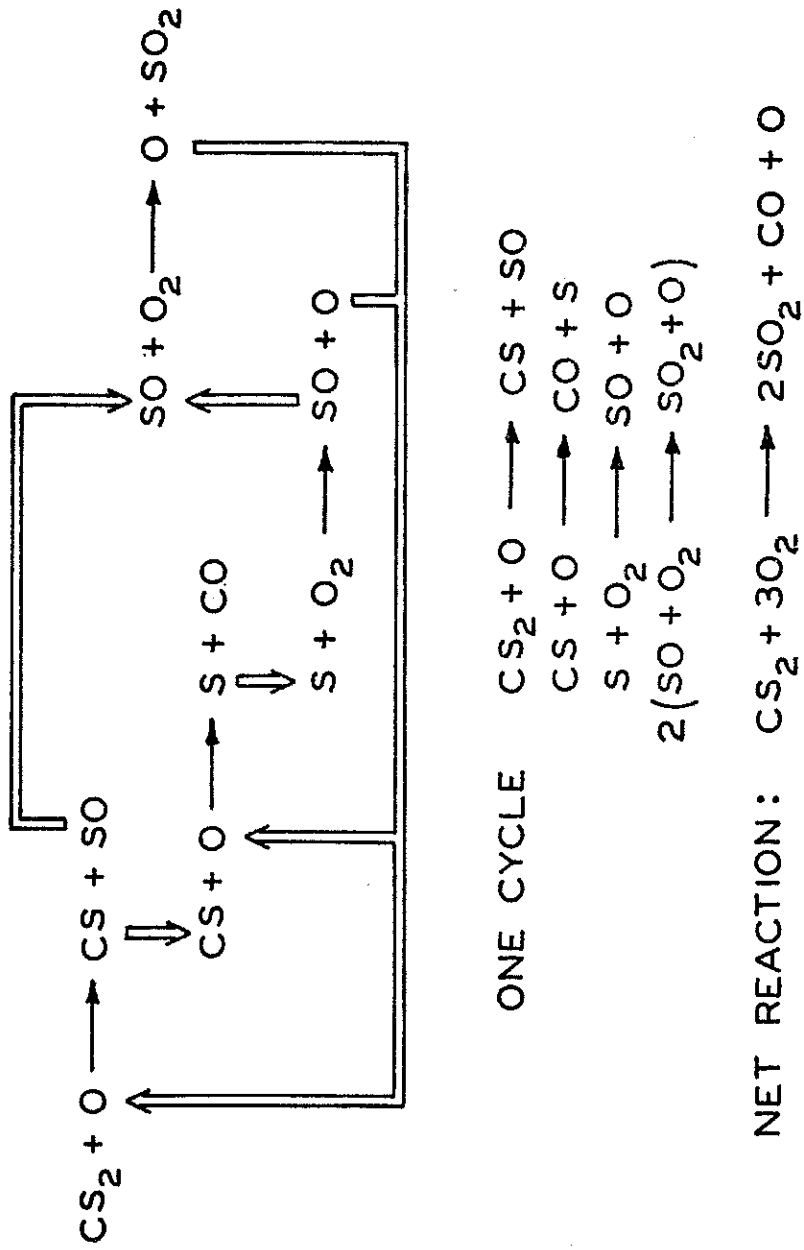

Figure 1-1. Chain Reaction Mechanism for the CS_2/O_2 Chemical Laser.

2. INITIAL CONDITIONS, INITIAL REACTIONS, AND INDUCTION PERIOD

The branching chain mechanism of the CS_2/O_2 flame can be used to explain the chemical dynamics of various types of lasers and of explosion phenomena. The significant influence of the chain mechanism for the widely-varying initial conditions is due to the high reaction rates and the behavior of branching chains. The consequence of a chain reaction which branches is that the chain carriers grow exponentially, tending to wipe out any relations to the details of the initial conditions.[84] The initial conditions for the various types of lasers, flames, and explosions shall be estimated and the chemistry associated with setting up the chain from these initial conditions will be developed.

2.1 Induction Period

Oscillatory behavior and existence of an induction time are two phenomena which are attributed to branching chain reactions. The CS_2/O_2 system exhibits induction time behavior. Any proposed reaction mechanism which is used to model CS_2/O_2 combustion should be able to predict this induction time and, roughly, its functional dependencies. The four-reaction chain mechanism which was deduced in Chapter 1 will be tested in this manner.

The initial conditions which are chosen for induction time calculations are those which provide a homogeneous mixture of CS_2 and O_2 with an O_2/CS_2 ratio of 10, a temperature of 300 K, and a pressure of 1 kPa. This mixture will include some small fraction of each of the intermediates; the initial amount of each of the intermedi-

ates is estimated by the following arguments.

A homogeneous mixture of CS_2 and O_2 can be expected to have a significant amount of the intermediate CS. Pure carbon disulfide does not decompose significantly at normal temperature and low pressures;[13] the equilibrium mole fraction of CS at 1 kPa is non-negligible only above 1000 K.[44] However, when oxygen is present, CS has been detected in mixtures with temperatures as low as 325 K (ref. 13). At 600 K and a pressure of 0.4 kPa , the ratio of CS concentration to the equilibrium concentration without O_2 has been measured at 10^9 (ref. 11, p. 665), where the ratio of CS to CS_2 was measured as 3×10^{-3}. The large nonequilibrium concentrations of CS must be explained by a dynamic, not equilibrium, process; it can be explained by the fast reaction between atomic sulfur and molecular oxygen (Table 2-1, number 3), preceded by carbon disulfide decomposition. The atomic sulfur required for the termolecular recombination reaction is thus absent. The atomic oxygen then begins the chain reaction, but combustion does not occur due to heterogeneous deactivation of the chain carriers. The maximum concentration available can be found by excluding heterogeneous reactions, assuming the steady-state approximation on CS, and assuming that the most important reactions of CS and CS_2 are those which are part of the chain mechanism (Table 2-1, numbers 1 and 2). Then the maximum CS/CS_2 ratio is

$$\frac{[CS]}{[CS_2]} \simeq \frac{K_1}{K_2} \quad , \tag{2.1}$$

where $[A]$ is the concentration of species A and K_i is the rate constant for reaction i from Table 2-1. From the approximation rates

given in Table 2-1, this maximum ratio is about 0.26 at 300 K. Since this fraction is very high, the observed concentrations of CS must be dependent on heterogeneous reactions. An important wall reaction converts CS to CS_2 and a carbon-rich deposit,[2] with a typical stoichiometry of

$$CS \xrightarrow{\text{wall}} 0.35\ CS_2 + 0.95\ (C_{0.68}S_{0.32}) \quad . \qquad (2.2)$$

A unimolecular rate, K_U, of around 5×10^{-2} s^{-1} at 300 K can be deduced from the decay data;[29, 85] the rate for a clean wall is at least an order of magnitude smaller. Employing this reaction with the homogeneous reaction between CS_2 and atomic oxygen and making the steady-state approximation, the concentration of CS is found to be dependent on the atomic oxygen concentration,

$$[CS] = \frac{K_1}{K_U} [CS_2][O] \quad . \qquad (2.3)$$

Under the conditions chosen for this investigation, i.e., a temperature of 300 K, a pressure of 10^3 Pa, and an O_2/CS_2 ratio of 10, the ratio of [CS] to [O] is approximately 2×10^6.

The sulfur monoxide molecule is relatively long-lived, as its most significant homogeneous method of elimination is with molecular oxygen, a reaction which is a few orders of magnitude slower than the reaction in which SO is produced (Table 2-1, number 1). Considering those two reactions, making the steady-state approximation on SO, and assuming a temperature of 300 K and an O_2/CS_2 ratio of 10, the ratio of [SO] to [O] of 3×10^5 is obtained. Consideration of heterogeneous deactivation should lower this ratio to a significantly lower value. Thus, the initial concentrations of the intermediates

will be small, except for that of CS.

2.2 Early Stages of the Induction Period

During the first part of the induction period, kinetics are dominated by the two reactions which form a small non-branching chain:

$$\begin{aligned} CS_2 + O &\rightarrow CS + SO \qquad K_1 \\ SO + O_2 &\rightarrow SO_2 + O \qquad K_4 \\ \text{net: } CS_2 + O_2 &\rightarrow CS + SO_2 \end{aligned} \tag{2.4}$$

Assuming that this chain is developed, then the concentrations of O and SO should be approximately constant.

Assume the steady-state approximations for the concentrations of SO and O in the reaction scheme of equation (2.4) to obtain

$$\frac{[SO]}{[O]} \simeq \frac{K_1[CS_2]}{K_4[O_2]} \; . \tag{2.5}$$

Since the CS_2 and O_2 concentrations will not change significantly during this initial stage, the ratio $[O]/[SO]$ can be expected to depend only on the initial fuel/oxidizer ratio.

The competitor for atomic oxygen is the intermediate CS, which is available in small, but significant, concentrations. This reaction produces atomic sulfur which in turn reacts with O_2 in the chain branching step. The four-reaction chain mechanism (Table 2-1, numbers 1 - 4) is operative with the expectation of an exponential growth of chain carriers. The rate of change of concentration of the four species S, O, CS, and SO are given, within this mechanism, as

$$\frac{d[CS]}{dt} = K_1[CS_2][O] - K_2[CS][O] ,$$

$$\frac{d[S]}{dt} = K_2[CS][O] - K_3[S][O_2] ,$$

$$\frac{d[O]}{dt} = K_4[SO][O_2] - K_1[CS_2][O] + K_3[S][O_2] - K_2[CS][O] \qquad (2.6)$$

$$\frac{d[SO]}{dt} = K_1[CS_2][O] + K_3[S][O_2] - K_4[O][SO]$$

2.3 Induction Time Estimate

In order to estimate the induction time, apply the steady-state approximation to the concentrations of S, CS, and O to obtain:

$$K_2[CS][O] \simeq K_3[S][O_2]$$

$$K_4[SO][O_2] \simeq K_1[CS_2][O] \qquad (2.7)$$

$$K_1[CS_2] \simeq K_4[CS]$$

Since the concentrations of CS_2 and O_2 as well as temperature are constant within this initial period, these approximations imply that the concentration of CS is constant, the ratio of SO to O concentration is constant, and the ratio of S to O concentration is also constant. The latter ratio is about 2×10^3 with the chosen initial conditions. Substitution of these approximations into the rate of change of [SO] equation from equations (2.4) yields the crude result:

$$\frac{d[SO]}{dt} \simeq K_4[O_2][SO] \quad . \qquad (2.8)$$

This can be rearranged and integrated over the induction period, where O_2 concentration is constant, to obtain:

$$[SO] \simeq [SO]_0 \exp(K_4[O_2]t) \quad , \qquad (2.9)$$

where the subscript 0 indicates the concentration of [SO] before the chain mechanism took over. The exponential growth of the intermediates and the constant ratio was experimentally verified during the induction period,[34] but the shock-wave ignition technique precludes any direct numerical comparisons. The induction time, τ_I, can be expected to be proportional to the growth constant, $K_4[O_2]$. Since the reaction rate is expected to have an Arrhenius form, the induction time should have the form

$$\tau_I \propto \frac{1}{[O_2]A_4\exp(-E_4/RT)} , \qquad (2.10)$$

where A_4 is the pre-exponential constant and E_4 is the activation energy of the reaction of Table 2-1, number 4. Induction time studies over the temperature range of 355-395 K with an O_2/CS_2 ration of 3 and a typical pressure of 4.3×10^3 Pa yield such an exponential relation.[9] Since the concentration of O_2 is proportional to pressure, at constant temperature the induction time should be inversely proportional to the pressure; such hyperbolic behavior was found for a pressure range of 0.4 kPa to 3 kPa, temperature of 398 K to 433 K, and O_2/CS_2 mixture ratios of 3 to 6.[10] The inverse relation between induction time and molecular oxygen concentration was qualitatively, but not quantitatively, observed.[10] The induction times of these studies[9, 10] ranged from 2 to 25 s, with the corresponding calculated time for growth, $(K_4[O_2])^{-1}$, being the order of tens of milliseconds. Since these induction times were taken as the time between introduction of the gases into a heated vessel and the detection of a flash of light, the induction times should be ex-

pected to be many times the calculated time for growth.

The same exponential growth can be obtained from the four-reaction scheme without the requirement of the steady-state approximation on atomic oxygen concentration. Assume the steady-state approximations on the concentrations of CS and S, then apply the results to the rates of production of O and SO to obtain:

$$\frac{d[O]}{dt} = K_4[SO][O_2] - K_1[CS_2][O]$$
$$\frac{d[SO]}{dt} = 2K_1[CS_2][O] - K_4[SO][O_2] \qquad (2.11)$$

These equations can be considered coupled linear equations with constant coefficients for the induction period. Let

$$\tau = t/K_4[O_2]$$
$$b = K_1[CS_2]/K_4[O_2]$$
$$x_1 = [O]/[O]_0 \qquad (2.12)$$
$$x_2 = [SO]/[O]_0$$

Then equations (2.8) become

$$\frac{dx_1}{d\tau} = x_2 - bx_1 \quad , \qquad \frac{dx_2}{d\tau} = 2bx_1 - x_2$$

or

$$\frac{d\underline{x}}{d\tau} = \begin{bmatrix} -b & 1 \\ 2b & 1 \end{bmatrix} \underline{x} \quad . \qquad (2.13)$$

Choose as initial conditions

$$x_1(0) = 1 \quad , \quad x_2(0) = r \quad , \qquad (2.14)$$

where r is the initial ratio of SO to atomic oxygen. The solution to equations (2.13) and (2.14) is given by

$$\underline{x}(\tau) = \left(\frac{b+r-\lambda_-}{\lambda_+ - \lambda_-}\right)\begin{bmatrix} 1 \\ \lambda_+ + b \end{bmatrix}\exp(\lambda_+\tau) + \left(\frac{b-r+\lambda_+}{\lambda_+ - \lambda_-}\right)\begin{bmatrix} 1 \\ \lambda_- + b \end{bmatrix}\exp(\lambda_-\tau) ,$$

$$\lambda_\pm = \left(\frac{1+b}{2}\right)\left[\pm\sqrt{1 + \frac{4b}{(1+b)^2}} - 1\right] . \tag{2.15}$$

Since $\lambda_+ > 0$ and $\lambda_- < 0$, the solution of interest is

$$\underline{x}(\tau) \sim \exp(\lambda_+\tau) . \tag{2.16}$$

A significant reduction is available since $b \gg 1$; then

$$\lambda_+ \to 1 ,$$

$$\lambda_- \to -b ,$$

and (2.17)

$$\underline{x}(\tau) \to r\begin{bmatrix} 1/b \\ 1 \end{bmatrix}\exp\{\tau\} .$$

Thus, [O] will be much smaller than [SO], and

$$[SO] \simeq [SO]_0 \exp(K_4[O_2]t) \tag{2.18}$$

which was obtained previously.

2.4 Initial Conditions for the Flame Laser

The initial conditions for the flame laser should be similar to those of the induction period, but with the additional influence of heat conduction and diffusion of chain carriers. The heat input raises the gas temperature, which increases the reaction rates, and thus accelerates production of the chain carriers. Upstream diffusion of the chain carriers further accelerates the rate of combustion and generation of chain carriers. The *a priori* knowledge of the mole fractions of the intermediate species is a significant cold boundary problem (ref. 86, chapter 11); the proper treatment will not be attempted here. However, the steady-state approximations, as applied earlier, indicate that the initial ratios of the chain carriers can be estimated. It is

expected that back diffusion would cause a change in the quantity of each species, but since the reaction rates are so high, the ratios of the species would remain approximately the same. The result is that only one species mole fraction, for any one of O, S, or SO, needs to be known a priori, the others being dependent on the reactant mole fractions. Since the products do not participate in the initial reactions, the initial mole fractions of the products can be assumed to be negligible.

2.5 Initial Conditions after Flash Photolysis

Carbon disulfide is dissociated into carbon monosulfide and atomic oxygen when a CS_2/O_2 mixture undergoes flash photolysis. The CS is formed vibrationally excited[40, 87] with at least three-quarters of the molecules with more than two vibrational quanta.[40] The amount of CS formed depends on the experimental arrangement, but is proportional to the flash energy and inversely proportional to the square root of the CS_2 concentration.[88] The fraction of CS_2 dissociated in a flash can be estimated at 0.03 to 0.10,[40, 88] where the lower value is typical of conditions under which lasing was observed.[88] At the low initial temperature, less than 300 K, which is typical of these lasers, there is not any significant concentration of the chain carriers. Thus, after the flash, the mixture will be composed of O_2, CS_2, CS, and S. The atomic sulfur will react with molecular oxygen in the chain branching reaction (Table 1-2, number 3), setting the chain in motion.

2.6 Initial Conditions for the Pulse Discharge Laser

Pulse discharge lasers typically have a gas mixture with a

large O_2/CS_2 ratio and a composition which is mostly diluent. The discharge dissociates the O_2 to atomic oxygen and the CS_2 into CS and atomic S. The amount of dissociation depends on the pulse energy and voltage[54] and is typically not measured. The CS and O generated by the discharge react immediately, but the chain is also at work since there is also a significant amount of atomic sulfur generated. Therefore, three of the four reactions in the chain mechanism (Table 1-2, numbers 1 - 3) start immediately. Since the output is proportional to the incident energy,[89] the chain mechanism cannot be the major factor in this type of laser. Another phenomenon which illustrates the lack of major importance of the chain mechanism is the monotonically decreasing CS concentration after the discharge;[54] the influence of the chain mechanism would cause the CS concentration to increase with time.

2.7 Thermal Dissociation Laser

Thermal dissociation of molecular oxygen followed by rapid expansion provides a supply of atomic oxygen into which cold CS_2 is injected. The initial reactants are atomic oxygen, molecular oxygen, and carbon disulfide, and are well diluted with inert gases. The typical initial ratios of inerts/O_2/CS_2/O are estimated to be $140/3/1/\frac{2}{3}$ (ref. 90). Therefore, the reaction between CS_2 and atomic oxygen (Table 1-2, number 1) begins the chain,which continues with the CS produced in the above reaction being immediately consumed by another atomic oxygen (Table 1-2, number 2). The full chain does not have a chance to set up due to the large amount of diluent and fast flow speeds.

Similarly, carbon disulfide can be thermally dissociated to form a mixture of CS_2, CS, S_2, atomic sulfur, and diluent, which can be frozen by rapid expansion. A mixture of molecular and atomic oxygen, which was generated in either a microwave or electric discharge, can be injected downstream of the expansion to form a mixture which initially contains a sizeable fraction of chain carrier. The chemiluminescent reaction (Table 2-1, number 2) begins immediately and is fed by the reaction between CS_2 and O (Table 2-1, number 1). The chain branching reaction between S and O_2 (Table 2-1, number 3) is also important. Although three of the four reactions which compose the chain mechanism are active for the initial kinetics of this type of laser, their importance is derived from the initial conditions, not the binding of a chain mechanism.

2.8 Electric Discharge Laser

Electric discharge lasers run the discharge through oxygen which is highly diluted with an inert, usually helium, to produce a mixture of atomic oxygen, molecular oxygen, and the inert. Typically, the ratio of atomic oxygen to molecular oxygen is around 0.1 (refs. 32, 91, 92). Carbon disulfide, or carbon disulfide plus the diluent, is injected into this mixture to form an initial mixture having a ratio of atomic oxygen to carbon disulfide concentration which is larger than or around 1. Since the CS_2 is separated from the oxygen supply until the mixing, the concentrations of all intermediates containing carbon and sulfur are negligible. Electric discharge lasers typically have a high flow speed of the order of 100 m s^{-1}. (32, 91, 92) As will be shown in Chapter 9, the flame speed for CS_2/O_2 flames is

of the order of 1 m s^{-1}; therefore, the flame processes of thermal conduction and diffusion cannot be important in this type of laser.

The initial reaction which is of importance is that between O and CS_2 (Table 2-1, number 1). This is followed immediately by the reaction between O and CS. Oxygen atom recombination is termolecular (Table 2-1, number 5), but must be considered when there is a high O atom concentration. At 300 K and a pressure of 1 kPa, the rate for this reaction is nearly four orders of magnitude slower than those of CS_2 and CS with which it competes. The chain mechanism never gets a chance to be fully set up due to the large flow speed and low temperature which is caused by the large amount of diluent. The gases transit the optical cavity in times typically corresponding to around 500 μs.[32, 92] The chain branching reaction between S and O_2 (Table 2-1, number 3) does produce a considerable amount of atomic oxygen in this time, due to the high reaction rate at low temperature and the relative abundance of O_2. But the fourth reaction in this chain (Table 2-1, number 4) does not occur rapidly enough at the low temperature to contribute much to the kinetics of this type of laser (note that the activation energy of 1.7 kJ mol^{-1} makes the reaction rate increase rapidly with temperature); even assuming a rapid build-up of SO_2 concentration, the characteristic time for this reaction, $K_4[O_2]$, is still large at about 2 s under typical conditions of a pressure of 0.7 kPa, $He/O_2/CS_2$ ratios of 67/33/1, and a temperature of 300 K.[92] This can be compared to the estimated characteristic time, $K_2[O_2]$, of about 1 μs for the chain branching reaction between S and O_2 (Table 2-1, number 3).

2.9 Microwave Discharge Laser

The kinetics and initial mixture of the microwave discharge correspond to those of the electric discharge laser. The microwave discharge is a more efficient dissociator of oxygen, yielding a ratio of atomic oxygen to molecular oxygen concentration of around 0.2 (refs. 71, 93). The flow speed is of the order of 100 m s^{-1}, (93-97) with the same consequences as for the electric discharge laser.

TABLE 2-1. Reactions of Importance During the Induction Period and for Initial Laser Kinetics

	Rate Constant
1. $CS_2 + O \rightarrow CS + SO$	K_1
2. $CS + O \rightarrow CO + S$	K_2
3. $S + O_2 \rightarrow SO + O$	K_3
4. $SO + O_2 \rightarrow SO_2 + O$	K_4
5. $O + O + M \rightarrow O_2 + M$	$K_5^b = cK_5$

where K_5^b is the effective bimolecular reaction rate.

The approximate reaction rates at 300 K and 1 kPa are:

$$K_1 \simeq 2 \times 10^6$$
$$K_2 \simeq 8 \times 10^6$$
$$K_3 \simeq 1 \times 10^6$$
$$K_4 \simeq 6 \times 10^0$$
$$K_5^b \simeq 4 \times 10^2$$

where the rates were taken from the tables of Chapter 1 and have the units of $m^3\ mol^{-1}\ s^{-1}$.

3. HISTORY OF THE CS_2/O_2 CHEMICAL LASER AND CHAIN MECHANISM

Both of the reactant molecules, carbon monosulfide and monatomic oxygen, which participate in the chemiluminescent reaction which has high vibrationally-excited carbon monoxide as its product are labile under conditions typically found in chemical lasers. These two labile species can be formed from the parent CS_2 and O_2 molecules by any of a number of methods. Consequently, there are many different techniques for initiating a CS_2/O_2 chemical laser.

3.1 Chemical Lasers

Laser action was first observed after flash photolysis of a CS_2/O_2 mixture.[98] The first laser emission from R-branch transitions was observed after flash photolysis, as was confirmation of cascading of vibrationally-excited CO.[99] Flash photolysis produces atomic sulfur and carbon monosulfide. The first step kinetics for this type of laser, as given in Table 3-1, is the reaction between atomic sulfur and molecular oxygen. Although only those lasers which use O_2 are of immediate interest here, it should be noted that lasing action has been observed from the reaction between CS and O when an electric discharge was placed in a mixture of CS_2 and NO_2.[100]

A spark discharge dissociates CS_2 and O_2 with a similar result as for flash photolysis, as is displayed in Table 3-1, and can result with laser action.[101] Continuous (cw) emission was obtained in a flowing system after moving the discharge out of the optical path, into the oxygen supply.[102] Since only oxygen is dissociated in this arrangement, the first step kinetics are limited to the reaction be-

tween CS_2 and O. The next step for a flowing system was the arrangement of the optical axis transverse to the flow direction.[32] Lasing was also found when the electric discharge was replaced with a microwave discharge to dissociate the oxygen.[103] The resulting kinetics, as indicated in Table 3-1, are of course the same as for the electric discharge. Another way to form CS and O for a laser is to place discharges in both the CS_2 and O_2 supply lines so that the chemiluminescent reaction occurs immediately at the confluence of the two streams (ref. 104).

Thermal dissociation of oxygen upstream of an expansion nozzle and CS_2 injection has resulted in lasing.[90] The initiation reactions are simply the high-temperature equilibrium reactions for oxygen dissociation and recombination, and the first step kinetics is that of the reaction of the atomic oxygen with CS_2.

A unique initiation technique results from the addition of atomic nitrogen to a CS_2/O_2 mixture.[105] The atomic nitrogen is formed from an electric discharge in molecular nitrogen. The atomic nitrogen reacts with CS_2 to form CS and with O_2 to form O. The CS and O then react in the usual chemiluminescent manner. The simplified reaction scheme is outlined in Table 3-1.

All of the above-mentioned methods of initiation yield lasers which are not pure chemical lasers[106] due to the requirement of the addition of energy to initiate the chemical reactions. At room temperature, CS_2 and O_2 are not hypergolic, but explosions can occur at elevated temperatures.[14] A free-burning flame must therefore provide sufficient feedback, by means of thermal conduction and

chain-carrier diffusion, to initiate the combustion process. Although the rate of the reactions and hence the production of vibrationally-excited CO is limited by combustion processes, complete population inversion was found in a CS_2/O_2 flame.[107] Subsequently, laser action was obtained from a free-burning CS_2/O_2 flame.[108]

For the discharge methods, an inert diluent, usually helium, is added to retard the recombination of atomic oxygen, while the atomic and molecular oxygen mixture is transported to the mixing zone; the inert is necessary for lasing in many of the systems.

The first non-diluent added gas which resulted in an increase in power was vibrationally-cold CO.[32] Increase in laser output with the addition of COS and N_2O was observed along with a decrease in power when N_2 and CO_2 were added.[97] These observations were explained as consequences of selective deactivation of CO vibrational levels by V-V energy exchange,[97] as will be described in Chapter 4.

3.2 Compendium of CO Chemical Lasers

A chronological listing of CO chemical lasers from the CS_2/O_2 parent molecules is given in Table 3-2. All of the lasers except those with an overwhelming quantity of diluent are run with excess oxygen. This is due to the dependency of the chemiluminescent reaction $CS + O \rightarrow CO + S$ on the availability of highly reactive atomic oxygen. Thus, a high concentration of molecular oxygen is desirable to ensure that the chain branching and chain propagation reactions occur readily. Also of importance is the low pressure, of around 1 kPa, which is common to these lasers; the low pressure is required to minimize collisional deactivation of vibrationally-excited CO as well as atomic

oxygen recombination.

The maximum power reported from a single CO chemical laser is 1 kW for pulsed operation[89] and 34 W for cw operation.[90] Perhaps efficiency, not power, is the best method for judging the relative performance of these lasers. However, there seems to be as many types and definitions of efficiencies as there are differing lasers. This is due, in part, to the significant number of diverse techniques for the CS_2/O_2 or, more precisely, the CS/O chemical laser. Although each of the electrical, thermal, mass flow, overall, and chemical efficiencies has its use, the only efficiency which can be consistently applied is that of molecular quantum efficiency. Since the reaction scheme for the carbon atoms is unidirectional for all of the lasers, the laser output per reactive carbon atom shall be the yardstick. For almost all of the lasing situations this reduces to the energy extracted per CS_2 molecule. Diluent or other added gases, such as vibrationally-cold CO, which will not participate in the reactions from CS_2 to vibrationally-excited CO, make no contribution to this efficiency calculation. Of the reports which supplied enough information for this molecular efficiency to be calculated, the highest efficiency was found to be 7.3×10^{-20} J per CS_2 molecule [93] for a laser which is initiated by a microwave discharge in O_2 and with N_2O as an added gas. Since a fundamental transition is about 3.8×10^{-20} J, this laser produces approximately 2 photons for every CS_2 molecule. The best reported efficiency for a flame laser corresponds to approximately 1 photon for every 3 fuel molecules.[118]

3.3 Chain Mechanism

The understanding of the chain mechanism of the CS_2/O_2 system has evolved as improved experimental techniques and increased knowledge of the characteristics of the intermediates become available. The CS_2/O_2 combustion mechanism has long been known to be a branching chain,[12] but the role of the intermediates, atomic sulfur and atomic oxygen, was not considered important compared to CS and SO. Correlation of spectroscopic measurements with orbital theories and activated complex theories improved the construction of the mechanism,[13] and provided a mechanism with SO as the main chain carrier. However, these arguments favored the wrong reaction channels.

Significant understanding of the chain mechanism was obtained only after the relative rates of the elementary reactions became known. An intermediate stage was obtained when a few of the reaction rates were used with macroscopic experimental evidence to deduce a mechanism which raised the importance of atomic oxygen, but still maintained SO as the most important chain carrier;[14] this mechanism missed some important elementary reactions, but had net reactions which are products of those fast elementary reactions.

The advent of the CS_2/O_2 chemical laser provided the impetus for many observers to add to the knowledge of the mechanism, which evolved rapidly as better reaction rates became available. Mechanisms deduced from the elementary reaction rates[34, 35] showed that atomic oxygen is the most important chain carrier. Elimination of the reaction between O_2 and CS from consideration[35] provided the step from which the four-reaction scheme, as discussed in Chapter 1,

could be reasoned. Once the importance of this four-reaction mechanism became accepted, the relative importance of the ancillary reactions and alternate reaction channels was questioned.

A comprehensive review of the CS_2/O_2 combustion reaction kinetics and macroscopic evidence[123] considers atomic oxygen and atomic sulfur as the active centers for chain propagation; thus, the two species which were often ignored in the past are now considered to be most important.

With the increased availability of elementary reaction rates came the useful application of computer simulation of the kinetic behavior of the CS_2/O_2 system. The four-reaction mechanism, given in figure 1-1, was found to describe the CS_2/O_2 flame.[124] The mechanism for $CS_2/O_2/O$ lasers was found to be described by only three of these reactions,[124, 125] excluding the reaction between SO and O_2.

TABLE 3-1. Methods of Initiation and First Step Kinetics of CS_2/O_2 Chemical Lasers

Method	Initiation Reactions	First Step Kinetics
Flash Photolysis	$CS_2 \rightarrow CS+S$ $O_2 \rightarrow O+O$	$CS_2+O \rightarrow CS+SO$ $CS+O \rightarrow CO^+ +S$
Electrical Discharge in Mixture	$CS_2 \rightarrow CS+S$ $O_2 \rightarrow O+O$	$CS_2+O \rightarrow CS+SO$ $CS+O \rightarrow CO^+ +S$
Electric or Microwave Discharge in O_2	$O_2 \rightarrow O+O$	$CS_2+O \rightarrow CS+SO$
Thermal Dissociations in O_2	$M+O_2 \rightleftarrows M+O+O$ in equilibrium	$CS_2+O \rightarrow CS+SO$
Reaction with Active N_2	$N_2 \rightarrow N+N$	$N+CS_2 \rightarrow CS+NS$ $N+O_2 \rightarrow NO+O$
Separate Discharges for CS_2 and O_2	$CS_2 \rightarrow CS+S$ $O_2 \rightarrow O+O$	$CS+O \rightarrow CO^+ +S$
Flame	O diffuses from flame front	$CS_2+O \rightarrow CS+SO$

CO^+ indicates vibrationally-excited CO.

TABLE 3-2. Chronological List of CS_2/O_2 Chemical Lasers

Method	Mode	Power	Pressure (kPa)	Ratio (O_2:CS_2)	Added Gas	Ratio (x:O_2:CS_2)	Upper V-Levels	Reference
Flash Photolysis	pulsed	0.5 W	20	1:1	He	150:1:1	6-14	98
Flash Photolysis	pulsed		1	6.5:1 1.3:1	Air Air	6.5:6.5:1 6.5:1.3:1	16-1	99
Electric Discharge in Mixture	pulsed		0.1 0.7	3:1 1:1	He	2:1:1	6-13	100
Electric Discharge in O_2	pulsed	0.1 W		5:1	He	115:5:1	10	109
Electric Discharge in O_2	cw	1 mW	2		He	15:1:?	8-12	101
Microwave Discharge in O_2	cw	mW	0.5	3:1			8-10	32
Electric Discharge in O_2	cw	70 mW	1.3	10:1	He	120:10:1	4-13	102
Microwave Discharge in O_2	cw	300 mW	0.4	8:1	He, CO	36:5:8:1	7-11	97
Electric Discharge in Mixture	pulsed	1 kW	4	12.5:1	He	27:12.5:1	2-13	89

TABLE 3-2 (continued). Chronological List of CS_2/O_2 Chemical Lasers

Method	Mode	Power	Pressure (kPa)	Ratio (O_2:CS_2)	Added Gas	Ratio (x:O_2:CS_2)	Upper V-Levels	Reference
Electric Discharge in Mixture	pulsed	1.9 W	1	2.7:1	He, CO	22:1.4:2.7:1	8-13	110
Free-burning Flame	cw	inversion	0.1	4:1	H_2	2:4:1	6-10	107
Free-burning Flame	cw	gain	0.9	7:1			8-10	111
Free-burning Flame	cw	1 mW	0.07		OCS		8-11	108
Free-burning Flame	cw cw	0.6 W 0.2 W		28:1 28:1	N_2O CO	2:28:1 6:28:1		112
Electric Discharge in Mixture	cw	0.4 W	14	25:1	He	1000:25:1	7-11	113
Electric Discharge in O_2	cw	250 mW	1.5		He	5:1:?	7-12	114
Microwave Discharge in O_2	cw	2.3 W	1.2	6:1	HeCO	60:3:6:1	7-11	96
Electric Discharge in Mixture	pulsed	6 W	9.3				3-12	115

TABLE 3-2 (continued). Chronological List of CS_2/O_2 Chemical Lasers

Method	Mode	Power	Pressure (kPa)	Ratio (O_2:CS_2)	Added Gas	Ratio (x:O_2:CS_2)	Upper V-Levels	Reference
Electric Discharge in O_2	cw	10 mW	1.0	23:1	He	48:23:1	2-16	91
Microwave Discharge in O_2	cw		0.5	33:1	He, CO	50:9:33:1	7-13	94
Thermal Dissociation of O_2	cw	34 W	40	3:1	He, Ar	100:40:3:1	4-13	90
Electric Discharge in O_2	cw	1.5 W	0.5	14:1	He, CO	60:8:14:1	7-12	116
Electric Discharge in CS_2	cw		7	10:1	He	42:10:1	6-14	73
Electric Discharge in CS_2	cw		0.6	9.5:1	He	42:9.5:1	16	117
Transfer from Active N_2	cw			6:1	N_2, N	100:1:6:1		105
Free-burning Flame	cw	6 W	2.7	18:1	N_2O	26:18:1		118

TABLE 3-2 (continued). Chronological List of CS_2/O_2 Chemical Lasers

Method	Mode	Power	Pressure (kPa)	Ratio (O_2:CS_2)	Added Gas	Ratio (x:O_2:CS_2)	Upper V-Levels	Reference
Flash Photolysis	pulsed		0.1	10:1	CO	1:10:1		88
Flash Photolysis in Mixture	pulsed		1.0	9:1	He	10:9:1		119
Microwave Discharge in CS_2; Electric Discharge in O_2	cw	2.2 W	0.4	3:1	He	5:3:1		103
Electric Discharge in O_2	cw	7 W			CO		10	120
Electric Discharge in Mixture	pulsed		0.4	42:1	He	100:42:1	14	54
Microwave Discharge in O_2	cw	22 W	0.7	23:1	He, N_2O	46:8:23:1	2-12	93, 121
Microwave Discharge in O_2	cw	1 W	0.6	33:1	He, CO	50:9:33:1		95

TABLE 3-2 (continued) Chronological List of CS_2/O_2 Chemical Lasers

Method	Mode	Power	Pressure (kPa)	Ratio (O_2:CS_2)	Added Gas	Ratio (x:O_2:CS_2)	Upper V-Levels	Reference
Electric Discharge in O_2	cw	4.5 W	0.7	33:1	He	57:33:1	14	92
Electric Discharge in Mixture	pulsed		0.5	3.8:1	He	40:3.8:1	1	122

4. VIBRATIONAL QUANTA KINETICS OF CO

The CO chemical laser has two distinct advantages over other diatomic molecule chemical lasers in its relatively slow vibration to translation (V-T) deactivation and preferential formation of molecules in the upper vibrational levels. Vibration to vibration (V-V) energy transfer is sufficiently faster than V-T for CO, so that V-V deactivation dominates. The product carbon monoxide from the reaction $CS + O \rightarrow CO + S$ is formed with almost all of its population in high vibrational states. As will be shown later in this chapter, a population inversion may be chemically formed for each of the first 13 vibrationally-excited states. The CS_2/O_2 chemical laser also has the advantage of fast chemical kinetics as compared to V-V deactivation.

4.1 Energy Levels

Carbon monoxide is a diatomic molecule which is held together by a very strong bond of 1077 kJ mol^{-1} (1.788 aJ),[26] and has the same molecular orbital designation as N_2.[126] This triple bond is the cause of the deep potential well of the CO ground state, which has 27 vibrational levels before reaching the lowest vibrational level on the lowest-lying electronically-excited state.[126, 127] The potential energy diagram for the CO ground state is given in figure 4-1. The ground state vibrational and rotational energy levels are given by the approximation formula:[126]

$$E(v, J) = \omega_e(v+\tfrac{1}{2}) - \omega_e x_e(v+\tfrac{1}{2})^2 + \omega_e y_e(v+\tfrac{1}{2})^3 + \omega_e z_e(v+\tfrac{1}{2})^4$$
$$+\left[B_e - \alpha_e(v+\tfrac{1}{2}) + \gamma_e(v+\tfrac{1}{2})^2\right] J(J+1) - \left[D_e + \beta_e(v+\tfrac{1}{2})\right] J^2(J+1)^2$$
$$+ He\, J^3(J+1)^3 \qquad (4.1)$$

when the vibrational and rotational constants are given in Table 4-1.

4.2 Chemical Excitation

The energy states of the product CO molecules from the reaction between carbon monosulfide and monatomic oxygen are presently only described in terms of the vibrational level. The information on the rotational level of the product molecules is too quickly erased by collisions; the rotational levels for each vibrational level reach a Boltzmann distribution within a few collisions, while V-V transfer for thermalization occurs on the order of once every thousand collisions (ref. 128).

The equilibrium vibrational distribution will not be a Boltzmann distribution due to anharmonic pumping which, under some circumstances, can lead to a Treanor distribution.[129, 130] However, due to spontaneous emission, which is important at the low pressures typical of CS_2/O_2 lasers, the vibrational distribution will be modified towards the lower levels,[131] leading to an irregular distribution.

The reaction $CS + O \rightarrow CO + S$ is unusual in that the product carbon monoxide is formed very vibrationally excited with little or no CO formed in the lower vibrational levels. The product energy distribution has been obtained by few investigators, and their experimental results are shown in figure 4-2. All of these independent measurements yield a distribution with an inverted population and each has a maximum at V = 12 or 13. High population of the lower levels was found by only one experimenter[54] while others[132, 133, 134] did not observe this behavior. The two additional measurements[95, 135] did

not cover the entire range of vibrational levels. The approximate relative population levels from these experiments and the experimental method are given in Table 4-2.

The heat of reaction of the reaction CS+O → CO+S is -310.9 kJ mol^{-1} (-0.5161 aJ) at 300 K and increases slightly to -312.9 kJ mol^{-1} (0.5195 aJ) at 2000 K when the standard heat of formation of 230.12 kJ mol^{-1} [25] for CS is employed. Comparing that energy with the vibration levels of CO,[126] the maximum vibrational level of CO which should result from this reaction is 12. But that is based on the assumption that most of the CS is in the zeroth vibrational level. However, the CS produced from the reaction with carbon disulfide and monatomic oxygen has a significant vibrational population in the first three vibrationally-excited levels;[49] 26 per cent of the total energy was found to have gone into vibrational energy of the products.

An independent measurement of the translational energy of the products indicates that a maximum of 10 per cent of the reaction energy goes into translational energy of the products CS and SO.[136,137] The harmonic constant, ω_e, and first anharmonic constant, $x_e\omega_e$, for the CS molecule are 2.55271×10^{-20} J and 1.28×10^{-22} J,[25] respectively; these indicate that for the first three vibrational levels of CS, each vibrational quantum can increase the maximum energetically possible CO vibrational level, at $v \simeq 13$, by one. Thus, the CO molecule can be formed in up to the 15^{th} vibrational level. The actual heat of formation of CS is probably around 40 kJ mol^{-1} larger than the standard one.[25] Three independent measurements place this heat of formation at 269 ±3 kJ mol^{-1},[138] 272 ± 2 kJ mol^{-1},[139]

and 293 ± 8 kJ mol^{-1}, [140] which would allow CO to be formed about 1, 2, or 3, respectively, vibrational levels above the previous discussions. With these considerations there is no doubt that the vibrational energy distributions of figure 4-2 and Table 4-2 are energetically feasible.

4.3 Radiative Decay

The dipole moment of 3.00×10^{-16} V [126] of carbon monoxide allows the radiative decay of vibrationally-excited CO. The spontaneous emission coefficients, $A_{v, v'}$, are determined from the dipole matrix elements[141] with the normalization based on emission measurements.[135] These coefficients are given in Table 4-3 for fundamental ($v \rightarrow v-1$), first overtone ($v \rightarrow v-2$), and second overtone ($v \rightarrow v-3$) emission from the lowest-lying 20 vibrational levels. The spontaneous emission coefficients increase with increasing vibrational level. The stimulated emission coefficients, $B_{v, v'}$, are determined from the spontaneous emission coefficients through the Einstein relation[142]

$$B_{v, v'} = \frac{c^3}{8\pi h \nu^3} A_{v, v'} , \qquad (4.2)$$

where c is the speed of light, h is the Planck constant, 6.626196×10^{-14} J s, and ν is the frequency of the emitted radiation.

The frequency of the emitted radiation will be centered according to equation (4.1) and the conversion of

$$\nu = E/h . \qquad (4.3)$$

The linewidth broadening to be considered here will be the two classic types of broadening, the Doppler and the Lorentz. The full width at

half height (FWHH) of a purely Doppler (or homogeneous) broadened line is given by (ref. 142, p. 44)

$$\Delta\nu_D = 2\frac{\nu_0}{c}\sqrt{\frac{2kT\ln 2}{m}} \quad , \tag{4.4}$$

where $\Delta\nu_D$ is the FWHH; ν_0 is the center frequency; k is the Boltzmann constant, 1.380622×10^{-23} J K^{-1}; T is temperature, and m is the mass of the molecule. The mass of the $C^{12}O^{16}$ molecule is 4.649×10^{-26} kg, so that the Doppler line width can be written as

$$\Delta\nu_D = 1.354 \times 10^{-7}\,\nu_0\sqrt{T}\;K^{-\frac{1}{2}} \quad . \tag{4.5}$$

The FWHH of a purely Lorentz (or inhomogeneous) broadened line is given by (ref. 142, p. 46)

$$\Delta\nu_L = Z/\pi \quad , \tag{4.6}$$

where Z is the collision frequency. The collision frequency for species i in a mixture of gases can be estimated by kinetic theory as (ref. 143, chapter III)

$$Z = n\left(\frac{8kT}{\pi m}\right)^{\frac{1}{2}} \sum_{j=1}^{N} X_j S_{ij}\left(1 + \frac{W_i}{W_j}\right)^{\frac{1}{2}} \quad , \tag{4.7}$$

where N is the number of species present, n is the particle density, X_j is the mole fraction of species j, S_{ij} is the collision cross section between species i and j, and W_i is the molecular weight of species i. The particle density can be represented in terms of the total pressure, p, and the temperature by

$$n = p/kT \quad . \tag{4.8}$$

Substituting the collision frequency and particle density into equation (4.6) and combining the constants yields the Lorentz linewidth as

$$\Delta\nu_L = 1.99 \times 10^{24} \left(\frac{K^{\frac{1}{2}} Hz}{Pa\ m^2}\right) \frac{p}{T^{\frac{1}{2}}} \sum_{j=1}^{N} X_j S_{ij} \left(1 + \frac{W_i}{W_j}\right)^{\frac{1}{2}} \quad . \tag{4.9}$$

For an estimate of the linewidth under conditions typically found in a CS_2/O_2 laser, assume a pressure of 1 kPa, a temperature of 1750 K, and a frequency of 5.64×10^{13} Hz, which corresponds to a v = 9 to 8 transition. Assume that only the three species, O_2, CO, and SO_2, are important and that the mole fractions can be assumed to be O_2: 0.67, SO: 0.22, and CO: 0.11. The collision cross section can be estimated by

$$S_{ij} = \pi(\sigma_i + \sigma_j)^2 \quad , \tag{4.10}$$

where σ_i is the molecular radius of species i. The Lennard-Jones molecular radii are:[86]

O_2: 0.177 nm, CO: 0.186 nm, and SO_2: 0.215 nm.

Since the interest is for $C^{12}O^{16}$, take the atomic weights as:

C: 0.012 kg mol^{-1}, O: 0.016 kg mol^{-1}, and S: 0.032 kg mol^{-1},

from which the molecular weights are approximated. Putting all this together yields a Doppler linewidth of 3.2×10^8 Hz and a Lorentz linewidth of 2.8×10^7 Hz. Since the separation of the two P-branch transitions, P(13) and P(12) with v = 9 to 8, is about 1.2×10^{11} Hz,[98] it is clear that under conditions typical of the CS_2/O_2 chemical laser, adjacent transitions do not overlap.

4.4 Collisional Decay

The vibrationally-excited carbon monoxide can be relaxed readily by V-V transfer with CO molecules in other vibrational states. The reaction

$$CO(v) + CO(v') \rightarrow CO(v-1) + CO(v'+1) + \Delta E \tag{4.11}$$

describes the general process of a quantum energy transfer in CO where the energy defect, ΔE, is transferred to (or from) translational and rotational energy. For $v > v'$, the process is endothermic, $\Delta E < 0$. If $v' = v-1$, then $\Delta E = 0$ and there is effectively no chemical change. If $v < v'$, then the reaction is exothermic, $\Delta E > 0$, and the molecule in the upper level, v', is pumped up one quantum. Since this type of exchange is exothermic, the tendency is for this reaction to be important; thus the upper levels are pumped at the expense of the lower levels. This phenomenon of anharmonic pumping is to be expected whenever the V-V transfer rates are fast compared to the V-T rates. Of particular interest in the CS_2/O_2 chemical laser is the vibrational relaxation by ground state CO molecules

$$CO(v) + CO(0) \rightarrow CO(v-1) + CO(1) + \Delta E \quad . \qquad (4.12)$$

The rates of these reactions at 300 K for v = 2 to 12 [128, 144] are given in Table 4-4 along with theoretical results[145] which allow extrapolation to v = 1 and v = 15 as well as to 700 K. The relaxation rates are greater for the lower vibrational levels, which implies preferential deactivation of the lower levels; thus, addition of vibrationally-cold carbon monoxide inserted with the reactants can help maintain a population inversion. However, this selectivity decreases with increasing temperature.

V-V transfer will cause selective depopulation of the lower vibrational levels of CO if the energy defect is smaller for the lower levels than for the upper levels. The probability of a V-V energy transfer is roughly an exponential function of the energy defect and a linear function of the vibration level;[128] the probability of energy

transfer in the reaction with unspecified polyatomic molecule, M ,

$$CO(v) + M \rightarrow CO(v-1) + M^{\dagger} + \Delta E \quad , \qquad (4.13)$$

where the superscript † indicates vibrational excitation, has the functional dependency

$$P_{v,v-1} \propto v \exp(-\Delta E) \quad . \qquad (4.14)$$

The energy defects for the vibrationally-cold diatomic gases CO, O_2, N_2, and triatomic gases COS, N_2O, CO_2, and CS_2 , and the first 20 excited vibrational levels of CO are presented in figure 4-3. From the position of COS in figure 4-3 , it would be expected that the energy transfer rates from CO to COS should be relatively large. This is confirmed by experimental data presented in Table 4-5, which indicates that the de-excitation of CO(5) by COS occurs in about one out of seven collisions. Selective population of the lowest levels of CO by N_2O can be expected due to the increasing energy defect with vibrational level as illustrated in figure 4-3 ; the relaxation data listed in Table 4-5 clearly illustrate this behavior. Both nitrogen and carbon dioxide exhibit slight perferential depopulation of the lower levels of CO.

The reactant species O_2 and CS_2 have a single quantum energy defect which, as illustrated in figure 4-2 , is smaller for increasing vibrational levels. The expectation is that these would tend to selectively depopulate the upper levels, which could tend to increase the population inversion in the intermediate levels. The near-resonant two-quanta transfer process

$$CS_2(000) + CO(1) \rightarrow CS_2(101) + CO(0) - 8.3 \times 10^{-22} \text{ J} \qquad (4.15)$$

has been shown to be efficient,[152] even though multi-quanta processes should not have a high probability. The rate for this exchange at 300 K is around 2.5×10^5 m^3 mol^{-1} s^{-1},[149, 152] about once every 620 collisions, which is two orders of magnitude below the quantum exchange between COS and CO(5). Similar multi-quanta excitation of CS_2 should have significantly lower rates for the higher CO levels, since overlapping of rotational bands, which provides the resonant exchange, will not occur.

The energy defect of SO_2 with CO(v) is too large to provide efficient V-V exchange; the rate with CO(1) was measured at 2.1×10^2 m^3 mol^{-1} s^{-1}.[149] This compares with the rate for deactivation by helium, which is given in Table 4-5. Since helium has no vibrational or rotational freedom, de-excitation of CO(v) occurs only by V-T transfer, and thus should have a lower rate than for polyatomic molecules. The data listed in Table 4-5 illustrate the importance of V-V as compared to V-T deactivation, which is represented by the rates for helium. Deactivation by other inerts should have a lower rate than that for helium, due to their larger mass; for example, the rate constant for deactivation of CO(1) by helium is about seven times that for argon.[148]

TABLE 4-1. Vibrational and Rotational Constants for the $C^{12}O^{16}$ Ground State

Symbol	Constant, J
ω_e	$4.3103193 \times 10^{-20}$
$\omega_e x_e$	2.64081×10^{-22}
$\omega_e y_e$	2.28×10^{-25}
$\omega_e z_e$	3.12×10^{-28}
B_e	3.836439×10^{-23}
α_e	3.4789×10^{-25}
γ_e	5.88×10^{-29}
D_e	1.2157×10^{-28}
β_e	-1.962×10^{-32}
H_e	1.163×10^{-34}

Data from ref. 126.

TABLE 4-2. Vibrational Distribution of the Product CO Molecules

Ref.	(132)	(132)	(135)	(133)	(94, 95)	(54)	(134)
v	Relative Populations						
1						2.38	0.09
2						1.13	0.08
3				0.35		0.82	0.07
4				0.35		0.52	0.11
5				0.37		0.55	0.18
6		0.05		0.40	0.37	0.58	0.29
7	0.06	0.17	0.10	0.44	0.44	0.62	0.48
8	0.27	0.32	0.21	0.50	0.69	0.67	0.64
9	0.61	0.41	0.49	0.51	0.81	0.71	0.78
10	0.66	0.55	0.61	0.62	0.91	0.80	0.89
11	0.80	0.65	0.73	0.74	1.00	0.89	0.94
12	0.87	0.85	0.91	0.90	1.00	0.97	1.00
13	1.00	1.00	1.00	1.00	1.00	1.00	0.85
14	0.61	0.90	0.92	0.88		0.77	0.59
15	0.20	0.58	0.30	0.52		0.56	0.32
16		0.32		0.24		0.34	0.14
17		0.18		0.14		0.13	
18				0.06			
19				0.02			
	intensity of first overtone emission	gain measurements	intensity of first overtone emission	gain measurements with CO probe laser	extrapolation from population ratios	extrapolation from population ratios	oscillation range measurements

TABLE 4-3. Carbon Monoxide Spontaneous Emission Coefficients

Fundamental $CO(v) \rightarrow CO(v-1) + h\nu$

First Overtone $CO(v) \rightarrow CO(v-2) + h\nu$

Second Overtone $CO(v) \rightarrow CO(v-3) + h\nu$

ν	$A_{\nu, \nu-1}$ (s^{-1})	$A_{\nu, \nu-2}$ (s^{-1})	$A_{\nu, \nu-3}$ (s^{-1})
1	33.4	-	-
2	64.5	0.9	-
3	92.9	2.8	0.01
4	118.0	5.6	0.05
5	142.0	9.3	0.12
6	164.3	13.9	0.26
7	182.0	19.0	0.45
8	200.1	25.1	0.7
9	214.1	32.0	1.1
10	227.1	39.3	1.6
11	238.8	47.7	2.3
12	248.5	56.2	3.1
13	256.3	65.6	4.1
14	262.5	75.0	5.2
15	268.3	85.8	6.5
16	271.9	95.8	8.2
17	275.2	106.8	10.1
18	278.5	118.0	12.2
19	279.6	129.2	14.4
20	281.2	140.9	15.6

The coefficients are from ref. 135, which are based on the matrix elements calculated in ref. 141.

TABLE 4-4. Vibrational Relaxation of CO(v) by CO(0)

$$CO(v) + CO(0) \rightarrow CO(v-1) + CO(1)$$

v	Experimental 300 K		Theoretical 300 K	Theoretical 700 K
1			1.0E6	7.8E5
2		1.1E6	1.5E6	1.2E6
3		1.6E6	1.9E6	1.7E6
4	1.2E6	1.9E6	1.8E6	2.1E6
5	7.8E5	1.2E6	1.1E6	2.2E6
6	3.8E5	5.9E5	4.4E5	1.9E6
7	2.0E5	2.8E5	1.6E5	1.3E6
8	1.0E5	1.4E5	8.3E4	8.7E5
9	6.6E4	9.8E4	5.2E4	5.7E5
10	3.7E4		4.3E4	4.7E5
11	2.8E4		3.3E4	3.8E5
12	2.0E4		2.5E4	3.2E5
13			2.0E4	2.9E5
14			1.8E4	2.6E5
15			1.3E4	2.3E5
reference	(128)	(144)	(145)	(145)

Notation: aEb is $a \times 10^b$

Reaction rates are in $m^3\ mol^{-1}\ s^{-1}$

The theoretical results were obtained from data in ref. 145 and conversion according to ref. 146.

TABLE 4-5. Vibrational De-excitation of CO(v) by a Few Molecules

$$CO(v) + M \rightarrow CO(v-1) + M$$

v	M: O_2	N_2	COS	N_2O	CO_2	He
1	4.E2	3.2E3	4.8E6	2.8E6	4.E4	3.5E1
2	-	-	-	1.E6	-	-
3	-	-	-	6.E5	-	-
4	-	1.4E3	2.4E7	3.0E5	1.8E4	-
5	-	1.0E5	3.6E7	1.5E5	1.0E4	-
6	-	6.0E2	3.4E7	9.0E4	9.6E3	-
7	-	5.1E2	2.2E7	5.9E4	9.0E3	-
8	-	4.3E2	9.0E6	5.2E4	9.6E3	-
9	-	2.8E2	4.3E6	5.2E4	1.3E4	9.0E1
10	-	2.4E2	2.3E6	6.0E4	2.0E4	1.6E2
11	-	1.3E2	1.9E6	6.0E4	3.2E4	2.0E2
12	1.3E4	-	1.1E6	6.0E4	5.2E4	3.2E2
13	2.6E4	-	6.0E5	5.4E4	7.2E4	3.8E2

Deactivation rates are in $m^3\ mol^{-1}\ s^{-1}$ and at 300 K.

Notation: aEb is $a \times 10^b$.

Rates for v=1 ; O_2, COS, N_2O, CO_2, He from refs. 147, 148, 149, 149, 150, and 151, respectively.

Rates for v=2, 3 from refs. 93 and 150; rates for v=4-13 from ref. 128.

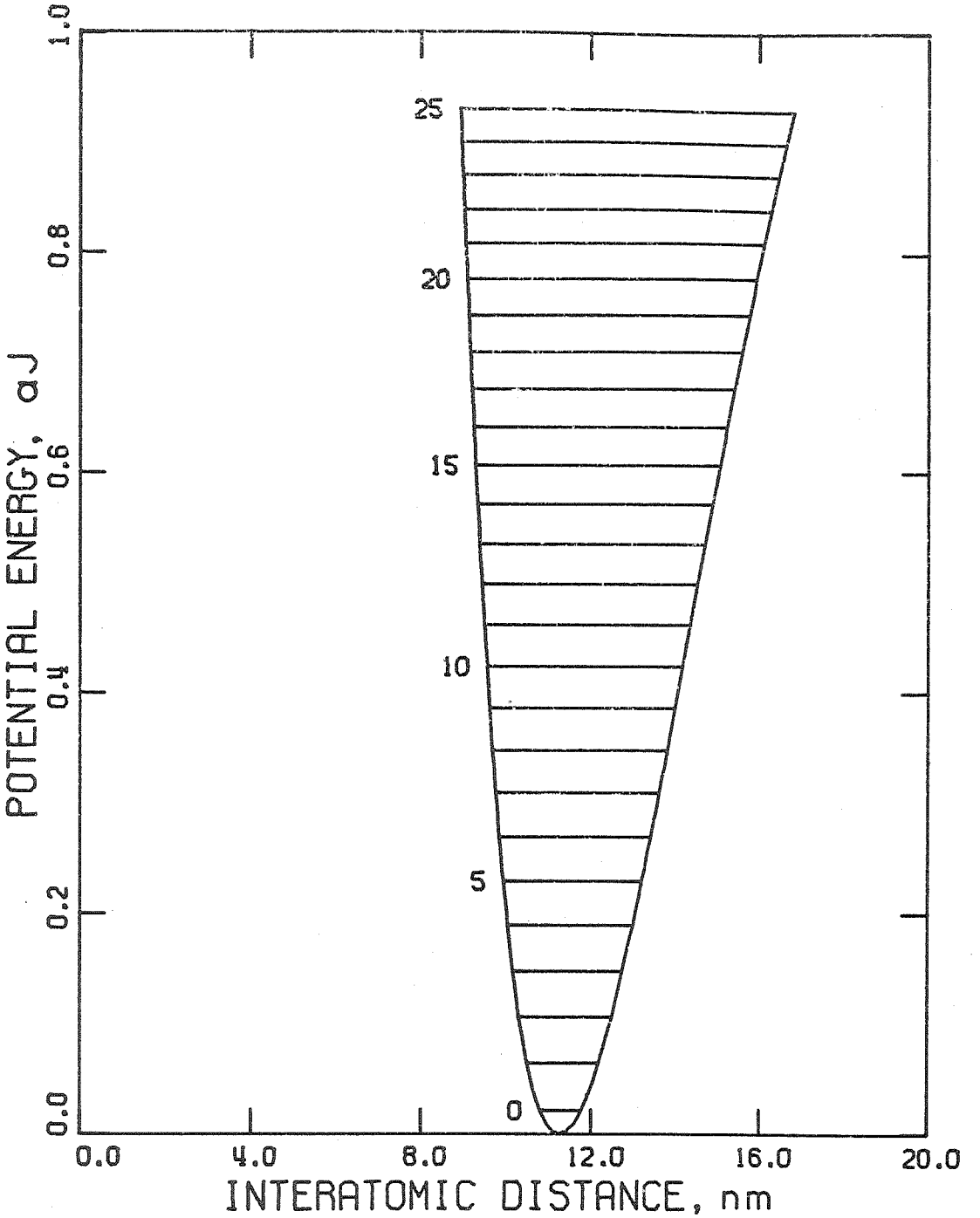

Figure 4-1. The Potential Energy Curve for the Electronic Ground State of $C^{12}O^{16}$ with the First Twenty-Six Vibrational States Indicated.

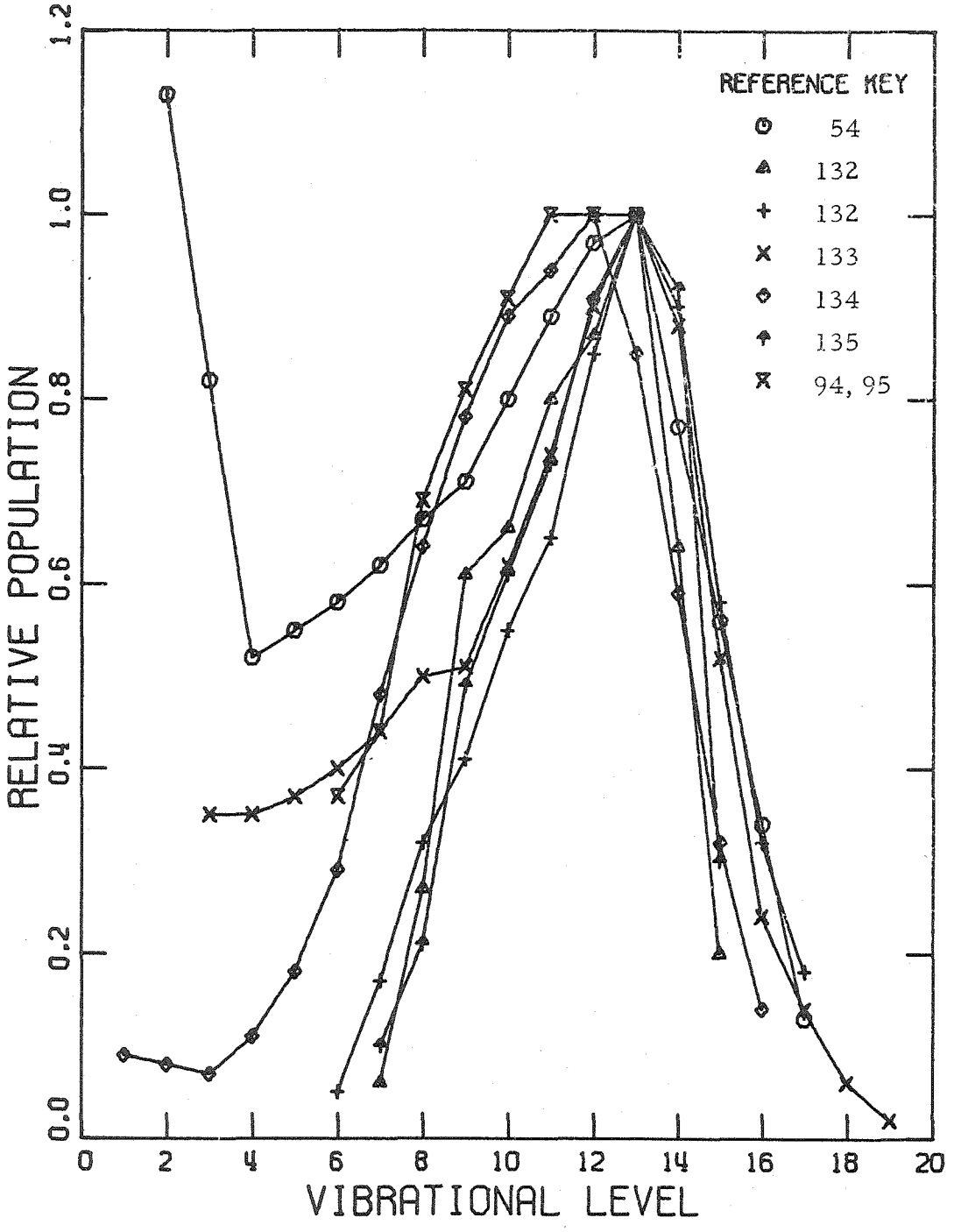

Figure 4-2. Product CO Energy Distribution from the Reaction $CS + O \rightarrow CO + S$.

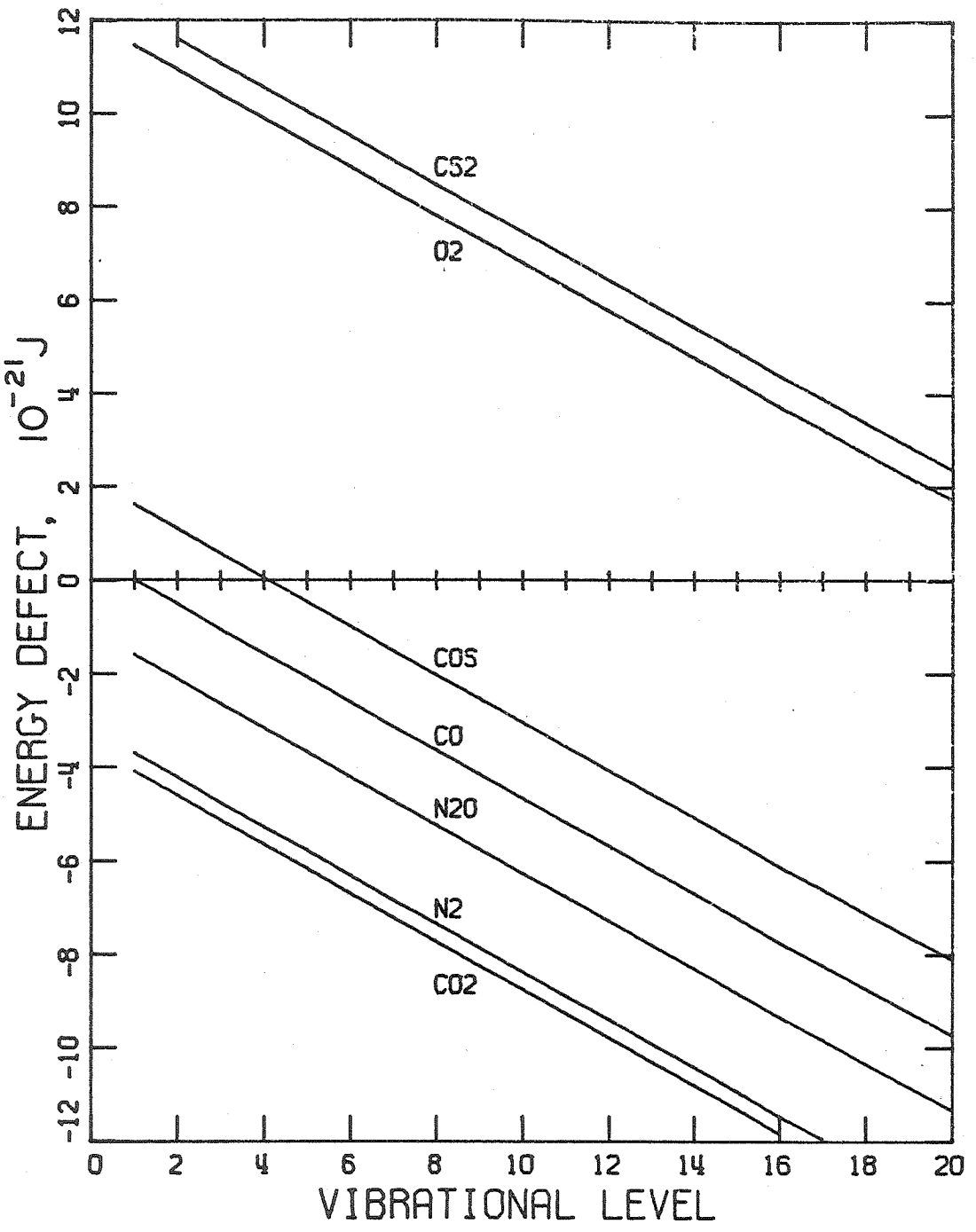

Figure 4-3. Energy Defect between CO(v) and Vibrationally-Cold Polyatomic Gases for a Quantum Exchange. The Defect Is Taken to the First Vibrational Level for the Diatomics and the First Asymmetric Stretch of the Triatomics.

5. VON KARMAN APPROXIMATIONS APPLIED TO THE CS_2/O_2 FLAME

The von Kármán approximations[153] provide a simple method of extracting information on the primary physical characteristics of one-dimensional laminar deflagrations. These methods allow an approximate determination of flame speed and flame structure. Apart from the usual assumptions of the theory of laminar flame propagation, the main implicit assumption is that the behavior of the major species near the hot boundary has the predominant influence on the flame properties; the initial reaction zone, where intermediate species and initial boundary conditions have a large influence, is downgraded and essentially ignored. The scope and accuracy of this method are limited due to the neglect of transient species, gross property assumptions, and the small number of reactions allowed for the kinetics scheme. However, rough functional dependencies are obtained from simple numerical computations. The assets, explicit assumptions, and limitations of the application of the von Kármán method are listed in Table 5-1.

In this chapter, the von Kármán method is applied to the lean CS_2/O_2 flame. The chemical kinetics are modeled by a five-reaction scheme which includes the four-reaction chain propagation mechanism discussed in Chapter 1. Numerical solutions are presented for the flame speed and flame structure for each of the three (zeroth, first, and second) approximations. Comparison of the calculations with experimental data is made in Chapter 9.

5.1 Development of the Problem

Following the formulation of von Kármán, the equations for

species conservation and for the diffusion relations are (ref. 153, eqs. 8a and 8b)

$$\frac{d\epsilon_i}{d\theta} = \frac{\lambda}{m^2 \overline{C}_p} \frac{w_i}{(\theta-1) + \sum_{j=1}^{N} \left(\frac{h_j^o}{\overline{C}_p T_f} \right) (\epsilon_j - \epsilon_{jf})} , \qquad (5.1)$$

$$\frac{dX_i}{d\theta} = \frac{\lambda}{\overline{C}_p} \left(\frac{RT}{p} \right) \frac{\sum_{J=1}^{N} \frac{1}{D_{ij}} \left[X_i \frac{\epsilon_j}{W_j} - X_j \frac{\epsilon_i}{W_i} \right]}{(\theta-1) + \sum_{j=i}^{N} \left(\frac{h_j^o}{\overline{C}_p T_f} \right) (\epsilon_j - \epsilon_{jf})} , \qquad (5.2)$$

where:

ϵ_j = mass flux fraction of species j ; additional subscript f indicates final value

θ = temperature, nondimensionalized by the adiabatic flame temperature

λ = thermal conductivity

m = mass flow rate

$\overline{C}_p$ = average specific heat capacity

h_j^o = standard specific heat of formation of species j

T_f = adiabatic flame temperature

N = number of species

X_i = mole fraction of species i

T = absolute temperature

R = ideal gas constant

p = absolute pressure

D_{ij} = binary diffusion coefficient

W_i = molecular weight of species i

The assumptions which lead to this formulation are: (i) steady state, (ii) one-dimensional plane flow, (iii) no body forces, (iv) no radiant energy transfer, (v) negligible bulk viscosity, (vi) negligible thermal diffusion, (vii) low velocity so that the integral of the momentum equation yields constant pressure, and (viii) all the species have the same constant heat capacity which allows the energy equation to be used to transform the independent variable from distance to temperature.

The net rate of production of species i by chemical reaction is given by:

$$w_i = W_1 \sum_{k=1}^{M} (\nu''_{i,k} - \nu'_{i,k}) K_k \prod_{j=1}^{N} \left(\frac{X_j p}{RT}\right)^{\nu'_{j,k}}, \quad i = 1, \ldots, N \qquad (5.3)$$

where:

M = number of elementary reactions,

$\nu'_{i,k}$ = stoichiometric coefficient for species i which is a reactant in reaction k,

$\nu''_{i,k}$ = stoichiometric coefficient for species i which is a product in reaction k,

K_k = rate constant for reaction k.

Consider the set of reactions:

1. $CS_2 + O \rightarrow CS + SO$
2. $CS + O \rightarrow CO + S$
3. $S + O_2 \rightarrow SO + O$
4. $SO + O_2 \rightarrow SO_2 + O$
5. $O + SO + M \rightarrow SO_2 + M$

with the eight species

1. O_2	2. CS_2	3. CS	4. CO
5. SO_2	6. S	7. SO	8. O

The initial conditions, $\theta = \theta_0$, are given by

$$\begin{aligned} X_1 &= 1 - X_0 \\ X_2 &= X_0 \qquad \text{for } X_0 < \tfrac{2}{7},\ \theta = \theta_0 \\ X_i &= 0\ , \quad i = 3, \ldots, 8 \end{aligned} \tag{5.4}$$

X_0 is the initial mole fraction of CS_2. The value of X_0 is limited to provide an excess of O_2 as CS_2/O_2 flame lasers invariable run with a lean mixture. The downstream conditions are determined from the physical reasoning that all of the CS has been reacted and that all intermediate species have disappeared, i.e., a limited equilibrium. Thus, the boundary conditions to be applied at $\theta = 1$ are:

$$\begin{aligned} X_1 &= \frac{1 - \frac{7}{2}X_0}{1 - \frac{1}{2}X_0} \qquad & X_5 &= \frac{2X_0}{1 - \frac{1}{2}X_0} \\ X_4 &= \frac{X_0}{1 - \frac{1}{2}X_0} \qquad & X_i &= 0\ , \quad i = 2, 3, \ldots, 6, 7, 8\ . \end{aligned} \tag{5.5}$$

This choice of kinetic scheme and boundary conditions corresponds to the overall reaction, equation (1.2), which was discussed in Chapter 1:

$$6.\quad CS_2 + \tfrac{5}{2}O_2 \rightarrow CO + 2SO_2\ .$$

Apply the steady-state approximation to the four transient species (CS, S, SO, O) to determine their mole fractions in terms of the reactant species (CS_2, O_2). Using these approximations, it is found that the net production of the major (reactant and product) species is related by:

$$w_i = \frac{\mu_i W_i}{\mu_j W_j}\, w_j\ , \tag{5.6}$$

where the μ are the stoichiometric coefficients of the overall reac-

tion, reaction 6; the stoichiometric coefficient is positive for a product species and negative for a reactant species. Choose species 4, CO, as the standard species since $\mu_4 = 1$, so that

$$w_i = \mu_i \frac{W_i}{W_4} w_4 \quad . \tag{5.7}$$

The steady-state approximations also simplify equations (5.3); the net rate of production of CO becomes

$$w_4 = \frac{1}{3} W_4 \, c \, \frac{K_1 K_4}{K_5} X_1 X_2 \quad , \tag{5.8}$$

where c is the total concentration,

$$c = p/RT \quad . \tag{5.9}$$

Substituting equation (5.7) into equation (5.1) yields:

$$\frac{d\epsilon_i}{d\theta} = \frac{\lambda}{m^2 \overline{C}_p} \frac{1}{W_4} \frac{w_4}{\sum_{j=1}^{N} \left(\frac{h_j^o}{\overline{C}_p T_f} \right) (\epsilon_j - \epsilon_{jf}) - (1-\theta)} \mu_i W_i \quad . \tag{5.10}$$

Collecting factors which are species dependent,

$$\frac{1}{\mu_i W_i} \frac{d\epsilon_i}{d\theta} = G(\theta) \quad . \tag{5.11}$$

Therefore,

$$\frac{1}{\mu_i W_i} \frac{d\epsilon_i}{d\theta} = \frac{1}{\mu_j W_j} \frac{d\epsilon_j}{d\theta} \quad . \tag{5.12}$$

Again choose species 4 and integrate to obtain

$$\epsilon_i - \epsilon_{if} = \mu_i \frac{W_i}{W_4} (\epsilon_4 - \epsilon_{4f}) \quad . \tag{5.13}$$

For the von Kármán approximations, the mole fractions and mass flux fractions of the intermediate species are considered to be negligible for evaluation of the species conservation equation and diffusion condi-

tion. The remaining ϵ_i can then be related to ϵ_4 by equation (5.13) so that one mass flux fraction is independent. The obvious choice is to remain with species 4, CO.

The energy conservation equation (ref. 1, eq. 7) with reduction by equations (5.13) is:

$$\frac{\lambda}{m\bar{C}_p}\frac{d\theta}{dz} = (\theta-1) + (\epsilon_4-\epsilon_{4f})\sum_{j=1}^{N}\left(\frac{h_j^o}{\bar{C}_p T_f}\right)\mu_j\frac{W_j}{W_4} \quad . \qquad (5.14)$$

Evaluate this equation for pre-flame conditions where the temperature derivative vanishes, $\epsilon_4 = 0$, and $\theta = \theta_0$, to find

$$-\epsilon_{4f}\sum_{j=1}^{N}\left(\frac{h_j^o}{\bar{C}_p T_f}\right)\mu_j\frac{W_j}{W_4} = 1-\theta_0 \quad . \qquad (5.15)$$

Equation (5.11) is equivalent to the global energy conservation equation which determines the adiabatic flame temperature. The differential equation for ϵ_4, equation (5.10) for $i = 4$, can be simplified with equations (5.13) and (5.15) to obtain

$$\frac{d\epsilon_4}{d\theta} = \frac{\lambda}{m^2\bar{C}_p}\frac{w_4}{(1-\theta_0)\left(1-\frac{\epsilon_4}{\epsilon_{4f}}\right)-(1-\theta)} \quad . \qquad (5.16)$$

For integration of equation (5.16), the von Kármán method represents the functions λ and w_4 in terms of the non-dimensional temperature. The mole fractions of the reactant species are approximated by functions which are linear with respect to θ between the two boundary points. The justification comes from the case of only two species which have a Lewis number of unity where, for this special case, the weight ratio of each species is exactly a linear function of temperature. This result is extrapolated to the current case of a

multicomponent mixture,

$$X_1 = 1 - \left[1 + \frac{5}{2}\left(\frac{\theta-\theta_0}{1-\theta_0}\right)\right] X_0$$
$$X_2 = \left(\frac{1-\theta}{1-\theta_0}\right) X_0 \tag{5.17}$$

The heat conductivity and reaction rates are approximated by the empirical relations

$$\lambda = \lambda_f \theta \ ,$$
$$\frac{K_1 K_4}{K_5} = A \exp\left(-\frac{\theta_a}{\theta}\right) \ . \tag{5.18}$$

Define the function ϵ and eigenvalue Λ by:

$$\epsilon = \frac{\epsilon_4}{\epsilon_{4f}} \ ,$$
$$\Lambda = \frac{1}{3} \frac{\lambda_f \rho_f}{m^2 \bar{C}_p} A \exp(-\theta_a) \ . \tag{5.19}$$

where ρ_f is the final density of the gases. Then equation (5.16) becomes

$$\frac{d\epsilon}{d\theta} = \Lambda\left[C_1 + C_2\left(\frac{1-\theta}{1-\theta_0}\right)\right]\left(\frac{1-\theta}{1-\theta_0}\right) \frac{\exp\left(-\theta_a \frac{1-\theta}{\theta}\right)}{(1-\theta_0)(1-\epsilon)-(1-\theta)}$$
$$\epsilon(\theta_0) = 0 \qquad \epsilon(1) = 1 \tag{5.20}$$

with

$$C_1 = \frac{1 - \frac{7}{2} X_0}{1 - \frac{1}{2} X_0} \quad \text{and} \quad C_2 = \frac{X_0(2 + \frac{1}{2} X_0)}{1 - \frac{1}{2} X_0} \ .$$

Define the functions y and η by:

$$y = 1 - \epsilon \quad \text{and} \quad \eta = \frac{1-\theta}{1-\theta_o} \ , \tag{5.21}$$

so that the hot boundary is located at $y(0) = 0$ and the cold boundary is

at $y(1) = 1$. Equation (5.20) is transformed to

$$\frac{dy}{d\eta} = \Lambda[C_1+C_2\eta]\frac{\eta}{y-\eta}\exp\left\{-\theta_a \frac{\eta}{\frac{1}{1-\theta_0}-\eta}\right\} \tag{5.22}$$

$$y(0) = 0 \quad , \quad y(1) = 1$$

5.2 Zeroth Order Approximation

For the zeroth approximation to the eigenvalue, the change of thermal enthalpy is neglected in comparison with the chemical energy production and heat transfer by conduction. This approximation eliminates the cold boundary problem by alteration of the basic equation. For the zeroth approximation, η is neglected in comparison to y in the denominator of equation (5.22). Thus, the equation becomes separable:

$$y\frac{dy}{d\eta} = \Lambda_z[C_1+C_2\eta]\eta\exp\left\{-\theta_a \frac{\eta}{\frac{1}{1-\theta_0}-\eta}\right\} . \tag{5.23}$$

Let

$$I = \int_0^1 [C_1+C_2\eta]\eta\exp\left\{-\theta_a \frac{\eta}{\frac{1}{1-\theta_0}-\eta}\right\} ; \tag{5.24}$$

then equation (5.23) can be integrated between the boundary points to obtain a relation for Λ_z :

$$\Lambda_z = 1/2I . \tag{5.25}$$

The zeroth order eigenvalue, Λ_z , provides an upper bound on the eigenvalue Λ of equation (5.22) (ref. 154, p. 111). From integration of equation (5.23), an approximation for y is also obtained:

$$y(\eta) = \left\{\frac{1}{I}\int_0^{\eta}[C_1+C_2\eta']\eta'\exp\left\{-\theta_a \frac{\eta'}{\frac{1}{1-\theta_0}-\eta'}\right\}d\eta'\right\}^{\frac{1}{2}} \tag{5.26}$$

where η' is a dummy variable for η.

5.3 First Order Approximation

A better approximation is obtained with a linear approximation for the change of thermal enthalpy, with the slope equal to its actual value at the hot boundary. Again, the cold boundary problem is eliminated by alteration of the equation. For the first approximation to the eigenvalue, η is considered as a linear function of y (or vice-versa) in the denominator of equation (5.22). Again the equation is separable. Let

$$\eta = \alpha y \tag{5.27}$$

in the denominator, and then evaluate α from the limit of y and η equal to zero to find

$$\alpha = \frac{\sqrt{1 + 4\Lambda_1 C_1} - 1}{2\Lambda_1 C_1} \quad . \tag{5.28}$$

The species conservation equation becomes

$$(1-\alpha)y \frac{dy}{d\eta} = \Lambda_1 [C_1 + C_2 \eta] \eta \exp\left\{-\theta_a \frac{\eta}{\frac{1}{1-\theta_0} - \eta}\right\} , \tag{5.29}$$

which, after integration between the boundary points, yields a relation for Λ_1, the first order approximation to the eigenvalue

$$\Lambda_1 = \frac{1}{2I}\left(1 - \sqrt{\frac{2I}{C_1}}\right) \tag{5.30}$$

and a relation for $y(\eta)$ which is identical to that of the zeroth approximation, equation (5.26).

5.4 Second Order Approximation

For the second approximation, the species conservation equation, equation (5.22), is integrated numerically with the additional

assumption of an ignition temperature. The ignition temperature is introduced simply by altering the cold boundary condition to

$$y(1-\delta) = 1$$
$$\delta = \frac{T_I - T_0}{T_f - T} > 0 \tag{5.31}$$

where T_I is the ignition temperature and T_0 is the initial temperature. Numerical methods are employed to find both the eigenvalue and the function y which satisfy the boundary conditions and equation (5.22).

An improvement on the approximation for the mole fraction can be made by consideration of the diffusion condition, equation (5-2). Assume that all of the binary diffusion coefficient are equal and that the Lewis number, $(\rho D\bar{C}_p)/\lambda$, is equal to unity. Then, with equations (5.13) and (5.15), it is found that

$$\frac{dX_i}{d\theta} = \bar{W} \frac{X_i \sum_{j=1}^{N} \frac{\epsilon_j}{\bar{W}_j} - \frac{\epsilon_i}{\bar{W}_i}}{(1-\theta_0)\left(1 - \frac{\epsilon_4}{\epsilon_{4f}}\right) - (1-\theta)} , \tag{5.32}$$

where $\bar{W}$ is the average molecular weight,

$$\bar{W} = \sum_{i=1}^{N} W_i X_i . \tag{5.33}$$

Substituting equation (5.13), expanding the sum, and employing previous notation yield

$$\frac{dX_i}{d\theta} = \frac{\bar{W}}{\bar{W}_f} \frac{X_i - X_{if} + (1-\epsilon)\left[\mu_i X_{4f} - \left(\sum_{j=1}^{N} \mu_j\right) X_i\right]}{(1-\theta_0)(1-\epsilon) - (1-\theta)} . \tag{5.34}$$

The linear approximation for the mole fraction is to be substituted into the right hand side of equation (5.34) and then this equation is to be integrated. The average molecular weight under the linear approximations for all mole fractions becomes

$$\bar{W} = \bar{W}_f\left[1 - \frac{X_0}{2}\left(\frac{1-\theta}{1-\theta_0}\right)\right] . \tag{5.35}$$

Consider again the species CO, and since for this case

$$\sum_{j=1}^{N} \mu_j = -\frac{1}{2}, \quad \mu_4 = 1 , \quad \text{and} \quad X_{4f} = \frac{X_0}{1 - \frac{X_0}{2}} , \tag{5.36}$$

apply the linear approximation, and transform to the y, η notation to obtain

$$\frac{\left(1 - \frac{X_0}{2}\right)}{X_0} \frac{dX_4}{d\eta} = \left(1 - \frac{X_0}{2}\eta\right)\left[-1 + \frac{y(1-\eta)}{2(y-\eta)}\right] . \tag{5.37}$$

The first term represents the contribution due to non-constant average molecular weight; for small values of the initial CS_2 mole fraction, the assumption of constant $\bar{W}$ can be seen to be valid. In order to determine the departure from linearity, let

$$x = \frac{X_4}{X_0}\left(1 - \frac{X_0}{2}\right) - \mu_4(1-\eta) . \tag{5.38}$$

Then equation (5.37) reduces to

$$\frac{dx}{d\eta} = \left(1 - \frac{X_0}{2}\eta\right)\frac{y(1-\eta)}{2(y-\eta)} + \frac{X_0}{2}\eta , \tag{5.39}$$

so that

$$x = \begin{cases} \displaystyle\int_0^{\eta} \left(1 - \frac{X_0}{2}\eta'\right) \frac{y(1-\eta')}{2(y-\eta')}\, d\eta' + \frac{X_0}{4}\eta \\ \qquad\qquad 0 \le \eta \le 1 \text{ for } 0^{th} \text{ or } 1^{st} \text{ approximation} \\ \qquad\qquad 0 \le \eta \le 1-\delta \text{ for } 2^{nd} \text{ approximation} \\ \displaystyle\int_0^{1-\delta} \left(1 - \frac{X_0}{2}\eta'\right) \frac{y(1-\eta')}{2(y-\eta')}\, d\eta' - \frac{1}{2}\left(1 - \frac{X_0}{4}\right)(1-\delta) + \frac{1}{2}\left(1 + \frac{X_0}{4}\right)\eta \\ \qquad\qquad 1-\delta < \eta \le 1 \text{ for } 2^{nd} \text{ approximation} \end{cases} \tag{5.40}$$

From the definitions of y and the mass flux fraction comes the relation:

$$y = 1 - \left(\frac{\overline{W}_f}{\overline{W}}\right) \frac{X_4}{X_{4f}} \left(1 - \frac{V_4}{v}\right) , \tag{5.41}$$

where V_4 is the diffusion velocity of species 4 and v is the mean flow velocity. Substituting the linear approximation for the mole fraction, the diffusion velocity is given by:

$$\frac{V_4}{v} = -1 + \left(1 - \frac{X_0}{2}\eta\right)\left(\frac{1-y}{1-\eta}\right) . \tag{5.42}$$

Since $y = 1$ at $\eta = 1-\delta$, then at the cold boundary $V_4 = -v$, which means that the product diffuses upstream with the speed of the flame speed.

If the physical dimension is given by z and the origin corresponds to the cold boundary, then the energy equation will provide the transformation from the temperature to space coordinate:

$$z = \frac{\lambda_f(1-\theta_0)}{m\overline{C}_p} \int_{\eta}^{1} \frac{\frac{1}{1-\theta_0} - \eta}{y - \eta}\, d\eta \quad . \tag{5.43}$$

The hot boundary, where $\eta = 0$, corresponds to $z = +\infty$.

5.5 Numerical Results

The eigenvalue integration requires numerical values for the constants representing the activation energy, θ_a, the initial temperature, θ_0, and the ignition temperature, δ. The values of these constants are dependent upon the adiabatic flame temperature and the rate constants of reactions 1, 4, and 5. The adiabatic flame temperature, T_f, can be found in the standard manner by solving the implicit equation

$$\sum_{i=1}^{N} H_i(T_f)X_{if} = \sum_{i=1}^{N} H_i(T_0)X_{i0} \quad , \tag{5.44}$$

where subscript 0 indicates the initial values and H_i is the molar enthalpy of species i. Details of the calculation of the flame temperature, as well as all the other numerical results presented in this chapter, are given in Appendix A. The enthalpies were calculated from a simple tabular form of the molear heat capacities whose values were taken from standard thermodynamic tables.[25] The resulting flame temperature as a function of the initial mole fraction of CS_2 and the resulting average heat capacity are displayed in figure 5-1.

The combined rate constant composed of the coefficient A and activation energy θ_a as given by equation (5.18) was determined by the values of the rate constants K_1,[46] K_2,[46] and K_5[63] given by

$$\begin{aligned} K_1 &= 5 \times 10^7 \exp\left(-\frac{960\ K}{T}\right)\ m^3\ mol^{-1}\ s^{-1} \\ K_4 &= 3.5 \times 10^5 \exp\left(-\frac{3300\ K}{T}\right)\ m^3\ mol^{-1}\ s^{-1} \\ K_5 &= 3.2 \times 10^5\ m^6\ mol^{-2}\ s^{-1} \end{aligned} \tag{5.45}$$

so that

$$A = 5.5 \times 10^{7} \ s^{-1} \ , \qquad \theta_a = \frac{4.2 \times 10^{3} \ K}{T_f} \ . \tag{5.46}$$

The value of the constant $1/(1-\theta_0)$ which appears initially in equation (5.22) is determined by the adiabatic flame temperature and the initial temperature, which is taken as 300 K. The variations of the activation energy constant and initial temperature value with X_0, the initial mole fraction of CS_2, are given in Figure 5-2.

With the previous numerical values, the eigenvalues for the zeroth, first, and second approximations can be generated. For the second approximation, an ignition temperature corresponding to $\delta = 0.05$ was chosen; the ignition temperature is plotted as a function of X_0 in Figure 5-1. These eigenvalues should form a lower bound on the eigenvalue, and hence an upper bound on the flame speed. The numerical results for the eigenvalues as a function of the initial mole fraction of CS_2 are presented in Figure 5-3. Notice that the better the approximation the lower the eigenvalue. Of course, these results do not necessarily bound the experimental flame speed due to the approximations used to produce a soluble model.

The mass flux fraction, ϵ, and the diffusion velocity ratio, $-V_4/v$, have been determined numerically as functions of the non-dimensional temperature $(\theta-\theta_0)/(1-\theta_0)$ for all three of the approximations. Since the functions ϵ and $-V_4/v$ are identical for the zeroth and first approximations, there are only two calculations for each function corresponding to the first and second approximations. The results are displayed for the case of $X_0 = 0.10$ for the mass

flux fraction in Figure 5-4 and the diffusion velocity ratio in Figure 5-5. The second approximation for these two functions is displayed with the initial mole fraction of CS_2 as a parameter in Figure 5-6 for ϵ and Figure 5-7 for $-V_4/v$.

The flame speed is determined from the eigenvalues through equation (5.19). The mass flux, and hence the flame speed, can be seen to be proportional to the inverse of the square root of the eigenvalue. Numerical values for the thermal conductivity were determined by taking advantage of a Lewis number of unity, and noting that the initial and final densities are related through the ideal gas law by

$$\frac{\rho_f}{\rho_0} = \frac{\bar{W}_f}{\bar{W}_0} \frac{T_0}{T_f} \quad . \tag{5.47}$$

Then the flame speed, v, can be given by

$$v = \sqrt{\frac{\overline{D_0 A \exp\{-\theta_a\}}}{3\left(1 - \frac{1}{2} X_0\right)}} \Lambda^{-\frac{1}{2}} \quad . \tag{5.48}$$

The numerical value for the diffusion coefficient at 300 K was approximated from data of the diffusion coefficient of O_2 with various neutral species and a pressure relation of[155]

$$D_0 = \left(\frac{1.013 \times 10^5 \text{ N m}^{-2}}{p} \right) D \quad , \tag{5.49}$$

choosing p as 1.0 kPa (0.01 atmosphere) and D as 1.5×10^{-5} m^2 s^{-1} (ref. 155), the diffusion coefficient is then taken as $D_0 = 1.5 \times 10^{-3}$ m^2 s^{-1}. The second approximation to the flame speed as a function of the initial mole fraction of CS_2 is shown in Figure 5-8.

The flame thickness and temperature profile are determined

from equation (5.43). The thermal conductivity is again evaluated by taking advantage of a Lewis number of unity, so that for the second von Kármán approximation,

$$z = \frac{D_0}{v}\left(\frac{1}{\theta_0} - 1\right)\int_{\eta}^{1} \frac{\frac{1}{1-\theta_0} - \eta}{y-\eta}\, d\eta \quad . \tag{5.50}$$

The temperature profile of θ as a function of distance non-dimensionalized by the coefficient of the integral of equation (5.50) is given in Figure 5-9 for five values of initial mole fraction of CS_2, X_0. The flame thicknesses for these cases vary from 1.5 mm to 5 mm.

5.6 Sensitivity of Numerical Results

The sensitivity of the eigenvalue and flame speed, calculated by the second von Kármán approximation, to changes in the ignition temperature and activation energy is obtained by approximation of the influence coefficient. The influence coefficients, α, are obtained by calculation of the partial derivatives in the form of

$$\frac{\partial \Lambda_2}{\Lambda_2} = \alpha \frac{\partial \theta_a}{\theta_a} \quad , \tag{5.51}$$

which relates the parameter θ_a to the dependent variable Λ_2. Thus, a fractional change of θ_a will result in approximately an α-fold fractional change in Λ_2. This influence coefficient is a means of presenting the instantaneous relation between θ_a and Λ_2 in a power form

$$\Lambda_2 \sim \theta_a^{\alpha} \quad . \tag{5.52}$$

Thus, an influence coefficient of unity implies a linear relationship and zero implies independence. The influence coefficients for the ignition temperature were approximated by decreasing δ by 10 per

cent and recalculating the von Kármán approximations. The results of the calculations, as summarized in Table 5-2, indicate that the eigenvalues and corresponding flame speed are nearly independent of the ignition temperature. The influence coefficients for the activation energy wer approximated by increasing θ_a by 10 per cent from the nominal case and recalculating the von Kármán approximations. The results of these calculations, as summarized in Table 5-3, indicate that the eigenvalue, Λ_2, and the flame speed are strongly dependent on the activation energy.

TABLE 5-1. Characteristics of the von Kármán Method

ASSETS

1. Includes diffusion effect for reactants and products.
2. Accurate for flames which have a single rate-controlling reaction with a large activation energy.
3. Simple computation.
4. Provides a lower bound of the computed flame speed.

EXPLICIT ASSUMPTIONS

1. Steady-state approximation on all intermediates.
2. Mole fractions of major species are linear with respect to temperature.
3. Heat capacities constant and equal.
4. Standard cold boundary difficulty removal for second approximation.

LIMITATIONS

1. Requires a reaction scheme with a single rate-determining step.
2. Intermediate species must have negligible concentrations.
3. Ignition zone kinetics ignored.
4. Chemical kinetic rates must be well known for accurate results.

TABLE 5-2. Influence Coefficients for the Ignition Temperature

X_0	Λ_2	Λ_2'	$\frac{\partial \Lambda_2}{\Lambda_2}$	$\frac{\partial \delta}{\delta}$	α_Λ	α_v
0.05	4.774	4.774	0	-0.1	0	0
0.10	3.246	3.246	0	-0.1	0	0
0.15	2.628	2.628	0	-0.1	0	0
0.20	2.351	2.350	4×10^{-4}	-0.1	+0.004	-0.002
0.25	2.252	2.250	9×10^{-4}	-0.1	+0.009	-0.004

TABLE 5-3. Influence Coefficients for the Activation Energy

X_0	Λ_2	Λ_2'	$\frac{\partial \Lambda_2}{\Lambda_2}$	$\frac{\partial \theta_a}{\theta_a}$	α_Λ	α_v
0.05	4.774	5.688	0.191	0.1	1.91	2.45
0.10	3.246	3.822	0.177	0.1	1.77	1.78
0.15	2.628	3.084	0.174	0.1	1.74	1.53
0.20	2.351	2.762	0.175	0.1	1.75	1.40
0.25	2.252	2.659	0.181	0.1	1.81	1.34

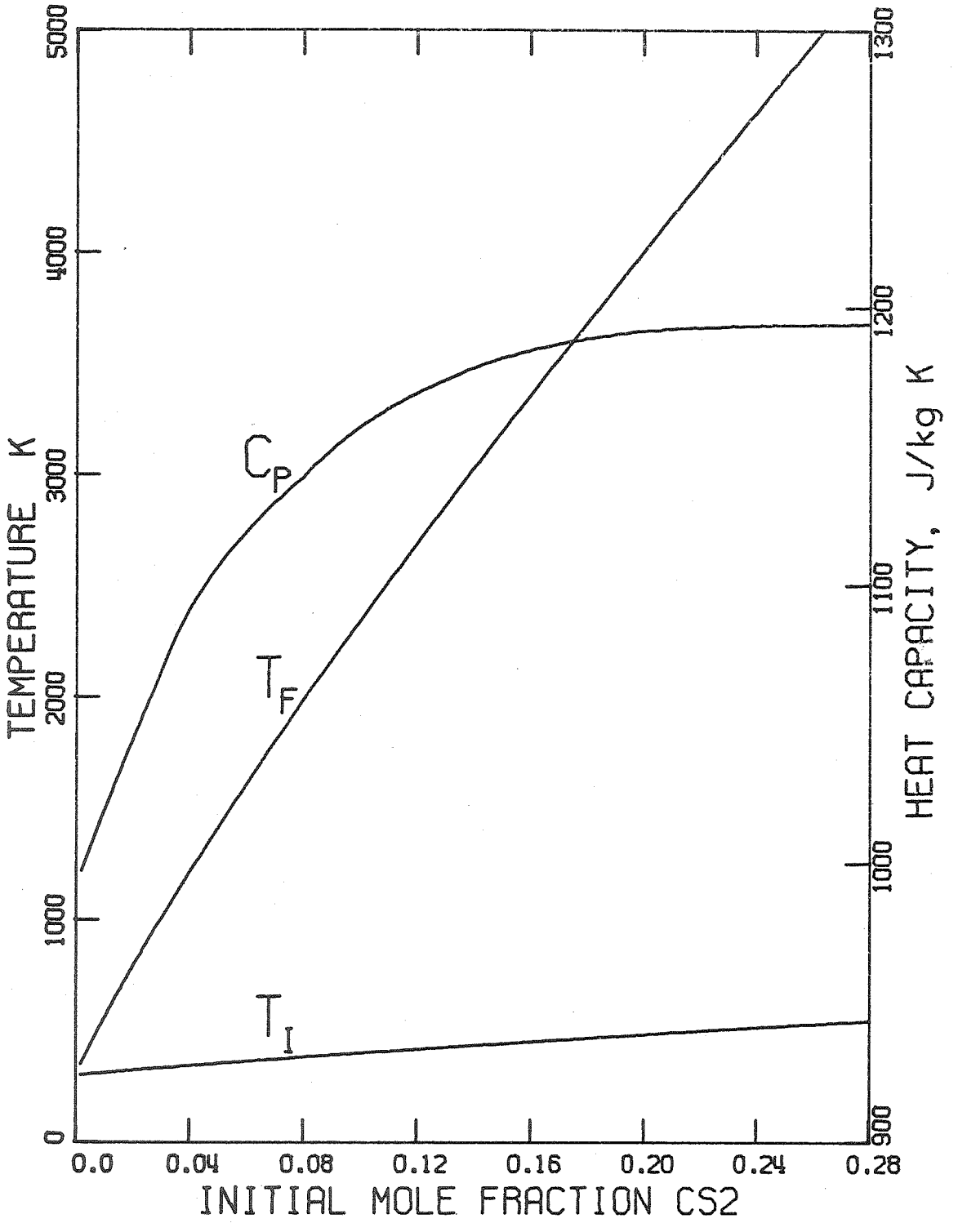

Figure 5-1. The Flame Temperature and Average Heat Capacity for All Three von Kármán Approximations and the Ignition Temperature for the Second Approximation.

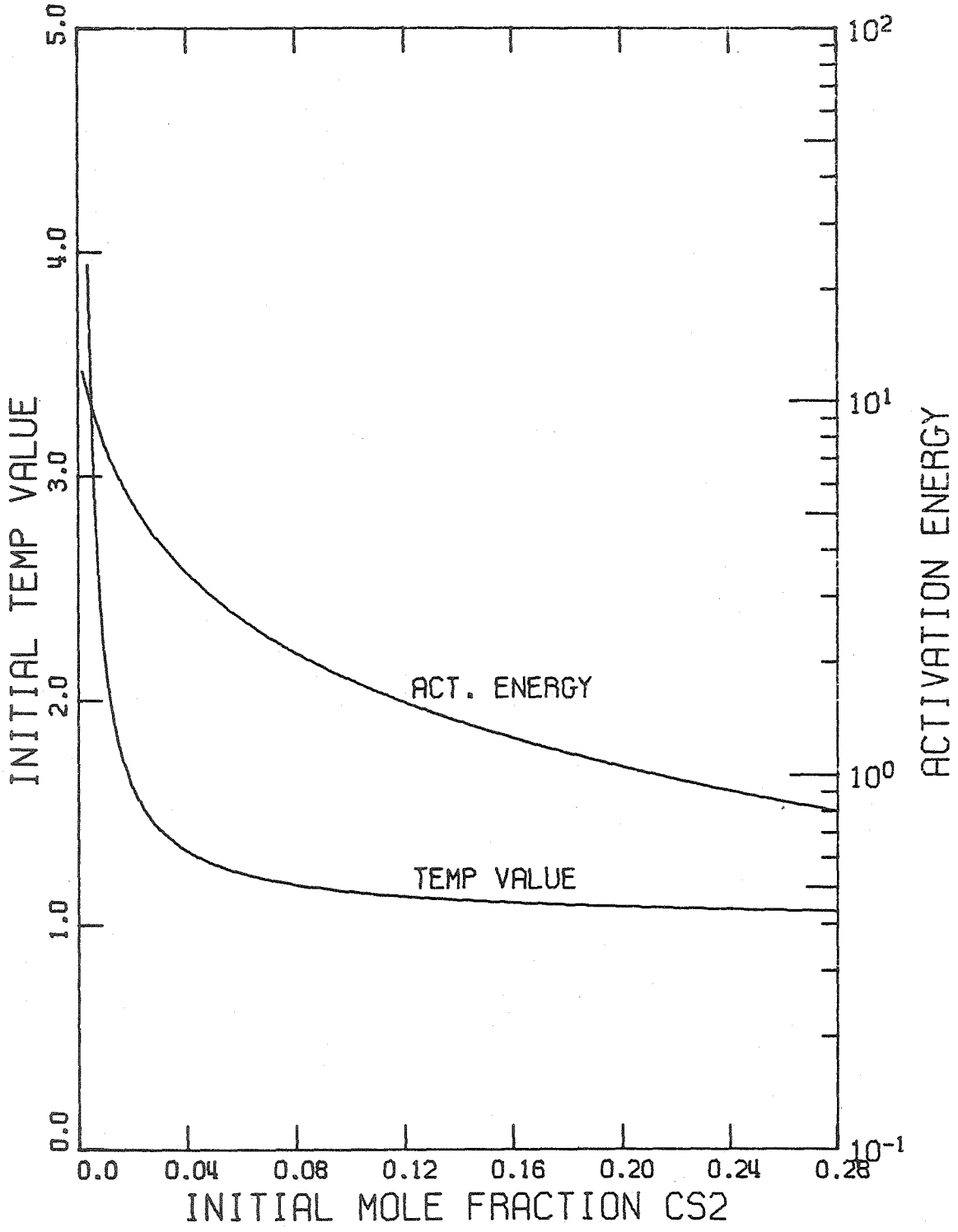

Figure 5-2. The Temperature Value, $1/(1-\theta_0)$, and the Activation Energy, θ_a, for the von Kármán Approximations, as a Function of the Initial Mole Fraction of CS_2.

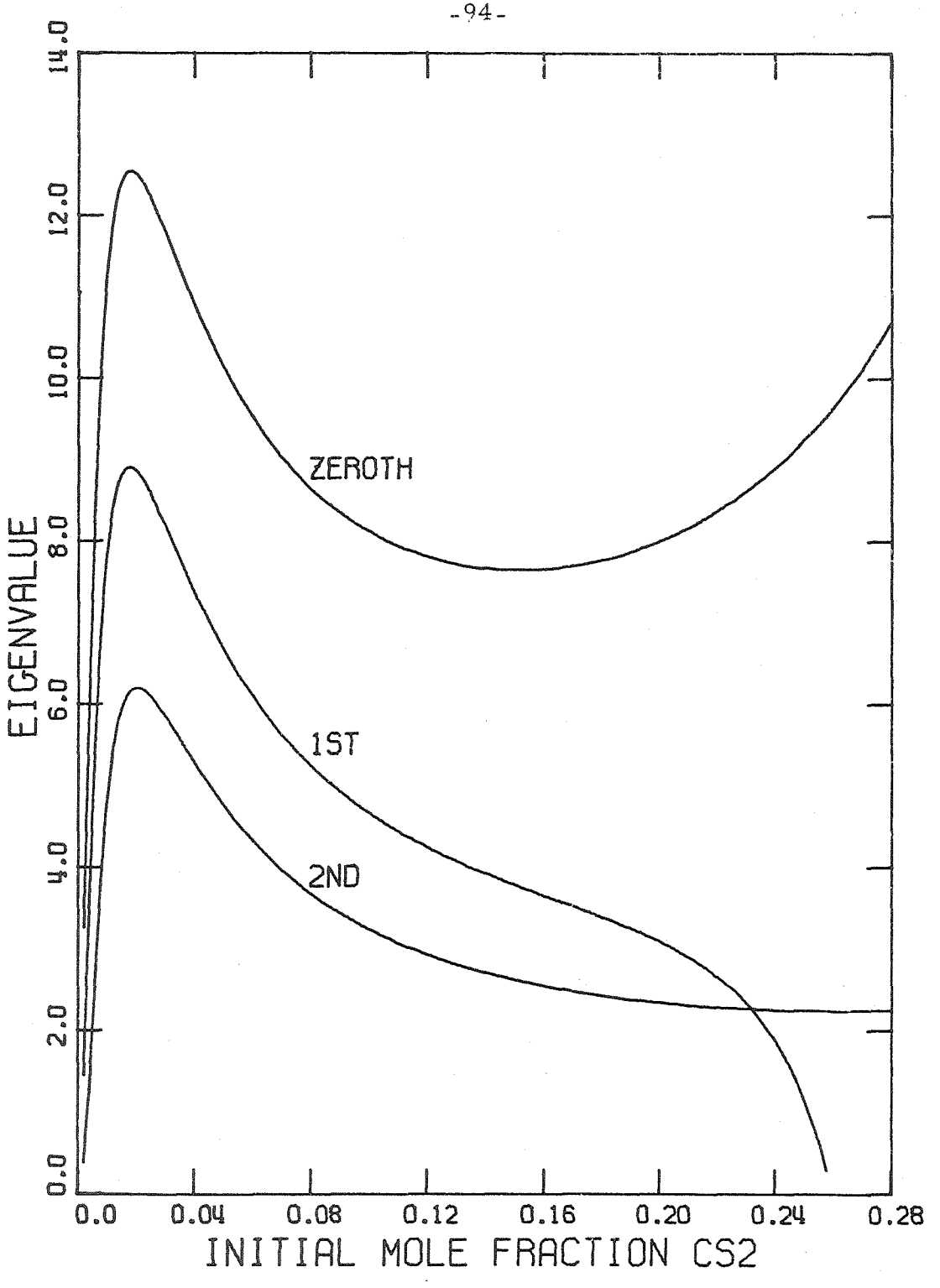

Figure 5-3. The Eigenvalues Which Were Calculated from the Zeroth, First, and Second von Kármán Approximations.

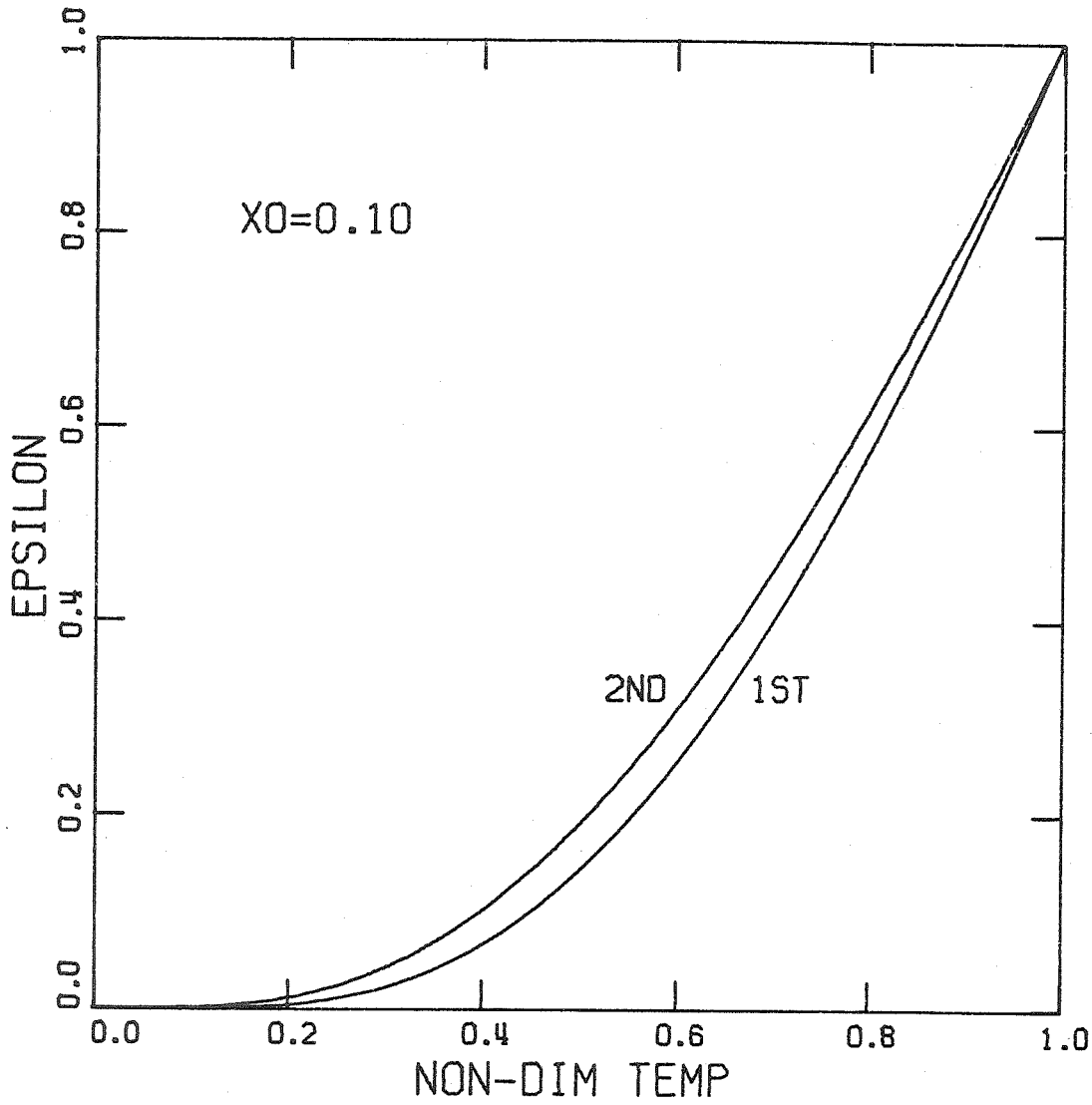

Figure 5-4. The Mass Flux Fraction, ϵ_4, as a Function of the Non-dimensional Temperature, θ, for the Case of $X_0 = 0.10$.

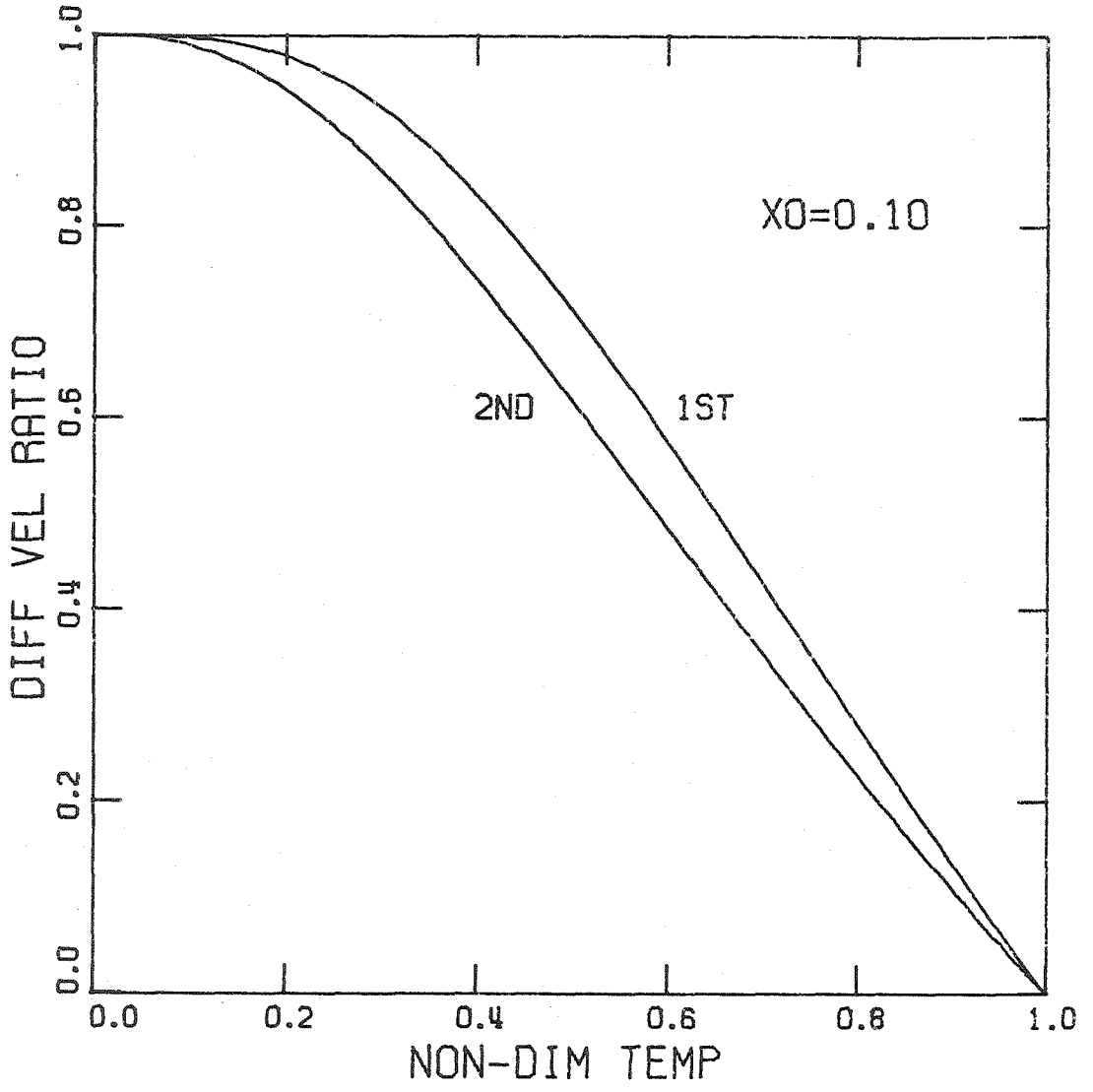

Figure 5-5. The Diffusion Velocity Ratio, V/v , as a Function of Non-dimensional Temperature, θ, for the Case of $X_0 = 0.10$.

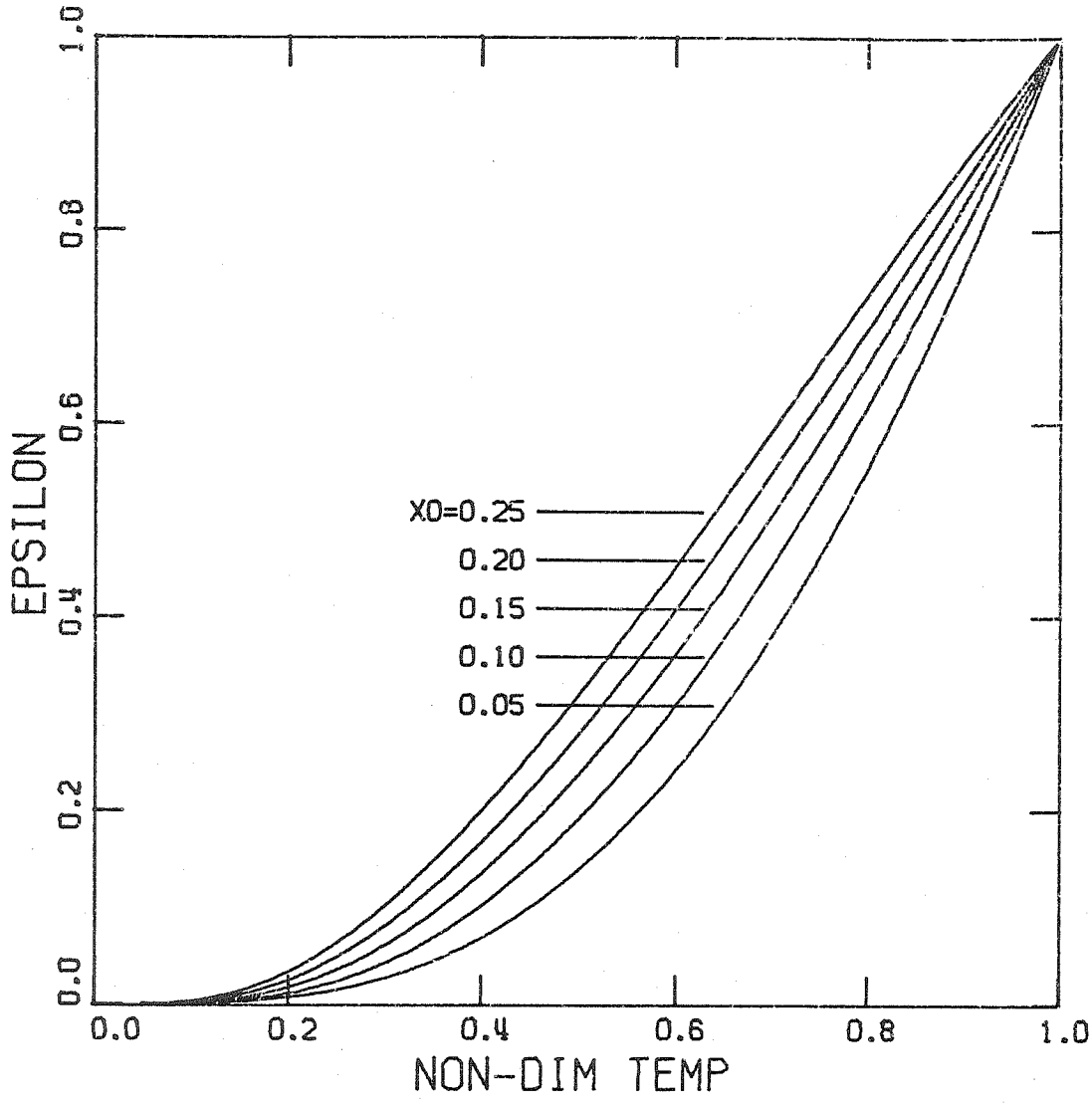

Figure 5-6. The Mass Flux Fraction, ε_4, of the Second von Kármán Approximation as a Function of Non-dimensional Temperature with X_0 as a Parameter.

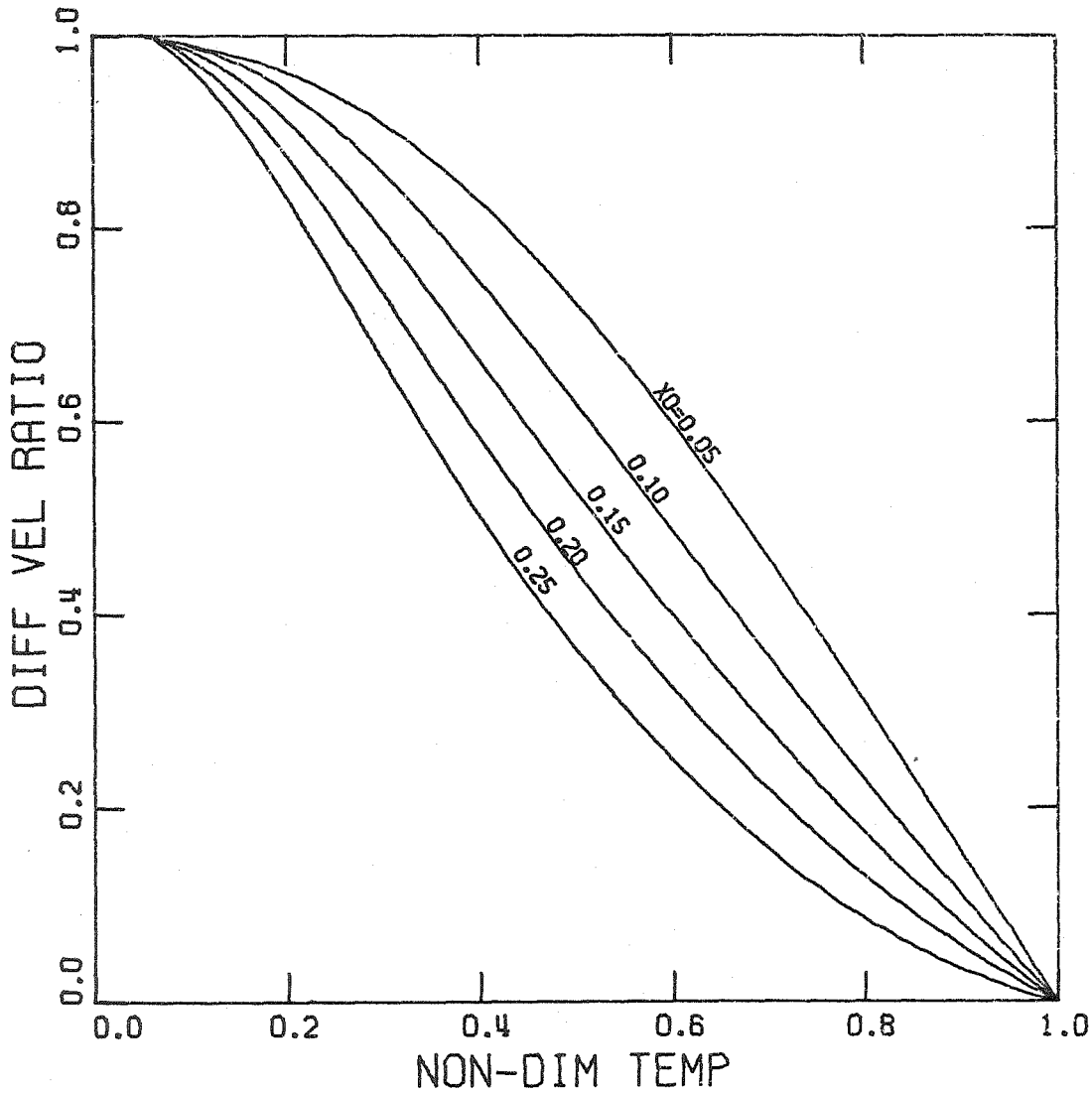

Figure 5-7. The Diffusion Velocity Ratio, V/v , of the Second von Kármán Approximation as a Function of Non-dimensional Temperature with X_0 as a Parameter.

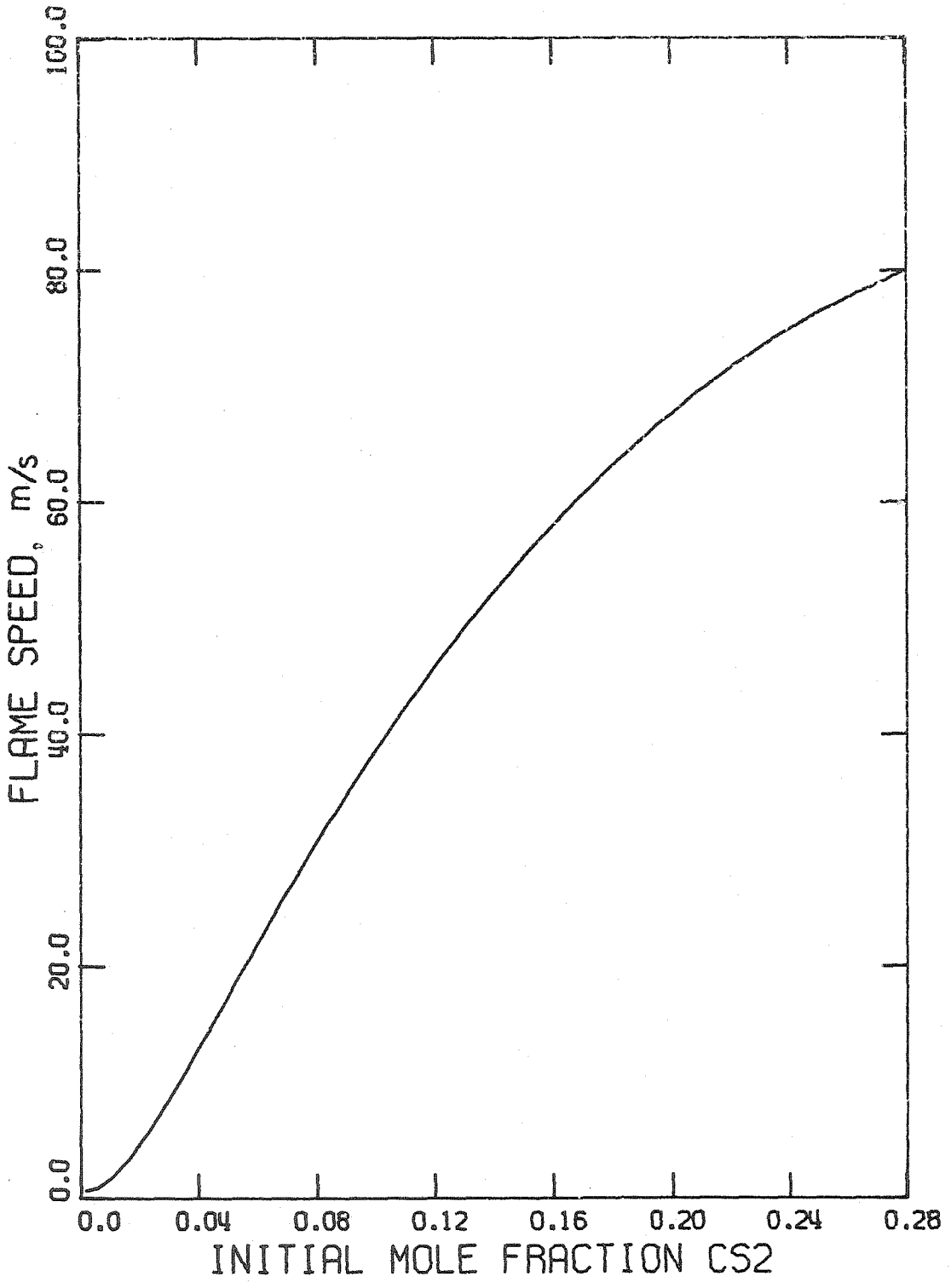

Figure 5-8. The Flame Speed Calculated from the Second von Kármán Approximation.

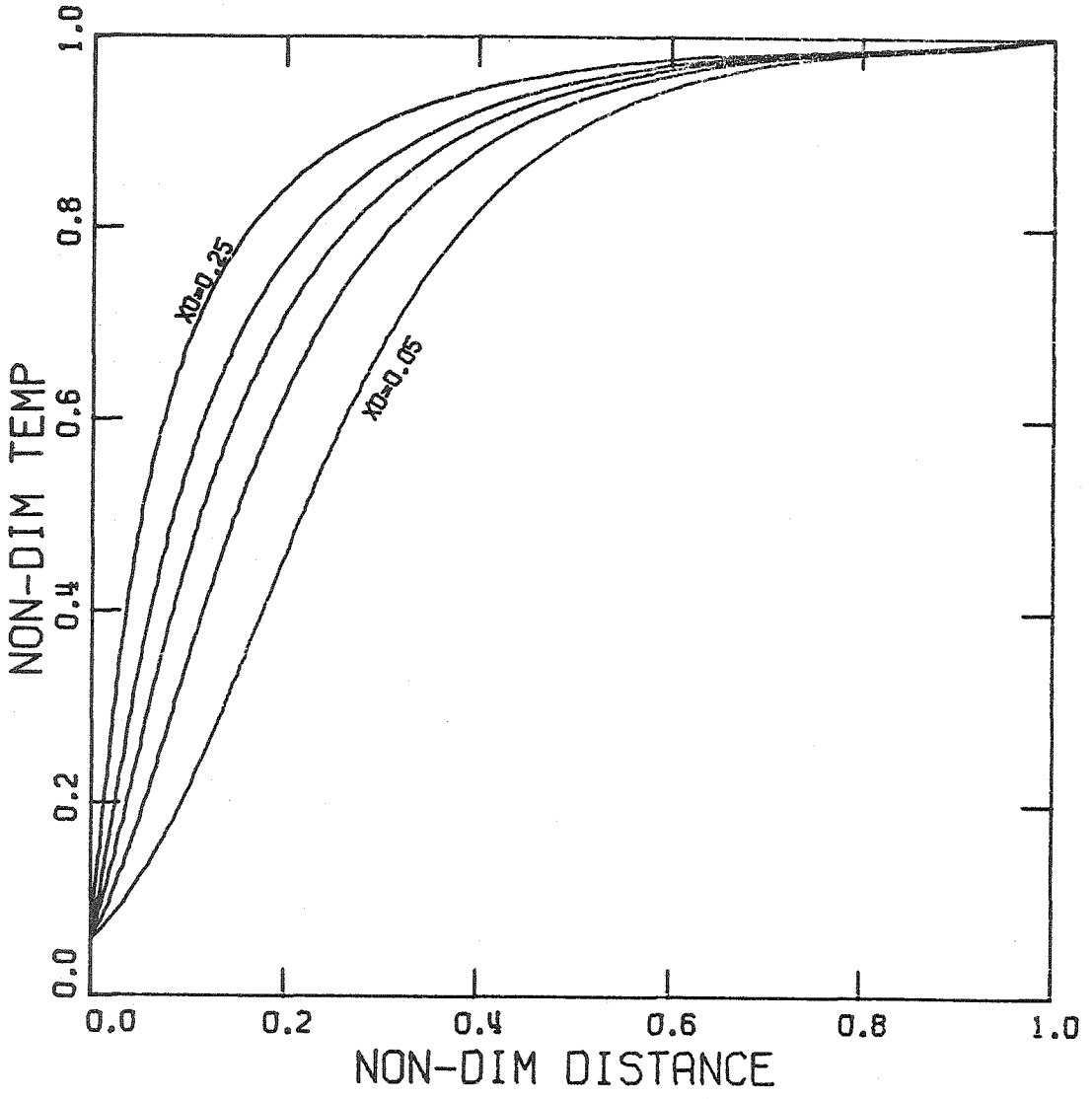

Figure 5-9. The Temperature Profile for the Second von Kármán Approximation with X_0 as a Parameter. The Flame Thicknesses, Which Non-dimensionalize the Distance, Are 1.6, 1.5, 1.9, 2.7, and 4.9 mm for X_0 of 0.05, 0.10, 0.15, 0.20, and 0.25, Respectively.

6. THERMAL THEORY APPROXIMATION TO THE CS_2/O_2 FLAME

The modeling of chemical reactions for lasers often involves complicated chemical kinetic schemes but the basic feedback mechanisms of the flame are ignored. These mechanisms of thermal conduction and diffusion distinguish a flame from a mass of rapidly moving gas which happens to be undergoing chemical change. For the CS_2/O_2 flame, both mechanisms can be important; thermal conduction upstream provides the heat which enables the reaction to proceed at a rapid rate, and diffusion provides the chain carriers required for the initiation of the chain reaction. In the extreme of the low-pressure isothermal diffusion flame, where the O_2/CS_2 ratio is large, the diffusion mechanism is dominant. For CS_2/O_2 flames with large flame temperatures, the heat conducted upstream provides for chain initiation with the unimolecular decay of the CS_2 molecule.

The model in which diffusion is neglected is called the thermal theory. This model as applied to the CS_2/O_2 laser will be discussed in this chapter and examples given for a simplified kinetic scheme. The assets, limitations, and explicit assumptions of the thermal theory are listed in Table 6-1. A model, which will be termed the single-species diffusion approximation, which allows for consideration of back-diffusion of one chain carrier while maintaining the ease of calculation of the thermal theory, is developed in Chapter 7. The object of these developments is to provide a model which contains the essence of the flame structure (and eventually laser kinetics) without the difficulties of a complete numerical solution

of the basic equations.

6.1 Thermal Theory Formulation

The one-dimensional thermal theory model which will be considered will treat the steady-state flame which has no body forces and no loss of energy by radiative heat transfer. Besides the assumption of negligible diffusion, the less important assumption of negligible bulk viscosity shall be made. Consider the case of the slow laminar flame, so that the velocity term can be ignored in the momentum equation and the flame can be considered isobaric. The continuity equation can be integrated to obtain

$$\rho v = m \quad , \text{ a constant} , \tag{6.1}$$

where ρ is the mass density, v is the mean flow velocity, and m is the mass flux. The energy equation can also be integrated to find that

$$m \sum_{i=1}^{N} h_i Y_i - \lambda \frac{dT}{dz} = mC_3 \quad , \quad \text{another constant} , \tag{6.2}$$

where Y_i is the mass fraction of species i.

The conservation of species is represented by

$$\frac{dY_i}{dz} = \frac{w_i}{m} \tag{6.3a}$$

$$w_i = W_i \sum_{\ell=1}^{M} (\nu''_{i,\ell} - \nu'_{i,\ell}) K_\ell \prod_{j=1}^{N} \left(X_j \frac{p}{RT} \right)^{\nu'_{j,\ell}} \tag{6.3b}$$

The ideal gas law provides an additional relation:

$$\frac{p}{R} = \frac{\rho T}{\overline{W}} \quad , \text{ a constant} . \tag{6.4}$$

Assume that the reactions go to equilibrium or completion; then X_i would be known. The final temperature, T_f, being the

flame temperature could then be calculated from standard thermodynamic tables, as explained in the previous chapter. Then the constant C_3 can be evaluated at the final condition, where the temperature derivative vanishes,

$$C_3 = \sum_{i=1}^{N} h_{if} Y_{if} \quad . \tag{6.5}$$

The cold boundary difficulty appears in this model due to an alternate evaluation of C_3 at the cold boundary:

$$C_3 = \sum_{i=1}^{N} h_{i0} Y_{i0} \quad . \tag{6.6}$$

This problem can be removed by any of a few equivalent techniques; the one used here will be the ignition temperature. The calculation will then have the boundary condition of the temperature being equal to the ignition temperature, T_I, at the spatial origin.

Transform the distance coordinate z to a new coordinate, $\zeta = z/m$, so that the equations become

$$\begin{aligned} \frac{dT}{d\zeta} &= m^2 \left[\frac{\sum_{i=1}^{N} h_i Y_i - \sum_{i=1}^{N} h_{if} Y_{if}}{\lambda} \right] \\ \frac{dY_i}{d\zeta} &= w_i \qquad\qquad i = 1, \ldots, N \end{aligned} \tag{6.7}$$

where Y_{i0}, T_I, and T_0 are to be specified, and then by the requirement of equilibrium or completion the Y_{if} are specified. The set of nonlinear equations, equations (6.7), is an eigenvalue problem with m^2 as its eigenvalue. Since the w_i are non-linear (except for the case of unimolecular decomposition), the powerful techniques for solution of the linear equations are not available, and hence these equations must be solved by other methods suitable to two-point boundary

value problems.

At the hot boundary the equations (6.7) must satisfy

$$\frac{dT}{d\zeta} \to 0 \ , \quad T \to T_f \ , \quad \text{and} \quad Y_i \to Y_{if} \quad . \tag{6.8}$$

The most important of these conditions is the last, since it implies both of the first two.

Define the molar enthalpy H_i as

$$H_i = W_i h_i \quad . \tag{6.9}$$

Since the mass fraction can be written in terms of the mole fraction,

$$Y_i = \frac{W_i X_i}{\overline{W}} \quad , \tag{6.10}$$

the enthalpy sum can be written as

$$\sum_{i=1}^{N} h_i Y_i = \frac{1}{\overline{W}} \sum_{i=1}^{N} H_i X_i \quad . \tag{6.11}$$

Substituting equation (6.10) into (6.7), the mass fractions can be eliminated. The resulting equations are

$$\frac{dT}{d\zeta} = m^2 \left[\frac{\frac{1}{\overline{W}} \sum_{i=1}^{N} H_i X_i - \frac{1}{\overline{W}_f} \sum_{i=1}^{N} H_{if} X_{if}}{\lambda} \right] \tag{6.12}$$

$$\frac{dX_i}{d\zeta} = \overline{W} \sum_{\ell=1}^{M} (\nu''_{i,\ell} - \nu'_{i,\ell}) K_\ell \prod_{j=1}^{N} \left(X_j \frac{p}{RT} \right)^{\nu'_{j,\ell}} \quad , \tag{6.13}$$

$$i = 1, \ldots, N$$

which is to be applied from the initial conditions of $X_i = X_{i0}$ and $T = T_I$ (the ignition temperature) to $T = T_f$ and $X_i = X_{if}$. The N+1 equations (6.12) represent an eigenvalue problem for the N+1 variables X_i and T, with the flame speed proportional to the square root of the

eigenvalue.

6.2 Numerical Solution

Numerical results have been obtained for the thermal theory approximation. The shooting method for solution of two-point boundary problems[156] was employed with the first two terms of a Taylor's expansion as the stepping method. The stepping in distance begins at $\zeta = 0$, with the temperature at the ignition temperature. The step size in ζ is varied according to the distance required for the temperature to rise a fixed amount. This is equivalent to having the temperature as the independent variable and the distance determined from equation (6.12).

To evaluate the thermal theory approximation, choose the four-reaction scheme

$$CS_2 + O \rightarrow CS + SO \qquad 1$$

$$CS + O \rightarrow CO + S \qquad 2$$

$$S + O_2 \rightarrow SO + O \qquad 3$$

$$SO + O_2 \rightarrow SO_2 + O \qquad 4$$

to represent the kinetics of the flame with the rate constants given by

$$\begin{aligned} K_1 &= 5 \times 10^7 \exp\left(-\frac{960\ K}{T}\right) \quad m^3\ mol^{-1}\ s^{-1} \\ K_2 &= 1 \times 10^8 \quad m^3\ mol^{-1}\ s^{-1} \\ K_3 &= 1 \times 10^7 \exp\left(-\frac{2800\ K}{T}\right) \quad m^3\ mol^{-1}\ s^{-1} \\ K_4 &= 4 \times 10^5 \exp\left(-\frac{3300\ K}{T}\right) \quad m^3\ mol^{-1}\ s^{-1} \end{aligned} \qquad (6.15)$$

The initial thermodynamic conditions chosen are temperature of 300 K and a pressure of 1.0 kPa. The initial mole fractions are based on the desired ratio of O_2/CS_2 and then on the steady-state approxima-

tions for the intermediate species. Since there are no thermal decomposition reactions in this kinetic scheme, a non-zero initial concentration of intermediate species is required to initiate the combustion. The initial mole fraction of the product CO is taken as zero, while the initial mole fraction of SO_2 is chosen to conserve atoms from a mixture which contained only CS_2 and O_2 molecules.

The enthalpies are obtained from integration of a least-squares fit of standard heat capacity data[25] to the three-parameter form

$$C_{pi} = a_{2i} + a_{3i}T + a_{4i}T^{-2} \qquad (6.16)$$

for the range of temperature from 300 K to 5000 K. The enthalpies are then given by

$$H_i = a_{1i} + a_{2i}T + \tfrac{1}{2}a_{3i}T^2 - a_{4i}T^{-1} \quad . \qquad (6.17)$$

The thermal conductivities for the individual gases have been fitted to a square-root temperature dependence[86] with a multiplicative factor correction which is applicable for the polyatomic species (ref. 157). The form for the polyatomic species is

$$\lambda_i = \ell_i \sqrt{T} \left[0.354 \frac{C_{pi}}{R} + 0.115 \right], \qquad (6.18)$$

where the approximately $T^{1/3}$ variation of the reduced transport integral with reduced temperature[158] has been ignored. The form for the monatomic species shows only the square root dependence on temperature,

$$\lambda_i = \ell_i \sqrt{T} \quad . \qquad (6.19)$$

The heat conductivity constants ℓ_i for the species O_2 and CO are based on experimental data at 1500 K [159] and for SO_2 on a datum at

900 K.[160] The constants ℓ_i for the remaining species were determined from the functional form[86]

$$\ell_i = \frac{2.63 \times 10^{-23}}{\sigma^2 \sqrt{W_i}} \text{ W m kg}^{\frac{1}{2}} \text{ K}^{-\frac{3}{2}} \text{ mol}^{-\frac{1}{2}} , \qquad (6.20)$$

where σ is the effective molecular diameter. The molecular diameter for CS_2 was taken as 4.44×10^{-10} m from a Lennard-Jones potential fit.[86] The effective diameters for oxygen and sulfur were taken from a table of atomic radii.[161] The molecular diameters for CS and SO were estimated at 4×10^{-10} m. The heat conductivity of the mixture of gases is taken as the homogeneous case,

$$\lambda = \sum_{i=1}^{N} \lambda_i X_i \quad . \qquad (6.21)$$

The logic and details of the computer program which calculates the thermal theory approximation are explained in Appendix B. The values of the constants a_{ji} and ℓ_i can be found in this appendix. The input variables chosen for the sample calculation to be displayed are as follows: step size is 0.05 K, O_2/CS_2 ratio of 10, and the initial relative volumes of

O_2	1.00	SO_2	4.31×10^{-3}
CS_2	9.57×10^{-2}	S	9.09×10^{-8}
CS	4.34×10^{-3}	SO	1.59×10^{-5}
CO	0.0	O	1.91×10^{-9}

The eigenvalue which satisfies the final conditions is 4.2125×10^{-5} kg^2 m^{-4} s^{-2}, which implies a flame speed of 0.450 m s^{-1}. The flame temperature for this composition is 1696.3 K. The temperature profile displays the expected sigmoidal shape, as shown

in Figure 6-1. The flame thickness of 56.5 mm can be found from this figure. The species mole fractions are given as a function of distance in Figure 6-3. The approximately steady values of the mole fractions of the species SO and CS should be noted, as should the rapid rise of atomic oxygen. The production rate of carbon monoxide as a function of distance is displayed in Figure 6-3. It can be seen that the highest production rate is found towards the end of the combustion process, with a coincident peak of CS mole fraction as can be determined from Figures 6-2 and 6-3.

6.3 Sensitivity of Numerical Results

The influence on the results of the thermal theory approximation by the choice for some of the critical parameters is found by calculation of the influence coefficients in the form

$$\frac{\partial A}{A} = \alpha_A \frac{\partial q}{q} \quad . \tag{6.22}$$

This form is discussed in Chapter 5. Two dependent variables, the eigenvalue, A , and maximum rate of production of CO, R_2 , were chosen to represent the influence of parameters on the calculations. First, the step size was increased by a factor of 2 to yield the influence coefficients α_A and α_{R_2} along with the influence coefficient for the flame speed, α_v , which are given in Table 6-2. Since the results show that the step size has little influence, the remaining calculations were made at the larger step size, 0.1 K. The ignition temperature was varied by decreasing the difference between the ignition and initial temperatures, and the reaction rates were varied by increasing the reaction rates by 10 per cent. The influence coefficients for these parameters are also given in Table 6-2. The only

reaction rate which cannot be considered as a limiting rate is K_3, the rate of the chain branching reaction, $S + O_2 \rightarrow SO + O$.

The approximate influence coefficients for the flame thickness, α_z, have also been calculated, and are given in Table 6-2. These influence coefficients are not to be considered as significant as the other coefficients. The flame thickness depends inversely on the enthalpy difference, which goes to zero as the temperature approaches the flame temperature. Consequently, as the reaction nears completion, the step size in distance becomes large with the final distance dependent on when the computation terminates.

To test the dominance of the four-reaction scheme, two double chain terminating reactions

$$O + SO + M \rightarrow SO_2 + M \qquad 5$$

$$O + O + M \rightarrow O_2 + M \qquad 6$$

were taken into consideration. Since these reactions do not conserve the number of moles, the computer program THERMAL was rewritten to calculate the thermal theory approximation based on equation(6.7). The rate of reaction chosen for the additional reactions are

$$K_5 = 3.2 \times 10^5 \ m^6 \ mol^{-2} \ s^{-1}$$

$$K_6 = 1.37 \times 10^6 \ T^{-1} \exp\left(-\frac{171 \ K}{T}\right) \ K \ m^6 \ mol^{-2} \ s^{-1} \qquad (6.23)$$

Adding these reactions, the thermal theory approximation made little difference in the species concentration profiles or the maximum rate of production of CO, R_2. The eigenvalue increased slightly, about 15 per cent, while the flame thickness increased by around a factor of 2. The flame thickness increase is due mostly to the extension of the definition of the flame thickness to include oxygen recombination.

TABLE 6-1. Characteristics of the Thermal Theory Approximation

Assets

1. Intermediates as important as major species.
2. Provides a good approximation for flame with a large temperature gradient.
3. Chemical kinetics are uncoupled from energy balance.

Assumptions

1. Diffusion effects are negligible.
2. Standard removal of the cold boundary difficulty.
3. Transport properties are the same as for an ideal homogeneous mixture.

Limitations

1. Ignores diffusion.
2. Large computational capability required for large reaction schemes.
3. Not applicable to isothermal phenomena.

TABLE 6-2. Influence Coefficients for the Thermal Theory Calculations

Parameter q	10^5 A ($kg^2 m^{-4} s^{-2}$)	$(R_2)_{max}$ ($mol\, m^{-3} s^{-1}$)	z_{max} (mm)	$\frac{\partial q}{q}$	α_A	α_{R_2}	α_v	α_z
ΔT	4.377	14.00	34.4	1.00	0.04	0.005	0.02	-0.4
T_I	4.49	14.00	34.3	-0.1	0.26	0.00	0.13	0.0
K_1	4.19	14.51	33.5	0.1	-0.43	0.36	-0.21	-0.3
K_2	4.665	13.78	31.9	0.1	0.65	-0.16	0.33	-0.7
K_3	4.385	14.08	34.4	0.1	0.02	0.06	0.01	0.0
K_4	4.725	15.03	43.5	0.1	0.80	0.74	0.40	2.7

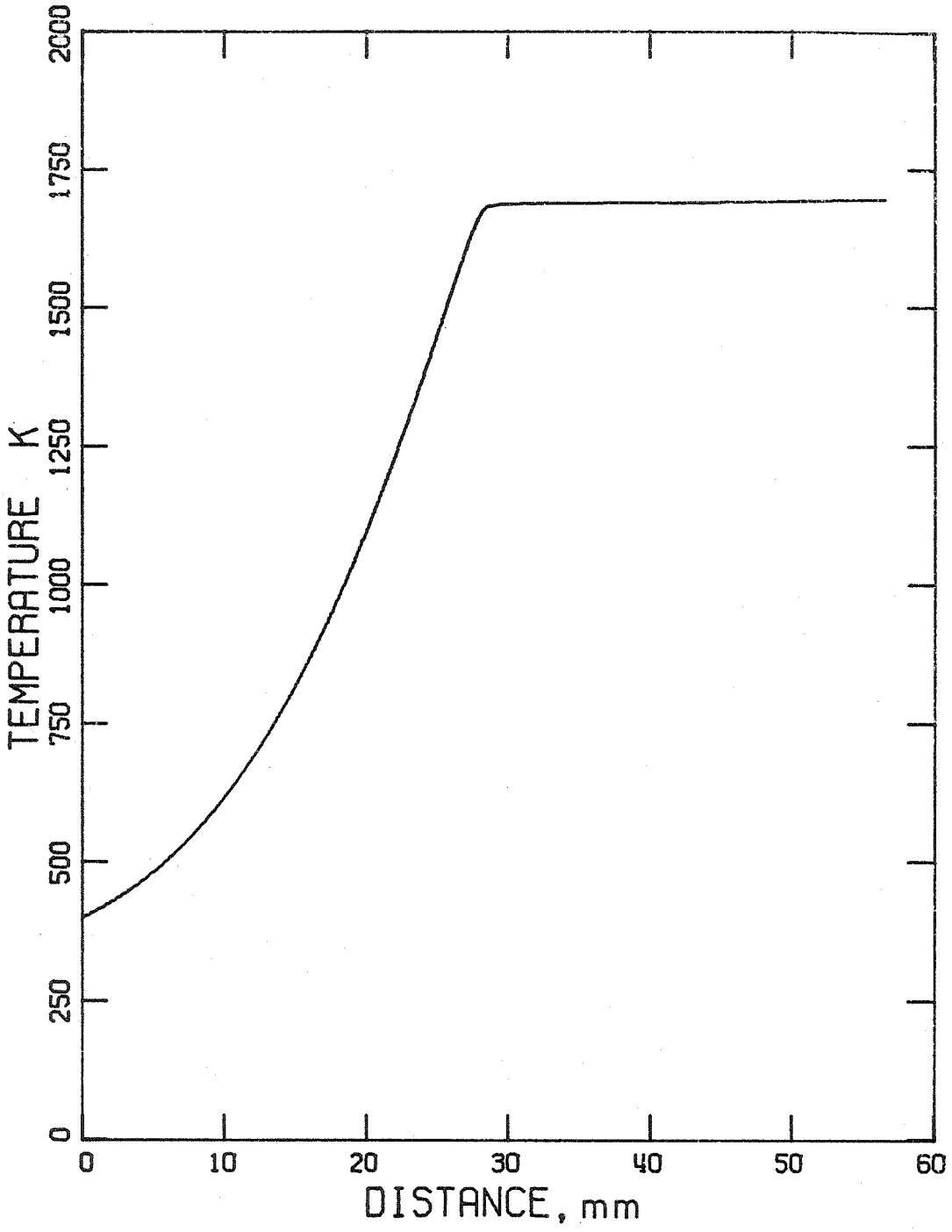

Figure 6-1. The Temperature Profile of the Thermal Theory Approximation for an O_2/CS_2 Ratio of 10.

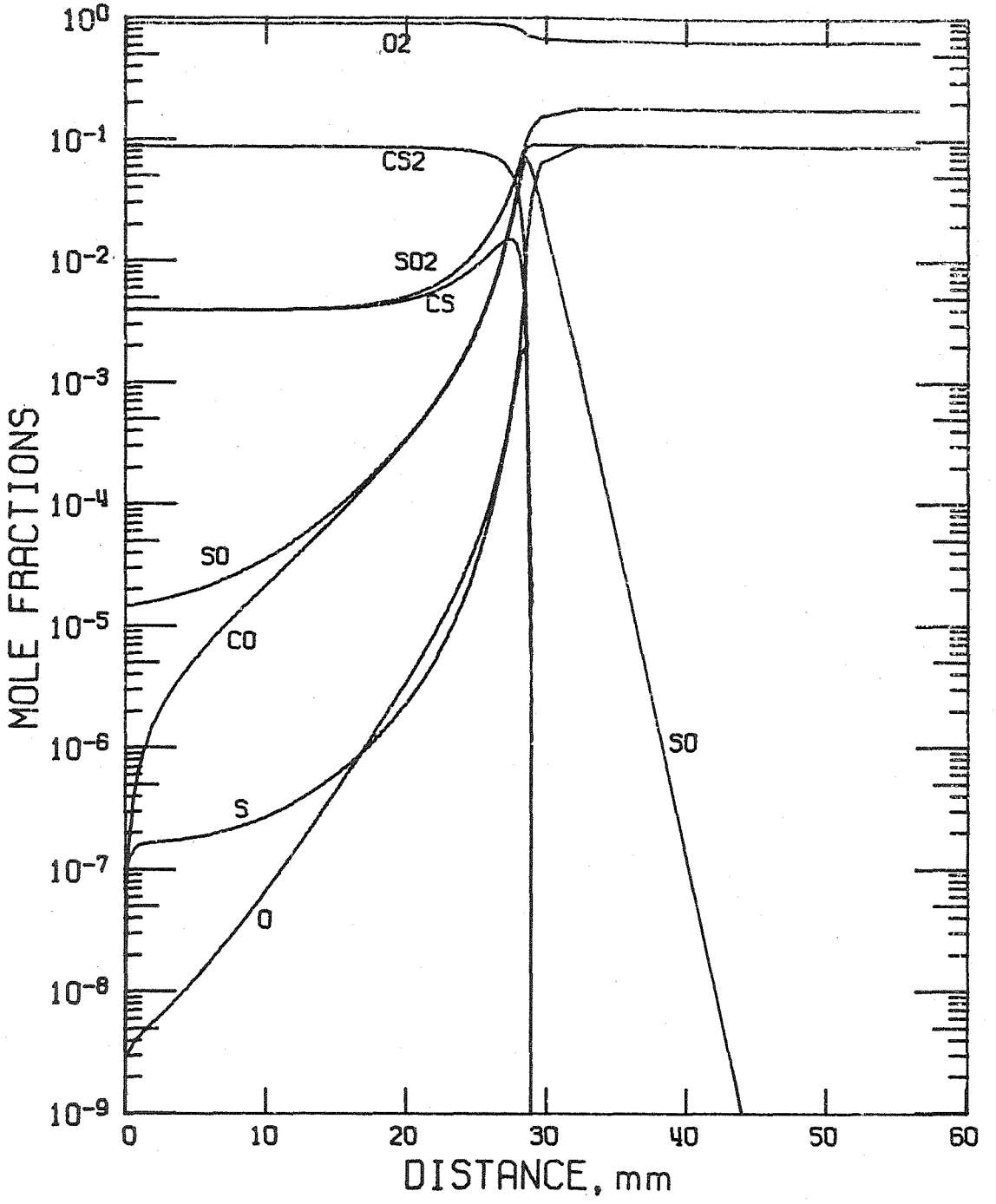

Figure 6-2. The Species Mole Fractions of the Thermal Theory Approximation as a Function of the Distance for an O_2/CS_2 Ratio of 10.

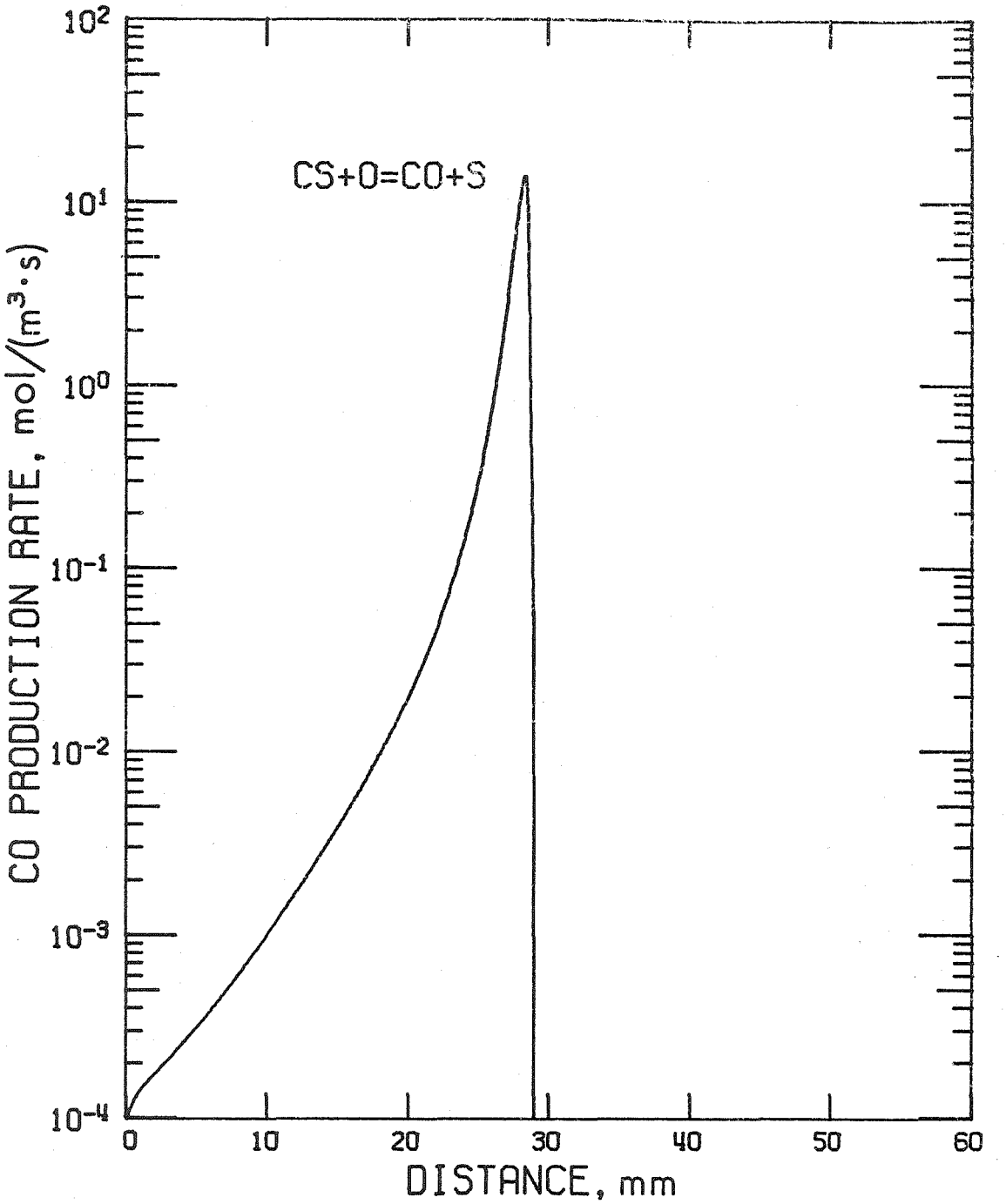

Figure 6-3. The Production Rate of CO from the Thermal Theory Approximation as a Function of Distance from the Ignition Point for the O_2/CS_2 Ratio of 10.

7. SINGLE SPECIES DIFFUSION APPROXIMATION

The typical method for determination of the flame structure from a complicated chemical kinetic scheme ignores the effects of diffusion and thermal conduction in order to provide a first-order, non-linear initial value problem. In flames where combustion occurs by a branching chain mechanism, such as the CS_2/O_2 flame, upstream diffusion of the chain carriers is important and is essential if chain carriers cannot be generated by thermal decomposition. For a flame driven by a chain mechanism mainly based on a single chain carrier, an additional assumption is justified which leads to a significant simplification of the one-dimensional steady flame problem. A method, termed the single species diffusion approximation, which allows for consideration of upstream diffusion of the most important chain carrier while maintaining the form of a first order initial value problem, is developed in this chapter.

This one-dimensional approximation incorporates independent diffusion for only one species, the active center. The diffusion effects of the remaining species are limited to that required for them to compensate for the diffusion of the active center. The single species diffusion approximation shall be developed for two cases; the first case ignores thermal conduction and the second includes it. The former case has application in the limit of isothermal combustion, while the latter is more useful for conditions of the CS_2/O_2 flame laser. The assets, limitations, and major assumptions of the single species diffusion approximations are given in Tables 7-1 and 7-2.

7.1 Formulation

The single species diffusion approximation will be developed for a steady flame with no body forces and no loss of energy by radiative heat transfer. Also, the assumptions of negligible thermal diffusion and negligible bulk viscosity shall be made. Again, the slow laminar flame simplification is made so that the combustion is isobaric. The continuity equation has the same result as for the thermal theory, as given in equation (6.1),

$$\rho v = m \quad , \quad \text{a constant} \quad . \tag{7.1}$$

The energy equation can be integrated and condensed to

$$\sum_{i=1}^{N} h_i \epsilon_i - \frac{\lambda}{m} \frac{dT}{dz} = C_4 \quad , \text{ a constant} \quad , \tag{7.2}$$

where ϵ_i is the mass flux fraction

$$\epsilon_i = Y_i \left(1 + \frac{V_i}{v} \right) \tag{7.3}$$

where V_i is the diffusion velocity of species i. The conservation of species retains the same form as for the thermal theory when written in terms of the mass flux fractions,

$$\frac{d\epsilon_i}{dz} = \frac{w_i}{m} \quad , \tag{7.4a}$$

$$w_i = W_i \sum_{\ell=1}^{M} (\nu''_{i,\ell} - \nu'_{i,\ell}) K_\ell \prod_{j=1}^{N} \left(X_j \frac{p}{RT} \right)^{\nu'_{j,\ell}} \quad . \tag{7.4b}$$

The ideal gas relation of equation (6.4) remains the same for this case,

$$\frac{p}{R} = \frac{\rho T}{\overline{W}} \quad , \text{ a constant} \quad . \tag{7.5}$$

The diffusion condition for one-dimensional flow is given by

$$\frac{dX_i}{dz} = m\left(\frac{RT}{p}\right) \sum_{j=1}^{N} \frac{1}{D_{ij}} \left[X_i \frac{\epsilon_j}{W_j} - X_j \frac{\epsilon_i}{W_i} \right] . \qquad (7.6)$$

For diffusion considerations, the approximation implies there are only two differentiable species, the active center and everything else. Consequently, assume that all of the binary diffusion coefficients are equal,

$$D_{ij} = D , \qquad (7.7)$$

so that equation (7.6) reduces to

$$\frac{dX_i}{dz} = \frac{1}{D} \left[X_i \sum_{j=1}^{N} V_j X_j - V_i X_i \right] . \qquad (7.8)$$

After some manipulation (ref. 154, chapter 1), Fick's law can be deduced from equation (7.8):

$$V_i = -D \frac{d}{dz} [\ell n\, Y_i] \quad , \qquad i = 1, \ldots, N \quad . \qquad (7.9)$$

Let species N be the chain carrier, so that species 1 through N-1 are considered everything else and hence will move with the same diffusion velocity:

$$\begin{aligned} V_i &= -D \frac{d}{dz} [\ell n(1-Y_N)] , \qquad i = 1, \ldots, N-1 \\ V_N &= -D \frac{d}{dz} [\ell n\, Y_N] \end{aligned} \qquad (7.10)$$

The relationship between V_i and V_N can readily be deduced as

$$V_i = -V_N \frac{Y_N}{1-Y_N} \qquad i = 1, \ldots, N-1 \qquad (7.11)$$

Equations (7.11) can be substituted into the definitions of the mass flux fractions to provide N-1 zeroth order relations and one first order relation,

$$Y_i = \epsilon_i \frac{1-Y_N}{1-\epsilon_N} \qquad i = 1, \ldots, N-1 \qquad (7.12)$$

$$\frac{dY_N}{dz} = \frac{v}{D}(Y_N - \epsilon_N) \quad . \tag{7.13}$$

Transform the distance coordinate, z, to the coordinate $\zeta = z/m$, so that equations (7.2), (7.4a), and (7.13) become

$$\sum_{i=1}^{N} h_i \epsilon_i - \frac{\lambda}{m^2}\frac{dT}{d\zeta} = C_4 \tag{7.14a}$$

$$\frac{d\epsilon_i}{d\zeta} = w_i \qquad i = 1, \ldots, N \tag{7.14b}$$

$$\frac{dY_N}{d\zeta} = \frac{m^2}{\rho D}(Y_N - \epsilon_N) \tag{7.14c}$$

7.2 First Case, Thermal Conduction Ignored

For the first case of the single species diffusion approximation, ignore thermal conduction so that the energy conservation equation, equation (7.14a), becomes

$$\sum_{i=1}^{N} h_i \epsilon_i = C_4' \quad . \tag{7.15}$$

The temperature and distance are implicitly related through this equation. The problem is then

$$\begin{aligned} &\sum_{i=1}^{N} h_i \epsilon_i = C_4' \\ &\frac{d\epsilon_i}{d\zeta} = w_i \qquad i = 1, \ldots, N \\ &Y_i = \epsilon_i \frac{1 - Y_N}{1 - \epsilon_N} \qquad i = 1, \ldots, N-1 \\ &\frac{dY_N}{d\zeta} = m^2 \frac{(Y_N - \epsilon_N)}{\rho D} \end{aligned} \tag{7.16}$$

This formulation of the one-dimensional steady combustion problem has the cold-boundary problem of lack of a priori knowledge

of the initial concentrations of the intermediate species. Although the initial concentrations can be obtained numerically from the unsteady case,[162] the initial concentrations for the intermediate species, except for the chain carrier, shall be approximated from the steady-state approximations on those intermediate species. Thus, assume that the initial concentrations X_{i0} are either given or approximated; then the mass fractions Y_{i0} can readily be found. Assume that no chain carrier is upstream of the flame, so that ϵ_N is initially zero. The mass flux fractions for the other species are obtained from equation (7.12), so that the initial conditions for the ϵ_i are:

$$\epsilon_{i0} = \frac{Y_{i0}}{1-Y_{N0}} \qquad i = 1, \ldots, N-1$$
$$\epsilon_{N0} = 0 \tag{7.17}$$

The set of 2N+1 non-linear equations, equations (7.16), for the 2N+1 variables Y_i, ϵ_i, and T along with the given initial conditions for Y_i and the initial conditions (7.17) represent an eigenvalue problem with m^2 as the eigenvalue. The flame speed is proportional to the square root of the eigenvalue.

7.3 Second Case, Thermal Conduction Considered

For the case of the single species diffusion approximation which considers thermal conduction, assume that the Lewis number

$$Le = \frac{\rho D \bar{C}_p}{\lambda} \tag{7.18}$$

is equal to unity. Then this problem becomes

$$\begin{aligned}
\frac{dT}{d\zeta} &= m^2 \frac{\sum_{i=1}^{N} h_i \epsilon_i - C_4}{\lambda} \\
\frac{d\epsilon_i}{d\zeta} &= w_i \qquad\qquad i = 1, \ldots, N \\
Y_i &= \epsilon_i \frac{1-Y_N}{1-\epsilon_N} \qquad\qquad i = 1, \ldots, N-1 \\
\frac{dY_N}{d\zeta} &= m^2 \frac{C_p}{\lambda} (Y_N - \epsilon_N)
\end{aligned} \tag{7.19}$$

The constant C_4 can be evaluated at the final condition, where the temperature derivative vanishes. At the final condition, the diffusion velocities vanish so that the final mass flux fractions are equal to the final mass fractions. Thus, as for the thermal theory,

$$C_4 = \sum_{i=1}^{N} h_{if} Y_{if} \ . \tag{7.20}$$

This formulation still has the cold-boundary problem of a priori knowledge of the initial concentrations of the intermediate species, but also has the flame holder problem. The ignition temperature technique will be used to solve the flame holder problem, so that the temperature is to be taken as the ignition temperature, T_I, at the spatial origin. The initial concentration considerations are the same as discussed for the previous case.

The set of 2N+1 non-linear equations, equations (7.19), for the 2N+1 variables ϵ_i, Y_i, and T along with the given conditions for Y_i, the initial conditions of (7.17), and the ignition temperature, represent an eigenvalue problem with m^2 as the eigenvalue. The flame speed is again proportional to the square root of the eigenvalue.

7.4 Numerical Solution

Numerical results have been obtained for the single species diffusion approximation. Many of the numerical techniques which were applied to the thermal theory approximation of Chapter 6 shall be applied to the single species diffusion approximation. The shooting method for solution of two-point boundary value problems was employed with the first two terms of a Taylor's expansion as the stepping method. The stepping in distance begins at $\zeta = 0$, and the step size in ζ is varied according to the distance required for the temperature to rise a fixed amount; this is equivalent to having the temperature as the independent variable and the distance determined from equation (7.15).

The four-reaction chain mechanism developed in Chapter 1 is again employed with the rate constants given in equations (6.15). The heat capacities are determined from the least-squares fit to the three-parameter form given by equation (6.16) with the average heat capacity, C_p, given by

$$\overline{C}_p = \frac{1}{\overline{W}} \sum_{i=1}^{N} X_i C_{pi} \quad . \tag{7.21}$$

The enthalpies are determined from integration of equation (6.16) and are given in the four-parameter form of equation (6.17). The thermal conductivity of the mixture is determined in the same manner as for the thermal theory approximation as given by equations (6.18) through (6.21). The combination ρD is assumed to have a square root dependence on temperature,

$$\rho D = \rho_0 D_0 (T/T_0)^{\frac{1}{2}} \tag{7.22}$$

since kinetic theory predicts a $T^{3/2}$ dependence of the diffusion coefficient.[143] The value of D_0 is determined in the same manner as for the von Kármán approximations of Chapter 5, from equation (5.49).

The logics and details of the computer programs which calculate the single species diffusion approximation are explained in Appendix C. The values of the input parameters which are chosen for a sample calculation of the case which ignores heat conduction are as follows: O_2/CS_2 ratio of 10, pressure of 1.0 kPa, step size of 0.1 K, initial temperature of 300 K, and the initial relative volume of

O_2	1.00	SO_2	4.28×10^{-3}
CS_2	9.57×10^{-2}	S	4.40×10^{-7}
CS	4.34×10^{-3}	SO	5.83×10^{-6}
CO	0.0	O	1.91×10^{-9}

The final conditions which must be satisfied by the calculation are determined by consideration of equations (7.16) at the hot boundary. Since the four-reaction scheme does not contain any reverse reactions, the chemistry must go to completion, as opposed to equilibrium. At completion, the distance derivatives should vanish. When all of the fuels are reacted, then the rates of species production or destruction, w_i, all vanish so that final condition on the second of equations (7.16) will be satisfied. It is therefore the last of equations (7.16) which provides the boundary condition at the hot boundary. This condition is the equality of the mass flux fraction and mass fractions for species N, which implies that the mass flux fractions and mass fractions of each of the species are equal.

This implies, from equation (7.3), that the diffusion velocities must be zero. Since these velocities are related through equation (7.11), the actual boundary condition to be applied at the hot boundary is the vanishing of the diffusion velocity, V_N. If this condition is satisfied at the hot boundary, then all of the other conditions which are associated with completion (or equilibrium) will be satisfied.

The eigenvalue which satisfies equations (7.16) and the initial and final conditions mentioned above is 2.765×10^{-4} kg^2 m^{-4} s^{-2}, which implies a flame speed of 1.15 m s^{-1}. The temperature profile, illustrated in Figure 7-1, indicates a thin flame zone with large gradients. The flame thickness from the initial conditions to the final conditions is 57.2 mm, but the zone which has significant combustion has a thickness of less than 2 mm. This zone may best be gauged by consideration of the rate of production of CO, given in Figure 7-2, which changes six orders of magnitude in about 2 mm. The mole fractions of the species are given as a function of distance in Figure 7-3. The maximum rate of production of CO can be seen to coincide with the maximum concentration of CS by comparison of Figure 7-2 and 7-3. The cause of the relatively slow temperature rise after the rapid jump can be identified as SO oxidation by noting the slow decay of SO in Figure 7-3. The negative of the ratio of diffusion velocity to flame speed,

$$-V_N/v \quad , \tag{7.23}$$

is shown in Figure 7-4 as a function of temperature. Although the diffusion speed of the active center is much faster than the flame speed, the concentration of the active center is small, so that the

diffusion velocity ratio for the other species, as related by equation (7.11), remains small.

7.5 Sensitivity of the Numerical Calculation

The influence on the results of the single species diffusion approximation by the choice for some of the critical parameters is found by calculation of the influence coefficients in the form given by equation (6.22). Two dependent variables, the eigenvalue, A, and the maximum rate of production of CO, R_2, were chosen to represent the influence of the parameters. The parameters which are most important to the single species diffusion approximation are the step size, initial concentration of atomic oxygen, and the four reaction rates. These six parameters were increased by 10 per cent, one at a time, and the corresponding eigenvalues were determined. The influence coefficients of the six parameters on the two variables are given in Table 7-3. Both the step size and initial concentration of atomic oxygen have little influence on the calculation, at least near the values chosen for the sample calculation. The only reaction rate which has a significant influence is K_4; therefore, the reaction between SO and O_2 must be the limiting reaction in this calculation.

TABLE 7-1. Characteristics of the Single Species Diffusion Approximation with Thermal Conduction Ignored

Assets

1. Intermediates as important as major species.
2. Chain reactions with a single active center can be represented.
3. Two-point boundary value problem can be solved as an initial value problem in a manner which is consistent with standard kinetic programs.

Assumptions

1. Diffusion of only one species is significant.
2. Diffusion effect is the same as if there were a binary mixture.
3. Heat transfer by conduction is ignored.

Limitations

1. Large computational capability required for large reaction schemes.
2. Only one chain carrier allowed.
3. Thermal conduction ignored.

TABLE 7-2. Characteristics of the Single Species Diffusion Approximation with Thermal Conduction Considered

Assets

1. Intermediates as important as major species.
2. Chain reactions with a single active center can be represented.
3. Two-point boundary value problem can be solved as an initial value problem in a manner which is consistent with standard kinetic programs.

Assumptions

1. Diffusion of only one species is significant.
2. Diffusion effect is the same as if there were a binary mixture.
3. Lewis number is unity.
4. Cold-boundary problem solved by ignition temperature.

Limitations

1. Large computational capability required for large reaction schemes.
2. Only one chain carrier allowed.

TABLE 7-3. Influence Coefficients for the Thermal Theory Calculation

Parameter q	$10^4 A$ ($kg^2 m^{-4} s^{-2}$)	$(R_2)_{max}$ ($mol\, m^{-3} s^{-1}$)	$\frac{\delta q}{q}$	α_A	α_{R_2}	α_v
ΔT	2.77	79.5	0.1	0.00	0.00	0.00
[O]	2.77	79.5	0.1	0.00	0.00	0.00
K_1	2.78	83.3	0.1	0.04	0.48	0.02
K_2	2.78	79.8	0.1	0.04	0.04	0.02
K_3	2.79	79.3	0.1	0.07	-0.03	0.04
K_4	3.00	83.1	0.1	0.83	0.45	0.42

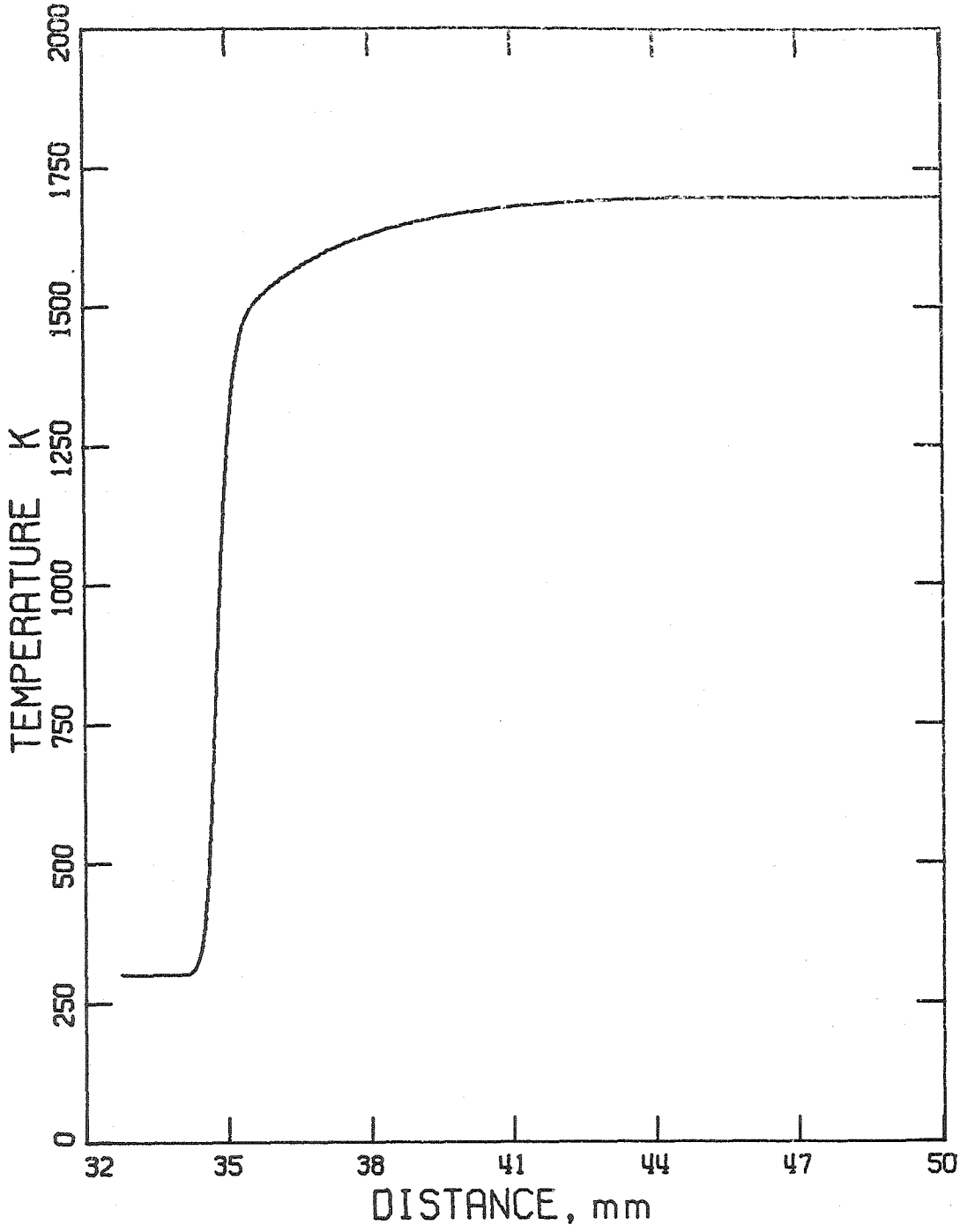

Figure 7-1. Temperature Profile of the Sample Calculation of the Single Species Diffusion Approximation with Heat Conduction Ignored. The O_2/CS_2 Ratio Is 10.

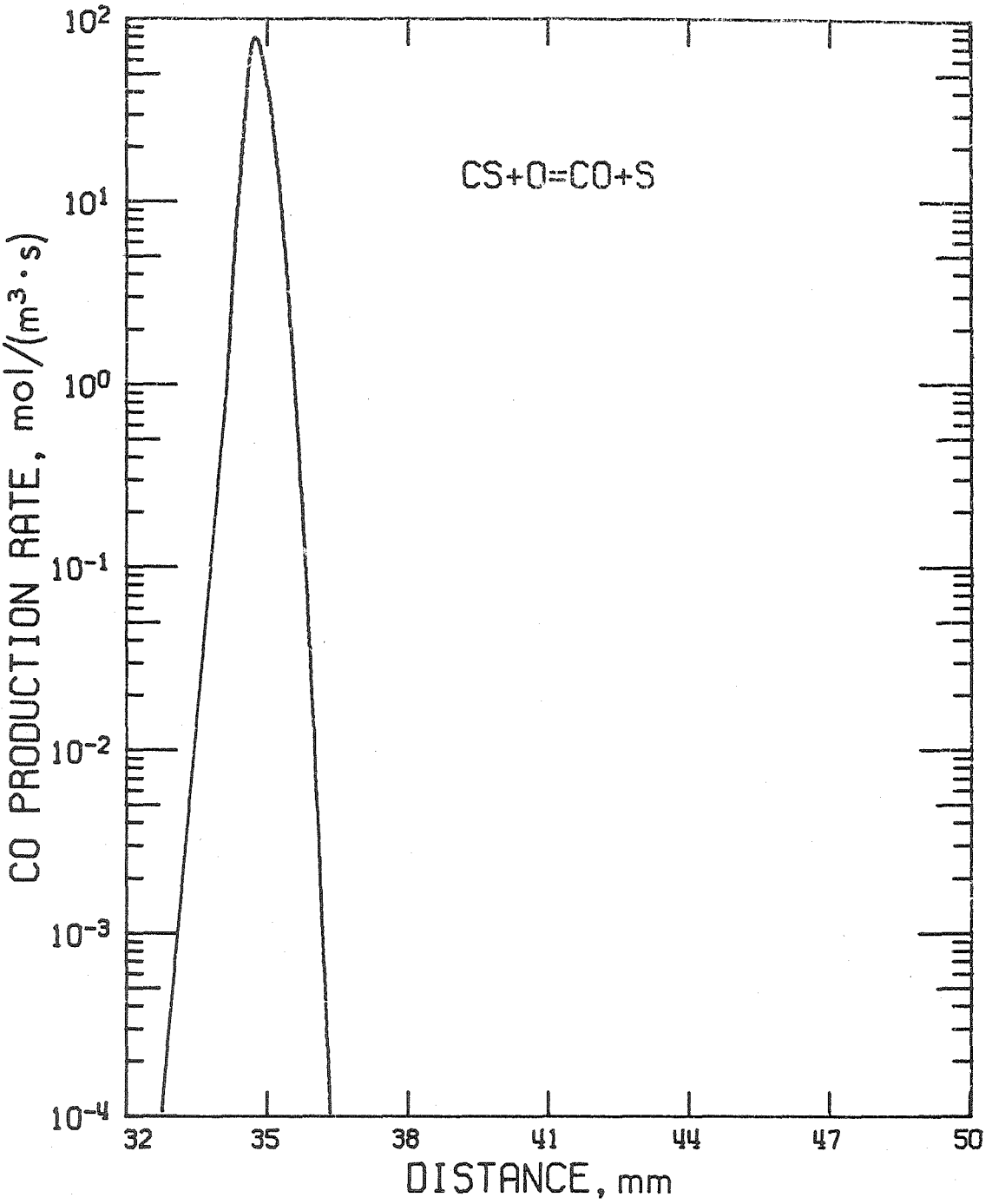

Figure 7-2. The Calculated Rate of Production of CO from the Chemiluminescent Reaction from the Single Species Diffusion Approximation for an O_2/CS_2 Ratio of 10.

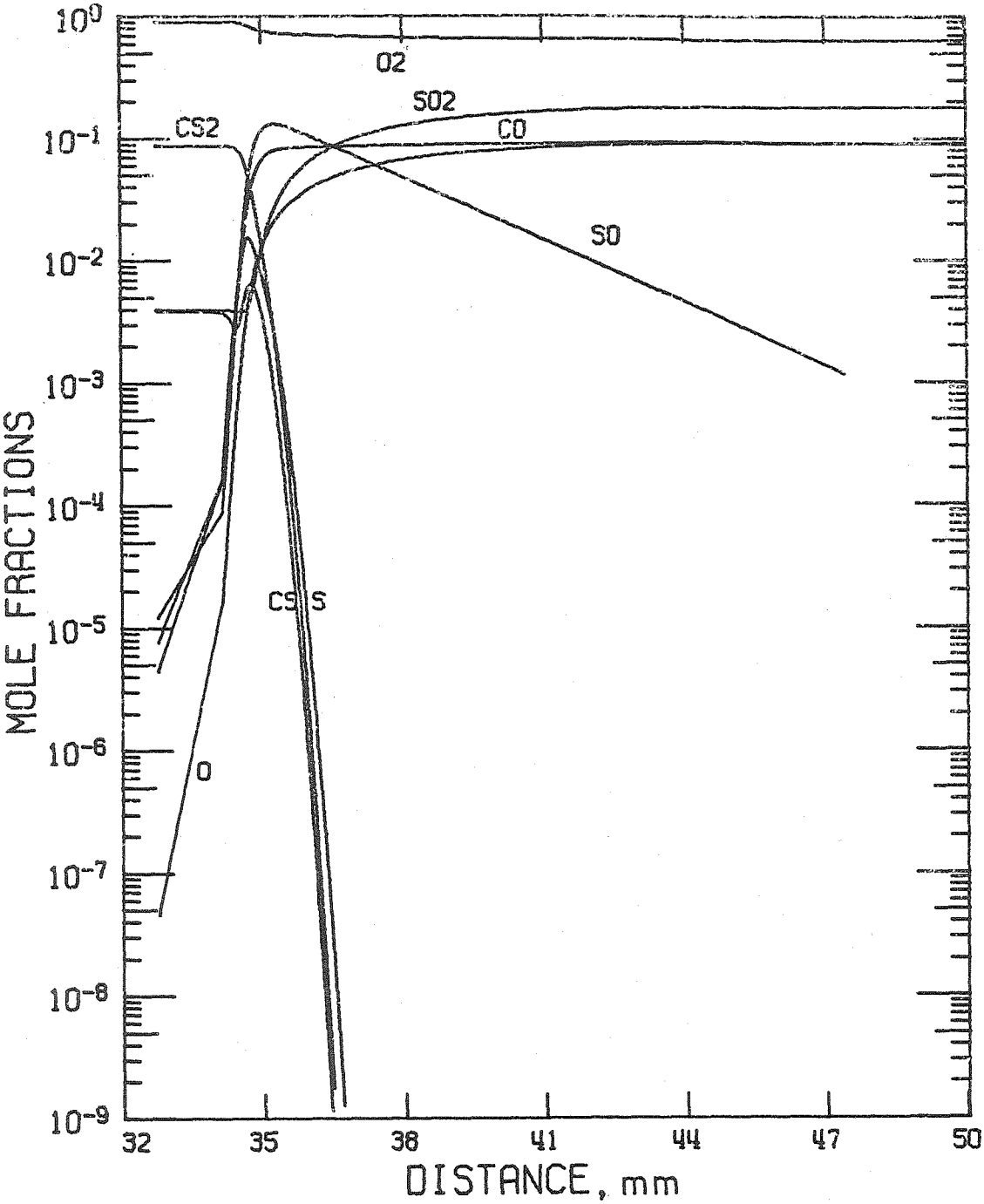

Figure 7-3. The Species Concentration Profiles for the Single Species Diffusion Approximation for an O_2/CS_2 Ratio of 10.

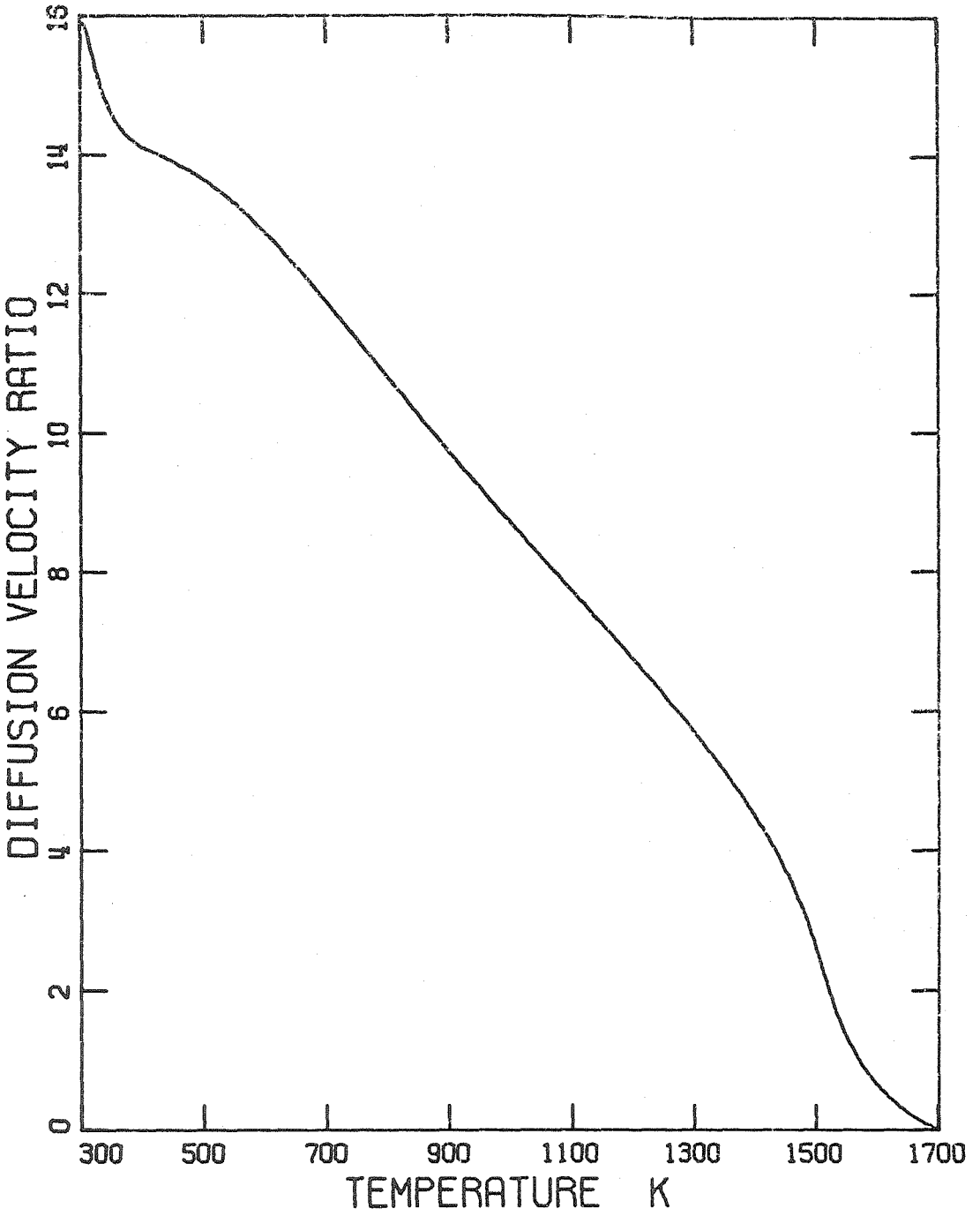

Figure 7-4. The Ratio of the Diffusion Velocity for Atomic Oxygen to the Flame Speed, $-V_N/v$, for the Single Species Diffusion Approximation with an O_2/CS_2 Ratio of 10.

8. APPARATUS

The apparatuses for the experimental work are divided into modular subsystems to provide flexibility and portability. The major subsystem is that of the chamber: as illustrated on Figure 8-1, all of the other subsystems connect to it. Each of the gases used in the experiments has its own independent module. The ignition, cooling water, and exhaust systems are also independent of each other. The optical apparatuses are both mechanically and functionally independent of the other subsystems, except for a support structure which is shared with the chamber.

8.1 Gas Supplies

The CS_2 supply subsystem comprises a plenum tank, flowmeter, metering valve, and other valves and pressure gauges as shown schematically in Figure 8-2.

The carbon disulphide is Mallinckrodt analytical reagent grade with no additional purifications. The pyrex tank has a volume of approximately 2.5×10^{-3} m^3 and is maintained with a maximum liquid CS_2 content of about 2×10^{-4} m^3. At room temperature, the vapor pressure of CS_2, and hence the tank pressure, is approximately one-half atmosphere. Under steady-state conditions during a typical run, evaporative cooling lowers the vapor pressure to about one-third atmospheric. As illustrated in Figure 8-2, the CS_2 flows through a rotameter flowmeter and a metering valve before it leaves the module. For typical operating conditions, the maximum and minimum measurable CS_2 flow rates with the present rotameter tube are 1.9 and 0.05 mmol s^{-1}.

A heater jacket is attached to the aluminum tank bottom to provide additional heat to the CS_2 in order to boost the tank pressure and CS_2 flow rate. If heat is supplied faster than that lost to the heat of vaporization, condensation occurs in the unheated tubing and rotameter. The chamber pressure is limited by the CS_2 tank pressure and the pressure drop in the flow system, as flow from, not to, the CS_2 tank is required. This upper limit on the chamber pressure is estimated to be about 25 kPa , which is greater than that required for the experiments which are considered here.

The oxygen supply subsystem is composed of a cylinder of Caltech grade O_2 , two-stage pressure regulator, flowmeter, metering valve, and other valves and pressure gauges as shown schematically in Figure 8-3. The oxygen flow is measured with a rotameter which has a tube whose maximum and minimum measurable flow rates under typical experimental conditions are 4.2 and 0.2 mmol s^{-1}. The nitrogen supply subsystem is composed of a cylinder of Caltech dry grade N_2 , two-stage pressure regulator, flowmeter, metering valve, and other hardware as shown schematically in Figure 8-4. The nitrogen flow is measured with a rotameter which has a tube whose maximum and minimum flow rates are 10 and 0.4 mmol s^{-1}.

The added gas supply system, as illustrated schematically in Figure 8-5, is composed of the same elements as the oxygen supply system. The two gases used in these experiments are carbon monoxide and nitrous oxide. The CO is CP grade supplied by the Matheson Company. The N_2O which is used is supplied in lecture bottle

quantity by the Matheson Company. The maximum/minimum flow rates measurable by the rotameter flowmeter for the added gases under typical operating conditions are approximately 4.3/0.2 mmol s^{-1} for CO and 3.5/0.2 mmol s^{-1} for N_2O. The added gas and gaseous CS_2 are combined in a simple counter flow mixer. The mixer and lines downstream from the mixer contain sufficient volume to provide a suitably large flow time so that complete mixing will occur.

8.2 Exhaust, Ignition, and Cooling Water

The exhaust system is composed of traps, vacuum pumps, and assorted valves, as illustrated schematically in Figure 8-6. The dual traps are custom designed to provide the maximum entrapment with conductance compatible with the largest vacuum pump used in these experiments. The conductance of the dual traps is about 0.8 $m^3 s^{-1}$. The first of these two traps is designed to be utilized as a dry ice/ethanol trap which operates at 195 K. Optimally, this trap captures CS_2, COS, and SO_2. The second trap is designed to be utilized as a liquid nitrogen trap operating at 77 K. This trap captures all the remaining species other than N_2 and probably O_2. a 2-inch Temescal gate valve throttles the flow to the main vacuum pump which can be either a 7.5×10^{-3} $m^3 s^{-1}$ Cenco model Hyvac 45, which was used for the majority of the experiments, or a 0.14 $m^3 s^{-1}$ Stokes model 412H. The auxiliary vacuum pump is a 5.8×10^{-4} $m^3 s^{-1}$ Welch model 1404, which is basically used for testing the vacuum and gas supply systems.

Vibration from the vacuum pumps is isolated from the chamber by the use of flexible tubing and one fixed clamp in combination

with a cantilevered clamp. The support for the traps removes the vertical vibration and damps the horizontal. The remaining vibration is removed in a vertical flexible line which connects the traps to a station which is fixed relative to the chamber.

The ignition system is an AC electric discharge whose components are schematically given in Figure 8-7. The input of the autotransformer is connected to a 230 V at 60 Hz source. The high voltage transformer steps up the output voltage of the autotransformer by approximately 70, yielding a maximum discharge voltage of about 16 kV. The high-voltage circuit is composed of a limiting resistance of 2.7 MΩ and a glow or spark discharge inside the chamber.

The water supplied to the chamber for cooling (or heating) purposes is industrial quality water at low gauge pressure. The water drain at atmospheric pressure is immediately downstream of the water exit port of the chamber. The compressed air is supplied to the chamber to flush the chamber and traps after the completion of a run. The compressed air is controlled by a low-pressure regulator and valves. The gases which are removed by this flush are very irritating, if not toxic: consequently, these gases are removed through a standard fume exhaust.

8.3 Chamber

The chamber is basically a 152 mm by 51 mm pyrex pipe cross with a 152 mm to 51 mm pyrex pipe reducer attached to the exhaust end. The flow axis coincides with the axis of the 152 mm pipe and the optical axis coincides with the axis of the 51 mm cross pipe. A third perpendicular axis corresponds with the vertical. The

volume of this chamber is approximately 11×10^{-3} m. The chamber is supported by two plates, one which is connected to the flange bolts which attach the cross and reducer and one which closes the other 152 mm end of the chamber.

The upstream end of the chamber is closed with an aluminum plate, through which pass the supply lines of O_2, CS_2, and cooling water. The air and N_2 supply lines empty into the chamber at the plate. The chamber pressure is measured by an absolute pressure gauge connected to one of the lines of this plate. The plate is rigidly attached to the structure which supports the chamber, detection equipment, and optics. The chamber and the aluminum end plate are sealed, as are all the parts, with a Teflon gasket.

A custom-designed pyrex fitting closes the exhaust end of the chamber. The fitting adapts the flange of the pyrex pipe to the tube of the traps. Additionally, this fitting provides access along the center of the flow axis for a thermocouple or high-voltage electrode. For the majority of the experiments, a stainless steel rod was inserted through the fitting; this rod was used as one of the electrodes of the ignition circuit.

There are four options for using the ports along the optical axis. A custom designed fitting was made to enable 75 mm round discs to close these ports. The viewing region is limited to the 51 mm inside diameter of the pyrex pipe. The four options for these ports are listed in Table 8-1. Option A is simply a pyrex disc which closes the port. Option B is a custom-designed pyrex ring to which either a NaCℓ or CaF_2 flat is cemented; this provides a 38 mm

viewing diameter through which both visible and infrared radiation can pass. Option C is a custom-designed Brewster angle attachment to which either a NaCℓ or CaF_2 flat is cemented; this provides a 22 mm viewing diameter which is 100 per cent transparent to one polarization for infrared radiation and almost 100 per cent transparent to the same polarization for visible radiation. Option D is a custom-designed aluminum plate through which a thermocouple rod is inserted. Motion along the direction of flow is adjustable, by motion of the entire plate, over a distance of about 15 mm. Motion of the rod along the optical axis is provided by a bored-through Swagelok fitting with nylon ferrules. The chromel-alumel thermocouple is composed of two 0.13 mm wires which extend from the stainless steel rod.

8.4 Injector

In order to promote the rapid mixing of CS_2 and O_2, a multiple slit injector was developed. The two gases are alternately injected from 155 slits, each 0.28 mm in width and 5 mm in length (O_2 is injected from both end slits), as illustrated in Figure 8-8. The slit spacing is 0.28 mm. The injector is constructed of 311 aluminum shims (1100 alloy) bolted tightly together. There are three distinct functions for these shims; spacer, CS_2 injector slit, and O_2 injector slit. The shims alternate in the series s, o, s, c, ... where s represents a spacer, o and c represent injection slits for O_2 and CS_2, respectively. Each injection slit shim provides a path from the appropriate reservoir in the injector to the outlet slit, as shown in Figure 8-1. Each reservoir is fed from both ends through the end

pieces.

The oxygen line is composed of aluminum and stainless steel tubing which provides a conductive path for the high-voltage discharge, so that the injector acts as an electrode for the ignition discharge. Nylon Swagelok ferrules connect the O_2 line to the end plate; thus, the entire injector can be moved along the flow axis of the chamber.

The total outlet area for each gas, with the added gas being included with CS_2, is $1.1 \times 10^{-4}\ m^2$. Therefore, the approximate gas velocity will be given by

$$u \simeq 12\left(\frac{kPa}{p}\right)\left(\frac{f}{mmol\ s^{-1}}\right) m\ s^{-1}\ , \qquad (8.1)$$

where u is the average gas velocity, p is the chamber pressure, and f is the total flow rate through the injector.

Below the injector is a water jacket which supports the injector so that the center of the optical axis runs along the face of the injector about 10 mm downstream and is approximately aligned with the center of the slits. An identical water jacket could be placed above the injector, but this is not required due to the high coefficient of heat conduction of aluminum, combined with the relatively high heat capacity and skin heat transfer coefficient of liquid water (as compared to gases at 1 kPa pressure). The top water jacket also blocks the flow of nitrogen around the injector, causing high flow speed at the edges of the injector.

The water jackets were first made of plexiglas, but when cracks and subsequent leaks developed, these jackets were replaced

with identical ones made of aluminum. The water jackets are attached to the machines surfaces of the aluminum shims with paper gaskets and gasket cement. Additionally, the jacket is fastened with screws to the end plates of the injector.

This injector can effectively be turned into a premixed configuration by the addition of two plates and a stainless steel mesh to the face. The first plate is a 1.2 mm thick spacer. A 40-mesh stainless steel screen is placed on the spacer and held in place by a 4.2 mm steel plate which has a single 22 × 100 mm slot centered around the CS_2 and O_2 slots. The average gas velocity from this slot is approximately given by

$$u \simeq 1.1\left(\frac{\text{kPa}}{p}\right)\left(\frac{f}{\text{mmol s}^{-1}}\right)\text{m s}^{-1} . \qquad (8.2)$$

A premixed slot burner is also available. The CS_2 and O_2 are mixed in a two-dimensional slot mixer inside the burner, and the mixture is injected from a 2.7 × 50 mm slot in its face. This burner is made from a solid block of aluminum machined as illustrated in Figure 8-10, and two aluminum end plates. The O_2, CS_2, and cooling water supply lines are attached to the end plates. The injector is supported by the cooling-water supply lines which rest on the chamber wall. The average gas velocity from this slot burner is approximated by

$$u \simeq 18\left(\frac{\text{kPa}}{p}\right)\left(\frac{f}{\text{mmol s}^{-1}}\right)\text{m s}^{-1} . \qquad (8.3)$$

8.5 Optical Subsystem

The optical subsystem provides numerous options for "look-

ing" at the flame. The options can be divided between two systems, photographic and photometric. The photographic system records information on film which must be sequentially processed, while the photometric systems provide real time information which is displayed electronically or electro-mechanically.

The photographic system consists of a 35 mm single-lens reflex camera (Minolta SRT 101) with an assortment of lenses and attachments. The camera is mounted on a tripod and looks into one of the optical ports of the chamber. Typically, a 55 mm, f/1.7 lens is used with an additional close-up lens or extension tube. Agfa-Gevaert Agfachrome CT 18 positive color transparency film was used for the majority of the work. The exposure index for this film is ASA 50 (DIN 18°). For shutter speeds longer than 1 s, the shutter was manually held and the time estimated; for shutter speeds of 1 s or shorter, the shutter control of the camera was employed.

The photometric optical system options can be divided into three groups: those which couple the chamber to the detector, the detector, and the detection electronics. These groups are broken down with a listing of their options in Table 8-2. Coupling from the chamber can be accomplished by any of four options and combinations of these options. Option (a), which is almost always employed, is an optical chopper.

This pneumatically driven chopper is custom designed to provide a 250 Hz chopping speed from a wheel with 6 equal-speed, quasi-rectangular holes, each subtending an arc of $\pi/6$ radians. An incandescent lamp and visible photocell are mounted on the chopper to

provide a signal for synchronization of electronics and chopping speed determination. Option (b) is a BaF_2 positive lens which is 25 mm in diameter and has a focal length of 250 mm. Option (c) is a McPherson model 2051, 1 m monochromator with a 150 lines per mm grating blazed at 4 μm. This monocchromator has a wavelength drive whose normal range includes 0 to 10.3 μm. The gearing chosen provides driving speeds with a maximum and minimum of 6.67×10^{-3} μm s^{-1} and 1.67×10^{-6} μm s^{-1}. Option (d) is a mirror or combination of mirrors which are mounted on an optical rail and aligned along the optical axis. There are three possible coupling mirrors: (i) dielectric coated flat germanium mirror whose nominal transmittance at 5.3 μm is 5 per cent and reflectance is 95 per cent; (ii) 100 per cent reflecting gold-coated concave mirror with -2 m radius of curvature and a 1 mm hole; and (iii) 100 per cent reflecting gold-coated flat mirror with a 2 mm hole. The mirror on the other side of the chamber has the additional options of: (iv) 100 per cent reflecting gold-coated concave mirror with a -2 m radius of curvature, and (v) 100 per cent reflecting gold-coated concave mirror with a -10 m radius of curvature. All of these mirrors have a diameter of 25 mm. Since the minimum mirror separation with the Brewster angle window attachments is 0.6 m, optically stable cavities can be obtained with any combination other than the two flat mirrors.

There are two photoconductive detector options available, PbS and Ge:Au. The lead sulfide detector is a 4 mm × 4 mm chip from the Santa Barbara Research Corporation. This chip operates at ambient temperature and is sensitive to radiation with wavelength

from the visible to about 3 μm. The gold-doped germanium detector is from Cryogenic Associates and is a 1 mm × 1 mm chip mounted in a dewar which has an Irtran 2 window. The Ge:Au chip operates at 77 K and is sensitive to radiation with wavelength from 2 μm to past 11 μm. Each of the detectors has a custom-built detection circuit which provides the appropriate bias current and load resistance.

The first option to display or measure the output is from the detection circuits themselves. The second option consists of adding an impedance-matching buffer and amplifier to the detection circuit. The next option adds a Burr-Brown four-pole, stagger-tuned band-pass filter with a Q of 20 and tuned to 250 Hz. The fourth option adds a custom-designed synchronous demodulator to the previous options. The signal can be displayed or measured with any of these options; the output of the first three AC and the last is DC. The remaining option is a Princeton Applied Research model HR-8 lock-in amplifier which connects to the detector circuits.

8.6 Observational Notes

Ignition occurs most readily at low flow rates (under 1 mmol s^{-1}) at approximately an O_2/CS_2 volume flow rate of 3/1. Once ignition has occurred, the discharge can be turned off, leaving a free-burning flame. The blue SO_2 emission provides a visible indication of the location of the flame. At low flow rates, e.g., 1 mmol s^{-1} and O_2/CS_2 ratio of 4, the flame boundary is parabolic in shape in the direction along the length of the slits and uniform along the optical axis. At higher flow rates, e.g., 3 mmol s^{-1} and O_2/CS_2 ratio of 4.4, the flame is roughly rectangular with the downstream end dif-

fuse and turning upward. Addition of nitrogen behind the injector minimizes the convective rise. At all flow rates attempted, the flame remains two-dimensional.

After the flame has been burning for less than 10^3 s, the chamber walls get quite hot, unless nitrogen is also flowing into the chamber. This additional nitrogen prevents explosions in the pumps and provides some protection for the optical windows along with cooling of the exhaust gases. The chamber walls do get warm in continuous operation, but an exterior fan cools the chamber walls.

After about 2×10^3 s of burning with the multi-slot burner without the screen attachment, the flame loses its two-dimensionality due to clogging of the CS_2 slits with deposits of carbon and sulfur. When the deposits are removed from the injector, there is no chemical action evident. This is consistent with the heterogeneous reaction mechanism of CS which is discussed in Chapter 2. Experiments with a dual slot injector with 0.5 mm slit width and no cooling yield no evidence of clogging or carbon deposition. The clogging problem is totally eliminated by the screen attachment. With this option, the flame burns with the front plate, not the screen, as the holder; the result being that neither the screen nor the slots become clogged.

The premixed injector forms a stable two-dimensional flame front. Under some flow conditions the ends of the flame are distorted, moving in the upstream direction. This distortion of the flame is dependent upon pressure, flow rate, and mixture ratio. The stability of this injector is not as great as that of the multi-slit injector.

TABLE 8-1. Viewing Port Options

Option	Viewing diameter (mm)
A. pyrex disc	50
B. pyrex ring	
(i) NaCl flat	38
(ii) CaF_2 flat	38
C. Brewster angle attachment	
(i) NaCl window	22
(ii) CaF_2 window	22
D. thermocouple	-

TABLE 8-2. Options for the Photometric Optical System

1. Coupling from the Chamber
   - (a) chopper
   - (b) imaging lens
   - (c) monochromator
   - (d) mirrors
     - (i) 95% R, 5% T at 5 μm, flat
     - (ii) 100% R, -2 m , 1 mm hole
     - (iii) 100% R, flat, 2 mm hole
     - (iv) 100% R, -2 m
     - (v) 100% R, -10 m
2. Detector
   - (a) PbS
   - (b) Ge:Au
3. Electronics, Display and Measurements
   - (a) detection circuit
   - (b) buffer and amplifier with (a)
   - (c) bandpass filter with (a) and (b)
   - (d) synchronous demodulator with (a), (b), and (c)
   - (e) lock-in amplifier with (a)

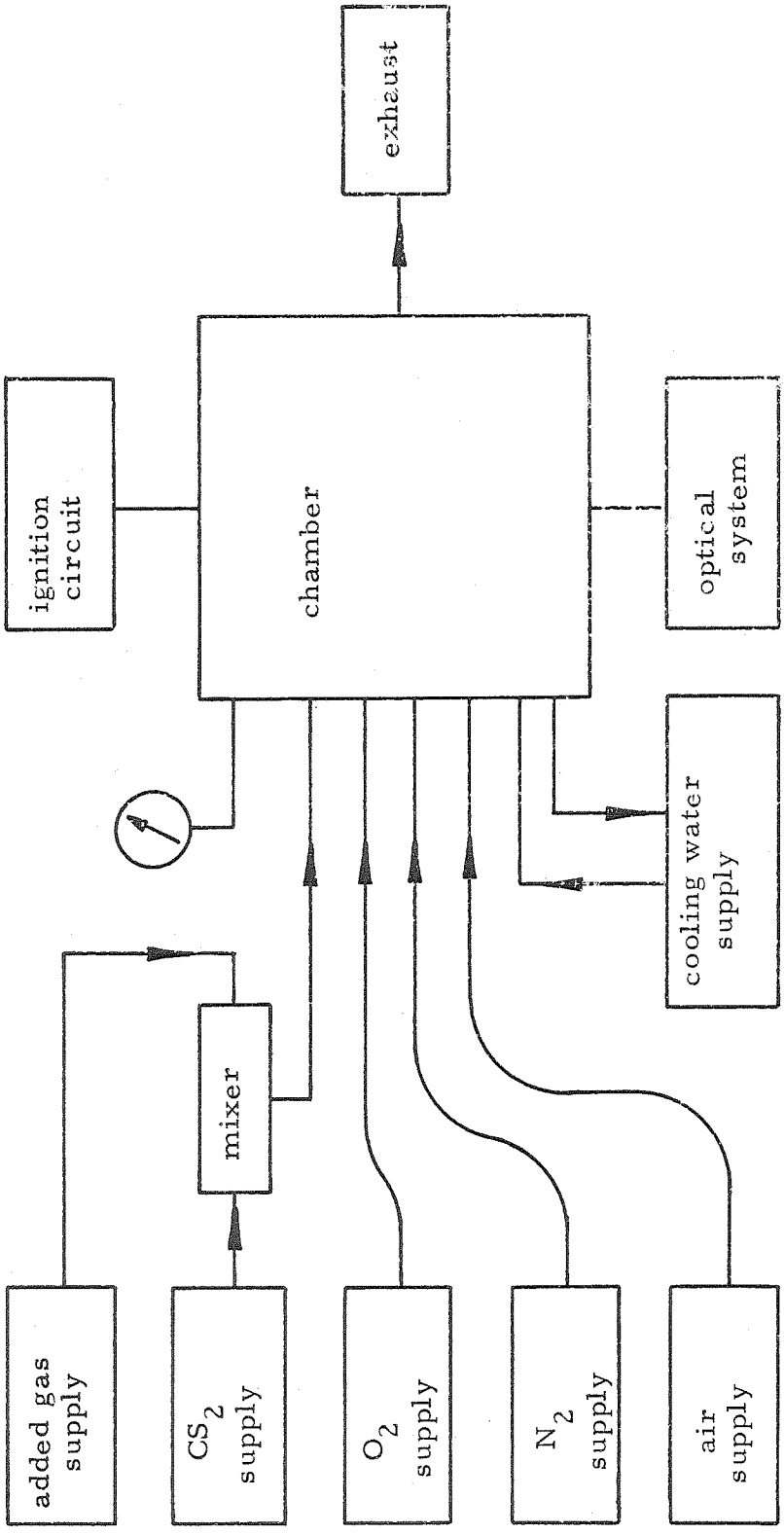

Figure 8-1. Block Diagram of the Apparatuses

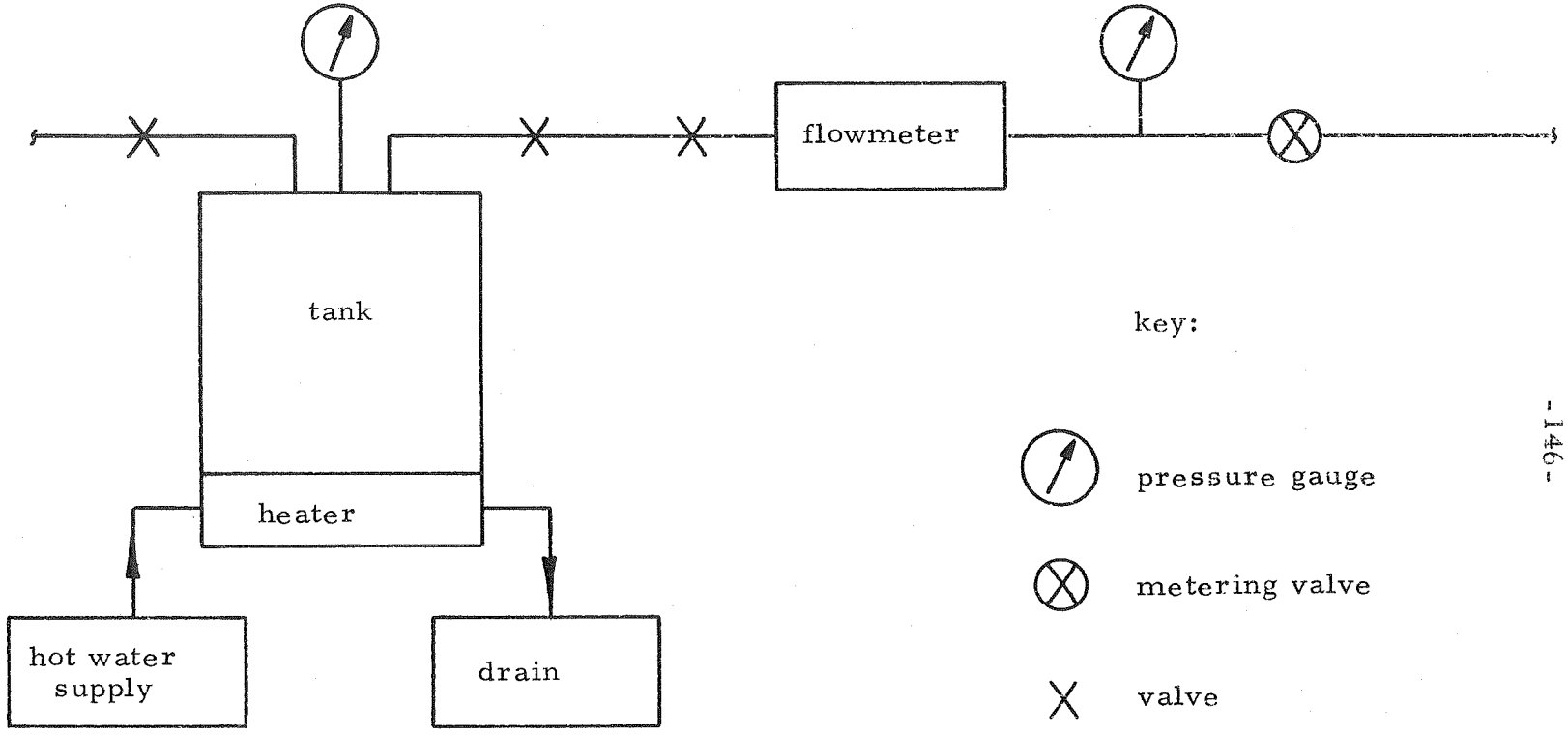

Figure 8-2. Schematic Diagram of the CS_2 Supply.

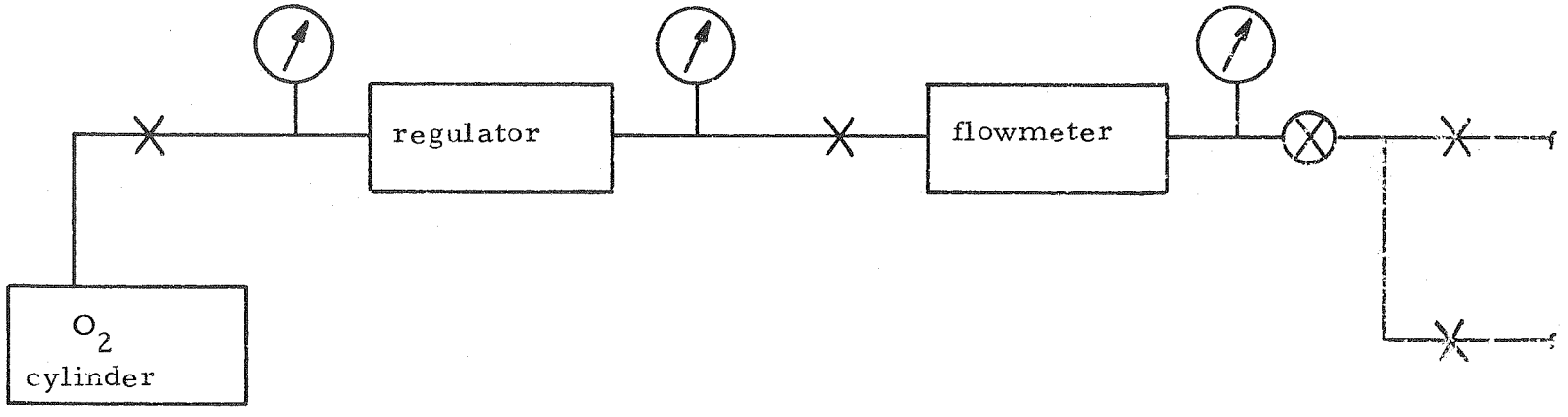

Figure 8-3. Schematic Diagram of the O_2 Supply.

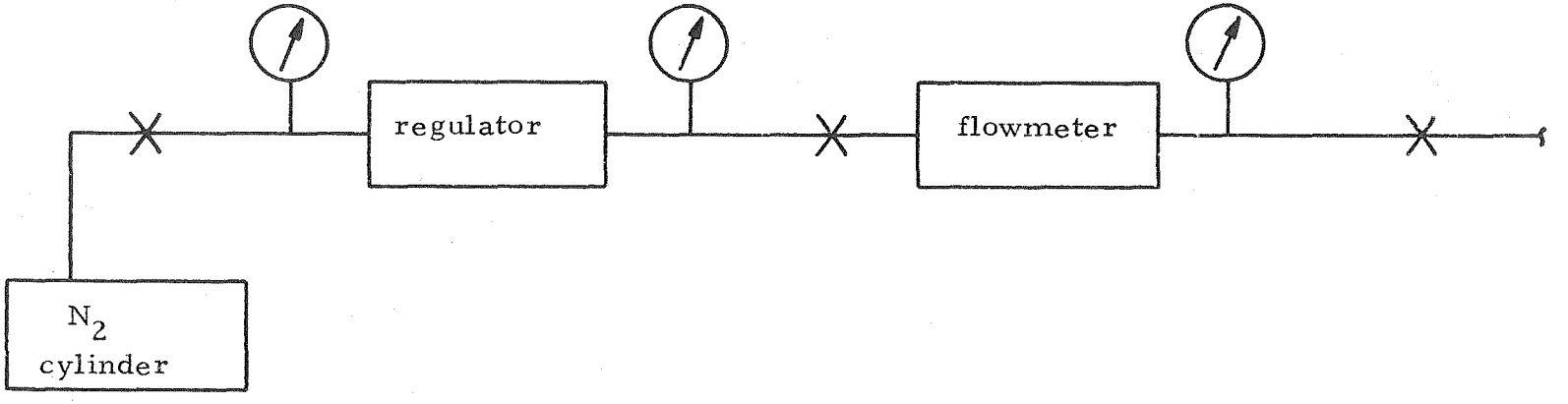

Figure 8-4. Schematic Diagram of the N_2 Supply.

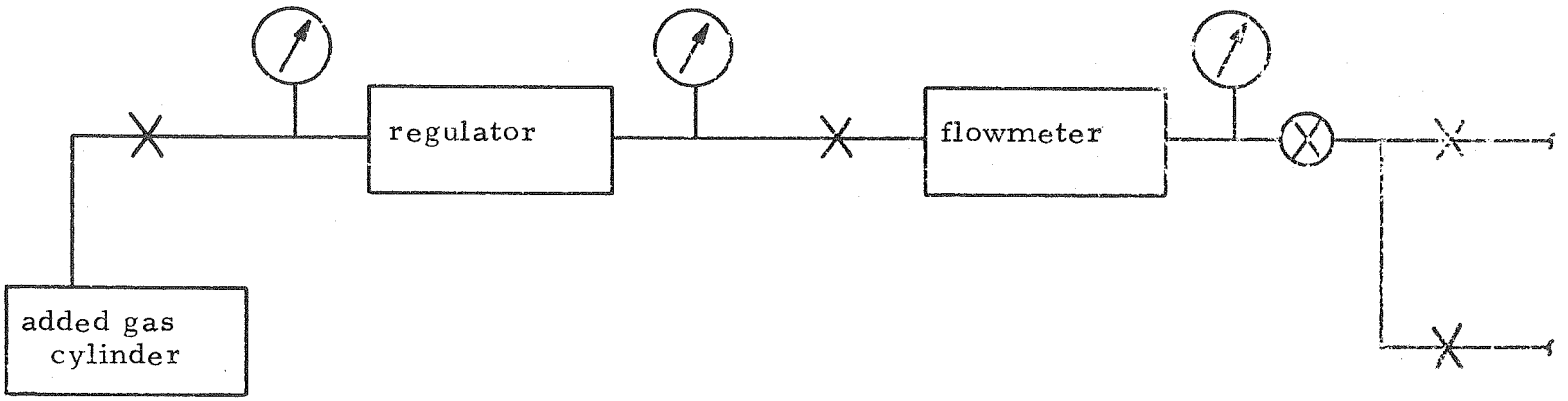

Figure 8-5. Schematic Diagram of the Added Gas Supply.

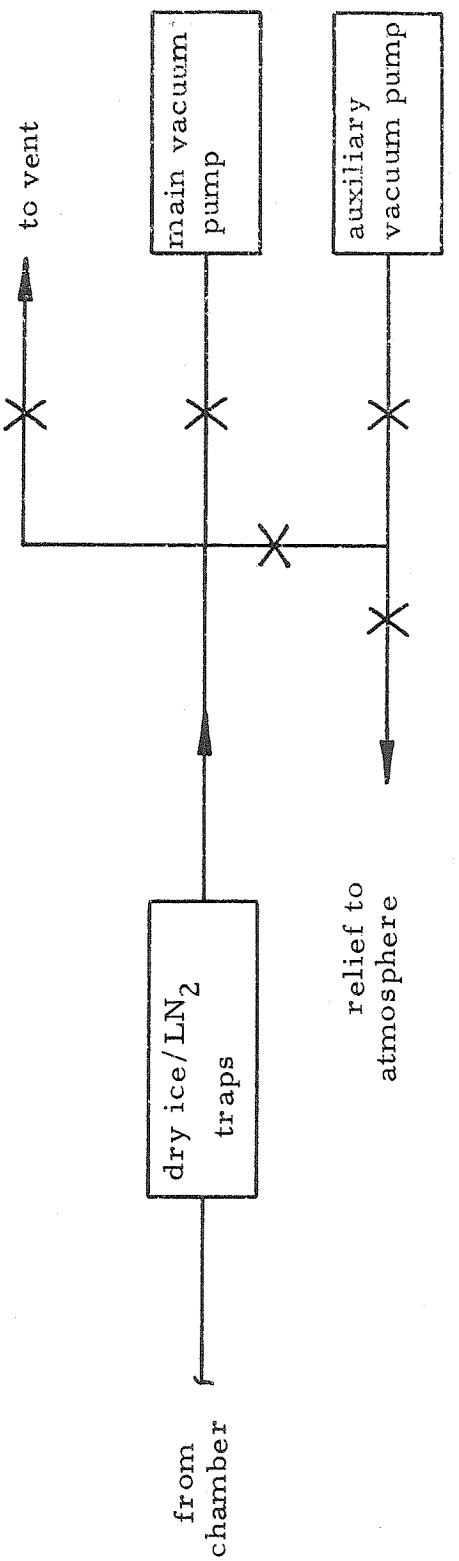

Figure 8-6. Schematic Diagram of the Exhaust System.

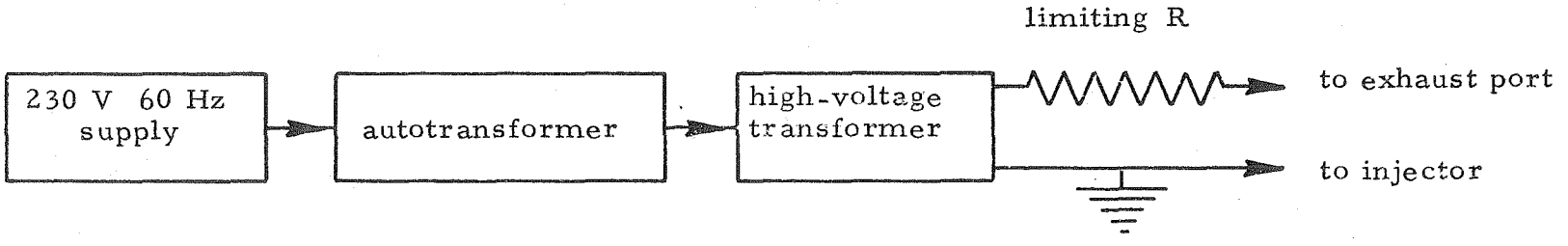

Figure 8-7. Schematic Diagram of the Ignition Circuit

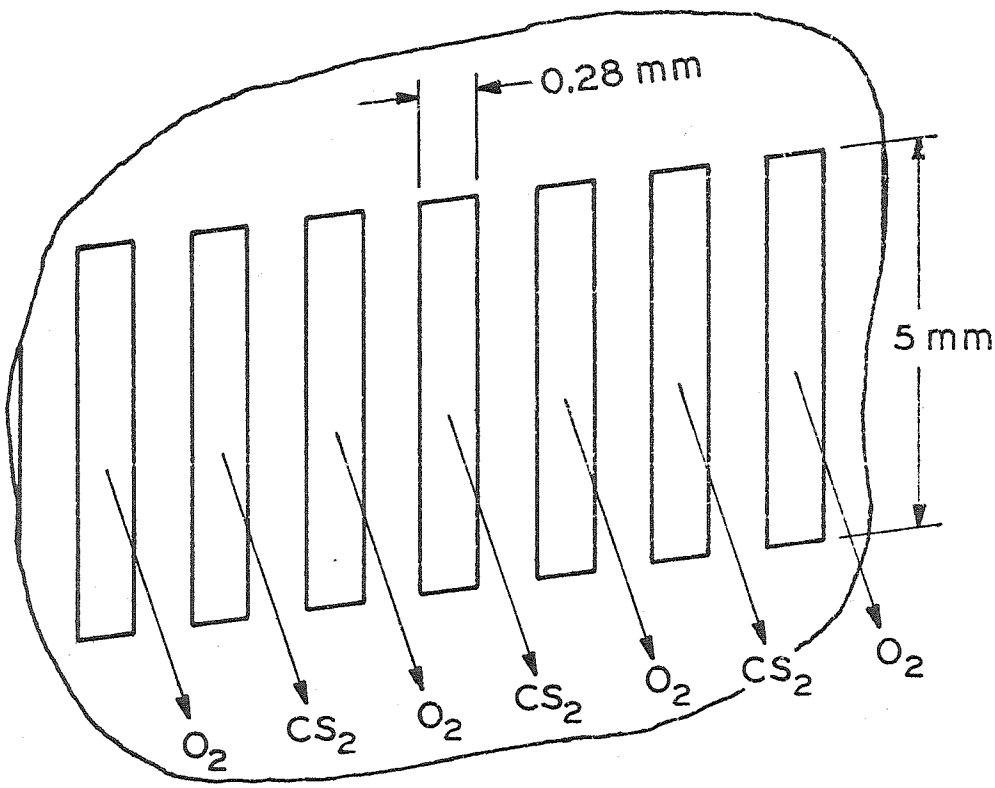

Figure 8-8. Cut-away View of Multi-slot Injector.

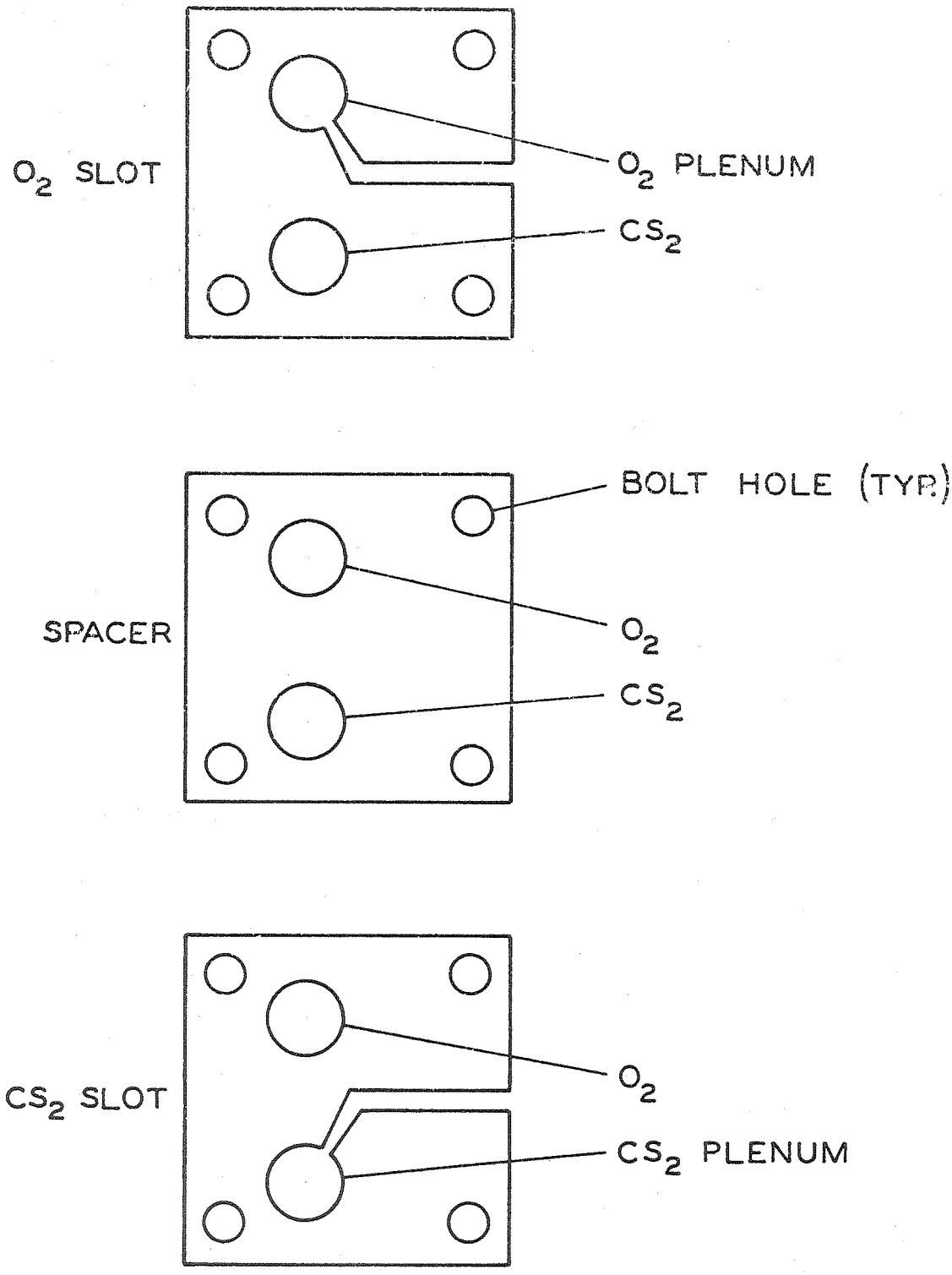

Figure 8-9. The Three Types of Shims Used to Make the Multi-slit Injector.

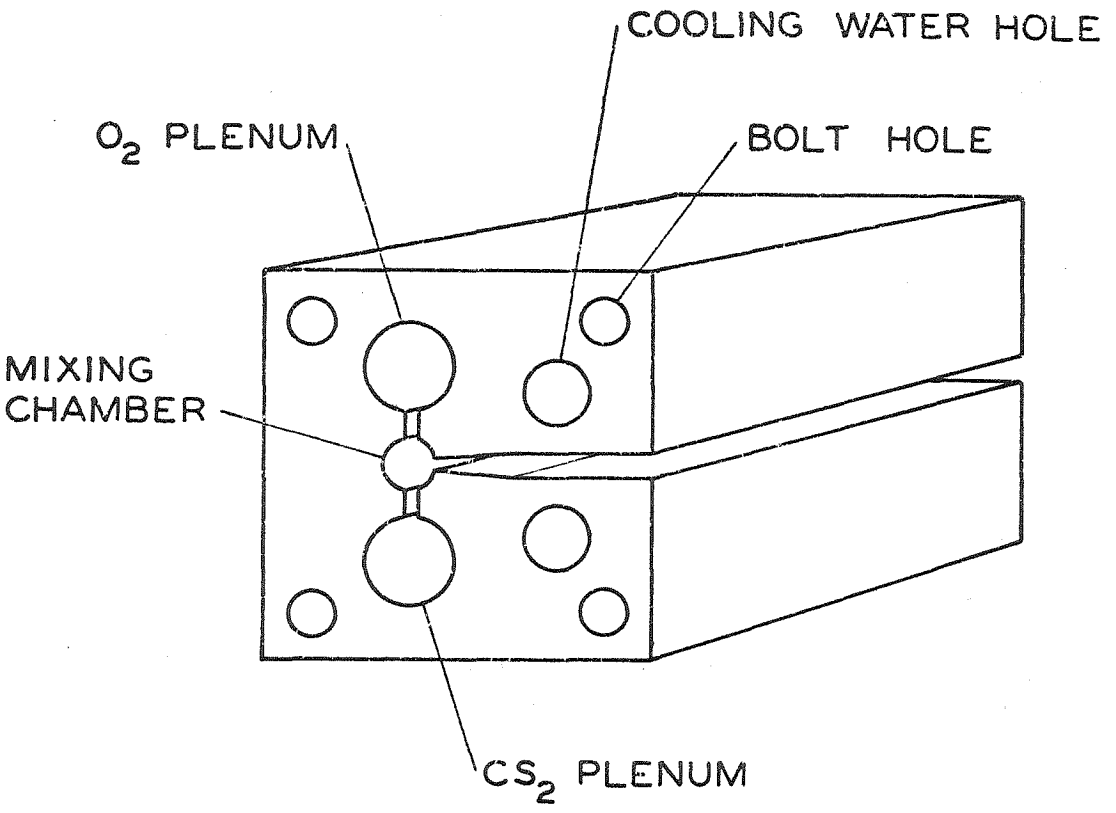

Figure 8-10. Representation of the Premixed Slot Burner.

9. FLAME SPEED

Flame speed is one of the important physical characteristics of flames which theoretical calculations must be able to estimate. To provide basic data on the flame speed under conditions typical of low speed, low pressure, non-diluted CS_2/O_2 flames, an experimental program was organized and executed. The flame speed was measured as a function of CS_2/O_2 ratio at 1 kPa and low flow rates.

9.1 Technique

The flame speed was measured by the method of Gouy (ref. 162, chapter IV) modified to account for the flame shape. This method is sufficient to give the burning velocity within ± 20 per cent, [88] which was deemed as accurate as required. For this approximation it is assumed that the burning velocity is constant over the entire surface of the flame front, and the fluid velocity at the flame front is assumed to be perpendicular to the front and has the magnitude of the flame speed. Continuity considerations yield

$$\rho v = \frac{f}{A_f} \quad , \tag{9.1}$$

where ρ is the pre-flame density, v is the flame speed, f is the particle flow rate, and A_f is the flame area. The ideal gas law determines the density from known pre-flame conditions. Let the arc length of the flame front at a typical cross section be given by h and ℓ be the length of the flame. Then the flame speed can be expressed in terms of measurable quantities:

$$v = \left(\frac{RT_0}{p}\right) \frac{f}{\ell h} \quad . \tag{9.2}$$

To approximate the loss of particle flow out of the ends of the flame

cylinder, assume that the flame area is approximately equal to half a circle of radius r whose half circumference is h . Since there are two ends of the cylindrical flame, the additional flame area, A_f', would be given by

$$A_f' = \frac{1}{\pi} h^2 = h\ell \left(\frac{1}{\pi} \frac{h}{\ell} \right) \quad . \tag{9.3}$$

Then with this correction, the flame speed is calculated by

$$v = \left(\frac{RT_0}{p} \right) \frac{f}{\ell h} \frac{1}{\left(1 + \frac{1}{\pi} \frac{h}{\ell} \right)} \quad . \tag{9.4}$$

Since consistent results can be expected for the flame speed measured by a slot burner when the length-to-width ratio of the burner is greater than 3,[164] the relation of equation (9.4) should only be used if $\pi\ell/h$ is greater than approximately 3 .

The multiple-slit injector, described in Chapter 8, was used with the mesh screen option to provide a flame for the flame speed measurements. The flow rates are measured by the supplies and method described in Chapter 8. The initial temperature can be approximated as that of the ambient temperature, which is the temperature at which the flow rate is measured. The pressure is measured by the chamber pressure gauge with the assumption of an isobaric flame. The flame length is taken as the length of the screen on the injector. The flame arc length, h , is measured from the projected images of 35 mm positive transparencies which contain a photographic image of the flame taken through the pyrex disc-covered viewing port. The inner boundary of the visible cone is measured as the flame arc length.

9.2 Data Acquisition

The first photographic run was made in order to determine the appropriate exposure for the transparencies. In addition to determining the approximate exposure limits for a typical flow and O_2/CS_2 ratio, a very rough estimate of the flame speed was obtained. The physical detail available from the transparencies was a function of the exposure, not of the aperture setting or shutter speed for the ranges which were used. The tabulation of the exposure settings and the flow conditions is contained in Table 9-1. The lower exposure slides (higher exposure value) are severely over-exposed with an optimum determined subjectively as an exposure value of 6 with good results for the inclusive range of 4 to 7. The flame arc length, h, was measured from a composite of these transparencies to be about 2.6×10^{-2} m, which implies a flame speed of $0.8\ m\ s^{-1}$.

In order to estimate the range of intensity expected from the CS_2/O_2 flame under the range of flow rates and mixture ratios for which a stable flame can be obtained, photometric data were collected with the Ge:Au detector. Although this detector is most sensitive in the infrared where the photographic emulsion is insensitive, the relative emissions should roughly correspond. The Ge:Au detector was pointed directly at the flame through one of the NaCl Brewster angle windows. The relative outputs of the flame with the corresponding flow conditions are listed in Table 9-2. These data indicate that the expected range of flame emission would vary about a factor of 4, which is equivalent to a change of exposure value (EV) of 2. Consequently, the next photographic data run would use the approximate

exposure value range of 4 EV.

For the second photographic data run, constant total flow through the injector was maintained while the O_2/CS_2 ratio was varied. At each flow case, given in Table 9-3, at least three transparencies were exposed with shutter speeds of 1/4 s, 1 s, and 4 s, which have the exposure value, compensated for the extension tube (ref. 165), as 7, 5, and 3, respectively. The transparencies corresponding to EVs of 7 and 5 were considered the most consistent, so these are used to measure the flame arc lengths. These arc lengths and their corresponding flame speeds are given in Table 9-3. A possible error in the recorded CS_2 pressure at the flowmeter was uncovered after this run. Consequently, the CS_2 flow may have been in error by at most a factor of $\sqrt{2}$ from the nominal. Although the resultant error in total injector flow could be at most 10 per cent, the O_2/CS_2 ratio could be greatly changed. The upper limits on flow and lower limits on O_2/CS_2 ratio corresponding to each case are given in Table 9-3. The flame speeds are all within the range of 1.3 to 2.7 m s^{-1}.

For the third photographic run, the total flow through the injector was maintained while the O_2/CS_2 ratio was varied. At each flow case given in Table 9-4 at least three transparencies were exposed with shutter speeds of 1/15, 1/4, and 1 s, corresponding to compensated EV of about 9, 7, and 5, respectively. The arc lengths and calculated flame speeds obtained from these transparencies are given in Table 9-4. The consistency of these measurements is illustrated in Figure 9-1, where the flame speeds for each O_2/CS_2

ratio can be seen to cluster. The means and standard deviations of the points of Figure 9-1 are given in Table 9-5. Transparencies other than those listed in Table 9-3 and taken at other exposures yielded flame speeds equal to or between those listed and were ignored in an attempt to provide a uniform data set.

Increasing flame speed with decreasing O_2/CS_2 ratio can be seen from Figure 9-1. Also evident from this figure is the trend towards higher flame speed for higher flow rates: this is expected as heat loss and heterogeneous elimination of active species at the injector wall decrease rate of combustion,[162] and these effects are less important at the higher flow rate which increases the length of the flame. The flame speed calculated from the transparencies listed in Table 9-1, i.e., 0.8 m s^{-1} at $O_2/CS_2 = 5$, fits well into the observed trend of Figure 9-1.

The measured flame speeds are in the ball park of previously published estimates. The flame speed for flame lasers has been calculated to be typically 2 m s^{-1} [112] where the O_2/CS_2 ratio is 34 ± 4 and the pressure is around 2 kPa. Another flame laser has a calculated flame speed (ref. 108, as corrected by ref. 112) of 1.5 m s^{-1} with an O_2/CS_2 ratio of 15 and a pressure of 1.3 kPa. The flame speed was estimated to be less than 2 m s^{-1} [13] for thermally initiated combustion of mixtures with O_2/CS_2 ratios from 3 to 6. For an atmospheric flame with an air/CS_2 ratio of around 14, the flame speed was reported to be 0.57 m s^{-1} (ref. 1, as reduced by ref. 166). Deletion of the inert (e.g. N_2) should increase the flame

speed, but the addition of water vapor should cause a smaller decrease.[1]

To provide a qualitative measure of the correlation of temperature with visual appearance along the flow axis, the fourth photographic run was made with a chromel-alumel thermocouple placed in the flame and moved along the flow axis. The inner edge of the visual flame as recorded by the transparencies has a temperature which is near, but below, the maximum temperature. The maximum temperature is reached just inside (about $1\frac{1}{2}$ mm for an O_2/CS_2 ratio of around 4.5 and relative flow of 40) the blue flame. The temperature remains constant along the flow axis for roughly the remainder of the blue emission, then decreases significantly by around a factor of 2. The large decrease in temperature can only be accounted for by mixing with the nitrogen which flows around the injector. The arc length which is measured from the transparencies must be longer than that length which ideally should be used for calculation of the flame speed. The actual flame speeds can thus be assumed to be larger than that calculated; this problem is not significant for hydrocarbon flames[1] as compared to the accuracy of the Gouy method, and so will not be considered important for this flame.

9.3 Estimate of the Limit of Error

The scatter of the flame speed data can be attributed more to the inadequate measurement of the CS_2 flow rate than to the measurement of the parameters from which the flame speed is calculated. The accuracy of the O_2/CS_2 ratio is strongly affected by error in the CS_2 flow rate, while the accuracy of the calculation of the flame

speed is only mildly affected.

The limit of error which may be expected has been estimated for both the flame speed and the O_2/CS_2 ratio. The limit of error was estimated for each of the measured quantities: these estimates are given in Table 9-6, where the mean or typical value of each of the limits has been given. The propagation of these limits was determined by standard methods[167] according to the mathematical operations which form the flame speed and O_2/CS_2 ratio. The limit of error for these two calculated quantities is given in Table 9-5 according to the O_2/CS_2 ratio and in averaged form in Table 9-6. The limits of error as given in Table 9-5 are plotted in Figure 9-2, where the center of the bars is chosen as the nominal O_2/CS_2 ratio and the mean of the flame speeds for that ratio. Also plotted on Figure 9-2 is a least-squares fit of the data from run number 3 to a linear relationship between the flame speed and O_2/CS_2 ratio. From this figure it can be seen that the spread in the data can easily be accounted for by the error in the control of the O_2/CS_2 ratio.

9.4 Calculated Flame Speeds

The flame speed, as calculated by the thermal theory approximation of Chapter 6 and the single species diffusion approximation of Chapter 7, is given as a function of O_2/CS_2 ratio in Figure 9-3. The four-reaction mechanism was chosen to represent the chemical kinetics, and the initial conditions were chosen according to the considerations presented in their respective chapters. Although the thermal theory approximation provides the correct dependency, the flame speed is below the experimental values and has a weaker de-

pendence on O_2/CS_2 ratio than might be expected from the experimental data. As shown in Figure 9-3, the single species diffusion approximation exhibits incorrect functional dependency below an O_2/CS_2 ratio of about 9, with the calculated flame speeds being above the measured values. Since the four-reaction scheme was developed for CS_2 combustion with an excess amount of O_2, these approximations are not expected to represent the chemical kinetics near the stoichiometric ratio, which is 3 for the four-reaction mechanism. The thermal theory approximation and single species diffusion approximation calculate the flame speed within a factor of 1.5.

The flame speed, as calculated by the von Kármán approximations of Chapter 5 and given in Figure 5-8, is more than an order of magnitude too high: however, the correct dependency with respect to O_2/CS_2 ratio is observed. These approximations use a five-reaction mechanism to represent the chemical kinetics and assume that the final concentrations of all intermediates are zero. Because of the assumptions made on the intermediate species and the consequent relation between the rates of reactions, the failure of the von Kármán approximations to predict the flame speed may be explained by the restriction of atomic oxygen to the role of an intermediate. It might be expected that consideration of the four-reaction mechanism with atomic oxygen as a product would yield more reasonable results; this has not been done here.

The slow speed and consequent isobaric assumptions are valid for the flames which are modeled. The pressure drop across the flame, Δp, is given by[163]

$$\Delta p = \rho_0 v^2 \left(\frac{\rho_0}{\rho_f} - 1 \right) \quad . \tag{9.5}$$

The thermal theory calculation for an O_2/CS_2 ratio of 10 yields a pressure drop of 1.4×10^{-2} Pa , which is a ratio of pressure drop to hydrostatic pressure of 1.4×10^{-5}. The pressure drop will increase with decreasing O_2/CS_2 ratio due to both the increase in flame speed and decrease in final density caused by higher flame temperatures. The maximum pressure drop for O_2/CS_2 combustion at 1 kPa is estimated at less than 1 Pa. The small pressure drop cannot be expected to be an important influence on the flame.

TABLE 9-1. Conditions for Photographic Run Number 1

$p = 1.2$ kPa

$\ell \simeq 0.1$ m

$O_2/CS_2 = 5$

$f = 1.1 \times 10^{-3}$ mol s^{-1}

O_2: 9.1×10^{-4} mol s^{-1}

CS_2: 1.9×10^{-4} mol s^{-1}

Transparency Number	Aperture (f/)	Shutter (s)	Exposure Value*
11	5.6	1/8	8
7	11	1	7
12	5.6	1/4	7
10	5.6	1/2	6
6	5.6	1	5
13	5.6	2	4
9	5.6	4	3
14	5.6	8	2
5	1.7	1	1.5
8	1.7	4	-0.5

*A difference of 1 EV (exposure value) is equivalent to 1 f/stop with EV = 1 equivalent to f/1 at 1 s.

55 mm focal length lens with +1 close-up lens

AGFA CT-18, ASA 50

TABLE 9-2. Relative Emission from the Flame

Ge:Au detector looking into flame

$p = 0.9 \pm 0.1$ kPa

N_2 flow into chamber = 0.7 mmol s^{-1}

Case	Flow Rates CS_2 (mmol s^{-1})	O_2 (mmol s^{-1})	O_2/CS_2 Ratio	Relative Total Flow*	Relative Emission
1	0.14	0.70	5	32	4.5
2	0.32	1.1	3.5	53	12
3	0.19	1.1	6	48	9
4	0.16	1.1	7	47	6
5	0.14	1.1	8	47	3.5
6	0.14	1.4	10	58	4

*Based on the linear scale where 100 is equivalent to 2.67 mmol s^{-1}.

TABLE 9-3. Conditions and Results of Photographic Run Number 2

Case	Nominal		Limit		EV ≃ 7		EV ≃ 5	
	Flow*	O_2/CS_2	Flow*	O_2/CS_2	Arc Length (mm)	Flame Speed ($m\ s^{-1}$)	Arc Length (mm)	Flame Speed ($m\ s^{-1}$)
7	40	3	44	2.1	19	1.3	17	1.5
8	40	4	43	2.8	12	2.2	11	2.4
9	40	5	43	3.5	14	1.9	12	2.2
10	40	6	42	4.2	13	2.0	13	2.0
11	40	7	42	5.0	18	1.4	17	1.5
12	50	4	54	2.8	18	1.8	15	2.1
13	50	5	54	3.5	14	2.3	14	2.3
14	50	6	53	4.2	16	2.0	14	2.3
15	50	7	53	5.0	17	1.9	16	2.0
16	50	8	53	5.7	18	1.8	17	1.9
17	50	9	52	6.4	21	1.5	20	1.6
18	60	4	65	2.8	23	1.6	22	1.7
19	60	5	64	3.5	17	2.2	15	2.5
20	60	6	64	4.2	17	2.2	14	2.7
21	60	7	63	5.0	20	1.9	18	2.1

*Based on the linear scale where 100 is equivalent to 2.67 mmol s^{-1}. $p = 10.0 \pm 0.7 \times 10^2$ Pa

N_2 flow into chamber: 1.1 mmol s^{-1} at 40, 0.9 mmol s^{-1} at 50, 0.8 mmol s^{-1} at 60. 55 mm focal length lens with 12 mm extension tube and f/8 aperture. AGFA CT-18, ASA 50; EV = 7 is at 1/4 s, EV = 5 is at 1 s. Mean flame speed is 1.96 m s^{-1} with 0.34 standard deviation.

TABLE 9-4. Conditions and Results of Photographic Run Number 3

Case	Relative Flow*	O_2/CS_2 Ratio	Flame Arc Length, mm EV: 9	7	5	Flame Speed, m s^{-1} 9	7	5
22	40	2.5	11	8.9	9.5	2.4	2.9	2.8
23	40	3.0	13	11	11	2.0	2.4	2.4
24	40	3.5	16	15	13	1.6	1.7	2.0
25	40	4.0	21	18	20	1.2	1.4	1.3
26	40	4.5	-	26	26	-	1.0	1.0
27	50	2.5	14	13	12	2.3	2.4	2.6
28	50	3.0	15	13	13	2.1	2.4	2.4
29	50	3.5	18	16	17	1.7	2.0	1.8
30	50	4.0	23	22	21	1.3	1.4	1.5
31	60	2.5	13	12	13	3.0	3.2	3.0
32	60	3.0	16	15	15	2.4	2.5	2.5
33	60	3.5	22	20	18	1.7	1.9	2.1

*Based on the linear scale where 100 is equivalent to 2.67 mmol s^{-1}.

$p = 10.0 \pm 0.3 \times 10^2$ Pa. N_2 flow into chamber 0.9 mmol s^{-1}.

55 mm focal length lens with 12 mm extension tube and f/8 aperture.

AGFA CT-18, ASA 50; EV = 9, 7, 5 at shutter speeds of 1/15, 1/4, 1 s.

TABLE 9-5. Flame Speed as a Function of O_2/CS_2 Ratio

O_2/CS_2 Ratio	Flame Speed ($m\ s^{-1}$) Mean	Std. Dev.	Limit of Error (per cent) O_2/CS_2	Flame Speed	Standard Deviation (per cent)
2.5	2.73	0.32	14.7	8.5	11.7
3.0	2.34	0.17	14.5	8.3	7.3
3.5	1.83	0.17	14.5	8.1	9.3
4.0	1.35	0.10	14.7	8.2	7.4
4.5	1.0		14.8	8.5	-

Experimental data and estimated limits of error for photographic run number 3.

TABLE 9-6. Limit of Error Estimates

Measurement	Symbol	Limit of Error (per cent)
ambient temperature	T	0.7
chamber pressure	p	3.0
flame length	ℓ	2.0
flame arc length	h	5.0
O_2 flow	f_{O_2}	5.6
CS_2 flow	f_{CS_2}	13.5
calculated variable		
flame speed	v	8.3
O_2/CS_2 ratio		14.6

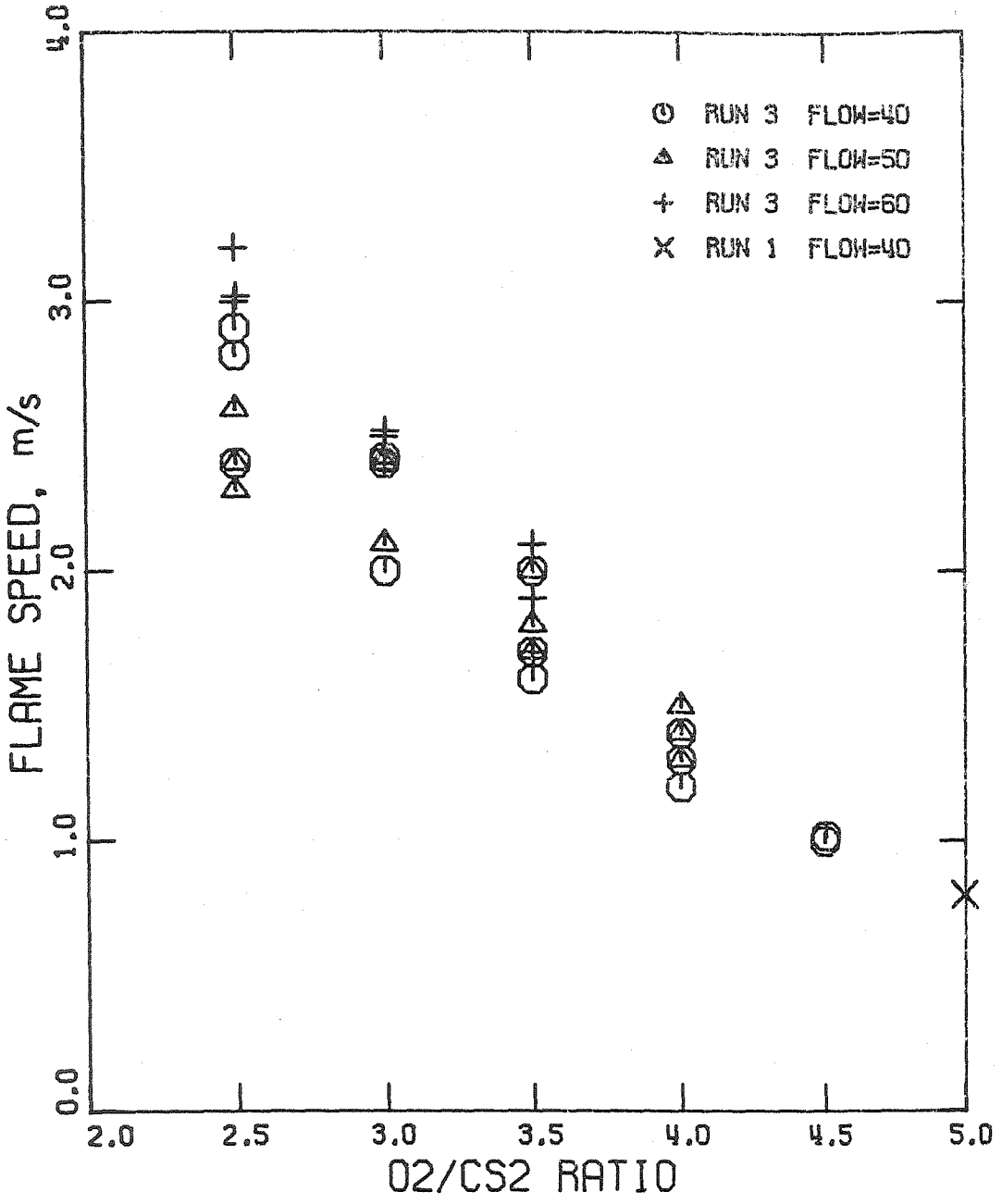

Figure 9-1. Experimental Flame Speed as a Function of O_2/CS_2 Ratio.

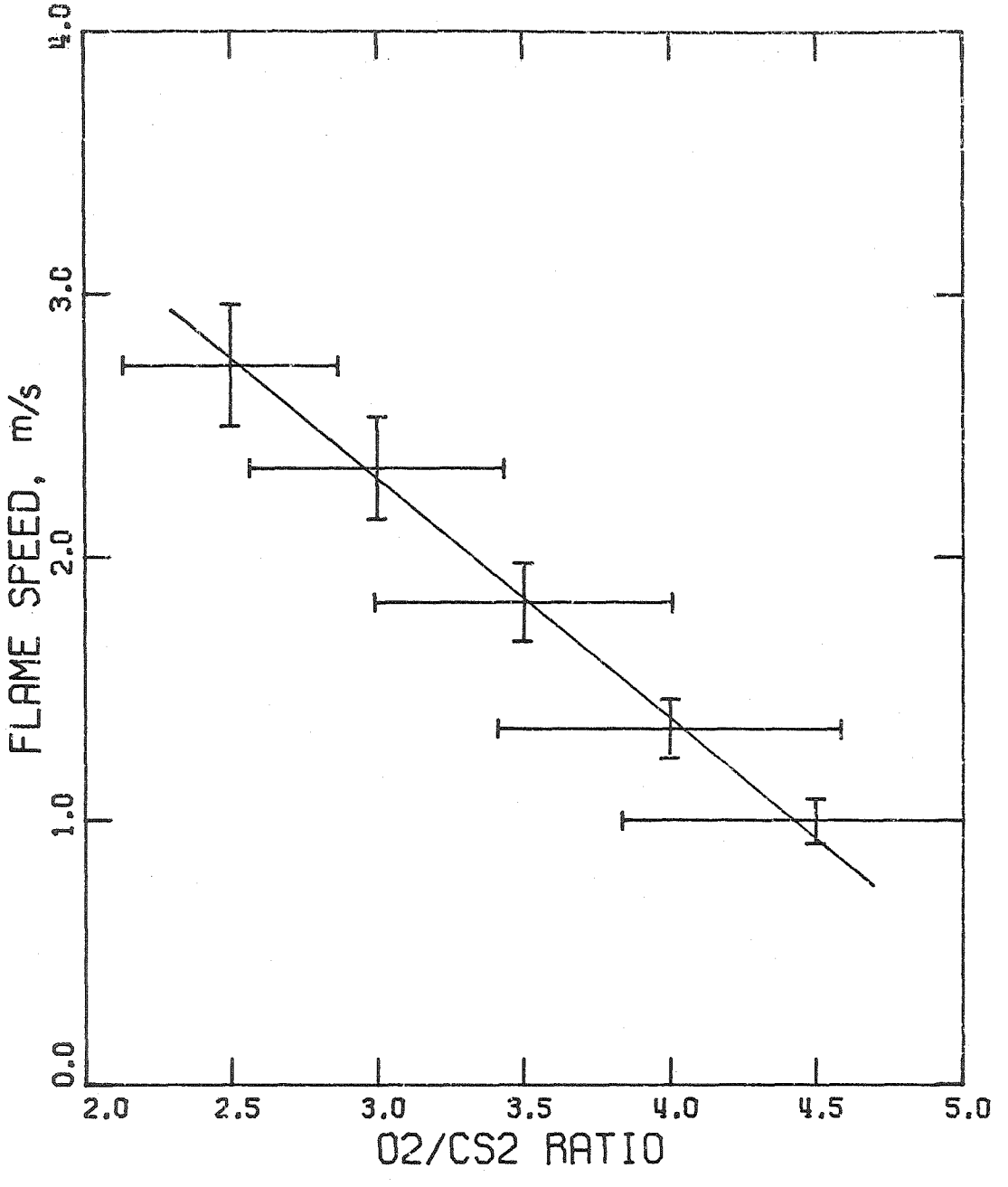

Figure 9-2. The Estimated Limits of Error for the Flame Speed Measurements and a Linear Least-squares Fit to the Data from Photographic Run Number 3.

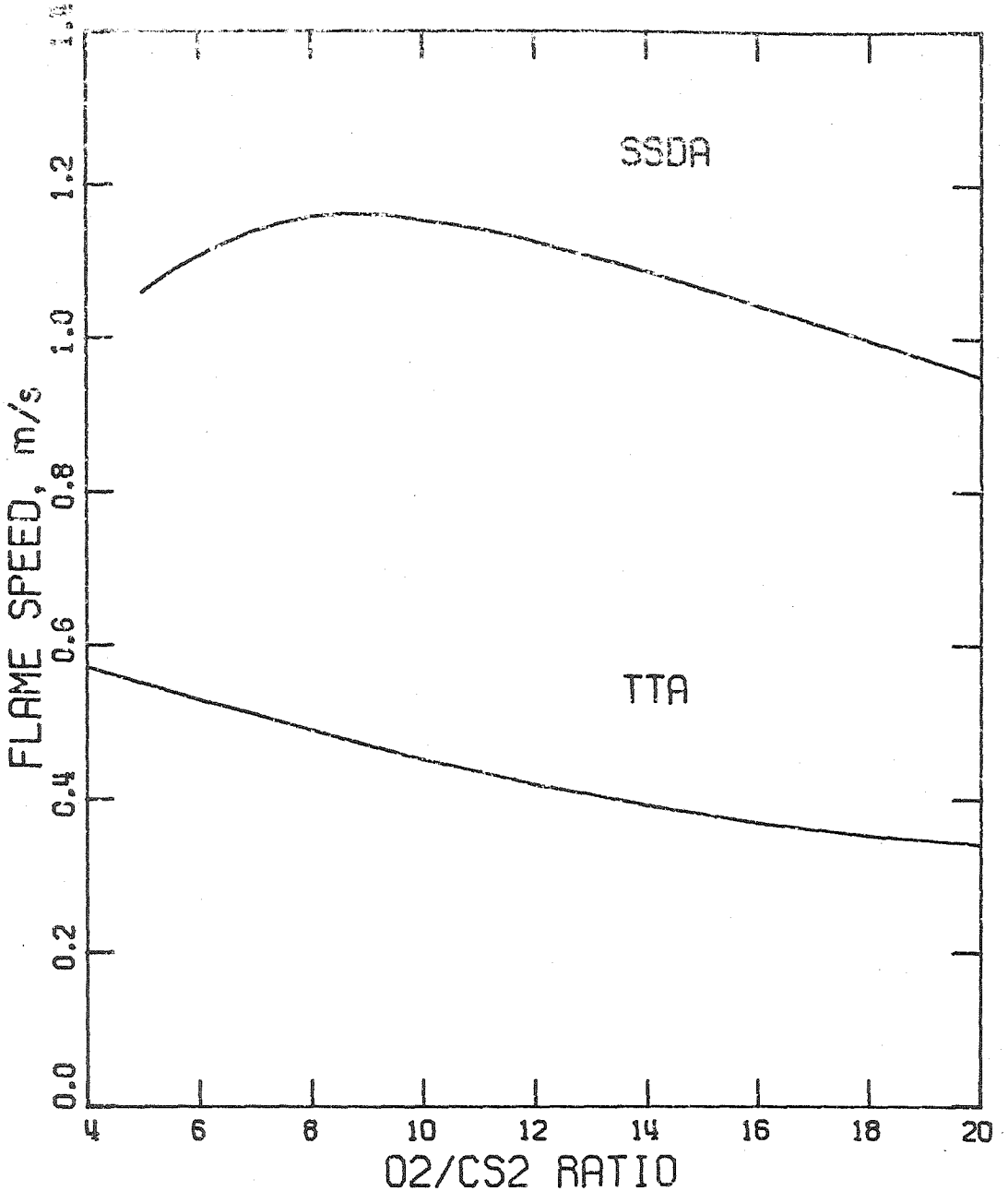

Figure 9-3. Calculated Flame Speed as a Function of O_2/CS_2 Ratio for the Thermal Theory Approximation (TTA) and the Single Species Diffusion Approximation (SSDA).

10. EMISSION MEASUREMENTS

The CO emission from the CS_2/O_2 flame can be used to deduce information on both the flame structure and the relative rates of population of the upper levels of CO by the chemiluminescent reaction. The spontaneous emission from the vibrational bands provides the means to determine the relative steady-state vibrational population in the flame. The technique for reduction of steady-state populations to relative rates of population of the vibrational levels of CO is developed in this chapter for the particular case of an O_2/CS_2 flame.

10.1 Vibrational Populations from Overtone Spectra

The relative distribution of vibrational energy of product CO from the reaction $CS + O \rightarrow CO + S$ can be obtained by an analysis of the overtone spectra of CO. The relative rates of formation of CO(v), R_v, are obtained from the relative steady-state populations, N_v, by consideration of the species conservation equations (with each CO(v) being a separate species) under steady-state conditions.[128, 135] Although this method implies many approximations, results for R_v under favorable conditions compare well, as can be seen in Figure 4-2 with the results for other techniques. This technique will be applied under conditions for the CS_2/O_2 chemical laser.

The steady-state populations of vibrationally-excited carbon monoxide can be estimated from the intensity of the emission from that band, for overtone emission[168]

$$N_v \propto \frac{I_{v,v-2}}{A_{v,v-2}\nu_{v,v-2}} \quad , \qquad (10.1)$$

where N_v is the relative steady-state population of CO(v), $I_{v, v-2}$ is the relative intensity of the emission from CO(v) to CO(v-2), $A_{v, v-2}$ is the spontaneous emission (Einstein) coefficient for the transition from CO(v) to CO(v-2), and $\nu_{v, v-2}$ is the frequency of the transition from CO(v) to CO(v-2). This relation is modified for fundamental transitions by replacing v-2 by v-1 in equation (10.1) and the associated nomenclature. The values of $I_{v, v-2}$ are obtained experimentally from the overtone spectra after correcting for optical system characteristics. The $I_{v, v-2}$ can be taken as the maximum intensity from each band or the integrated intensity of each band; since the peak intensity method has been shown to be as effective as other techniques,[135] this method shall be used. The steady-state analysis of the species conservation equation yields the relation for R_v in terms of N_v,[128, 135]

$$R_v = \sum_{n=1}^{v} A_{v, v-n} N_v - \sum_{n=1}^{v_{max}} A_{v+n, v} N_{v+n}$$

$$+ \sum_{\text{all } q} \left(\sum_{n=1}^{v} K^q_{v, v-n} c X_q N_v - \sum_{n=1}^{v_{max}} K^q_{v+n, v} c X_q N_{v+n} \right) + (K_w + K_p) N_v \qquad (10.2)$$

where

R_v is the relative rate of population of CO(v) for the reaction $CS + O \rightarrow CO(v) + S$,

v_{max} is the highest vibrational level of CO under consideration ,

$K^q_{v, v-n}$ is the n-quantum deactivation rate between species q and CO(v) ,

c is the concentration of the gases,

X_q is the mole fraction of species q ,

K_w is the rate of deactivation of CO(v) at the walls,

K_p is the rate of removal of CO(v) from the zone from which intensities are obtained .

This relation is derived for a homogeneous macroscopic control volume where the residence time of a molecule is large compared to the deactivation time and all production in the v-level occurs in this volume. This method is particularly useful when the residence time is large compared to the half-life for radiative decay, as the spontaneous emission coefficients are more accurately known than the other coefficients of equation (10.2).

Due to the low probability for multi-quanta V-V or V-T transfers, only single quantum exchanges need be considered. Due to the small spontaneous emission coefficients for many quanta emission, emission of only the fundamental and overtone bands will be considered.

Since the CS_2/O_2 flame is free of wall influence except near the flame holder, the rate of deactivation by the walls, K_w, can be ignored. After these three assumptions, the relations of equation (10.2) become

$$R_v = (A_{v,v-1}+A_{v,v-2})N_v - A_{v+1,v}N_{v+1} - A_{v+2,v}N_{v+2}$$

$$+ c\sum_q X_q (K^q_{v,v-1}N_v - K^q_{v+1,v}N_{v+1}) + K_p N_v \quad . \qquad (10.3)$$

Because of the high temperatures and added cold CO which occur in the flame laser, two additional considerations need be made. The rate of convection of CO(v) into the homogeneous control

volume, to which equation (10.2) applies, must be considered. This is due to the significant thermal contribution to the lower vibrational levels. The convection term can be represented by subtraction of the term

$$K_p N_v^I \tag{10.4}$$

from the right hand side of equation (10.3); the superscript I indicates the relative population of CO(v) in the gas which is added to the control volume. The fast V-V transfer of CO and the consequent anharmonic pumping phenomenon supplies the justification for consideration of a collisional pumping process. The single quantum V-V exchanges can be represented by addition of the term

$$c \sum_q X_q (K^q_{v,\,v+1} N_v - K^q_{v-1,\,v} N_{v-1}) \tag{10.5}$$

to the right hand side of equation (10.3). After these two considerations are made, equation (10.3) becomes

$$\begin{aligned} R_v = {} & (A_{v,\,v-1} + A_{v,\,v-2}) N_v - A_{v+1,\,v} N_{v+1} - A_{v+2,\,v} N_{v+2} \\ & + c \sum_q X_q \left[(K^q_{v,\,v-1} + K^q_{v,\,v+1}) N_v - K^q_{v+1,\,v} N_{v+1} - K^q_{v-1,\,v} N_{v-1} \right] \\ & + K_p (N_v - N_v^I) \quad . \end{aligned} \tag{10.6}$$

The sum over the species can be significantly reduced because contributions from only a few molecules dominate the contributions from the others.

10.2 Experimental Arrangement

To measure the intensity of emission in the vibrational bands from the CS_2/O_2 flame, the apparatuses which are detailed in Chapter 8 were employed with the following options. The multi-slot in-

jector with its screen option provided the flame. Vacuum was supplied by the 7.5×10^{-3} m^3 s^{-1} vacuum pump. The viewing ports were closed by NaCℓ flats mounted on the pyrex disc. The emission from the chamber was chopped at 263 Hz before it entered the monochrometer. Both the Ge:Au and Pbs detectors were employed with detection from a combination of their detection circuits and the lock-in amplifier. The output of the lock-in amplifier was recorded with a chart recorder.

Fundamental emission was recorded with the Ge:Au detector and overtone emission was observed with the PbS detector. Since the signal-to-noise ratio was better by more than 10 for the overtone emission with the PbS detector, overtone emission measurements were chosen to provide useful data. Masking of the flame to follow a single streamline, the center streamline, reduced the emission intensity so that accurate intensity measurement could not be made for each of the overtone bands. Thus, the determination of N_v as a function of distance along a streamline could not be made with these apparatuses.

Masking of the flame indicated that most of the emission occurs in a region from the edge of visible emission to a few millimeters downstream. The choice was made to measure the total emission from the flame and to deduce an average population in the vibrational levels. Since the largest signal was obtained when the 100 per cent reflecting, -10 m focal length mirror was placed on the far side of the optical axis and the BaF_2 lens was placed on the near side, this arrangement was used for emission measurements.

10.3 Experimental Data

Intensity of overtone spectra was recorded for the $v = 2 \rightarrow 0$ to $v = 20 \rightarrow 18$ transitions under eight different flow conditions. The flow conditions for these eight cases is given in Table 10-1. The relative populations of CO(2) to CO(19) for these cases, as determined by reduction according to equation (10.1), after correction for optical system characteristics, are given in Table 10-2. These relative populations indicate the highly non-equilibrium nature of the CO(v) in the flame. The relative populations for case 39 are plotted as a function of vibrational level in Figure 10-1. Also plotted on Figure 10-1 is an approximation to the Boltzmann distribution, normalized to CO(2), for the adiabatic flame temperature of 2680 K. A least-squares fit of the relative populations to a Boltzmann distribution yields a vibrational temperature of 10660 K for case 39; the other cases yield least-squares fit temperatures from 9230 to 11790 K. The population distribution in the flame does not represent a Treanor distribution; meaningful least-squares fits to the Treanor distribution could not be obtained for any of the cases. The shape of the curve presented in Figure 10-1 is explained by chemical population of the upper levels of CO, combined with V-V exchange between the upper and lower levels of CO and between all CO levels and other molecules.

The combined effects of the V-V exchanges spread the vibrational populations with the majority of the excited CO cascading downward (smaller v), with some pumped upward toward higher v levels.

10.4 Rate of Population of CO(v)

The rate of population of the vibrational levels of CO by chemical means was estimated using equations (10-6). The control volume considered corresponded to the region of flame from which the emission was observed; that includes the region in which flame reactions predominate to the limit of view of the optical system. As shown in Chapters 6 and 7, the region in which the majority of CO is produced is expected to be quite small, with the flame properties leveling out downstream. So the assumption of homogeneity for the derivation of equations (10.6) may not be grossly violated.

There were quite a few approximations made in order to calculate the R_v from the N_v. The amount of CO(v) produced in the control volume is assumed to be much larger than that flowing in, so that the N_v^I can be ignored for the upper levels. The temperature which is implicitly required is estimated from a linear fit with respect to O_2/CS_2 ratio to thermal theory calculations. The rate of pumping, K_p, is chosen as the inverse of the residence time in the control volume, which in turn is estimated as the gas velocity divided by the estimated zone thickness of 6 mm. The gas velocity is estimated from the experimentally-determined flame speed, extended by the thermal theory calculations for high O_2/CS_2 ratio, and the conservation of mass, ρv = constant, for a cylindrically expanding gas. The three species O_2, CO(0), and CO(1) were considered to have the predominant influence on the collisional process.

The rate of deactivation by O_2 was estimated by the assumption of a functional dependence of the rate on the energy defect as

given in equation (4.13). The rates were normalized to an experimental rate for the v = 12 to 11 transition[128] and an empirical constant[128] for the coefficient in the exponential. The rates for deactivation by CO(0) and CO(1) and activation by CO(1) were calculated from theoretical rates[129] normalized to experimental data for the v = 4 to 2 rate[128] for deactivation by CO(0).

The mole fraction of the O_2 was estimated by assuming that the reaction to form CO went to completion. The mole fraction of CO(0) was estimated by assuming that 25 per cent of the CO formed chemically from the reaction and 75 per cent of the added CO were in the ground state. Similarly, the mole fraction of CO(1) was estimated by assuming 15 per cent and 25 per cent, respectively.

The relative rates of population, R_v, were calculated from the N_v for the eight cases mentioned previously. The normalized rates are given in Table 10-3 for vibrational levels 3 through 18. The rates for the lower vibrational levels were thought to be high due to cascading from upper levels; the result of this effect could not be accurately determined. The rates of population for v = 7 through 18 were re-normalized to determine the fractional contribution within these levels.

Since the results for the R_v should ideally be independent of the flow conditions, the results of the eight cases were combined. The mean and standard deviation of these rates is given in Figure 10-2. These data indicate that there is a maximum rate of production of CO(15) which is two levels higher than expected from the experimental results obtained by others and displayed in Figure 4-2.

Rather than this being due to the high temperature in the flame, this behavior of a shifted maximum is probably due to the approximations made to obtain V-V exchange rates.

TABLE 10-1. Flow Conditions for Overtone Emission Measurements

Case	Relative Flow*	O_2/CS_2 Ratio	CO/O_2 Ratio	Pressure (kPa)	Adiabatic Flame Temp.†, K
34	100	6	0	1.36	2630
35	100	7	0	1.44	2570
36	100	5	0	1.31	2680
37	100	4	0	1.23	2740
38	100	3.5	0	1.24	2770
39	100	5	0.13	1.25	2680
40	77	5	0.34	1.28	2680
41	110	10	0	2.07	2430

* Based on the linear scale where 100 is equivalent to 2.67 mmol s^{-1}.

† Calculated.

TABLE 10-2. Relative Populations of CO(v) from Emission Measurements

v / Case:	34	35	36	37	38	39	40	41
2	1.00	1.00	1.00	1.00	1.00	1.00	1.00	1.00
3	0.60	0.66	0.56	0.53	0.58	0.55	0.51	0.56
4	0.35	0.41	0.30	0.28	0.31	0.29	0.24	0.39
5	0.25	0.29	0.20	0.18	0.18	0.19	0.15	0.31
6	0.20	0.24	0.15	0.13	0.13	0.15	0.11	0.27
7	0.18	0.22	0.13	0.12	0.11	0.13	0.083	0.24
8	0.16	0.20	0.11	0.10	0.096	0.11	0.069	0.21
9	0.14	0.18	0.10	0.087	0.079	0.097	0.061	0.19
10	0.13	0.16	0.089	0.075	0.066	0.086	0.053	0.16
11	0.11	0.14	0.079	0.066	0.059	0.078	0.049	0.14
12	0.096	0.12	0.073	0.060	0.053	0.068	0.043	0.11
13	0.085	0.10	0.068	0.058	0.050	0.060	0.039	0.093
14	0.072	0.088	0.056	0.053	0.046	0.051	0.035	0.076
15	0.054	0.070	0.046	0.046	0.040	0.042	0.026	0.060
16	0.039	0.042	0.033	0.035	0.033	0.031	0.017	0.034
17	0.024	0.023	0.021	0.025	0.022	0.018	0.010	0.019
18	0.013	0.011	0.012	0.015	0.014	0.010	0.005	0.008
19	0.006	0.004	0.006	0.008	0.008	0.006	0.003	0.004
20	0.002	0.002	0.003	0.004	0.004	0.002	0.001	0.001

TABLE 10-3. Relative Rates of Population of CO(v)

v / Case:	34	35	36	37	38	39	40	41
3	1.00	1.00	1.00	1.00	1.00	1.00	1.00	1.00
4	0.41	0.55	0.44	0.44	0.46	0.33	0.28	0.85
5	0.25	0.20	0.23	0.22	0.18	0.17	0.16	0.36
6	0.041	0.045	0.060	0.073	0.066	0.077	0.074	0.221
7	0.054	0.017	0.037	0.067	0.063	0.042	0.039	0.024
8	0.036	0.034	0.044	0.072	0.065	0.037	0.020	0.020
9	0.059	0.043	0.036	0.050	0.049	0.035	0.022	0.065
10	0.053	0.061	0.037	0.035	0.022	0.026	0.014	0.240
11	0.051	0.095	0.016	0.028	0.023	0.036	0.019	0.205
12	0.040	0.045	0.014	0.008	0.017	0.030	0.015	0.219
13	0.062	0.067	0.064	0.030	0.018	0.034	0.014	0.222
14	0.121	0.112	0.061	0.044	0.030	0.034	0.032	0.271
15	0.101	0.255	0.078	0.062	0.033	0.045	0.027	0.763
16	0.130	0.175	0.087	0.056	0.046	0.052	0.020	0.451
17	0.096	0.122	0.060	0.056	0.032	0.029	0.012	0.415
18	0.057	0.079	0.044	0.037	0.017	0.016	0.007	0.191

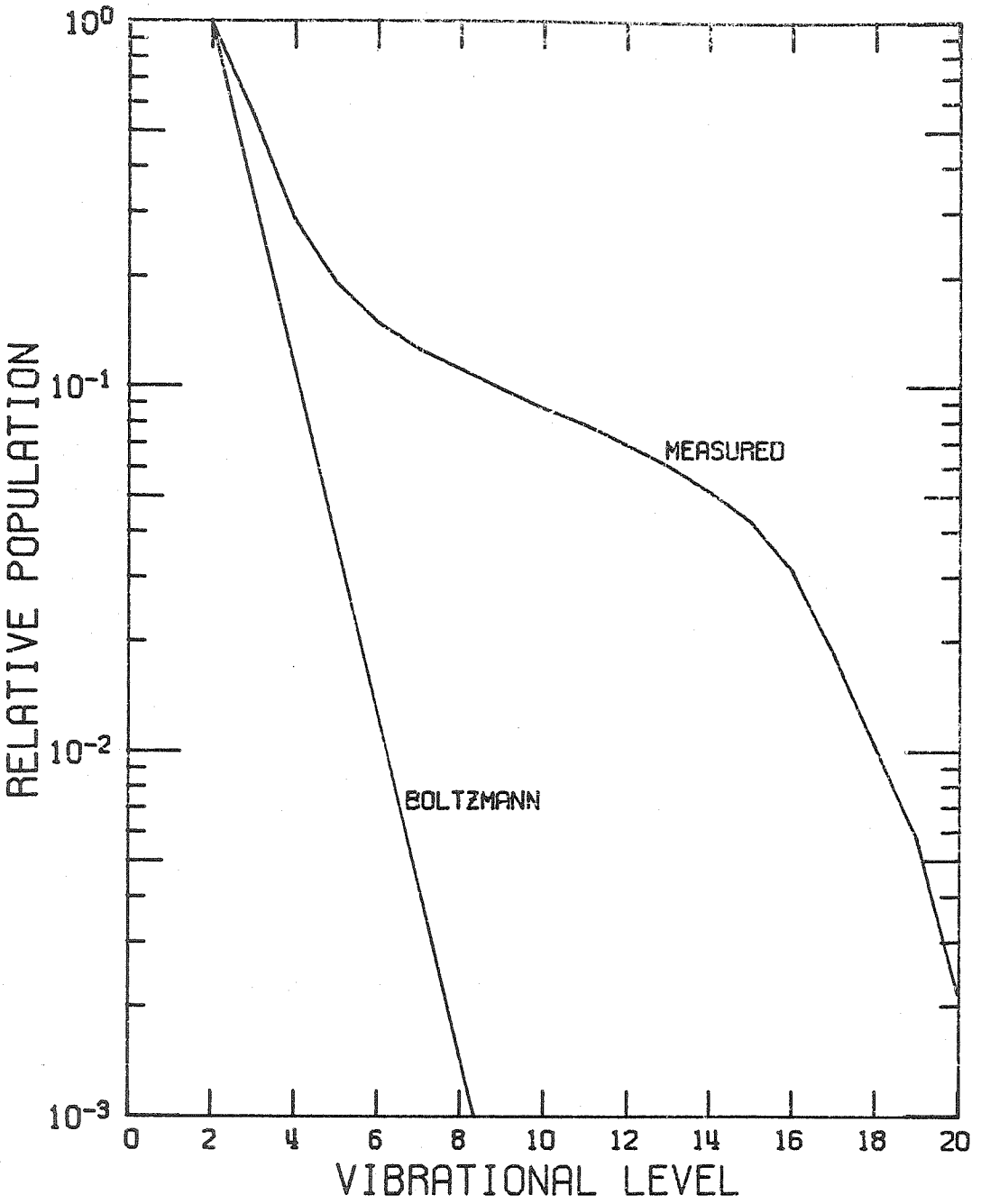

Figure 10-1. The Measured Relative Population in the Flame for Case 39. The Boltzmann Distribution Corresponds to the Calculated Flame Temperature.

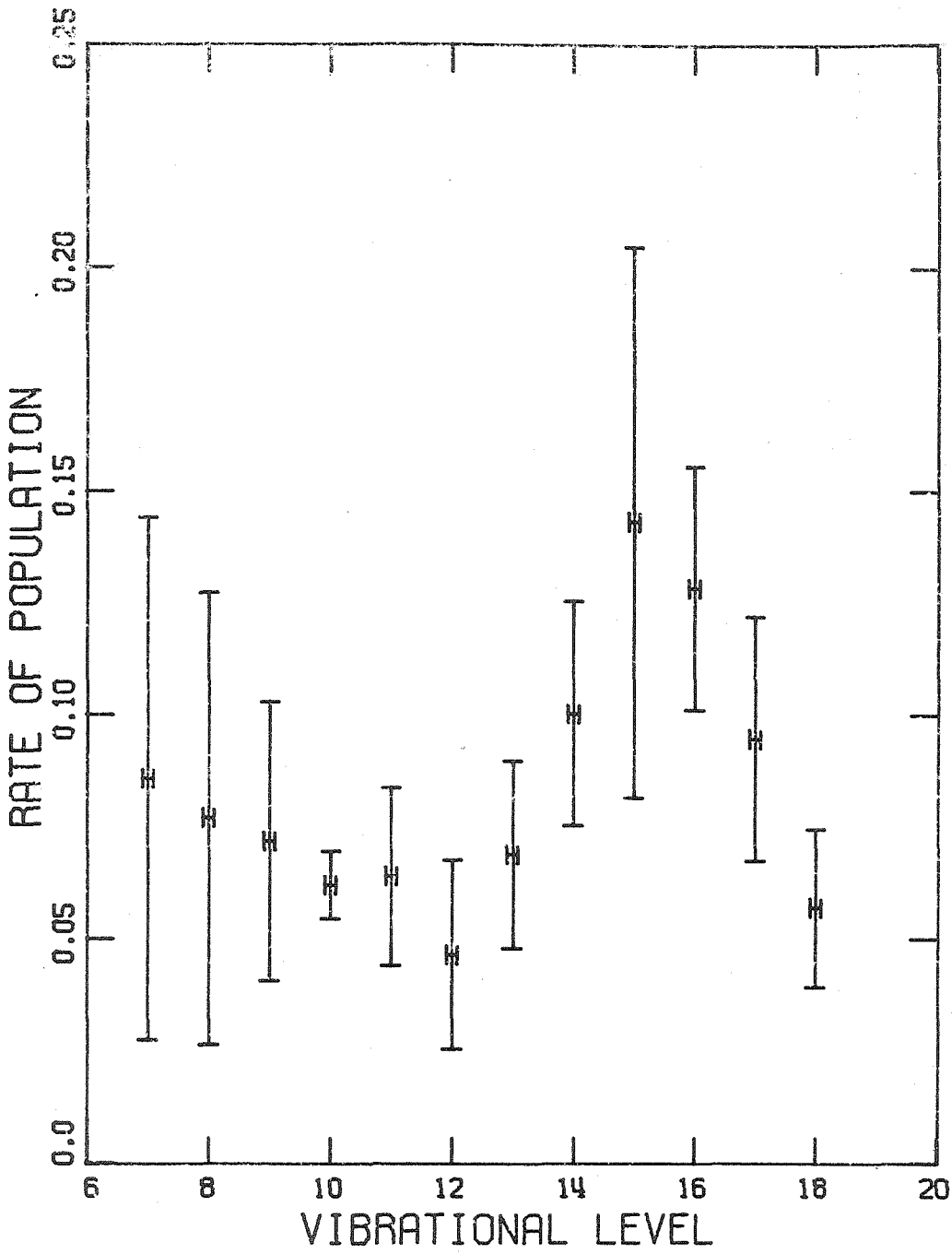

Figure 10-2. The Relative Rates of Population of CO(v) from a Composite of Eight Cases. The Rates Were Normalized So That the Sum over the Levels Shown Is Equal to One. The Mean Is Shown with One Standard Deviation Error Bars.

11. GENERALIZED KINETICS AND THERMODYNAMICS PROGRAMS

The kinetics and thermodynamical calculations which have been discussed were modified or developed specifically to model lean CS_2/O_2 combustion. Two computer programs which were developed elsewhere have been utilized for calculation of some of the important aspects of CS_2/O_2 combustion. One of these programs, designated by the name CEC 72, [169] performs equilibrium calculations; while the other, designated by the program name GKAP, [170] performs kinetics calculations coupled with fluid mechanics considerations.

11.1 The CEC 72 Program

The program CEC 72 [169] computes chemical equilibria for complex chemical systems by minimization of the free energy of these systems. This program considers both gaseous and condensed species. Besides calculation of chemical equilibrium for thermodynamic states fixed by two thermodynamic state functions, CEC 72 calculates theoretical rocket performance, shock properties, and Chapman-Jouget detonation properties.

Equilibrium calculations with assigned enthalpy and pressure were performed with CEC 72. This corresponds to isobaric, adiabatic combustion from a given initial state to the final state, which is calculated by the program. The initial conditions chosen for these calculations are a mixture of gaseous CS_2 and O_2 at 300 K with a pressure of 1 kPa. The equilibrium mole fractions of the products are given as a function of initial mole fraction of CS_2 in Figure 11-1.

Of particular interest is the high equilibrium concentration of atomic oxygen. This implies that the four-reaction mechanism might represent the kinetics better than expected; application of the four-reaction mechanism implicitly implies that the excess atomic oxygen, which is formed as a consequence of this scheme with no termination or recombination reaction, does not decay in the combustion zone.

The adiabatic flame temperature for the chosen initial conditions is given as a function of initial mole fraction of CS_2 in Figure 11-2. The high temperatures and low pressure provide the explanation of the large equilibrium concentrations of the species which would be considered intermediates.

The sonic velocity, as given as a function of initial mole fraction of CS_2 in Figure 11-2, is many times that of the measured and calculated flame speeds discussed in Chapter 9; therefore, the assumption of low speed flow is justified.

11.2 The GKAP Program

The program GKAP [170] calculates the chemical kinetics and fluid mechanics of chemically-reacting gaseous mixture which flows along a stream tube. The conservation equations for frictionless one-dimensional flow of a mixture of chemically-reacting gases are integrated along a pressure-defined stream tube. Mass, momentum, and energy may be added to the stream tube. This program can approximate a well-stirred reactor and can calculate the fluid mechanics for an area-defined stream tube. If the vibrational levels of a species are considered as separate species, then GKAP can calculate the zero power gain between the vibrational levels. The GKAP pro-

gram also can screen the input set of reactions to determine which ones are not important to the case being considered.

The GKAP program was modified by elimination of those options and calculations which were thought not to be required for modeling CS_2/O_2 lasers and combustion. The assumption of an isobaric flame enabled simplification of the fluid mechanics, as did the elimination of mass, momentum, and energy addition capability. The normal shock and oblique shock calculations were deleted, as shocks do not occur in low speed flow. The well-stirred reactor capability was also removed.

The GKAP program was used to screen a large reaction set for a case of a flame laser and for a case of a $CS_2/O_2/O$ laser. The initial conditions for the flame laser were the same as for the thermal theory calculation of Chapter 6, and the initial conditions for the other case were taken from a $CS_2/O_2/O$ laser[96] which is described in Chapter 3. The reaction set consisted of 32 reactions which contained 13 species. These reactions and the corresponding reaction rates, taken from the Tables of Chapter 1, were used for all GKAP calculations and are listed in Table 11-1.

The GKAP program had trouble with the implied extra body reactions involving SO_3 and CO_2; this was caused by the implicit assumption of a quasi-equilibrium between all third body reactions and their inverses. This technique is used to speed the integration as the chemistry nears equilibrium, but leads to reversal of some implied extra body reactions by the program. In order to obtain reasonable results, the third body reactions involving SO_3 and CO_2 were

dropped: to preserve some uniformity, all other reactions involving those two species, neither of which is considered a primary product, were dropped. This left a reaction scheme composed of 23 reactions which involve 11 species.

These 23 reactions were screened by the GKAP program. Six reactions were found to be significantly less important than the others and were dropped from consideration; these reactions are designated by R3, R5, R11, R13, R18, and R23 in Table 11-1. Since these include all of the ozone production reactions, the two ozone destruction reactions, R12 and R22, were also dropped, thus eliminating consideration of the species O_3. After this first screening, the reaction set consisted of 15 reactions involving 10 species.

These 15 reactions were screened to determine which of the remaining reactions are least important. A group of six reactions was found to be expendable; these reactions are designated as R17, R19, R21, R26, R27, and R30 in Table 11-1. When these reactions are dropped, the species COS is eliminated from consideration.

After this second screening, the reaction set consisted of 9 reactions involving 9 species. A third screening found all of the 9 reactions much more important than the ones which were previously eliminated. The three least important reactions of these which were remaining are designated as R2, R20, and R31 in Table 11-1. After these three reactions were dropped, the species S_2 was no longer under consideration. This left a reaction scheme consisting of six reactions which involves eight species.

The fourth screening found the reactions designated as R14

and R25 in Table 11-1 as the least important. After dropping these reactions, the four-reaction mechanism which was deduced in Chapter 1 remained. The importance of each of these reactions is shown by the failure of the computation to produce an ignition when any one of these reactions is eliminated. Thus, a reaction mechanism which represents both the CS_2/O_2 flame and $CS_2/O_2/O$ lasers should contain at least the four reactions which are designated as R1, R4, R6, and R7 in Table 11-1 and are discussed repetitively in this thesis.

TABLE 11-1. Reactions and Rates for the CKAP Program

Designation	Reaction	Rate* A†	N	B
R1	$CS_2+O \rightarrow CS+SO$	5. E7	0	956
R2	$CS_2+O \rightarrow CO+S_2$	2. E4	0	0
R3	$CS_2+O \rightarrow COS+S$	1. E6	0	0
R4	$CS+O \rightarrow CO+S$	1. E8	0	0
R5	$CS+O_2 \rightarrow CO+SO$	2. E8	0	24200
R6	$S+O_2 \rightarrow SO+O$	1. E7	0	2820
R7	$SO+O_2 \rightarrow SO_2+O$	4. E5	0	3270
R8	$CO+O_2 \rightarrow CO_2+O$	3. E6	0	25200
R9	$COS+O \rightarrow CO_2+SO$	6. E7	0	2770
R10	$COS+SO \rightarrow CO_2+S_2$	1. E5	0	0
R11	$SO+SO \rightarrow SO_2+S$	4. E3	0	0
R12	$SO+O_3 \rightarrow SO_2+O_2$	1. 5E6	0	1060
R13	$SO+O \rightarrow SO_2$	3. E2	0	0
R14	$SO+O+M \rightarrow SO_2+M$	3. E5	0	0
R15	$SO_2+O+M \rightarrow SO_3+M$	3. E3	0	0
R16	$SO_3+M \rightarrow SO_2+O+M$	8. E-4	0	0
R17	$S_2+O \rightarrow S+SO$	4. E6	0	0
R18	$O_2+O_2 \rightarrow O+O_3$	1. 3E7	0	50620
R19	$O+O_3 \rightarrow O_2+O_2$	1. 2E7	0	2410
R20	$O_2+M \rightarrow O+O+M$	2. 8E7	1	59880
R21	$O+O+M \rightarrow O_2+M$	1. 4E6	1	170
R22	$O_3+M \rightarrow O_2+O+M$	2. E2	0	11420
R23	$O_2+O+M \rightarrow O_3+M$	2. E2	0	0
R24	$CO+O+M \rightarrow CO_2+M$	2. E1	0	0

*Rate is given as $A\,T^{-N}\exp\{-B/T\}$

A in $(m^3\ mol^{-1})^{n-1}\ K^N\ s^{-1}$, where n is the order of the reaction; B in K.

† aEb is equivalent to $a \times 10^b$.

TABLE II-1 (continued). Reactions and Rates for the GKAP Program

Designation	Reaction	Rate A	N	B
R25	$CS_2+M \rightarrow CS+S+M$	4.E3	0	40400
R26	$CS_2+SO \rightarrow COS+S_2$	2.E1	0	0
R27	$COS+M \rightarrow CO+S+M$	1.5E2	0	30500
R28	$SO_3+O \rightarrow SO_2+O_2$	3.E8	0	6040
R29	$SO_2+M \rightarrow SO+O+M$	3.E2	0	55400
R30	$COS+S \rightarrow S_2+CO$	2.E4	0	0
R31	$S+S+M \rightarrow S_2+M$	3.E4	0	0
R32	$CO_2+O \rightarrow CO+O_2$	2.E7	0	26700

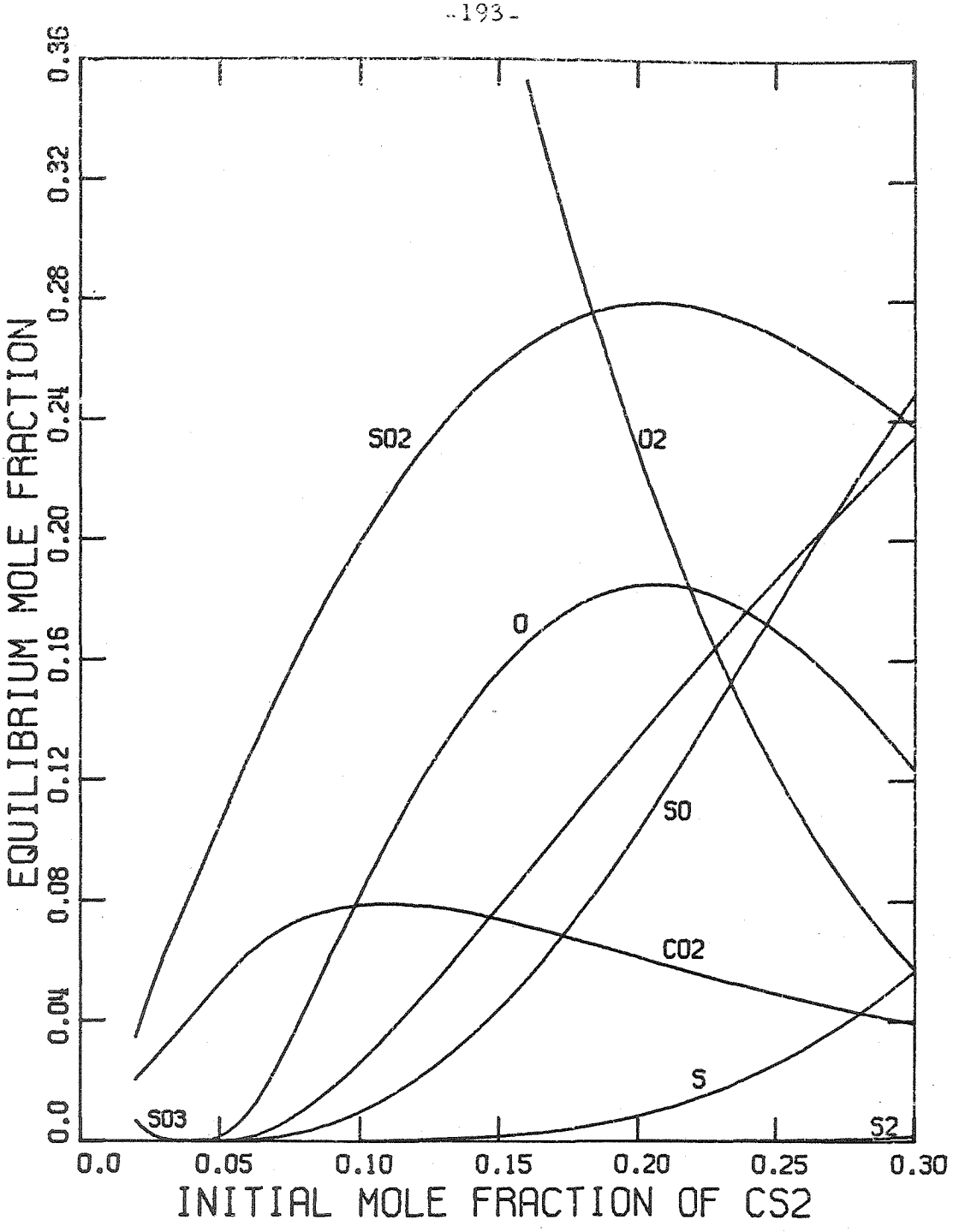

Figure 11-1. The Equilibrium Mole Fractions Calculated for Isobaric Adiabatic Combustion of a Gaseous Mixture of CS_2 and O_2 at a Pressure of 1 kPa.

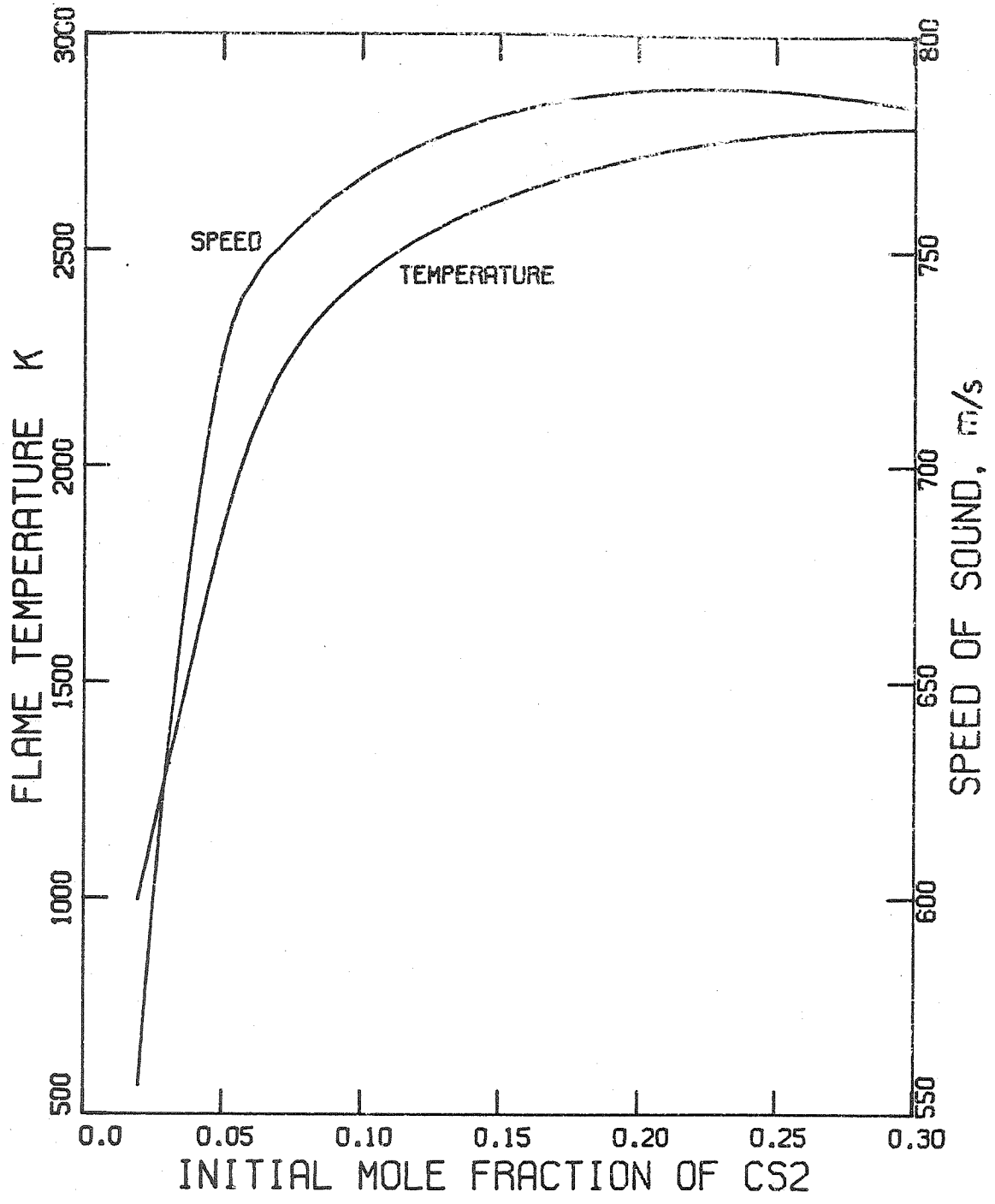

Figure 11-2. The Adiabatic Flame Temperature for a Gaseous Mixture of CS_2 and O_2 at a Pressure of 1 kPa.

CONCLUDING REMARKS

This study has produced some new and interesting ideas about the CS_2/O_2 combustion laser. The most significant advances involve the application of flame theories with selected chemical kinetics to predict the behavior of quantum phenomena. The CS_2/O_2 flame is shown to operate premixed under conditions similar to those of the flame laser, i.e., low pressure, low speed, lean flame. Thus, the theoretical analyses for one-dimensional, low-speed deflagrations can be applied with the expectation that the results will resemble the actual flame more closely than the analyses which are intended for more complicated flows.

The accuracy of the theoretical analyses is dependent upon proper considerations for the chemical changes in the flame. Although the kinetic data for the elementary reaction rates are sparse and not well known, those data are used along with macroscopic experimental observations, made by others, to determine the most important reactions in the flame. The important reactions are reduced in number by deduction of the sequence of reactions which occur in the flame. The most important reactions, which are four in number, form a branching chain mechanism for the CS_2/O_2 flame. Although this four-reaction mechanism had been proposed previously, the arguments which were presented were not sufficient to choose conclusively this mechanism over any of the others which had also been proposed.

The arguments which oppose this four-reaction mechanism are shown to be incorrect or not important. The energetic feasibility

of chemical population of the upper vibration levels of CO from the reaction between carbon monosulfide and atomic oxygen is shown by consideration of recent thermochemical data and the vibrational content of the reactant CS. Equilibrium calculations for isobaric adiabatic CS_2/O_2 combustion indicate that there is a large equilibrium mole fraction of atomic oxygen; this implies that the four-reaction mechanism, which provides a large amount of atomic oxygen at the end of the flame, is a better model of the CS_2/O_2 flame than was expected. The four-reaction mechanism is further supported by an independent screening of the reactions with a kinetics calculation which does not account for diffusion and heat conduction; this computer screening indicated that the four reactions in the proposed mechanism are the most important reactions of those which have been considered.

The proposed mechanism was used to estimate the induction behavior exhibited by explosions of mixtures of CS_2 and O_2. The functional behavior of the induction time with respect to initial molecular oxygen concentration and initial temperature compares favorably to the experimental data of other experimenters. The experimental evidence of a constant ratio of SO to O_2 during the induction period is explained by consideration of a steady-state approximation applied to the proposed mechanism. The actual value of the induction time is more difficult to calculate, but the theoretical estimates are in the correct range. The heterogeneous reactions are not yet sufficiently well understood to provide a good estimate of either the exact induction time or the boundaries of the explosion peninsula.

Three different one-dimensional laminar flame theories are

applied to lean CS_2/O_2 deflagration under the conditions which are similar to the CS_2/O_2 combustion laser. These theoretical analyses are applicable to premixed flames and take into consideration at least one of the feedback mechanisms which typify a flame calculation. The analyses are eigenvalue problems with the eigenvalue related to the flame speed.

The approximations suggested by von Kármán are applied to the lean CS_2/O_2 flame with a five-reaction scheme chosen to represent the chemical kinetics of the flame. This five-reaction scheme, which has the four-reaction chain mechanism as a subset, was chosen to fit the requirements of the von Kármán approximations that all intermediates disappear at the boundaries. The von Kármán approximations allow for heat conduction and some diffusion effects, but place severe restrictions on the independence of the concentrations of the species. Because of these restrictions, the von Kármán approximation does not provide a good representation of the flame structure.

The thermal theory approximation, which does not include diffusion effects, is based on thermal conduction as the dominant feedback mechanism. This approximation is applied to the lean CS_2/O_2 flame with the chemical kinetics described by the four-reaction chain mechanism. The flame speed and flame thickness determined by this approximation are reasonable; the structure behaves reasonably, but there are no experimental data to match.

The single-species diffusion approximation, which is based on diffusion of only one chain carrier, is developed for and applied to the lean CS_2/O_2 flame. The four-reaction mechanism is used to describe

the chemical kinetics of the flame. The calculated flame speed is reasonable, but the calculated reaction zone is too small; the flame structure behaves reasonably. The single-species diffusion approximation calculation indicates that the reaction $SO + O \rightarrow SO_2 + O$ is the rate-determining step for diffusion-controlled kinetics.

The flame speed of the premixed CS_2/O_2 flame is experimentally determined for a pressure of 1 kPa, initial temperature of about 300 K, and an O_2/CS_2 ratio in the range of 2.5 to 5. The flame speed decreases approximately linearly (within the error of the data) from a value around 3 m s^{-1} at the stoichiometric ratio of 2.5 to less than 1 m s^{-1} at the lean limit of these experiments. The flame speed calculated by the three previously mentioned theoretical approximations is compared to the experimental data. The von Kármán approximation yields a similar dependency, but is the wrong order of magnitude. The von Kármán approximation does not adequately describe the flame because of the failure of this particular version to allow for a significant concentration of atomic oxygen. The thermal theory approximation yields the correct dependency and yields a good approximation to the flame speed. The single-species diffusion approximation provides the correct dependency for O_2/CS_2 greater than 4 and is a little higher than the data. Application of the four-reaction mechanism must be limited to lean flames in order to preserve the conditions for which it was deduced; the theoretical calculations should not be expected to be valid for O_2/CS_2 ratios approaching stoichiometric.

The vibrational population of CO in the flame is determined

from spontaneous emission intensity. Determination of the vibrational population as a function of distance along a streamline would provide one measure of the flame structure. Sufficient spatial resolution could not be obtained with the available apparatus for the structure to be deduced from emission measurements. The average vibrational population of CO in the flame is determined experimentally. The average vibrational population is not found to be inverted, but is found to be highly non-equilibrium.

The rate of vibrational population of CO by the chemiluminescent reaction is obtained by combining the measured spontaneous emission intensities with theoretical rates for vibrational energy transfer. A steady-state analysis, which is considered accurate under favorable conditions, is employed to calculate the rate of vibrational population of CO in the flame. The rates for V-V exchange could not be estimated accurately enough to ensure that the results for the flame case are meaningful.

The points which are of main concern are the chain mechanism and the theoretical flame calculations. The branching-chain mechanism, given in figure 1-1, is responsible for most of the phenomena associated with CS_2/O_2 explosion, deflagration, and laser action. The one-dimensional flame theories adequately predict the behavior of the low pressure, isobaric CS_2/O_2 flame.

REFERENCES

1. W. T. Olson, Ed., Basic Considerations in the Combustion of Hydrocarbon Fuels with Air, NACA Report 1300 (1957).

2. V. V. Azatyan, U. M. Cershenson, E. N. Sarkissyan, G. A. Sachyan, and A. B. Nalbandyan, "Investigation of Low-Pressure Flames of a Number of Compounds Containing Sulfur by the ESR Method," Twelfth Symposium (International) on Combustion, pp. 989-994, The Combustion Institute (1969).

3. V. Kondratiev, "The Radiation of the Low-Temperature Flame of Carbon Disulphide," Acta Physicochimica URSS, Vol. 12, pp. 637-646 (1940).

4. M. A. A. Clyne and B. A. Thrush, "The Kinetics of the Carbon Monoxide Flame Bands," Ninth Symposium (International) on Combustion, pp. 177-183, Academic Press (1963).

5. K. G. P. Sulzmann, B. F. Myers, and E. R. Bartle, "CO Oxidation. I. Induction Period Preceding CO_2 Formation in Shock-Heated $CO-O_2$-Ar Mixtures," J. Chem. Phys., Vol. 42, pp. 3969-3979 (1965).

6. A. Sharma, J. P. Padur, and P. Warneck, "Chemiluminescent Reactions of CS_2, COS, and H_2S with Atomic Oxygen," J. Chem. Phys., Vol. 43, pp. 2155-2156 (1965).

7. K. F. Greenough and A. B. F. Duncan, "The Fluorescence of Sulfur Dioxide," J. Am. Chem. Soc., Vol. 83, pp. 555-560 (1961).

8. C. J. Halstead and B. A. Thrush, "The Kinetics of Elementary Reactions Involving the Oxides of Sulfur. III. The Chemiluminescent Reaction between Sulfur Monoxide and Ozone," Proc. Roy. Soc. (London), Vol. A295, pp. 380-398 (1966).

9. A. L. Myerson and F. R. Taylor, "The Ignition Limits of 1-3 Mixtures of Carbon Disulfide and Oxygen," J. Am. Chem. Soc., Vol. 75, pp. 4348-4350 (1953).

10. F. R. Taylor and A. L. Myerson, "First Limit Induction Time Studies of CS_2-O_2 Explosions," Seventh Symposium (International) on Combustion, pp. 72-79, Butterworths (1959).

11. V. N. Kondratiev, Chemical Kinetics of Gas Reactions, Addison-Wesley (1964).

12. N. Semenoff, "On the Kinetics of Complex Reactions," J. Chem. Phys., Vol. 7, pp. 683-699 (1939).

13. A. L. Myerson, F. R. Taylor, and P. L. Hanst, "Ultraviolet Absorption Spectra and the Chemical Mechanism of CS_2-O_2 Explosions," J. Chem. Phys., Vol. 26, pp. 1309-1320 (1957).

14. W. P. Wood and J. Heicklen, "Kinetics and Mechanism of the Carbon Disulfide - Oxygen Explosion," J. Phys. Chem., Vol. 75, pp. 861-866 (1971).

15. C. W. Allen, Astrophysical Quantities, the Athlone Press, 2nd Edition (1963).

16. J. L. Franklin and J. G. Dillard, Ionization Potentials, Appearance Potentials, and Heats of Formation of Gaseous Positive Ions, NSRDS-NBS Circular 26 (1969).

17. J. Troe and H. G. Wagner, "Unimolekulare Reaktionen in Thermischen Systemen," Berichte der Bunsengesellschaft für Physikalische Chemie, Vol. 71, pp. 937-979 (1967).

18. H. S. Johnson, Gas Phase Reaction Kinetics of Neutral Oxygen Species, NSRDS-NBS Circular 20 (1968).

19. H. A. Olschewski, J. Troe, and H. G. Wagner, "Unimolekularer Zerfall von CS_2 in Stoβwellen," Zeitschr. für Physikalische Chemie Neue Folge, Vol. 45, pp. 329-338 (1965).

20. H. A. Olschewski, J. Troe, and H. G. Wagner, "Der unimolekulare Zerfall von SO_2," Zeitsch. für Physikalische Chemie Neue Folge, Vol. 44, pp. 173-183 (1965).

21. M. A. Nettleton and R. Stirling, "Formation and Decomposition of Sulfur Trioxide in Flames and Burned Gases," Twelfth Symposium (International) on Combustion, pp. 635-641, The Combustion Institute (1969).

22. R. K. Hanson, "Shock-tube Study of Carbon Monoxide Dissociation Kinetics," J. Chem. Phys., Vol. 60, pp. 4970-4976 (1974).

23. W. Braun, A. M. Bass, D. D. Davis, and J. D. Simmons, "Flash Photolysis of Carbon Suboxide: Absolute Rate Constants for Reactions of $C(^3P)$ and $C(^1D)$ with H_2, N_2, CO, NO, O_2, and CH_4," Proc. Royal Soc. (London), Vol. A312, pp. 417-434 (1969).

24. F. F. Martinotti, M. J. Welch, and A. P. Wolf, "The Reactivity of Thermal Carbon Atoms in the Gas Phase," Chemical Communications, Vol. 1968, pp. 115-116 (1968).

25. D. R. Stull and H. Prophet, JANAF Thermochemical Tables, NSRDS-NBS Circular 37 (1971).

26. B. Darwent, Bond Dissociation Energies in Simple Molecules, NSRDS-NBS Circular 31 (1970).

27. L. P. Blanchard and P. Le Goff, "Mass Spectrometric Study of the Species CS, SO, and $CC\ell_2$ Produced in Primary Heterogeneous Reactions," Canadian J. of Chemistry, Vol. 35, pp. 89-98 (1957).

28. S. J. Arnold and G. H. Kimbell, "Observations on the Visible Emission from Electronically Excited CS_2," Canadian J. of Chemistry, Vol. 49, pp. 4110-4114 (1971).

29. R. J. Richardson, H. T. Powell, and J. D. Kelley, "Heterogeneous Loss Reaction of Carbon Monosulfide," J. Phys. Chem., Vol. 77, pp. 2601-2604 (1973).

30. H. G. Wagner and J. Wolfrum, "Reaction of Atoms," Angewandte Chemie, International Edition, Vol. 10, pp. 604-619 (1971).

31. U. Bonne, K. H. Homann, and H. G. Wagner, "Carbon Formation in Premixed Flames," Tenth Symposium (International) on Combustion, pp. 503-512, The Combustion Institute (1965).

32. W. Q. Jeffers and C. E. Wisnall, "A Transverse-Flow CO Chemical Laser," App. Phys. Letters, Vol. 17, pp. 67-69 (1970).

33. A. Tewarson and H. B. Palmer, "Origins of Chemiluminescent Emission in Low-Pressure Flames of Sulfur-Containing Compounds," Thirteenth Symposium (International) on Combustion, pp. 99-107, The Combustion Institute (1971).

34. D. B. Sheen, "Shock-Tube Study of the Oxidation of Carbon Disulfide," J. Chem. Phys., Vol. 52, pp. 648-655 (1970).

35. G. Hancock and I. W. M. Smith, "Infrared Chemiluminescence from Vibrationally Excited CO," Trans. Faraday Soc., Vol. 67, pp. 2586-2597 (1971).

36. F. J. Wright, "Flash Photolysis of Carbon Disulfide and Its Photochemically Initiated Oxidation," J. Phys. Chem., Vol. 64, pp. 1648-1652 (1960).

37. R. J. Donovan and D. J. Little, "The Rate of the Reaction $S(3^3P_J) + O_2$," Chem. Phys. Lett., Vol. 13, pp. 488-490 (1972).

38. J. J. McGarvey and W. D. McGrath, "Kinetic Spectroscopy in the Vacuum Ultra-violet Region. I. The Dissociation Energy of SO and the Combustion of Hydrogen Sulphide, Carbon Disulfide, and Carbonyl Sulphide," Proc. Roy. Soc. (London), Vol. A278, pp. 490-504 (1964).

39. M. DeSorgo, A. J. Yarwood, O. P. Strauz, and H. E. Gunning, "The Photolysis of Carbon Disulfide and Carbon Disulfide - Oxygen Mixtures," Canadian J. of Chemistry, Vol. 43, pp. 1886-1891 (1965).

40. A. B. Callear, "Flash Photolysis of Carbon Disulphide," Proc. Roy. Soc. (London), Vol. A276, pp. 401-412 (1963).

41. R. J. Donovan, D. Husain, and P. T. Jackson, "Spectroscopic and Kinetic Studies of the SO Radical and the Photolysis of Thionyl Chloride," Trans. Faraday Soc., Vol. 65, pp. 2930-2940 (1969).

42. N. Basco and R. D. Morse, "The Adiabatic Flash Photolysis of NO_2 and SO_2," Proc. Roy. Soc. (London), Vol. A321, pp. 129-139 (1971).

43. N. Cohen and J. Heicklen, "The Oxidation of Inorganic Non-metallic Compounds," Comprehensive Chemical Kinetics, Vol. 6, Elsevier, pp. 1-128 (1972).

44. A. G. Gaydon, G. H. Kimbell, and H. B. Palmer, "A Shock-Tube Study of the Kinetics of Decomposition of Carbon Disulfide," Proc. Roy. Soc. (London), Vol. A279, pp. 313-326 (1964).

45. I. W. M. Smith, "Relaxation of Vibrationally Excited CS Produced in the Reaction: $O(^3P) + CS_2 \rightarrow SO+CS$," Trans. Faraday Soc., Vol. 64, pp. 3183-3191 (1968).

46. K. H. Homann, G. Krome, and H. G. Wagner, "Schwefelkohlenstoff-Oxydation, Geschwindigkeit von Elementarreaktionen," Berichte der Bunsengesellschaft für Physikalische Chemie, Vol. 72, pp. 998-1004 (1968).

47. A. A. Westenberg and N. deHaas, "Atom-Molecule Kinetics Using ESR Detection. V. Results for $O+OCS$, $O+CS_2$, $O+NO_2$, and $H+C_2H_4$," J. Chem. Phys., Vol. 50, pp. 707-719 (1969).

48. I. W. M. Smith, "Rate Parameters for Reactions of $O(2^3P)$ with CS_2, NO_2, and Olefins," Trans. Faraday Soc., Vol. 64, pp. 378-389 (1968).

49. I. W. M. Smith, "Experimental and Computer Studies of the Kinetics and Distribution of Vibrational Energy in Both Products of the Reaction $O(^3P)+CS_2 \rightarrow SO+CS$," Discussions of the Faraday Society, Vol. 44, pp. 194-204 (1967).

50. A. B. Callear and I. W. M. Smith, "Measurement of the Rate Parameters for Reaction of $O(2^3P)$ with Carbon Disulphide and Olefines, by Flash Spectroscopy," Nature, Vol. 213, pp. 382-383 (1967).

51. G. Hancock and I. W. M. Smith, "Infrared Chemiluminescence from the Reaction $O+CS \rightarrow CO+S$," Chem. Phys. Lett., Vol. 3, pp. 573-576 (1969).

52. I. R. Slagle, J. R. Gilbert, and D. Gutman, "Kinetics of the Reaction between Oxygen Atoms and Carbon Disulfide," J. Chem. Phys., Vol. 61, pp. 704-709 (1974).

53. D. D. Davis, R. B. Klemm, and M. Pilling, "A Flash Photolysis-Resonance Fluorescence Kinetics Study of Ground-State Sulfur Atoms: I. Absolute Rate Parameters for Reaction of $S(^3P)$ and $O_2(^3\Sigma)$," Int. J. Chem. Kinetics, Vol. 4, pp. 367-382 (1972).

54. S. Tsuchiya, N. Nielsen, and S. H. Bauer, "Lasing Action and the Relative Populations of Vibrationally Excited Carbon Monoxide Produced in Pulse-Discharged Carbon Disulfide - Oxygen - Helium Mixtures," J. Phys. Chem., Vol. 77, pp. 2455-2464 (1973).

55. R. W. Fair, A. Van Roodselaar, and O. P. Strausz, "The Reaction of $S(^3P)$ Atoms with Molecular Oxygen," Canadian J. of Chemistry, Vol. 49, pp. 1659-1664 (1971).

56. R. W. Fair and B. A. Thrush, General Discussions, Discussions of the Faraday Society, Vol. 44, pp. 236-237 (1967).

57. N. Basco and A. E. Pearson, "Reactions of Sulfur Atoms in Presence of Carbon Disulphide, Carbonyl Sulphide, and Nitric Oxide," Trans. Faraday Soc., Vol. 63, pp. 2684-2694 (1967).

58. P. Fowles, M. DeSorgo, A. J. Yarwood, O. P. Strausz, and H. E. Gunning, "The Reactions of Sulfur Atoms. IX. The Flash Photolysis of Carbonyl Sulfide and the Reactions of $S(^1D)$ Atoms with Hydrogen and Methane," J. Am. Chem. Soc., Vol. 86, pp. 1352-1362 (1967).

59. E. L. Merryman and A. Levy, "Kinetics of Sulfur-Oxide Formation in Flames. II. Low Pressure H_2S Flames," J. Air Pollution Control Association, Vol. 17, pp. 800-806 (1967).

60. A. Sharma, J. P. Padur, and P. Warneck, "The Chemiluminescent Reactions of Atomic Oxygen with Carbonyl Sulfide and Hydrogen Sulfide," J. Phys. Chem., Vol. 71, pp. 1602-1607 (1967).

61. D. J. Williams, "The Reaction $SO+O_2 \rightarrow SO_2+O$," Combustion and Flame, Vol. 12, pp. 165-168 (1968).

62. T. R. Rolfes, R. R. Reeves, and P. Harteck, "The Chemiluminescent Reaction of Oxygen Atoms with Sulfur Monoxide at Low Pressures," J. Phys. Chem., Vol. 69, pp. 849-853 (1965).

63. C. J. Halstead and B. A. Thrush, "The Kinetics of Elementary Reactions Involving the Oxides of Sulfur. II. Chemical Reactions in the Sulfur Dioxide Afterglow," Proc. Roy. Soc. (London), Vol. A295, pp. 363-379 (1966).

64. J. O. Sullivan and P. Warneck, "Mass Spectrometric Investigation of the Reaction between Oxygen Atoms and Carbonyl Sulfide," Berichte der Bunsengesellschaft für Physikalische Chemie, Vol. 69, pp. 7-11 (1965).

65. C. J. Halstead and B. A. Thrush, "Chemiluminescent Reaction of SO," Photochemistry and Photobiology, Vol. 4, pp. 1007-1013 (1965).

66. K. Hoyermann, H. G. Wagner, and J. Wolfrum, "Bestimmung der Geschwindigkeit der Reaktion $O+COS \rightarrow CO+SO$," Berichte der Bunsengesellschaft für Physikalische Chemie, Vol. 71, pp. 603-606 (1967).

67. V. N. Kondratiev and E. I. Intezarova, "Interaction between CO and O," Int. J. Chem. Kinetics, Vol. 1, pp. 105-111 (1969).

68. M. C. Lin and S. H. Bauer, "Bimolecular Reaction of N_2O with CO and Recombination of O and CO as Studied in a Single-Pulse Shock Tube," J. Chem. Phys., Vol. 50, pp. 3377-3391 (1969).

69. T. A. Brabbs and F. E. Belles, "Recombination of Carbon Monoxide and Atomic Oxygen at High Temperatures," Eleventh Symposium (International) on Combustion, pp. 125-135, The Combustion Institute (1967).

70. R. S. Brokaw, "Ignition Kinetics of the Carbon Monoxide - Oxygen Reaction," Eleventh Symposium (International) on Combustion, pp. 1063-1073, The Combustion Institute (1967).

71. H. L. Peterson and C. B. Kretschmer, Kinetics of Recombination of Atomic Oxygen at Room Temperature, Aerojet Report TN-38, Aerojet-General Corp. (1960), AFOSR TN-60-1478.

72. W. P. Wood and J. Heicklen, "The Photooxidation of Carbon Disulfide," J. Phys. Chem., Vol. 75, pp. 854-860 (1971).

73. F. G. Sadie, P. A. Buger, and O. G. Malan, "Reaction Mechanisms of the CS_2-O_2 Chemical Laser," J. App. Phys., Vol. 43, pp. 5141-5142 (1972).

74. F. Stuhl and H. Niki, "Measurements of Rate Constants for Termolecular Reactions of $O(^3P)$ with NO, O_2, CO, N_2, and CO_2 Using a Pulsed Vacuum-uv Photolysis-Chemiluminescent Method," J. Chem. Phys., Vol. 55, pp. 3943-3953 (1971).

75. B. H. Mahan and R. B. Solo, "Carbon Monoxide - Oxygen Atom Reaction," J. Chem. Phys., Vol. 37, pp. 2669-2677 (1962).

76. D. C. Krezenski, R. Simonaitis, and J. Heicklen, "The Reactions of $O(^3P)$ with Ozone and Carbonyl Sulfide," Int. J. Chem. Kinetics, Vol. 3, pp. 467-482 (1971).

77. F. Kaufman, "Reactions of Oxygen Atoms," Progress in Reaction Kinetics, Vol. 1, pp. 3-39 (1961).

78. F. Kaufman, "The Air Afterglow and Its Use in the Study of Some Reactions of Atomic Oxygen," Proc. Roy. Soc. (London), Vol. A247, pp. 123-139 (1958).

79. M. F. R. Mulcahy, J. R. Stevens, and J. C. Ward, "The Kinetics of Reaction between Oxygen Atoms and Sulfur Dioxide: an Investigation by Electron Spin Resonance Spectrometry," J. Phys. Chem., Vol. 71, pp. 2124-2131 (1967).

80. M. F. R. Mulcahy, J. R. Steven, J. C. Ward, and D. J. Williams, "Kinetics of Interaction of Oxygen Atoms with Sulfur Oxides," Twelfth Symposium (International) on Combustion, pp. 323-329, The Combustion Institute (1969).

81. E. R. Allen and R. D. Cadle, "A Study of the Effect of Molecular Oxygen on Atomic Oxygen-Hydrocarbon Reactions," Photochemistry and Photobiology, Vol. 4, pp. 979-987 (1965).

82. D. D. Davis, J. Prusazcyk, M. Dwyer, and P. Kim, "A stop-Flow Time-of-Flight Mass Spectrometry Kinetics Study. Reaction of Ozone with Nitrogen Dioxide and Sulfur Dioxide," J. Phys. Chem., Vol. 78, pp. 1775-1779 (1974).

83. K. J. Olszyma and J. Heicklen, "The Reaction of Ozone with Carbon Disulfide," J. Phys. Chem., Vol. 74, pp. 4188-4198 (1970).

84. A. N. Oraevskii, "A Chemical Laser Based on Branched Reactions," Soviet Physics JETP, Vol. 28, pp. 744-747 (1969).

85. J. E. Wollrab and R. L. Rasmussen, "Lifetime of Gas-phase Carbon Monosulfide," J. Chem. Phys., Vol. 58, pp. 4702-4703 (1973).

86. J. O. Hirschfelder, C. F. Curtiss, and R. B. Bird, Molecular Theory of Gases and Liquids, Wiley and Sons (1964).

87. A. B. Callear and R. G. W. Norrish, "Formation of Vibrationally Excited Carbon Monosulphide and Sulphur by the Flash Photolysis of Carbon Disulphide," Nature, Vol. 188, pp. 52-53 (1960).

88. E. B. Gordon, V. S. Pavlenko, Y. L. Moskvin, M. S. Drozdov, P. S. Vinogradov, and V. L. Tal'roze, "Kinetics of a Pulsed Chemical Carbon Monoxide Laser with Photoinitiated Oxidation of Carbon Disulfide," Soviet Physics JETP, Vol. 36, pp. 611-618 (1973).

89. T. V. Jacobson and G. H. Kimbell, "Transversely Spark-Initiated Chemical Laser with High Pulse Energies," J. App. Phys., Vol. 41, pp. 5210-5212 (1970).

90. L. R. Boedeker, J. A. Shirley, and B. R. Bronfin, "Arc-excited Flowing CO Chemical Laser," App. Phys. Lett., Vol. 21, pp. 247-249 (1972).

91. F. G. Sadie, P. A. Buger, and O. G. Malan, "Continuous-Wave Overtone Bands in a CS_2-O_2 Chemical Laser," J. App. Phys., Vol. 43, pp. 2906-2907 (1972).

92. C. J. Ultee and P. A. Bonczyk, "Performance and Characteristics of a Chemical CO Laser," IEEE J. Quantum Electronics, Vol. QE-10, pp. 105-110 (1974).

93. W. Q. Jeffers and C. E. Wiswall, "Efficient Low-band Operation of a CO Chemical Laser," App. Phys. Lett., V. 23, pp. 626-627 (1973).

94. K. D. Foster, "Initial Distribution of $CO^{\dagger}$ from the Reaction $O+CS \rightarrow CO^{\dagger}+S$," J. Chem. Phys., Vol. 57, pp. 2451-2455 (1972).

95. K. D. Foster and G. H. Kimbell, "Characteristics of a CS_2/O_2 Chemical Laser with Flow Transverse to the Optical Axis," Fourteenth Symposium (International) on Combustion, pp. 203-210, The Combustion Institute (1973).

96. R. D. Suart, P. H. Dawson, and G. H. Kimbell, "CS_2/O_2 Chemical Lasers: Chemistry and Performance Characteristics," J. App. Phys., Vol. 43, pp. 1022-1032 (1972).

97. R. D. Suart, S. J. Arnold, and G. H. Kimbell, "Power Enhancement of a CO Chemical Laser by the Addition of Vibrationally Cool Gases," Chem. Phys. Lett., Vol. 7, pp. 337-340 (1970).

98. M. A. Pollack, "Laser Oscillation in Chemically Formed CO," App. Phys. Lett., Vol. 8, pp. 237-238 (1966).

99. D. W. Gregg and S. J. Thomas, "Analysis of the CS_2-O_2 Chemical Laser Showing New Lines and Selective Excitation," J. App. Phys., Vol. 39, pp. 4399-4404 (1968).

100. S. Rosenwaks and S. Yatsiv, "CO Chemical Laser by Flash Photolysis of $CS_2 + NO_2$," Chem. Phys. Lett., Vol. 9, pp. 266-268 (1971).

101. S. J. Arnold and G. H. Kimbell, "Chemical Laser Action in Electrically Pulsed Flowing CS_2-O_2 Mixtures," App. Phys. Lett., Vol. 15, pp. 351-353 (1969).

102. C. Wittig, J. C. Hassler, and P. D. Coleman, "Constant-Wave Laser Oscillation in a Carbon Monoxide Chemical Laser," Nature, Vol. 226, pp. 845-846 (1970).

103. R. D. Suart, G. H. Kimbell, and S. J. Arnold, "Continuous-Wave Stimulated Emission in Flowing Carbon Disulfide-Oxygen Mixtures," Chem. Phys. Lett., Vol. 5, pp. 519-520 (1970).

104. W. Q. Jeffers, C. E. Wiswall, J. D. Kelley, and R. J. Richardson, "cw CO Chemical Laser Directly Fueled by Carbon Monosulfide," App. Phys. Lett., Vol. 22, pp. 587-589 (1973).

105. Y. Hirose, J. C. Hassler, and P. D. Coleman, "A CW-CO Chemical Laser from the Reaction of Active Nitrogen with O_2+CS_2," IEEE J. Quantum Electronics, Vol. QE-9, pp. 114-117 (1973).

106. A. N. Chester, "Chemical Lasers: a Status Report," Laser Focus, Vol. 7, pp. 25-30 (1971).

107. K. D. Foster and G. H. Kimbell, "Vibrational Population Inversion of CO in a Free-Burning CS_2/O_2 Flame," J. Chem. Phys., Vol. 53, pp. 2539-2540 (1970).

108. H. S. Piloff, S. K. Searles, and N. Djeu, "cw CO Laser from the CS_2-O_2 Flame," App. Phys. Lett., Vol. 19, pp. 9-11 (1971).

109. C. Wittig, J. C. Hassler, and P. D. Coleman, "Carbon Monoxide Chemical Laser Utilizing a Fast Flow System," App. Phys. Lett., Vol. 16, pp. 117-118 (1970).

110. A. Lecuyer and N. Legay-Sommaire, "Étude d'un laser à oxyde de carbone formé chimiquement," Comptes Rendus Acad. Sc. (Paris), Vol. B271, pp. 1212-1215 (1970).

111. N. Djeu, H.S. Pilloff, and S.K. Searles, "Determination of Optical Gain for CO Transitions in a CS_2-O_2 Flame by Oscillation-Range Measurements," App. Phys. Lett., Vol. 18, pp. 538-540 (1971).

112. S.K. Searles and N. Djeu, "Characteristics of a CW CO Laser Resulting from a CS_2-O_2 Additive Flame," Chem. Phys. Lett., Vol. 12, pp. 53-56 (1971).

113. C.J. Utlee, "Premixed cw Electric-Discharge CO Chemical Lasers," App. Phys. Lett., Vol. 19, pp. 535-537 (1971).

114. C. Wittig, J.C. Hassler, and P.D. Coleman, "Continuous Wave Carbon Monoxide Chemical Laser," J. Chem. Phys., Vol. 55, pp. 5523-5532 (1971).

115. B. Ahlborn, P. Gensel, and K.L. Kompa, "Transverse-Flow Transverse-Pulsed Chemical CO Laser," J. Appl. Phys., Vol. 43, pp. 2487-2489 (1972).

116. W.Q. Jeffers, "R-branch Emission from a cw CO Chemical Laser," App. Phys. Lett., Vol. 21, pp. 267-269 (1972).

117. F.G. Sadie, P.A. Buger, and O.G. Malan, "Investigations on the CS_2-O_2 Chemical Laser," Z. Naturforschung, Vol. 27, pp. 1260-1263 (1972).

118. M.J. Linevsky and R.A. Carabetta," cw Laser Power from Carbon Bisulfide Flames," App. Phys. Lett., Vol. 22, pp. 288-291 (1973).

119. S. Rosenwaks and I.W.M. Smith, "Laser Emission from CO Formed in the Flash-initiated Reactions of $O(^3P)$ Atoms with Cs and CSe," Faraday Transactions II, Vol. 69, pp. 1416-1424 (1973).

120. Y. Hirose, Y. Nachshon, T.A. DeTemple, and P.D. Coleman, "Single-line Operation of a 2-W Longitudinal cw CO Chemical Laser with No Frequency-selective Element in the Optical Cavity," App. Phys. Lett., Vol. 23, pp. 195-197 (1973).

121. W.Q. Jeffers and C.E. Wiswall, "Experimental Studies of the $O/O_2/CS_2$ CW CO Chemical Laser," IEEE J. Quantum Electronics, Vol. QE-10, pp. 860-869 (1974).

122. J. Stricker and S. H. Bauer, "Stimulated CO Emission of the (1→0) Band in a Pulse Initiated (CS_2+O_2) Chemical Laser," Chem. Phys. Lett., Vol. 28, pp. 98-100 (1974).

123. V. N. Kondratiev, "The Mechanism of Carbon Disulfide Oxidation," Kinetics and Catalysis, Vol. 13, pp. 1223-1235 (1973).

124. D. W. Howgate and T. A. Barr, Jr., "Dynamics of the CS_2-O_2 Flame," J. Chem. Phys., Vol. 59, pp. 2815-2829 (1973).

125. T. J. Menne, Laser Kinetic Data Development, McDonnell-Douglas Research Laboratories, Technical Report RK-CR-73-7 (1973).

126. P. H. Krupenic, The Band Spectrum of Carbon Monoxide, NSRDS-NBS Circular 5 (1966).

127. J. T. Yardley, "Laser Action in Highly-Excited Vibrational Levels of CO," J. Molec. Spectroscopy, Vol. 35, pp. 314-324 (1970).

128. G. Hancock and I. W. M. Smith, "Quenching of Infrared Chemiluminescence. ". The Rates of De-Excitation of CO($4 \leq v \leq 13$) by He, CO, NO, N_2, O_2, OCS, N_2O, and CO_2," Applied Optics, Vol. 10, pp. 1827-1842 (1971).

129. S. D. Rockwood, J. E. Brau, W. A. Proctor, and G. H. Canavau, "Time-Dependent Calculations of Carbon Monoxide Laser Kinetics," IEEE J. Quantum Electronics, Vol. QE-9, pp. 120-129 (1973).

130. C. E. Treanor, J. W. Rich, and R. C. Rehm, "Vibrational Relaxation of Anharmonic Oscillators with Exchange-dominated Collisions," J. Chem. Phys., Vol. 48, pp. 1798-1807 (1968).

131. J. T. Yardley, "Population Inversion and Energy Transfer in CO Lasers," Applied Optics, Vol. 10, pp. 1760-1767 (1971).

132. G. Hancock, C. Morley, and I. W. M. Smith, "Vibrational Excitation of CO in the Reaction: O+CS → CO+S," Chem. Phys. Lett., Vol. 12, pp. 193-196 (1971).

133. H. T. Powell and J. D. Kelley, "Vibrational Distribution of Carbon Monoxide from O+CS → S+CO(v)," J. Chem. Phys., Vol. 60, pp. 2191-2192 (1974).

134. N. Djeu, "Quantitative Laser Measurement of Very Small Absorptions: Studies of the O+CS → CO(v)+S Reaction," J. Chem. Phys., Vol. 60, pp. 4109-4115 (1974).

135. G. Hancock, B. A. Ridley, and I. W. M. Smith, "Infrared Chemiluminescence from Vibrationally Excited CO, Part 2. Product Distribution from the Reaction O+CS → CO+S," J. Chem. Soc., Faraday Transactions II, Vol. 68, pp. 2117-2126 (1972).

136. P. L. Moore, P. N. Clough, and J. Geddes, "A Study of the Reaction O+CS_2 → SO+CS Using Crossed Molecular Beams," Chem. Phys. Lett., Vol. 17, pp. 608-610 (1972).

137. J. Geddes, P. N. Clough, and P. L. Moore, "Crossed Molecular Beam Study of Reactive Scattering," J. Chem. Phys., Vol. 61, pp. 2145-2149 (1974).

138. V. H. Dibeler and J. A. Walker, "Mass-Spectrometric Study of Photoionization. VI. O_2, CO_2, COS, and CS_2," J. Optical Soc. Amer., Vol. 57, pp. 1007-1012 (1967).

139. H. Okabe, "Photodissociation of CS_2 in the Vacuum Ultraviolet; Determination of D_o^o (SC-S)," J. Chem. Phys., Vol. 56, pp. 4381-4384 (1972).

140. D. L. Hildbrand, "Thermochemistry of the Molecules CS and CS^+," Chem. Phys. Lett., Vol. 15, pp. 379-380 (1972).

141. L. A. Young and W. J. Eachus, "Dipole Moment Function and Vibration-Rotation Matrix Elements for CO^+," J. Chem. Phys., Vol. 44, pp. 4195-4206 (1966).

142. B. A. Lengyel, Introduction to Laser Physics, Wiley and Sons (1966).

143. E. A. Kennard, Kinetic Theory of Gases, McGraw-Hill (1938).

144. Y. Fushiki and S. Tsuchiya, "Vibration-to-Vibration Energy Transfer of CO in the States of v = 2 ~ 9," Japanese J. Appl. Phys., Vol. 13, pp. 1043-1049 (1974).

145. W. Q. Jeffers and J. D. Kelley, "Calculations of V-V Transfer Probabilities in CO-CO Collisions," J. Chem. Phys., Vol. 55, pp. 4433-4437 (1971).

146. I. W. M. Smith and C. Wittig, "Vibrational Energy Transfer in Carbon Monoxide at Low Temperatures," J. Chem. Soc., Faraday Transactions II, Vol. 69, pp. 939-951 (1973).

147. D. J. Miller and R. C. Millikan, "Vibration-Vibration Energy Exchange between Carbon Monoxide and Oxygen," Chem. Phys. Lett., Vol. 27, pp. 10-13 (1974).

148. W. H. Green and J. K. Hancock, "Measurement of CO(v=1) Vibrational Energy Transfer Rates Using a Frequency-doubled CO_2 Laser," J. Chem. Phys., Vol. 59, pp. 4326-4335 (1973).

149. J. K. Hancock, D. F. Starr, and W. H. Green, "Measurement of the Rate of Excitation and Deactivation of OCS(001), N_2O(001), CS_2(001), and C_2N_2(00100) Using Laser Excited CO as a Pumping Source," J. Chem. Phys., Vol. 61, pp. 3017-3025 (1974).

150. A. B. Peterson and C. Wittig., "A Chemically Pumped CO_2 Laser from the CS_2/O_2 Reaction," Chem. Phys. Lett., Vol. 27, pp. 442-444 (1974).

151. G. C. Berend and R. L. Thommarson, "Vibrational Relaxation of Carbon Monoxide by Helium," J. Chem. Phys., Vol. 58, pp. 1256-1257 (1973).

152. D. C. Richman and R. C. Millikan, "Collisional Exchange of Vibrational Energy between CO(v=1) and CS_2: Evidence for Dominant Multiquantum Effects," J. Chem. Phys., Vol. 61, pp. 4263-4266 (1974).

153. T. von Kármán, "Structure and Propagation of Laminar Flames," Sixth Symposium (International) on Combustion, pp. 1-11, Reinhold (1957).

154. F. A. Williams, Combustion Theory, Addison-Wesley (1965).

155. W. E. Forsythe, Smithsonial Physical Tables, 9th Revised Edition, Smithsonian Institute publication 4169 (1964).

156. S. D. Conte, Elementary Numerical Analysis, McGraw-Hill (1965).

157. J. O. Hirschfelder, "Heat Conductivity in Polyatomic, Electronically Excited, or Chemically Reacting Mixtures, III," Sixth Symposium (International) on Combustion, pp. 351-366, Reinhold (1957).

158. J. H. Ferziger and H. G. Kaper, Mathematical Theory of Transport Processes in Gases, North-Holland (1972).

159. S. C. Saxena and G. P. Gupta, "Column Method of Measuring Thermal Conductivity of Gases: Results on Carbon Monoxide and Oxygen," Progress in Astronautics and Aeronautics, Vol. 23, pp. 45-62 (1970).

160. Y. S. Touloukian, P. E. Liley, and S. C. Saxena, Thermal Conductivity, Nonmetallic Liquids and Gases, IFI/Plenum (1970).

161. B. H. Mahan, University Chemistry, Addison-Wesley (1965).

162. D. B. Spalding and P. L. Stephenson, "Laminar Flame Propagation in Hydrogen + Bromine Mixtures," Proc. Roy. Soc. (London), Vol. A324, pp. 315-337 (1971).

163. A. G. Gaydon and H. G. Wolfhard, Flames, Their Structure, Radiation, and Temperature, 3rd Edition, Chapman and Hall (1970).

164. J. M. Singer, "Burning-Velocity Measurements on Slot Burners; Comparison with Cylindrical Burner Determinations," Fourth Symposium (International) on Combustion, pp. 352-358, Williams and Wilkins (1953).

165. Anonymous, Kodak Master Photoguide for Still Picture-Taking, Eastman Kodak Co. (1968).

166. R. M. Fristrom and A. A. Westenberg, Flame Structure, McGraw-Hill (1965).

167. Y. Beers, Introduction to the Theory of Error, Addison-Wesley (1957).

168. G. Herzberg, Molecular Spectra and Molecular Structure, I. Spectra of Diatomic Molecules, 2nd Edition, Van Nostrand (1950).

169. S. Gordon and B. J. McBride, Computer Program for Calculation of Complex Chemical Equilibrium Compositions, Rocket Performance, Incident and Reflected Shocks, and Chapman-Jouguet Detonations, NASA SP-273 (1971).

170. G. R. Nickerson, H. M. Grey, and D. E. Coats, Generalized Kinetic Analysis Program, Ultrasystems, Inc., Irvine, California (1971).

APPENDIX A.

The computer program which has been written to calculate the von Kármán approximations is designated as KARMAN4. The ten subprograms which comprise KARMAN4 are written in Fortran IV G. The flow diagram of Figure A-1 displays the relationship between the ten subprograms, and Table A-1 contains a brief statement on the main purpose of each of the subprograms. The variables of the coding, which is given in Figures A-2 through A-6, were made to correspond to the last transformation of Chapter 5, equation (5.21).

Common Blocks

There are seven common blocks in these programs. These blocks are utilized to transmit data from BLOCK DATA, transmit constants from TFLAME, or supply data to KARAPP for punch output.

The common block FBLOCK contains the thermodynamic tables used to calculate the adiabatic flame temperature. It appears in the programs TFLAME and BLOCK DATA. The flame temperature is calculated from six-entry tabular forms of the heat capacity and enthalpy in the following manner.

The flame temperature is calculated from the implicit equation:

$$\sum_{i=1}^{N} H_i(T_f)X_i(\infty) = \sum_{i=1}^{N} H_i(T_0)X_i(-\infty) \quad . \qquad (A.1)$$

Substituting the initial mole fraction from equation (5.4), the final mole fractions from equation (5.5), and dropping the subscript on X_0, the implicit equation becomes

$$\left[\frac{1-\frac{7X}{2}}{X}\right] H_i(T_f) + H_4(T_f) + 2H_5(T_f)$$

$$= \left[1 - \frac{X}{2}\right] H_2(T_0) + \frac{\left[1 - \frac{X}{2}\right]\left[1-X\right]}{X} H_1(T_0) \quad . \quad (A.2)$$

Assume a piece-wise linear approximation to the heat capacity so that the heat capacity and enthalpy can be represented by

$$C_p = a_{2i} + a_{3i} T \quad , \qquad (A.3)$$

$$H_i(T) = a_{1i} + a_{2i}T + \frac{a_{3i}}{2} T^2 \quad .$$

The flame temperature equation then becomes explicit and quadratic:

$$\left[\left(\frac{1}{X} - \frac{7}{2}\right)a_{31}+a_{34}+2a_{35}\right] T_f^2 + \left[\left(\frac{1}{X} - \frac{7}{2}\right)a_{21}+a_{24}+2a_{25}\right] T_f$$

$$= \left(2 + \frac{X}{2}\right) a_{11} + \left(1 - \frac{X}{2}\right)a_{12} - a_{14} - 2a_{15} \quad . \qquad (A.4)$$

The flame temperature is then found easily.

To provide a reasonably accurate heat capacity approximation, the heat capacity data are broken into six temperature regions. The flame temperature is then calculated from the lower bound of the region in which it falls. The seven arrays, each array corresponding to the temperature table, and one scalar, which are contained in this block and their association with the above calculation are:

A1: array which contains the constants a_{21}

A2: array which contains the sum $a_{24}+2a_{25}$

B1: array which contains the constants $a_{31}/2$

B2: array which contains the sum $a_{34}/2 + a_{35}$

H1: array which contains the constants a_{11}

H2: array which contains the sum $-a_{14}-2a_{15}$

TC: array which contains the temperatures corresponding to the table for the above arrays

HZ: scalar which contains the enthalpy of CS_2 at 300 K

The common block PBLOCK contains the average heat capacity and the adiabatic flame temperature. It appears in the programs TFLAME and KARAPP. This block is utilized to transmit data from TFLAME to KARAPP for punch output. The two scalars held in PBLOCK and their meanings are:

C: average heat capacity, $\bar{C}_p$

T: adiabatic flame temperature, T_f

The common block TBLOCK contains the constants required for the von Kármán approximations. This block occurs in the programs KARAPP, EKAR, VDUF, ZINT, and THREE along with the program TFLAME in which these constants are calculated. The scalars in this block and the constants which they represent are:

A: activation energy, θ_a

B: initial temperature constant, $\frac{1}{1-\theta_0}$

D: ignition temperature constant, δ

The common block UBLOCK contains the distance array and is used to transmit this array from ZINT to KARAPP for punch output. The array contained on UBLOCK and its meaning are:

U: array which contains the distances corresponding to the non-dimensional temperature variables η, z

The common block VBLOCK contains the diffusion velocity ratio and is used to transmit this array from VDUF, where it is filled, to KARAPP, where it may be used for punch output. The array contained in VBLOCK and its meaning are:

V: array which contains the diffusion velocity ratio, V_4/v

The common block YBLOCK contains the initial mole fraction of CS_2 and the array related to the mass flux fraction. This block appears in the six subprograms KARAPP, EKAR, VDUF, FIND3, THREE, and ZINT. The variables contained in YBLOCK and their meanings are:

X: initial mole fraction of CS_2 , X_0

Y: array containing the variable which is related to the mass flux fraction, $y = 1-\varepsilon$

The common block ZBLOCK contains the approximations to the eigenvalue based on the initial mole fraction of CS_2. This block transmits the data from BLOCK DATA to EGUESS, where it is used. The array and its meaning are:

Z: array containing approximations to the eigenvalue of the second von Kármán approximation

MAIN

The program MAIN reads in the number of cases and the initial mole fraction of CS_2 for each of the cases. This value is checked to be sure that it is within the bounds required for the calculations to be valid; that is, a lean flame.

This program calls subroutine KARAPP for the von Kármán approximation to be made. The scalar variables unique to this program are:

N: number of cases

I: counter for the cases

X: initial mole fraction of CS_2 , X_0

KARAPP

The subroutine KARAPP contains the logic for the calculation of the three von Kármán approximations. This subroutine calls the subprograms TFLAME, EKAR, VDUF, EGUESS, FIND3, and ZINT, while not performing any calculations. Punch output is most readily taken from this program. The scalars appearing in this program are:

XXXX: initial mole fraction of CS_2, X_0

E: approximation to the eigenvalue for the second von Kármán approximation

TFLAME

The subroutine TFLAME calculates and sets the constant required for the von Kármán approximations. This program calls no others, and it calculates the three constants contained in the common block TBLOCK and the two constants contained in the common block PBLOCK. The scalars of this program and their meanings are:

TZ: initial temperature, T_0

X: initial mole fraction of CS_2, input from the calling sequence, X_0

I: integer whose value determines which part of the thermodynamic tables are used to calculate the flame temperature

Z: intermediate storage variable

C: average heat capacity, $\bar{C}_p$

V: intermediate storage variable

U: intermediate storage variable

T: adiabatic flame temperature, T_f

TI: ignition temperature, T_I

EKAR

The subroutine EKAR calculates the zeroth and first von Kármán approximations. The integral I defined in equation (5.24) is evaluated by Simpson's method*, and then the zeroth and first approximations are calculated by equations (5.25) and (5.30), respectively. This program calls no others. The scalar variables which appear in this program and their meanings are:

Z: non-dimensional temperature variable, η

S: intermediate constant

T: intermediate constant

I: counter for evaluating the integrand and for the integration

R: intermediate storage variable

Q: intermediate storage variable

EZ: eigenvalue for zeroth von Kármán approximation, Λ_Z

E1: eigenvalue for first von Kármán approximation, Λ_1

VDUF

The subroutine VDUF calculates the diffusion velocity from the mass flux fraction. This program does not call any other, with the mass flux fraction being transmitted through the common block YBLOCK. The diffusion velocity is calculated from equation (5.42) for either the first or the second approximation. The integer constant in the calling sequence is the indicator; if N is greater than one, then the diffusion velocity of the second approximation is calculated. The variables of this program and their meanings are:

*S. D. Conte, Elementary Numerical Analysis, McGraw-Hill (1965).

H: step in non-dimensional temperature

N: indicator whose value determines whether the diffusion velocity ratio for the first or second approximation is to be calculated

Z: non-dimensional temperature, η

I: counter for evaluating the diffusion velocity at each point that the mass flux fraction is known

R: constant equal to $X_0/2$

EGUESS

The subroutine EGUESS makes an approximation to the eigenvalue of the second von Kármán approximation. The approximation is based on the value of the initial mole fraction, which is inputed through the calling sequence, and an array of previously determined eigenvalues. This program calls no other. The variables for this program and their meanings are:

N: array location corresponding to the nearest whole per cent of initial mole fraction at CS_2 below that of the input

X: initial mole fraction of CS_2, X_0

M: array location corresponding to the nearest per cent of initial mole fraction of CS_2 above that of the input

W: floating point representation of the variable N described above

C: intermediate value used for linear interpolation of table

E: the estimated eigenvalue which is outputed through the calling sequence

FIND3

The subroutine FIND3 contains the iteration scheme for convergence on the eigenvalue of the second von Kármán approximation.

The estimation to the eigenvalue, which was inputed through the calling sequence, is tried along with another estimate which is the inputed one divided by 1.2. If the former is too high, it is divided by 2 and the new one tried. If both the original estimates are too low (which is desired), then the secant method* is employed to find a new estimate. The secant method is employed on successive approximations until either convergence to within the convergence criterion or the estimated eigenvalue is too high. When the estimated eigenvalue is too high, a new estimate is made based on the bisection method* but with the new estimate one-tenth the span from the best previous estimate to the last estimate. After convergence is achieved, the intermediate values of the mass flux fraction variable are normalized by the final value. If convergence is not reached within fifty iterations, the program returns after writing an error message. This program calls subroutine THREE for the integration. The variables of this program and their meanings are:

CRITN: the convergence criterion in difference from the solution of 1

J: counter for the number of the iterations

JMAX: the maximum number of iterations

E: estimate to the eigenvalue

U: result from the integration with estimated eigenvalue

F: previous estimate to the eigenvalue

V: result of the integration with previous estimate

G: second previous eigenvalue estimate

---

*Ibid.

I: counter for normalizing mass flux fraction variable

THREE

The subroutine THREE integrates the species conservation equation. The second order Runge-Kutta method is applied to integrate equation (5.22) with the ignition temperature boundary conditions given in equation (5.31). This program calls no others. The scalars of this program and their meanings are:

S, T: integration constants whose value depends on X_0

H: step size in the integration

W: variable related to a temperature half-step for the Runge-Kutta method

Z: variable related to the temperature step for the integration

E: eigenvalue estimate for which the integration is performed

G: partial evaluation of the integrand

I: counter for the integration

F: partial evaluation of the integrand

C1, C2, C3, C4: partial evaluations of integrands

J: counter for the number of iterations on the eigenvalue; it is inputed and outputed through the calling sequence and incremented at the end of this program

ZINT

The subroutine ZINT calculates the transformed distances corresponding to the values of the temperature variable for the second von Kármán approximation; thus, it determines the temperature profile. The integral of equation (5.43) is evaluated using Simpson's method. The constant preceding the integral is used to non-dimensionalize the distance so that the output of this program is a non-

dimensional distance,

$$\frac{m\,\bar{C}_p}{\lambda_f(1-\theta_0)}\,z \quad . \tag{A.5}$$

This program calls no other. The scalars of this program and their meanings are:

Z: variable related to the non-dimensional temperature

J: counter for evaluation of the integrand

I: counter for performing the integral

E: step in non-dimensional temperature divided by 3

R, Q: holding locations for integrand evaluations

S: value of integral

C: step in non-dimensional temperature

BLOCK DATA

The non-executable program BLOCK DATA contains the fixed constants required for the von Kármán approximations. These constants are discussed under the common blocks FBLOCK and ZBLOCK.

TABLE A-1. Main Purpose of Each of the Subprograms of KARMAN4

MAIN:	provides for input of the initial mole fraction of CS_2
KARAPP:	driver program for calculation of the three von Kármán approximations
TFLAME:	calculates the non-dimensional constants required for the approximations
EKAR:	calculates the zeroth and first von Kármán approximations
EGUESS:	provides an estimate of the eivenvalue of the second approximation
FIND3:	contains the iteration scheme for the eigenvalue of the second approximation
THREE:	performs the integration for the eigenvalue of the second approximation
VDUF:	calculates the diffusion velocity ratio for all of the approximations
ZINT:	calculates the distance as a function of non-dimensional temperature for the second approximation
BLOCK DATA:	holds the constants required for the approximations

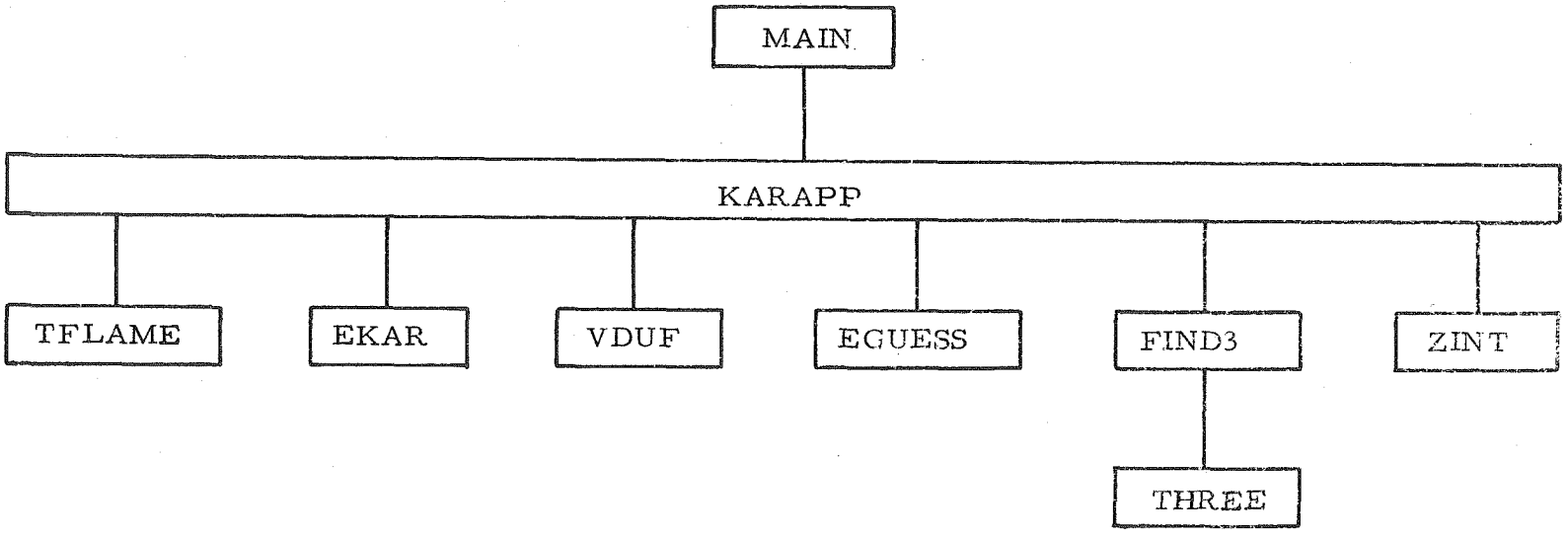

Figure A-1. Flow Diagram for the Computer Program KARMAN4 Which Calculates the von Kármán Approximations.

```
      READ(5,20) N
      DO 2 I=1,N
      READ(5,21) X
      IF(X.LE.0.0.OR.X.GT.0.285714) GO TO 1
      CALL KARAPP(X)
      GO TO 2
    1 WRITE(6,3) X
    2 CONTINUE
      STOP
    3 FORMAT(1H1,'INITIAL MOLE FRACTION OF CS2 IS OUT OF BOUNDS',1PE9.2)
   20 FORMAT(I10)
   21 FORMAT(F10.4)
      END



      SUBROUTINE KARAPP(XXXX)
      COMMON/PBLOCK/ C,T
      COMMON/TBLOCK/ A,B,D
      COMMON/UBLOCK/U(101)
      COMMON/VBLOCK/V(101)
      COMMON/YBLOCK/ X,Y(101)
      X=XXXX
      CALL TFLAME(X)
      CALL EKAR
      CALL VDUF(1)
      CALL EGUESS(X,E)
      CALL FIND3(E)
      CALL VDUF(2)
      CALL ZINT
      RETURN
      END



      BLOCK DATA
      COMMON/FBLOCK/A1(6),A2(6),B1(6),B2(6),H1(6),H2(6),TC(6),HZ
      COMMON/ZBLOCK/Z(30)
      REAL*4 A1/29.39,34.89,37.79,39.97,41.57,42.50/,
     1 A2/109.06,142.19,152.74,156.28,158.50,160.33/,
     2B1/7.852E-3,2.900E-3,2.184E-3,1.594E-3,0.938E-3,0.502E-3/,
     3 B2/47.324E-3,10.558E-3,3.536E-3,2.222E-3,1.824E-3,1.686E-3/,
     4H1/0.0,24.15E3,63.39E3,106.7E3,152.3E3,198.1E3/,
     5 H2/704.4E3,606.5E3,448.5E3,286.9E3,122.8E3,-43.9E3/,
     6 TC/3.E2,1.E3,2.E3,3.E3,4.E3,5.E3/,HZ/117.1E3/
      REAL*4 Z/0.0  ,4.741,6.208,5.863,5.299,4.774,4.336,3.976,3.681,
     13.445,3.246,3.079,2.938,2.817,2.715,2.628,2.553,2.469,2.435,2.389,
     22.351,2.319,2.293,2.274,2.260,2.252,2.249,2.250,2.25 ,2.25 /
      END
```

Figure A-2. Coding for the Main Program Designated as MAIN, Subroutine KARAPP, and the program BLOCK DATA.

```
      SUBROUTINE TFLAME(X)
      COMMON/PBLOCK/ C,T
      COMMON/TBLOCK/ A,B,D
      COMMON/FBLOCK/A1(6),A2(6),B1(6),B2(6),H1(6),H2(6),TC(6),HZ
      TZ=300.
      IF(X.GT.0.1359) GO TO 3
      IF(X.GT.0.02785) GO TO 1
      I=1
      GO TO 6
    1 IF(X.GT.0.07855) GO TO 2
      I=2
      GO TO 6
    2 I=3
      GO TO 6
    3 IF(X.GT.0.1969) GO TO 4
      I=4
      GO TO 6
    4 IF(X.GT.0.2602) GO TO 5
      I=5
      GO TO 6
    5 I=6
    6 Z=1./X-3.5
      C=1.-X/2.
      V=Z*B1(I)+B2(I)
      U=Z*A1(I)+A2(I)+TC(I)*V
      Z=HZ*C+H2(I)-Z*H1(I)
      D=(SQRT(1.+(2.*V*Z)/(U*U))-1.)*U/V
      T=D+TC(I)
      D=T-300.
      C=(HZ+H2(1)/C)*X/D
      B=T/D
      A=4.2E3/T
      TI=D/20.
      D=0.05
      WRITE(6,7) X,T,TZ,TI,A,B,C,D
      RETURN
    7 FORMAT(5H1 X =,F10.4/10X,'TF',13X,'TZ', 8X,'TI - TZ',11X,'A',13X,
     1 'B',13X,'C',13X,'D'/2F14.1,F14.2,3F14.3,F14.5//)
      END


      SUBROUTINE EGUESS(X,E)
      COMMON/ZBLOCK/Z(30)
      N=INT(X*100.+1.001)
      M=N+1
      W=FLOAT(N)
      C=W-X*100.
      E=Z(M)+(Z(N)-Z(M))*C
      E=E/(1.+0.05*C*(1.-C))
      RETURN
      END
```

Figure A-3. Coding for the Subroutines TFLAME and EGUESS.

```
      SUBROUTINE EKAR
      COMMON/YBLOCK/ X,Y(101)
      COMMON/TBLOCK/ A,B,D
      Y(1)=0.0
      Z=0.0
      S=1.-X/2.
      T=(1.-3.5*X)/S
      S=X*(2.+X/2.)/S
      DO 1 I=2,101
      Z=Z+0.01
    1 Y(I)=Z*(T+S*Z)*EXP(-A*Z/(B-Z))
      R=Y(1)
      DO 2 I=3,101,2
      Q=Y(I-1)
      Y(I-1)=Y(I-2)+0.005*(R+Q)
      S=Y(I-2)+0.01*(R+Y(I)+4.*Q)/3.
      R=Y(I)
    2 Y(I)=S
      EZ=0.5/Y(101)
      E1=EZ*(1.-SQRT(1./(EZ*T)))
      WRITE(6,4) EZ,E1
      DO 3 I=2,101
    3 Y(I)=SQRT(Y(I)/S)
      WRITE(6,5) (I,Y(I),I=2,101)
      RETURN
    4 FORMAT(' EZ = ',E20.6/' E1 = ',E20.6//' MASS FLUX FRACTION'/)
    5 FORMAT(5(I10,F14.5))
      END


      SUBROUTINE THREE(E,J)
      COMMON/YBLOCK/ X,Y(101)
      COMMON/TBLOCK/ A,B,D
      S=1.-X/2.
      T=(1.-3.5*X)/S
      S=X*(2.+X/2.)/S
      H=0.01*(1.-D)
      Y(1)=0.0
      W=H/2.
      Z=H
      Y(2)=(1.+SQRT(1.+4.*E*T))*H/2.
      G=E*(T+S*Z)*EXP(-A*Z/(B-Z))
      DO 1 I=2,99
      W=W+H
      F=E*(T+S*W)*EXP(-A*W/(B-W))
      C1=H*G/(Y(I)/Z-1.)
      C2=H*F/((Y(I)+C1/2.)/W-1.)
      C3=H*F/((Y(I)+C2/2.)/W-1.)
      Z=Z+H
      G=E*(T+S*Z)*EXP(-A*Z/(B-Z))
      C4=H*G/((Y(I)+C3)/Z-1.)
    1 Y(I+1)=Y(I)+(C1+C4+2.*(C2+C3))/6.
      Y(101)=Y(100)+SQRT(E*(1.-X)*EXP(-A/(B-1.)))*H
      J=J+1
      RETURN
      END
```

Figure A-4. Coding for the Subroutines EKAR and THREE.

```
      SUBROUTINE FIND3(E)
      COMMON/YBLOCK/ X,Y(101)
      CRITN=1.E-4
      J=0
      JMAX=50
      WRITE(6,9) X
      IF(X.LT.0.27) GO TO 1
      E=2.250
      WRITE(6,14) E
      RETURN
    1 CALL THREE(E,J)
      U=Y(101)
      WRITE(6,10) J,E,U
      IF(U.LT.1..AND.(1.-U).LT.CRITN) GO TO 7
      F=E/1.2
      CALL THREE(F,J)
      V=Y(101)
      WRITE(6,10) J,F,V
      IF(V.LT.0.0) GO TO 2
      IF(V.LT.1.0) GO TO 3
      IF(J.GT.JMAX) GO TO 6
    2 E=E/2.
      GO TO 1
    3 IF(U*(1.-U).LT.0.0.OR.V.GT.U) GO TO 5
    4 IF((U-V)/U.LT.3.E-7.OR.(E-F)/E.LT.3.E-7) GO TO 7
      G=(E*(1.-V)-F*(1.-U))/(U-V)
      F=E
      V=U
      E=G
      CALL THREE(E,J)
      U=Y(101)
      WRITE(6,10) J,E,U
      IF(J.GT.JMAX) GO TO 6
      IF(U*(1.-U).LT.0.0.OR.V.GT.U) GO TO 5
      IF(1.-U.LT.CRITN) GO TO 7
      GO TO 4
    5 E=(E-F)/10.
      IF((U-1.)*(1.001-U).GT.0.0) E=E*9.
      E=E+F
      CALL THREE(E,J)
      U=Y(101)
      WRITE(6,10) J,E,U
      IF(J.GT.JMAX) GO TO 6
      IF(U*(1.-U).LT.0.0.OR.V.GT.U) GO TO 5
      IF(1.-U.LT.CRITN) GO TO 7
      GO TO 4
    6 WRITE(6,11)
    7 WRITE(6,12) X,E
      DO 8 I=1,101
    8 Y(I)=Y(I)/Y(101)
      WRITE(6,13) (I,Y(I),I=1,101)
      RETURN
    9 FORMAT(29H1EIGENVALUE ITERATION FOR X =,F10.4/)
   10 FORMAT(I20,1PE20.5,E20.7)
   11 FORMAT(' TOO MANY ITERATIONS ')
   12 FORMAT(1H1,' X =',F10.4,10X,'EIGENVALUE =',1PE15.6//
     1' MASS FLUX FRACTION'/)
   13 FORMAT(5(I10,F14.5))
   14 FORMAT('EIGENVALUE LIMIT NEAR STOICH IS' ,1PE15.4)
      END
```

Figure A-5. Coding for the Subroutine FIND3.

```
      SUBROUTINE VDUF(N)
      COMMON/YBLOCK/ X,Y(101)
      COMMON/TBLOCK/ A,B,D
      COMMON/VBLOCK/V(101)
      R=X/2.
      V(1)=0.0
      H=0.01
      IF(N.GT.1) H=H*(1.-D)
      Z=H
      DO 1 I=2,100
      V(I)=1.-(1.-R*Z)*(1.-Y(I))/(1.-Z)
    1 Z=Z+H
      V(101)=1.0
      WRITE(6,2)
      WRITE(6,3) (I,V(I),I=1,101)
      RETURN
    2 FORMAT(1H1,' DIFFUSION VELOCITY RATIO '//)
    3 FORMAT(5(I10,F14.5))
      END


      SUBROUTINE ZINT
      COMMON/TBLOCK/ A,B,D
      COMMON/UBLOCK/U(101)
      COMMON/YBLOCK/ X,Y(101)
      C=0.0095
      Z=0.95
      DO 1 J=1,100
      I=102-J
      U(I)=(B-Z)/(Y(I)-Z)
    1 Z=Z-C
      U(101)=1.E77
      E=C/3.
      C=C/2.
      R=U(1)
      U(1)=0.0
      DO 2 I=3,101,2
      Q=U(I-1)
      U(I-1)=U(I-2)+C*(R+Q)
      S=U(I-2)+E*(R+U(I)+4.*Q)
      R=U(I)
    2 U(I)=S
      WRITE(6,3)
      WRITE(6,4) (I,U(I),I=1,100)
      RETURN
    3 FORMAT(//' DISTANCE FUNCTION'//)
    4 FORMAT(5(I10,1PE14.4))
      END
```

Figure A-6. Coding for the Subroutines VDUF and ZINT.

APPENDIX B.

The computer program which has been written to calculate the thermal theory approximation is designated as THERMAL. The eight subprograms which comprise THERMAL are written in Fortran IV G. The flow diagram of Figure B-1 displays the relationship between the eight subprograms, and Table B-1 contains a brief statement on the main purpose of each of the subprograms. The dimensionalization of the variables of the coding, which is given in Figures B-2 through B-6, is the same as for the related variables of Chapter 6.

The program THERMAL uses an iterative shooting method of trial solutions to the eigenvalue problem of Chapter 6, equations (6.12) and (6.13). The Taylor's expansion stepping method, as explained in Chapter 6, is effectively a piece-wise integration of the species conservation equations, equation (6.13).

Common Blocks

There are six common blocks in these programs. The common blocks are utilized to transmit data from BLOCK DATA and to retain the values of important variables between the steps of the shoot.

The common block CBLOCK transmits constants from BLOCK DATA. It appears in LAMBDB, TINF, and ENTH along with BLOCK DATA. The constants which are in CBLOCK and their meanings are:

CA: array which contains the constants a_{2i}

CB: array which contains the constants a_{3i}

CD: array which contains the constants a_{4i}

HZERO: array which contains the heat of formation of the species at 300 K

HZ: array which contains the constants a_{1i}

HB: array which contains the constants $\frac{1}{2}a_{3i}$

CL: array which contains the constants ℓ_i

The common block IBLOCK retains the initial values required for re-initializing the shooting iteration along with some final constants which are calculated in STARTT. It appears in the subroutines STARTT and AGAINT. The values which are on IBLOCK and their meanings are:

XI: array which contains the initial mole fractions, X_{i0}

XF: array which contains the final mole fractions, X_{if}

TF: flame temperature, T_f, K

TI: ignition temperature, T_I, K

CI: initial concentration, mol m^{-3}

UI: initial average molecular weight, kg mol^{-1}

DUC: initial density, kg m^{-3}

P: pressure, p, K

R: initial O_2/CS_2 ratio

The common block SPNAME contains alpha-numeric representations of the species. It appears in the subroutine AGAINT and the subprogram BLOCK DATA. There is only one array in this block, and it is:

SN: array which contains the alpha-numeric representations of the species

The common block WBLOCK contains the molecular weights of the species. It appears in STARTT, RATEST, and with the values in

BLOCK DATA. There is only one array in this block and it is:

W: array which contains the species molecular weight, W_i, kg mol^{-1}

The common block XBLOCK transmits current data from program to program. It appears in four programs: STARTT, AGAINT, RATEST; and LAMBDB. The variables which are in XBLOCK and their meanings are:

X: array which contains the current mole fractions, X_i

T: temperature, T, K

U: average molecular weight, $\overline{W}$, kg mol^{-1}

The common block ZBLOCK holds the variables and constants of the integration. It appears in STARTT, AGAINT, and most importantly in RATEST. The variables and constants which are contained in ZBLOCK and their meanings are:

Z: a double precision variable which contains the distance, ζ, m^3 s kg^{-1}

A: current eigenvalue estimate, kg^2 m^{-4} s^{-2}

C: concentration, mol m^{-3}

C3: sum of enthalpies constant, C_3, J kg^{-1}

DT: step in temperature, K

H: array which contains the species molar enthalpies, H_i, J mol^{-1}

KMX: number of steps between print-out

PR: pressure divided by the gas constant, mol K m^{-3}

TS: temperature above which integration terminates, K

TDBL: double precision temperature, T, K

MAIN

The program MAIN controls the flow of the calculations as well as provides for entry of the critical parameters from input data cards. This program reads in two estimates of the eigenvalue, one which has previously been found to be smaller than and one larger than the actual eigenvalue. This program continues to converge on the eigenvalue by making better approximations by using the bisection method until the predetermined number of iterations has been performed or until the estimated eigenvalue is sufficiently close to the actual eigenvalue.

This program calls STARTT, AGAINT, and RATEST. The scalar functions and their uses are given in the following:

NA: maximum number of eigenvalue iterations before termination, an inputed variable

DTEMP: the step in temperature for the shooting method, an inputed variable, K

KTEMP: the number of steps in temperature between point-outs, an inputed variable

A1: the current lower bound on the eigenvalue, a variable whose initial value is inputed

NCASES: number of cases to be run, a variable whose value is inputed

A2: the current upper bound on the eigenvalue, a variable whose initial value is inputed

IA: counter for the number of eigenvalue iterations

K: counter whose value determines when print-outs are obtained and whose output value is an indication of the reason for termination of the shooting integration

KS: counter for the total number of steps in each integration

AA: the new approximation to the eigenvalue

ICASES: counter for the cases

STARTT

The initial values and constants are calculated in the program STARTT. This program provides the logic for calculation of the final conditions and the constant C_3. It also sets the ignition temperature after having the flame temperature calculated.

This program calls TINF and ENTH. The scalar variables and their meanings are:

DTEMP: step in temperature, K

KTEMP: number of steps between variables

I: counter for the species

S: normalization factor for initial mole fractions

UF: final average molecular weight, kg mol^{-1}

AGAINT

The initial values required for the shooting integration are set in the program AGAINT. It also calculates the flame speed corresponding to the eigenvalue which is input in the calling sequence.

This program does not call any other. The scalar variables unique to this program and their meanings are:

AA: estimated eigenvalue, $kg^2\ m^{-4}\ s^{-2}$

I: counter for the species

V: flame speed, v, $m\ s^{-1}$

RATEST

The program RATEST makes a step in the integration. The reaction rates and rate of species change, w_i, are calculated in

order that the second term in the Taylor's expansion can be found. The mole fractions, temperature, distance, and average molecular weight at the end of the step are calculated. This program checks for conditions for which the integration should end. For each termination condition, an identifying message is printed and the counter K, from the calling sequence, obtains a unique value, making the counter an indicator.

The program calls the routines ENTH and LAMBDB. The variables which are unique to this program and their meanings are:

TC: thermal conductivity of the mixture, λ, $W\,m^{-1}\,K^{-1}$

S: dummy variable used as the sum of the enthalpies and the renormalization factor

I: counter for the species

K: counter for number of steps since previous printout and indication for cause of termination of integration

DZ: step in transformed distance, $m^3\ s\ kg^{-1}$

CC: concentration squared, $mol^2\ m^{-6}$

R1, R2, R3, R4: intermediate storage values

WW: array which contains the rate of species change, w_i

RR: array which contains the rates of the reactions

LAMBDB

The thermal conductivity of the mixture is calculated in the subroutine LAMBDB. The thermal conductivities of each species are calculated; then they are combined to obtain the single value required in the program RATEST.

This program does not call any other program. The vari-

ables of this program and their meanings are:

TT: temperature squared, K^2

ST: square root of the temperature, $K^{\frac{1}{2}}$

I: counter for the species

TC: thermal conductivity of the mixture, λ, $W\,m^{-1}K^{-1}$

CPI: array containing the heat capacities of the species, C_{pi}, $J\,mol^{-1}\,K^{-1}$

TCI: array containing the thermal conductivities of the species, λ_i, $W\,m^{-1}\,K^{-1}$

TINF

The adiabatic flame temperature corresponding to the initial mixture is calculated in subroutine TINF. This program uses a combination of the secant method and the bisection method to find the zero of a temperature-dependent enthalpy function.

This subroutine does not call any other. The variables of this program and their meanings are:

CONV: convergence criterion

S1,S2,S3,S4: constants related to the final enthalpy

I: counter for the species

TF: approximation to the flame temperature, K

FF: enthalpy function whose zero indicates the flame temperature

J: the number of iterations on TF

T2: approximation that is higher than the flame temperature

T1: approximation that is lower than the flame temperature

F2: enthalpy function corresponding to T2

FI: enthalpy function corresponding to TI

XF: array containing the final mole fractions of the species, X_{if}

X: array containing the initial mole fractions, X_{i0}

T: initial temperature, T_I, K

ENTH

The enthalpies of the species are calculated in the subroutine ENTH. This program does not call any other. The variables associated with this program are:

I: counter for the species

T: temperature, T, K

H: array which contains the species enthalpies, H_i, J mol^{-1}

BLOCK DATA

The non-executable program BLOCK DATA contains the constants which are required for the calculation of the heat capacities, enthalpies, and thermal conductivities. It also contains the molecular weights and alpha-numeric representations of the species.

TABLE B-1. Main Purpose of Each of the Subprograms of THERMAL

MAIN:	driver which controls the flow of the calculation
STARTT:	performs calculations of initial values and constants
AGAINT:	sets initial conditions for the shooting method
RATEST:	makes a step for the shooting method; calculates the reaction rates and changes the species mole fractions
TINF:	calculates the adiabatic flame temperature
LAMBDB:	calculates the coefficient of thermal conduction
ENTH:	calculates the enthalpy of each species

BLOCK DATA: holds the necessary constants for these programs

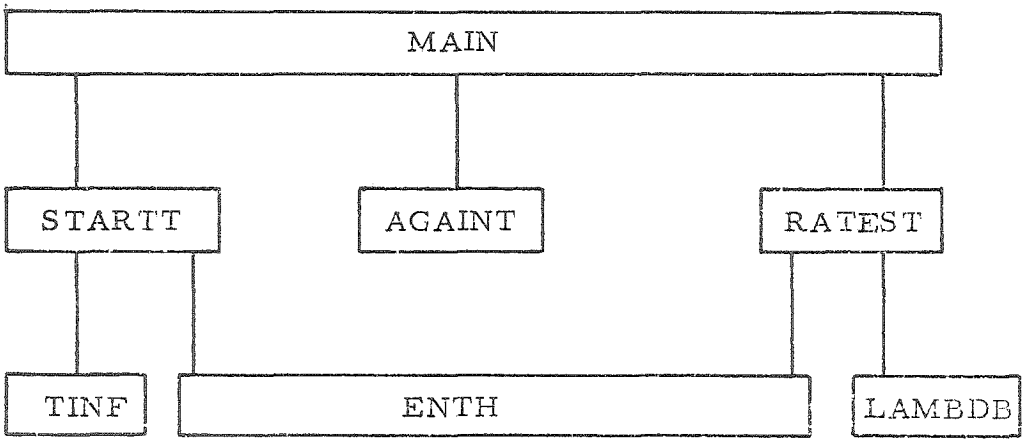

Figure B-1. Flow Diagram for the Computer Programs Which Calculate the Thermal Theory Approximation.

```
      READ(5,21) NCASES
      DO 7 ICASE=1,NCASES
      READ(5,20) NA,DTEMP,KTEMP,A1,A2
      IF(A2.GT.A1) GO TO 1
      WRITE(6,11) A1,A2
      GO TO 7
    1 CALL START(DTEMP,KTEMP)
      DO 6 IA=1,NA
      K=1000
      KS=0
      AA=(A1+A2)/2.
      CALL AGAINT(AA)
    2 KS=KS+1
      CALL RATEST(K)
      IF(K.LT.2000) GO TO 2
      WRITE(6,12) KS
      IF(K.EQ.10000) GO TO 7
      IF(K.EQ.30000) GO TO 3
      A1=AA
      GO TO 6
    3 A2=AA
    6 CONTINUE
    7 CONTINUE
      STOP
   11 FORMAT(1H1,' PROGRAM NOT EXECUTED DUE TO ERROR IN INPUT EIGENVALUE
     *S'//' A1 =',1PE15.5,20X,'A2 =',1PE15.5)
   12 FORMAT(1HO,' RATEST WAS CALLED',I8,' TIMES')
   20 FORMAT(I10,F10.3,I10,2E20.5)
   21 FORMAT(I10)
      END



      BLOCK DATA
      COMMON/CBLOCK/CA(8),CB(8),CC(8),HZERO(8),HZ(8),HB(8),CL(8)
      COMMON/SPNAME/SN(8)
      COMMON/WBLOCK/W(8)
      DATA CA/33.76,59.77,35.91,33.35,55.14,20.49,36.27,20.40/
      DATA CB/.1936E-2,.7739E-3,.5696E-3,.1129E-2,.1366E-2,.5078E-3,
     *.5197E-3,.2282E-3/
      DATA CC/-.5794E6,-.1494E7,-.6899E6,-.5939E6,-.1663E7,.3392E6,
     *-.6648E6,.1490E6/
      DATA CL/1.48E-3,4.86E-4,7.83E-4,1.54E-3,5.50E-4,3.40E-3,7.50E-4,
     *9.49E-3/
      DATA HZERO/0.0,117.1E3,230.1E3,-110.5E3,-296.8E3,279.0E3,6.9E3,
     *249.2E3/
      DATA HZ/-.828502E4,.104114E6,.221700E6,-.118577E6,-.307961E6,
     *.271801E6,-.178873E4,.242673E6/
      DATA HB/.9681E-3,.3869E-3,.2848E-3,.5647E-3,.6838E-3,.2539E-3,
     *.2598E-3,.1141E-3/
      DATA SN/4HO2  ,4HCS2 ,4HCS  ,4HCO  ,4HSO2 ,4HS   ,4HSO  ,4HO   /
      DATA W/.032,.07613,.04407,.02801,.06406,.03206,.04806,.016/
      END
```

Figure B-2. Coding for the Main Program, Designated MAIN, and the Non-executable program BLOCK DATA.

```
      SUBROUTINE STARTT(DTEMP,KTEMP)
      REAL*8 Z,TOBL
      COMMON/IBLOCK/XI(8),XF(8),TF,TI,CI,UI,DUC,P,R
      COMMON/WBLOCK/W(8)
      COMMON/XBLOCK/X(8),T,U
      COMMON/ZBLOCK/Z,TOBL,A,C,C3,DT,HK(8),KMX,PR,TS
      DT=DTEMP
      KMX=KTEMP
      T=300.
      P=1.E3
      PR=P/8.314
      CI=PR/T
      READ(5,20) XI
      R=XI(1)/(XI(2)+XI(3))
      S=XI(1)
      DO 1 I=2,8
    1 S=S+XI(I)
      UI=0.0
      DO 2 I=1,8
      XI(I)=XI(I)/S
    2 UI=UI+W(I)*XI(I)
      DUC=CI*UI
      XF(1)=XI(1)-3.*XI(2)-2.*(XI(3)+XI(6))-XI(7)
      XF(2)=0.0
      XF(3)=0.0
      XF(4)=XI(4)+XI(2)+XI(3)
      XF(5)=XI(5)+2.*XI(2)+XI(3)+XI(6)+XI(7)
      XF(6)=0.0
      XF(7)=0.0
      XF(8)=XI(8)+XI(2)+XI(3)+2.*XI(6)+XI(7)
      CALL TINF(TF,XF,XI,T)
      CALL ENTH(TF,H)
      C3=0.0
      UF=0.0
      DO 5 I=1,8
      C3=C3+H(I)*XF(I)
    5 UF=UF+W(I)*XF(I)
      C3=C3/UF
      TI=400.
      TS=TF+5.*DT
      RETURN
   20 FORMAT(8E10.2)
      END


      SUBROUTINE ENTH(T,H)
      COMMON/CBLOCK/CA(8),CB(8),CD(8),HZERO(8),HZ(8),HB(8),CL(8)
      DIMENSION H(8)
      DO 1 I=1,8
    1 H(I)=HZ(I)+T*(CA(I)+T*HB(I))-CD(I)/T
      RETURN
      END
```

Figure B-3. Coding for the Programs ENTH and STARTT.

```
      SUBROUTINE ACAINT(AA)
      REAL*8 Z,TOBL
      COMMON/IBLOCK/XI(8),XF(8),TF,TI,CI,UI,DUC,P,R
      COMMON/SPNAME/SN(8)
      COMMON/XBLOCK/X(8),T,U
      COMMON/ZBLOCK/Z,TOBL,A,C,C3,DT,HK(8),KMX,PR,TS
      A=AA
      Z=0.0
      TOBL=TI-DT
      T=TOBL
      C=CI
      U=UI
      DO 1 I=1,8
    1 X(I)=XI(I)
      V=SQRT(A)/DUC
      WRITE(6,10)DT,(I,SN(I),X(I),XF(I),I=1,8),R,TI,TF,C,U,V,C3,P,A
      RETURN
   10 FORMAT(1H1,' INITIAL CONDITIONS AND CONSTANTS'//// 5X,'STEP IN TEM
     *P IS',F9.3,' K'// 6X,' SPECIES',13X,'X(I)',15X,'XF(I)'//8(I8,2X,A4
     1,2E20.6/)// 8X,'O2/CS2 RATIO =',F9.2
     2   // 8X,'IGITION TEMP =',F9.1,' K'//10X,'FLAME TEMP =',F 9.1,' K'
     3// 7X,'CONCENTRATION =',F 9.4,' MOL/M3'// 6X,
     4 'AVE MOL WEIGHT =',F 9.5 ,' KG/MOL'//9X,'FLAME SPEED =',F9.4,' M/
     5S'//18X,'C3 =',F9.0,' J/KG'//12X,'PRESSURE =',F9.1,' N/M2'//
     6 10X,'EIGENVALUE =',1PE14.4,' KG2 M4/S2'/1H1)
      END



      SUBROUTINE LAMBDB(TC)
      COMMON/CBLOCK/CA(8),CB(8),CD(8),HZERO(8),HZ(8),HB(8),CL(8)
      COMMON/XBLOCK/X(8),T,U
      DIMENSION CPI(8),TCI(8)
      TT=T*T
      ST=SQRT(T)
      DO 1 I=1,5
      CPI(I)=CA(I)+T*CB(I)+CD(I)/TT
    1 TCI(I)=CL(I)*ST*(0.0426*CPI(I)+0.155)
      TCI(6)=CL(6)*ST
      CPI(7)=CA(7)+T*CB(7)+CD(7)/TT
      TCI(7)=CL(7)*ST*(0.0426*CPI(7)+0.155)
      TCI(8)=CL(8)*ST
      TC=X(1)*TCI(1)+X(2)*TCI(2)+X(3)*TCI(3)+X(4)*TCI(4)+X(5)*TCI(5)+
     *X(6)*TCI(6)+X(7)*TCI(7)+X(8)*TCI(8)
      RETURN
      END
```

Figure B-4. Coding for the Programs LAMBDB and ACAINT.

```
      SUBROUTINE RATEST(K)
      REAL*8 Z,TOBL
      COMMON/WBLOCK/W(8)
      COMMON/XBLOCK/X(8),T,U
      COMMON/ZBLOCK/Z,TOBL,A,C,C3,DT,H(8),KMX,PR,TS
      DIMENSION WW(8),RR(4)
      CALL ENTH(T,H)
      S=X(1)*H(1)
      DO 1 I=2,8
    1 S=S+X(I)*H(I)
      S=S/U-C3
      IF(S/C3.GT.1.E-7) GO TO 2
      K=20000
      GO TO 8
    2 CALL LAMBDA(TC)
      DZ=DT*TC/(S*A)
      C=PR/T
      CC=C*C
      RR(1)=X(2)*X(8)*5.0E7*EXP(-960./T)*CC
      RR(2)=X(3)*X(8)*1.0E8*CC
      RR(3)=X(6)*X(1)*1.0E7*EXP(-2800./T)*CC
      RR(4)=X(7)*X(1)*4.0E5*EXP(-3300./T)*CC
      R1=RR(1)*U
      R2=RR(2)*U
      R3=RR(3)*U
      R4=RR(4)*U
      WW(1)=-R3-R4
      WW(2)=-R1
      WW(3)=R1-R2
      WW(4)=R2
      WW(5)=R4
      WW(6)=R2-R3
      WW(7)=R1+R3-R4
      WW(8)=R3+R4-R1-R2
      S=0.0
      DO 3 I=1,8
      X(I)=X(I)+WW(I)*DZ
      IF(X(I).LT.1.E-30) X(I)=0.0
    3 S=S+X(I)
      U=0.0
      DO 4 I=1,8
      X(I)=X(I)/S
    4 U=U+X(I)*W(I)
      Z=Z+DZ
      TOBL=TOBL+DT
      T=TOBL
      IF(X(2)+X(3)+X(6)+X(7).LT.1.E-15) GO TO 6
      IF(T.GT.TS) GO TO 7
      K=K+1
      IF(K.LT.KMX) RETURN
      K=0
      GO TO 8
    6 K=10000
      WRITE(6,12)
      GO TO 8
    7 K=30000
      WRITE(6,13)
    8 WRITE(6,10) Z,T,X,A,C,TC,U,S,RR
      RETURN
   10 FORMAT(1HO,' AT Z = ',D20.10,9X,' TEMPERATURE =',F10.1//
     *' X',8E15.4//' A,C,TC,U,S',5E18.6//' RR',4E22.5/)
   12 FORMAT(1HO,' NO MORE REACTANTS ')
   13 FORMAT(1HO,' TEMPERATURE IS TOO HIGH'/)
      END
```

Figure B-5. Coding for the Program RATEST.

```
      SUBROUTINE TINF(TF,XF,X,T)
      COMMON/CBLOCK/CA(8),CB(8),CD(8),HZERO(8),HZ(8),HB(8),CL(8)
      DIMENSION X(8),XF(8)
      CONV=1.E-6
      S1=0.0
      S2=0.0
      S3=0.0
      S4=0.0
      DO 1 I=1,8
      S1=S1+XF(I)*CA(I)
      S2=S2+XF(I)*HB(I)
      S3=S3+XF(I)*CD(I)
    1 S4=S4+HZERO(I)*(X(I)-XF(I))
      S4=S4+(S2*T+S1)*T-S3/T
      TF=((27628.3*X(2)-21871.3)*X(2)+17305.6)*X(2)+318.457
      FF=TF*(S1+TF*S2)-S3/TF-S4
      IF(ABS(FF/S4).LT.CONV) RETURN
      J=1
      IF(FF.LT.0.0) GO TO 3
    2 T2=TF
      F2=FF
      TF=TF-20.
      FF=TF*(S1+TF*S2)-S3/TF-S4
      IF(ABS(FF/S4).LT.CONV) RETURN
      J=J+1
      IF(J.GT.50) GO TO 8
      IF(FF.GT.0.0) GO TO 2
      T1=TF
      F1=FF
      GO TO 4
    3 T1=TF
      F1=FF
      TF=TF+20.
      FF=TF*(S1+TF*S2)-S3/TF-S4
      IF(ABS(FF/S4).LT.CONV) RETURN
      J=J+1
      IF(J.GT.50) GO TO 8
      IF(FF.LT.0.0) GO TO 3
      T2=TF
      F2=FF
    4 TF=(T1*F2-T2*F1)/(F2-F1)
      IF((TF-T1)*(T2-TF).LE.0.0) GO TO 7
    5 FF=TF*(S1+TF*S2)-S3/TF-S4
      IF(ABS(FF/S4).LT.CONV) RETURN
      J=J+1
      IF(J.GT.50) GO TO 8
      IF(FF.LT.0.0) GO TO 6
      T2=TF
      F2=FF
      GO TO 4
    6 T1=TF
      F1=FF
      GO TO 4
    7 TF=(T1+T2)/2.
      GO TO 5
    8 WRITE(6,10) TF
      RETURN
   10 FORMAT(1H1,' CAUTION  CONVERGENCE NOT ACHIEVED IN TINF ',E15.6//)
      END
```

Figure B-6. Coding for the Program TINF.

APPENDIX C

The computer program which has been written to calculate the single species diffusion approximation is designated as SINGLED. The seven subprograms which comprise SINGLED are written in Fortran IV G. The flow diagram of Figure C-1 displays the relationship between the subprograms, and Table C-1 contains a brief statement on the main purpose of each of the subprograms. The dimensionalization of the variables of the coding, which is given in Figures C-2 through C-4, is the same as for the related variables of Chapter 7.

The single species diffusion approximation, with heat conduction ignored, as represented by equations (7.16), is calculated by SINGLED. The program SINGLED is structured in the same manner as THERMAL, which is described in Appendix B. The iterative shooting method of trial eigenvalues is the same, as is the stepping method.

Common Blocks

There are seven common blocks in these programs. The common blocks are utilized to transmit data from BLOCK DATA and to retain the values of important variables between the programs.

The common block CBLOCK transmits data from BLOCK DATA. It appears in STARTS, HEAT, and TINF, along with BLOCK DATA. This block is identical to the CBLOCK of the thermal theory; the constants and their meanings are given in Appendix B.

The common block IBLOCK retains the initial values required for re-initializing the shooting iteration and retains some of

the final constants which are calculated in STARTS. It appears in the initiating programs STARTS and AGAINS. This block contains all of the values of the IBLOCK of the thermal theory program as given in Appendix B with the additions and alterations of:

EI: array which contains the initial mass flux fractions, ε_{i0}

YI: array which contains the initial mass fractions, Y_{i0}

DUC: constant related to the diffusion coefficient, $(\rho D/T^{\frac{1}{2}})_0$, kg m^{-1} s^{-1} $K^{-\frac{1}{2}}$

The common block SPNAME contains the species names in alpha-numeric format. It appears in the subroutine AGAINS along with BLOCK DATA. This block is identical to the SPNAME of Appendix B.

The common block WBLOCK contains the molecular weights of the species. It appears in STARTS and RATESS along with BLOCK DATA. This block is identical to the WBLOCK of Appendix B.

The common block XBLOCK transmits current data from program to program. It appears in three programs: AGAINS, HEAT, and RATESS. This block is identical to the XBLOCK of Appendix B.

The common block ZBLOCK holds information required for the integration. It appears in AGAINS, STARTS, and most importantly in RATESS. The variables and constants which are contained in this block are the same as those of the ZBLOCK of Appendix B,with the deletion of C3, C, H, and TS and with the addition of:

B: constant related to the eigenvalue

E: array which contains the current mass flux fractions, ϵ_i

Y: array which contains the current mass fractions, Y_i

DH: array which contains the heats of reaction, ΔH^0_{300}, J mol^{-1}

XMN: value of the mole fraction of O_2 which terminates the integration

MAIN

The program MAIN controls the flow of the calculations as well as calculating eigenvalue approximations. This program reads in two estimates of the eigenvalue, which have previously been found to surround the actual eigenvalue, from which a new eigenvalue estimate is obtained. Convergence to the actual eigenvalue is continued, using the bisection method until the predetermined number of iterations is performed or until the estimated eigenvalue is sufficiently close to the actual eigenvalue. This program calls STARTS, AGAINS, and RATESS. The scalar functions and their uses are given in the following:

NA: maximum number of eigenvalue iterations before termination, an inputed variable

A1: the current lower bound on the eigenvalue, a variable whose initial value is inputed

A2: the current upper bound on the eigenvalue, a variable whose initial value is inputed

IA: counter for the number of eigenvalue iterations

K: counter whose value determines the print-out frequency and whose output value is an indication of the reason for the termination of the shooting integration

KS: counter for the total number of steps in each integration

AA: the new approximation to the eigenvalue

STARTS

The initial values and constants are calculated in the subroutine STARTS. This program provides the logic for calculation of the constant C_4. This program calls TINF. The scalar variables of this program and their meanings are:

I: counter for the species

S: normalization factor for initial mole fractions

D: diffusion coefficient at the initial temperature, D, $m^2\ s^{-1}$

YIE: constant which relates the initial mass fractions and mass flux fractions

AGAINS

The initial values required for the shooting integration are set in the subroutine AGAINS. It also calculates the flame speed corresponding to the eigenvalue which is input in the calling sequence. This program does not call any other. The scalar variables unique to this program and their meanings are the same as those of the subroutine AGAINT of Appendix B.

RATESS

The subroutine RATESS makes a step in the integration. The reactions rates and rate of species change, w_i, are calculated in order that the second term in the Taylor's expansion for the mass flux fraction can be found. The mass flux fractions, mass fractions, mole fractions, temperature, distance, and average molecular weight at the end of the step are calculated. This program checks for conditions for which the integration should end. For each termination

condition, an identifying message is printed and the counter K, from the calling sequence, obtains a unique value, making the counter an indicator. This program calls the subroutine HEAT. The variables which are unique to this program and their meanings are:

I: counter for the species

K: counter for the number of steps since the previous print-out and indicator for the cause of termination of the integration

CP: average heat capacity of the mixture, C_p, J kg^{-1} K^{-1}

YE: constant relating the mass fractions and mass flux fractions

DZ: step in transformed distance, m^3 s kg^{-1}

CC: concentration squared, c^2, mol^2 m^{-6}

R1, R2, R3, R4: rate of production or annihilation of species for four reactions, mol m^{-3} s^{-1}

Q: renormalization factor

HEAT

The specific heat capacity is calculated in the subroutine HEAT. The individual molar heat capacities for each of the species are calculated and combined assuming a homogeneous mixture. The resultant average molar heat capacity is divided by the average molecular weight to obtain the specific heat capacity. This program calls no others. The variables of this program are:

CP: average specific heat capacity, C_p, J kg^{-1} K^{-1}

TT: temperature squared, T^2, K^2

TINF

The adiabatic flame temperature which corresponds to the initial conditions is calculated in TINF. This subroutine does not call

any other. TINF is detailed in Appendix B.

BLOCK DATA

The non-executable program BLOCK DATA contains the constants which are used in these programs. This program contains all of the constants of the BLOCK DATA for the thermal theory approximation of Appendix B.

TABLE C-1. Main Purpose of Each of the Subprograms of SINGLED

MAIN:	driver which controls the flow of the calculation
STARTS:	performs calculations of initial values and constants
AGAINS:	sets initial conditions for the shooting method
RATESS:	makes a step for the shooting method; calculates the reaction rates and changes the species mole fractions
TINF:	calculates the adiabatic flame temperature
HEAT:	calculates the specific heat capacity of the mixture
BLOCK DATA:	holds the necessary constants for these programs

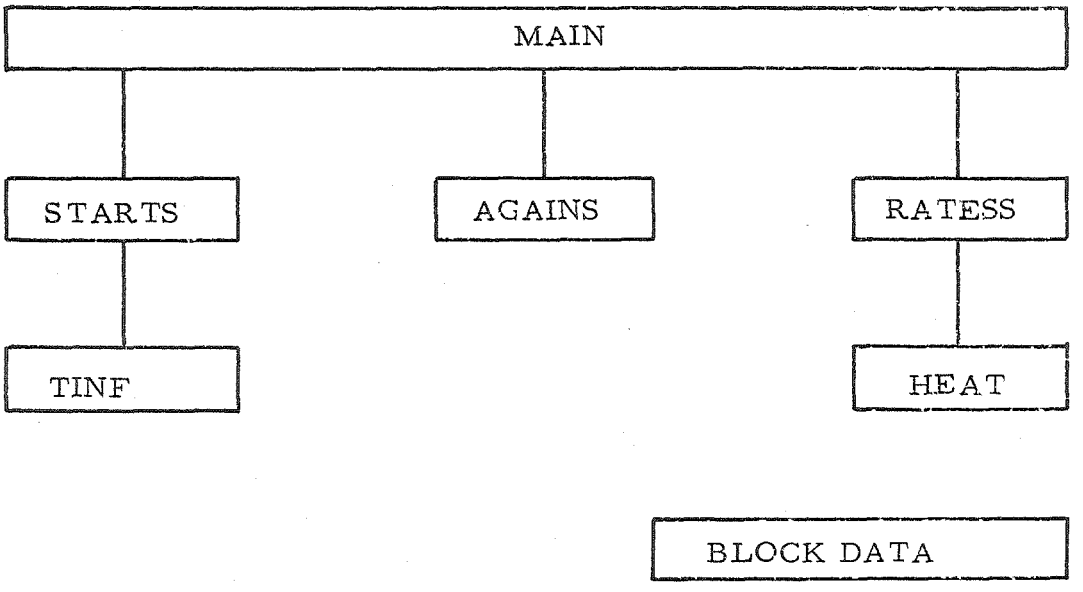

Figure C-1. The Flow Diagram for the Programs Which Calculate the Single Species Diffusion Approximation.

```
      READ(5,20) NA,A1,A2
      IF(A2.GT.A1) GO TO 1
      WRITE(6,11) A1,A2
      GO TO 7
    1 CALL STARTS
      DO 6 IA=1,NA
      K=1000
      KS=0
      AA=(A1+A2)/2.
      CALL AGAINS(AA)
    2 KS=KS+1
      CALL RATESS(K)
      IF(K.LT.2000) GO TO 2
      WRITE(6,12) KS
      IF(K.EQ.10000) GO TO 7
      IF(K.EQ.30000) GO TO 3
      A1=AA
      GO TO 6
    3 A2=AA
    6 CONTINUE
    7 STOP
   11 FORMAT(1H1,' PROGRAM NOT EXECUTED DUE TO ERROR IN INPUT EIGENVALUE
     *S'//' A1 =',1PE15.5,20X,'A2 =',1PE15.5)
   12 FORMAT(1HO,' RATESS WAS CALLED',I8,' TIMES')
   20 FORMAT(I10,2E20.5)
      END



      SUBROUTINE AGAINS(AA)
      REAL*8 Z,TOBL,E
      COMMON/IBLOCK/CI,DUC,EI(8),P,TF,TI,UI,XF(8),XI(8),YI(8)
      COMMON/SPNAME/SN(8)
      COMMON/XBLOCK/X(8),T,U
      COMMON/ZBLOCK/Z,TOBL,E(8),A,B,DH(4),DT,KMX,PR,XMN,Y(8)
      A=AA
      B=A/DUC
      TOBL=TI
      T=TOBL
      U=UI
      V=SQRT(A)/(UI*CI)
      DO 1 I=1,8
      X(I)=XI(I)
      Y(I)=YI(I)
    1 E(I)=EI(I)
      WRITE(6,10) DT,(I,SN(I),X(I),Y(I),EI(I),XF(I),I=1,8),TI,TF,CI,
     *U,V,P,A
      RETURN
   10 FORMAT(1H1,' INITIAL CONDITIONS AND CONSTANTS'////5X,'STEP IN TEMP
     * =',F9.3,' K'// 3X,' SPECIES',11X,'X(I)',12X,'Y(I)',12X,'E(I)',11X
     *,'XF(I)'//8(I6,A7,1P4E16.5/)// 8X,'INITIAL TEMP =',0PF9.1,' K'//
     *                                10X,'FLAME TEMP =',F9.1,' K'/
     *                       / 7X,'CONCENTRATION =',F9.4,' MOL/M3'// 6X,'A
     *VE MOL WEIGHT =',F9.5,' KG/MOL'// 9X,'FLAME SPEED =',F9.4,' M/S'//
     *12X,'PRESSURE =',F9.1,' PA'//10X,'EIGENVALUE =',1PE14.4,' KG2/(M4
     *S2)'/1H1)
      END
```

Figure C-2. The Coding for the Main Program, Designated MAIN, and Subroutine AGAINS.

```
      SUBROUTINE STARTS
      REAL*8 Z,TDBL,E
      COMMON/CBLOCK/CA(8),CB(8),CD(8),HZERO(8),HZ(8),HB(8),CL(8)
      COMMON/IBLOCK/CI,DUC,EI(8),P,TF,TI,UI,XF(8),XI(8),YI(8)
      COMMON/WBLOCK/W(8)
      COMMON/ZBLOCK/Z,TDBL,E(8),A,B,DH(4),DT,KMX,PR,XMN,Y(8)
      DIMENSION XR(8)
      TI=300.
      P=1.E9
      PR=P/8.314
      D=1.5E-5*(1.E5/P)
      CI=PR/TI
      READ(5,20) DT,KMX,XR
      S=XR(1)
      DO 1 I=1,7
    1 S=S+XR(I)
      DO 2 I=1,7
    2 XI(I)=XR(I)/S
      XI(8)=0.0
      XF(1)=XI(1)-3.*XI(2)-2.*(XI(3)+XI(6))-XI(7)
      XF(2)=0.0
      XF(3)=0.0
      XF(4)=XI(4)+XI(2)+XI(3)
      XF(5)=XI(5)+2.*XI(2)+XI(3)+XI(6)+XI(7)
      XF(6)=0.0
      XF(7)=0.0
      XF(8)=XI(8)+XI(2)+XI(3)+2.*XI(6)+XI(7)
      CALL TINF(TF,XF,XI,TI)
      UI=0.0
      S=S+XR(8)
      DO 3 I=1,8
      XI(I)=XR(I)/S
    3 UI=UI+W(I)*XI(I)
      DUC=UI*CI*D/SQRT(TI)
      DO 4 I=1,8
    4 YI(I)=XI(I)*W(I)/UI
      EI(8)=0.0
      YIE=1.-YI(8)
      DO 6 I=1,7
    6 EI(I)=YI(I)/YIE
      XMN=XF(1)*0.99
      DH(1)=HZERO(2)+HZERO(8)-HZERO(3)-HZERO(7)
      DH(2)=HZERO(3)+HZERO(8)-HZERO(4)-HZERO(6)
      DH(3)=HZERO(1)+HZERO(6)-HZERO(7)-HZERO(8)
      DH(4)=HZERO(1)+HZERO(7)-HZERO(5)-HZERO(8)
      RETURN
   20 FORMAT(F10.4,I10/8E10.2)
      END


      SUBROUTINE HEAT(CP)
      COMMON/CBLOCK/CA(8),CB(8),CD(8),HZERO(8),HZ(8),HB(8),CL(8)
      COMMON/XBLOCK/X(8),T,U
      TT=T*T
      CP=0.0
      DO 1 I=1,8
    1 CP=CP+X(I)*(CA(I)+T*CB(I)+CD(I)/TT)
      CP=CP/U
      RETURN
      END
```

Figure C-3. The Coding for the Subroutines STARTS and HEAT.

```
      SUBROUTINE RATESS(K)
      REAL*8 Z,TOBL,E
      COMMON/WBLOCK/W(8)
      COMMON/XBLOCK/X(8),T,U
      COMMON/ZBLOCK/Z,TOBL,E(8),A,B,DH(4),DT,KMX,PR,XMN,Y(8)
      C=PR/T
      CC=C*C
      R1=X(2)*X(8)*5.0E7*EXP(-960./T)*CC
      R2=X(3)*X(8)*1.0E6*CC
      R3=X(6)*X(1)*1.0E7*EXP(-2800./T)*CC
      R4=X(7)*X(1)*4.0E5*EXP(-3300./T)*CC
      CALL HEAT(CP)
      DZ=DT*CP/(DH(1)*R1+DH(2)*R2+DH(3)*R3+DH(4)*R4)
      Y(8)=Y(8)+(Y(8)-E(8))*DZ*B/SQRT(T)
      IF(Y(8).LT.1.E-25) Y(8)=0.0
      E(1)=E(1)+DZ*W(1)*(-R3-R4)
      E(2)=E(2)+DZ*W(2)*(-R1)
      E(3)=E(3)+DZ*W(3)*(R1-R2)
      E(4)=E(4)+DZ*W(4)*(R2)
      E(5)=E(5)+DZ*W(5)*(R4)
      E(6)=E(6)+DZ*W(6)*(R2-R3)
      E(7)=E(7)+DZ*W(7)*(R1+R3-R4)
      E(8)=E(8)+DZ*W(8)*(R3+R4-R1-R2)
      YE=(1.-Y(8))/(1.-E(8))
      U=Y(8)/W(8)
      Q=Y(8)
      DO 1 I=1,7
      Y(I)=E(I)*YE
      IF(Y(I).LT.1.E-25) Y(I)=0.0
      Q=Q+Y(I)
    1 U=U+Y(I)/W(I)
      U=Q/U
      DO 2 I=1,8
      Y(I)=Y(I)/Q
    2 X(I)=Y(I)*U/W(I)
      Z=Z+DZ
      TOBL=TOBL+DT
      T=TOBL
      IF(X(1).LT.XMN) GO TO 7
      IF(E(8).GT.Y(8)) GO TO 3
      IF(X(2)+X(3)+X(6)+X(7).LT.1.E-15) GO TO 6
      K=K+1
      IF(K.LT.KMX) RETURN
      K=0
      GO TO 8
    3 K=20000
      WRITE(6,13) A
      GO TO 8
    6 K=10000
      WRITE(6,12) A
      GO TO 8
    7 K=30000
      WRITE(6,14) A
    8 WRITE(6,10) Z,T,C,U,CP,X,Y,E
      RETURN
   10 FORMAT(1HO,' AT Z =',D18.10,9X,'T=',F7.1,9X,'C=',F9.4,9X,'U=',F9.5
     *,9X,'CP=',F8.1//3X,'X',1P8E15.4/3X,'Y',8E15.4/3X,'E',8D15.4/)
   12 FORMAT(1HO,' NO MORE REACTANTS',10X,'EIGENVALUE =',1PE15.4/)
   13 FORMAT(1HO,' E(8) IS LARGER THAN Y(8) FOR',1PE16.5/)
   14 FORMAT(1HO,' X(1) IS TOO SMALL FOR',1PE16.5/)
      END
```

Figure C-4. The Coding for the Subroutine RATESS.